TR-DA1636
25 NOVEMBER 1967

EXPERIMENTAL STUDY OF SOLAR CELL PERFORMANCE AT HIGH SOLAR INTENSITIES

BY D.C. BRIGGS

Contract No. NAS2-4248

Submitted to:
AMES RESEARCH CENTER
NATIONAL AERONAUTICS AND SPACE ADMINISTRATION

PHILCO-FORD CORPORATION
Space & Re-entry Systems Division
Palo Alto, California

TR-DA1636

EXPERIMENTAL STUDY OF SOLAR CELL PERFORMANCE AT HIGH SOLAR INTENSITIES

By D. C. Briggs

November 15, 1967

Prepared under Contract No. NAS 2-4248 by
PHILCO-FORD CORPORATION
Space and Re-entry Systems Division
Palo Alto, California

for

AMES RESEARCH CENTER
NATIONAL AERONAUTICS AND SPACE ADMINISTRATION

TABLE OF CONTENTS

TABLE OF CONTENTS (Cont)

TABLE OF CONTENTS (Cont)

LIST OF TABLES

LIST OF ILLUSTRATIONS

LIST OF ILLUSTRATIONS(Cont)

LIST OF ILLUSTRATIONS (Cont)

LIST OF ILUSTRATIONS (Cont)

LIST OF ILLUSTRATIONS (Cont)

SECTION 1

SUMMARY

An analytical and experimental program was undertaken to evaluate solar cell performance at elevated temperatures in combination with high intensity insolation. Optical characteristics of the solar cell covers were evaluated to analytically determine equilibrium temperatures for particular solar cell configurations with the cells bonded to, but thermally insulated from, a spinning spacecraft. Experimental efforts included the measurement of solar cell-cover composite performance at insolation levels approximating those encountered at 1.0, 0.5, and 0.4 A.U.

The report presents a detailed investigation of solar cell performance for intensities as high as 7.6 suns for three basic types of solar cells: (1) experimental cells specifically designed for high intensity, (2) earlier production type cells, and (3) recently produced improved 2 x 2cm cells. The results illustrate the improvement that can be obtained in solar cell output by designing solar cells specifically for high intensity. Also illustrated is the importance of low series resistance and reduced temperature on improving solar cell performance at high intensities.

SECTION 2

INTRODUCTION

This report continues the investigation of solar cell performance applicable to space missions requiring near sun approaches. (References 1, 2, and 3). The objective of this report is to provide an extensive experimental evaluation of silicon solar cell performance applicable for spacecraft missions between 1.0 and 0.4 A.U. with particular emphasis on experimental and analytical evaluation of the functional relationships between temperature, insolation (intensity), and angle of incidence. These investigations were performed to establish a more complete understanding of the performance of solar cell assemblies under equilibrium temperature conditions at high solar intensities, as well as to evaluate the experimental solar cells produced for high intensity operation under NASA Contract NAS2-3613 (Reference 4).

This program included a detailed experimental evaluation of three types of silicon solar cells at one, three, and six times air mass zero (AMZ) solar intensity (140 mW/cm). The primary emphasis has been placed on applications where the solar cells were to be bonded to, but thermally insulated from, a spinning spacecraft. The work reported includes (1) a detailed investigation of the solar cell performance under "standard conditions" for comparison with general data and (2) the experimental evaluation of solar cell performance at solar intensities up to 7.6 suns.

The efforts and continual interest of Mr. B. Mamula and Mr. D. Spratling through the experimental phases of this work contributed significantly to the successful performance of the work presented in this report. Their efforts to continually improve the experimental apparatus has generated major reductions in experimental uncertainty which the author gratefully acknowledges.

SECTION 3

SYMBOLS

A - Constant

a - Semiconductor Materials Property

A U - Astronomical Units

A - Areas, Square Meters

B - Constant

E_g - Effective Thermal Band-gap, Electron Volts

F - Fraction of Light, watts/cm^2

I - Current, amps

I_L - Light Generated Current, amps

I_t - Energy Intensity, watts/cm^2

I_{rs} - Energy Reflected from Surface S, watts/cm^2

I_o - Junction Current, amps.

k - Boltzmann's Constants - 1.38×10^{-23} joule/^oK

K - $\epsilon A \sigma T^3_{ave}$

N - Multiplier - Number of Suns

n - Junction Characteristic - Dimensionless

p - Power, watts/$meters^2$

q - Charge of electron - 1.602×10^{-19} coulombs

Q - Heat Input, watts/$meter^2$

r - Reflectivity - Dimensionless

R - Resistance - Ohms

S - Solar Constant (140 mW/cm^2)

s - Solar Distribution (mW/cm^2micron)

T - Temperature ^oC

t - Transmittance - Dimensionless

V - Voltage - Volts

α - Absorptivity, Dimensionless

φ - Incident Angle, degrees

ϵ - Emissivity, Dimensionless

η - Efficiency, Dimensionless

θ - Time, Seconds

λ - Wavelength - microns

σ - Stefan-Boltzmann Constant - 4.88×10^{-8} kg-cal/sq m)(hr)($^{o}K^{4}$)

λ_1 - Cut On Wavelength - microns

λ_2 - Cut Off Wavelength - microns

λ_3 - Cut On Wavelength - microns

τ - Transmissivity - Dimensions

Subscripts

a - Area

B - Base

C - Coating

F - Filter

L - Load

m - Maximum

O - Reference Value - Normal

OC - Open Circuit

P - Parallel

r - Reflectivity

s - Series

S - Surface

sc - Short Circuit

T - Temperature

t - Total

1 - Initial

Superscripts

' - Second

* - Normalized

SECTION 4

GENERAL BACKGROUND

4.1 GENERAL

The measurement of solar cell performance at high insolation requires careful design of the experimental apparatus, as well as an intimate knowledge of expected solar cell performance. This section will review the solar cell lumped parameter model and attempt to provide a basis for predicting solar cell performance at high intensities. A general review of measurement techniques will also be presented, with particular emphasis placed on the determination of the series resistance in a silicon solar cell. Additionally, a review of the thermal analysis of a rotating solar cell will be presented to illustrate the technique used in establishing the equilibrium temperatures.

4.2 SOLAR CELL MODEL

The ability of photovoltaic cells to convert solar energy directly into electrical energy is well known (References 5, 6, 7, and 8). The p-n junction causes the flow of carriers created in the semiconductor by incident photons whose energy exceeds the band gap energy. This separation of charge (electrons and holes) results in a forward bias of the junction and, hence, delivery of current to an external load. The most generally employed model is represented below:

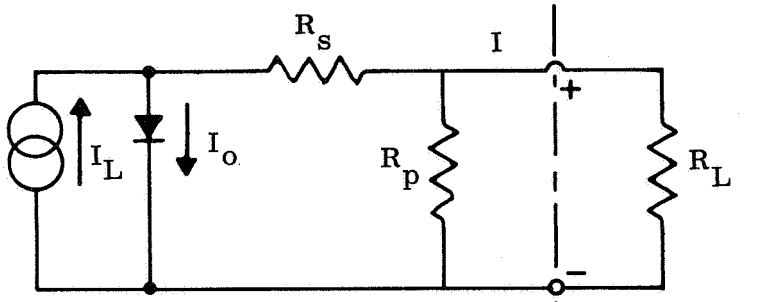

The current-voltage relationship derived from this model was first proposed by Shockley (Reference 17) and later expanded to be most generally approximated by the following equation with the generated current being defined as positive for convenience:

$$I = I_L - I_0 \left\{ e^{q(V+IR_s)/nkT} - 1 \right\} - V/R_p \qquad (4\text{-}1)$$

Thus, the dependence of the solar cell characteristics on temperature and insolation may be determined from the corresponding dependence on the parameters I_0, I_L, R_s and n. The reverse saturation current I_0 is insensitive to incident intensity and its temperature dependence is approximated by (Reference 9):

$$I_o = aT^3 e^{(-E_g/nkT)} \qquad (4\text{-}2)$$

where "E_g" is the band gap energy and the quantity "a" depends on the detailed properties of the semiconductor.

The light-generated current is directly proportional to the collection efficiency of the junction for photon-generated carriers. Thus the light-generated current is directly proportional to the intensity up to the junction saturation point. Second order effects show that the light-generated current is also dependent upon temperature. In the study of solar cell performance, careful distinction must be made between light-generated current and short-circuit current. The short-circuit current is defined as the junction current when the terminal voltage is zero. The light-generated current is the photovoltaically-generated current. The two are often confused because at one-sun intensities and normal operating temperatures, the short-circuit current is approximately equal to the light-generated current.

To determine the variation of open circuit voltage with intensity, equation 4-1 may be approximated by the following equation (neglecting parallel

resistance):

$$V_{OC} = (nk/q)\ T\ \ln\ (I_L/I_0) \qquad (4\text{-}3)$$

Equation 4-3 illustrates the relationship between the open circuit voltage, the junction temperature and the intensity. Thus, assuming I_0 and T are constant, V_{OC} varies linearly with the natural logarithm of the light-generated current.

These considerations, combined with the following discussion on series resistance, allow a general prediction of the solar cell performance at high temperatures and high insolation.

4.3 SERIES RESISTANCE OF A SOLAR CELL

As early as 1955, Prince (Reference 7) pointed out the importance of series resistance in solar cell performance. Studies by Wysocki (Reference 10) and Wolf and Rauschenback (Reference 11) have shown that series resistance is a limiting factor in the output efficiency of cells at high illumination levels. An exhaustive study of the components of series resistance allowed Berman (Reference 12) to establish a mathematical model of series resistance.

In the most elementary form, series resistance affects the shape of the characteristic I-V curve. Increasing the series resistance causes a rounder knee and, conversely, decreasing the series resistance sharpens the knee. The ramifications of this will become apparent in the discussion of test results.

A review of Berman's model illustrates the effect of base resistivity upon series resistance. Test books such as Runyan's (Reference 13) show that the base resistivity is a function of impurity concentration and temperature, and that, regardless of the impurity concentration, the series resistance can be expected to increase with increasing temperatures in the range of interest. It can thus be concluded that temperature effects on series resistance will detrimentally affect the shape of the I-V characteristics.

A review of Equation 4-1 illustrates that the meaningful measure of light-generated current (assuming a very large shunt resistance and hence neglecting the V/R_p term) must be made when the junction voltage is equal to the negative product of junction current and series resistance ($V = IR_s$), because then:

$$I = I_L \qquad (4\text{-}4)$$

The value of negative bias solar cell measurements becomes obvious when short-circuit current no longer approximates the light-generated current. Obtaining data for the light-generated current will provide solar cell performance predictions superior to those obtained by deriving the detailed relationship between temperature, light intensity, series resistance, and short-circuit current.

4.4 SOLAR CELL MEASUREMENTS AND SERIES RESISTANCE

Reference 5 presents a review of the most commonly used methods of obtaining the I-V characteristics of solar cells. Included in this reference is the presentation of the two-light intensity method employed throughout this project for determination of series resistance. This method is the one most generally employed; however, the accuracy with which it can be determined tends to make the values obtained for particular cells questionable. As an alternative, the method proposed by W. T. Picciano (Reference 14) is an iterative approach using the solar cell equation and the data from a single I-V curve, which is worthy of consideration. While this approach is approximate, preliminary evaluation tends to show very good agreement with actual test data, and might be of value in analyzing high intensity solar cell performance, especially if data at two light intensities is not available.

4.5 EQUILIBRIUM TEMPERATURE ANALYSIS

Appendix A presents the energy balance analysis employed in this project to determine the equilibrium temperature of a particular solar cell configuration with the cells bonded to, but thermally insulated from, a spinning

spacecraft. The method employed is a condensed version of that presented in Reference 2, which follows the general approach of Fairbanks (Reference 7). This method assumes that the rotational velocity is large enough to insure that pertubations around the mean temperature are small and can be neglected. The solution requires rather detailed knowledge of the spectral response of the solar cell, the spectral properties of the cover assembly, the solar absorptivity, and the total hemispherical emissivity. The power generated by the cell is approximated by the product of the solar intensity, the solar conversion efficiency, the temperature efficiency and a filter efficiency which accounts for the optical characteristics of the cover. Additionally, it is assumed that the power and solar absorptivity vary with the cosine of the angle of incidence. This cosine approximation is not rigorous. However, a more refined analysis of the angle-of-incidence shows very little effect on the calculated equilibrium temperature. More generally, if the solar cell is tested at either the short-circuit or open-circuit points, the electrical power generated is equal to zero; then the energy balance can be expressed as

$$Q_{in} + Q_{rad} = 0$$

from which the cell temperature can be directly obtained. It is obvious that when the cell is generating electrical power, the temperature is correspondingly reduced; the temperature difference caused by neglecting the power term was shown in Table 6 to be only a few degrees centigrade, so the assumption of cosine dependence is easily justified for thermal analysis.

SECTION 5

EXPERIMENTAL APPROACH

5.1 GENERAL

This section describes the test procedures, the test apparatus, and the calibration procedures used in this program.

5.2 TASK DESCRIPTIONS

The following task descriptions define the experimental program presented in this report.

5.2.1 Task I - Preliminary Measurements

This task consisted of a series of measurements on each solar cell and cover used in this program. These preliminary measurements established the base-line characteristics of the components which were used in evaluating any possible performance degradation resulting from the succeeding tests, and formed the basis of the analytical efforts. These measurements consisted of two groups of tests:

a. Solar Cell Characteristics. I-V curves were obtained on all solar cells used in this program. These tests were conducted under the following conditions:

1. OCLI Solar Simulator at 140mW/cm^2
2. Solar Cell Temperature of 28 ± 1°C
3. Insolation Normal to the Surface

In addition, the spectral response of selected samples of each type of solar cell was obtained. Sufficient samples were taken to define the range and dispersion in the data.

b. Solar Cell Cover Characteristics. The transmission characteristics of four samples of each type of filter and cover were measured as a function of wavelength in the spectral range from 0.35 to 2.0 microns.

5.2.2 Task II - One Sun Performance

Filters and covers were assembled to the solar cells with Dow Corning XR63488 adhesive so that at least five test samples were obtained for each of the following categories:

a. High Intensity Experimental Cells (Type A) (Ref. 4)

1. As received (0.001" integral cover)
2. 6 mil cover glass with A/R coating
3. Blue-red interference filters
4. A/R coating applied to external surface of the integral cover.

b. Cells Used in Previous Work (Type B) (Ref. 2)

1. Bare Cells
2. 6 mil cover glass with A/R coating
3. Blue-red interference filters

c. Late Production 2 x 2cm N/P Silicon Cells (Type C)

1. Bare cells
2. 6 mil cover glass with A/R coating
3. Blue-red interference filters

After the test samples were assembled, the performance evaluation tests were performed on samples in each category. Solar cell output was determined using the calibrated OCLI solar simulator with the intensity adjusted to 140mW/cm^2. The measurements performed in this task consisted of the following:

a. Spectrophotometric measurements were performed on the samples to determine the reflectivity as a function of wavelength. The total hemispherical surface emissivity was also measured using the emissometer.

b. The angle of incidence performance was determined by measuring I-V curves at specific angles of incidence.

c. The temperature effects were obtained by measuring I-V curves at selected cell temperatures covering the range from 28°C to 150°C.

5.2.3 Task III - High Intensity Measurements

Following the determination of the solar absorptivity and infra-red emissivity, the equilibrium temperature of each cell configuration was calculated, assuming that the cell was bonded to, but thermally insulated from, a rotating spacecraft with the sun incidence perpendicular to the axis of rotation. Tests were performed on samples of each category using the Strong Carbon Arc solar simulator at insolations approximately equivalent to one, three, and six suns (AMZ) with the cells thermally controlled so that they operated at their respective calculated equilibrium temperatures. I-V curves were obtained at specific angles of incidence for each case.

5.2.4 Task IV - Data Analysis

A complete review of the test data was performed and is presented in Section 6. The purpose of this task was to evaluate the test results and study the effects of angle-of-incidence and predict the performance of a solar cell mounted on a spinning spacecraft. The results are presented and summarized, providing comparisons of the various solar cell types for particular applications. Particular emphasis is also placed upon the effect of series resistance at high temperatures and high insolations.

5.3 SOLAR CELL CONFIGURATIONS

Three types of solar cells and three types of covers were employed in this project. The selections were based upon the objective of providing the most comprehensive test data applicable to the general requirements of this program. The solar cells were selected in three groups: (1) high intensity experimental cells, (2) cells identical to those used in the previous work, and (3) recent production cells. The covers were essentially in three groups: (1) integral covers on the experimental cells, (2) fused silica cover glass with anti-reflective coating, and (3) blue-red interference filter on a fused silica cover glass. The components and the final assembly leading to the categories described in Section 5.2.2 are discussed below.

5.3.1 Solar Cells

5.3.1.1 High Intensity Experimental Cells (Type A)

These cells were manufactured under NASA Contract NAS 2-3613 for NASA Ames Research Center and are described in Reference 4. These cells were designed specifically for operation in a near-sun mission at 0.2 A.U.

The objective of the design was to optimize the short-circuit current at one-sun intensity, open-circuit voltage at 25-sun intensity, and maximum power over all intensities. The cells were manufactured to the following cell specifications:

Size and Type

n on p, 1 by 2 by 2.5 x 10^{-2}cm

Grid Geometry and Type

11 grids, contact strip along 2 cm side, sintered silver-titanium

Base Resistivity

0.2 to 1.2 ohm cm

Diffused Junction Depth

0.6 to 0.8 μm

Series Resistance

0.1 to 0.2 ohms

Short-Circuit Current at AM = 1 (100mW/cm^2)

≥ 40 mA

Open-Circuit Voltage at AM = 1 (100mW/cm^2)

> 0.55 volts

Cover Glass

integral, 2.5 x 10^{-3}cm thick SiO_2

5.3.1.2 Cells Used in Previous Work (Type B)

The solar cells used in the work reported in Reference 2 are cells typical of early production quality, reflecting production techniques which have been substantially improved since their manufacture. These cells are not designed for high intensity, and hence have substantially higher series resistance. These cells have the following characteristics:

Size and Type

n on p, 1 by 2 by 4.06 x 10^{-2}cm

Grid Geometry and Type

5 grids, contact strip along 2 cm side, plated contacts

Efficiency

58 mA at 400 mV

Series Resistance

$\sim 1\ \Omega$

Anti-Reflection Coating

SiO anti-reflective coating on active area

5.3.1.3 Late Production Cells (Type C)

The solar cells selected for this category were to be representative of the most recent production solar cells used in near-earth orbits (solar intensities of $\approx 140 mW/cm^2$). These cells were selected to represent the performance of a spacecraft if the power subsystem employed typical current production cells. It was realized that small quantities of experimental type cells are available with characteristics more suitable for near-sun operation than those selected in this category;

however, it was felt beneficial to the mission analysis to have accurate data on current production type solar cells at high intensities. Thus, the cells used were typical of those currently being employed by Philco-Ford in their communication satellite programs. These cells have the following characteristics:

Size and Type

n on p silicon, 2 x 2 x 3.55 x 10^{-2}cm

Grid Geometry and Type

6 silver-titanium grids, thin collector strip, solder-dipped corner dart contacts

Base Resistivity

5 to 14 ohm-cm

Diffusion Junction Depth

approximately 0.3 microns

Electrical Output (AMZ based upon JPL balloon standard 28 ± 2°C)

Short Circuit Current

142.1 mA - minimum

Open Circuit Voltage

555 mV - minimum

Current at 452 mV

132 mA - minimum

Anti-Reflection Coating

SiO on active surface

5.3.2 Solar Cell Covers

Three basic types of solar cell covers were employed in this program: (1) integral covers, (2) microsheet covers with anti-reflective coating, and (3) blue-red interference filters. The integral covers were only deposited on the high intensity experimental cells (Type A). The integral covers were part of the contract to develop the experimental solar cells, hence all the Type A cells were received with integral covers. The following descriptions from Reference 4 delineate the details of each of these covers.

5.3.2.1 Integral Covers

The integral covers were quartz-evaporated onto bare (without A/R coating) Type A solar cells. The cells were placed in a fixture which masked the contact strip and were exposed to the evaporator source for a sufficient time to give a 25 μm coating. As described in Reference 4, the coating thickness was limited to this value. Many stress lines, cracks and large areas of delamination were observed in the covers as received, and will be discussed in detail in following sections of this report.

5.3.2.2 Microsheet Covers with Anti-Reflective Coatings

These covers were purchased from Optical Coating Laboratory, Inc. and are typical of microsheet covers used in many satellite applications. These covers were 0.0152 cm (0.006 inches) thick Corning 0211 microsheet and had an anti-reflection coating. OCLI solar cell covers are produced with an anti-reflection coating on one surface which is designed to minimize the loss of energy to the solar cells in the region of peak spectral response. A single layer coating is applied to produce reflections of less than 2 percent in the wavelength region from 600 to 800 millimicrons. Figure 1 illustrates the characteristics of the anti-reflection coating. The effect of the A/R coating for improving solar cell performance is presented in detail by Ralph and Wolf (Reference 30).

5.3.2.3 Blue-Red Interference Filters

These covers were also purchased from OCLI and are typical of the blue-red wide bandpass filters used for solar cell covers. The results of Reference 2 indicated that, for a spinning spacecraft exposed to solar intensities up to six suns, a nominal filter bandpass approximately equal to the solar cell spectral response region would provide optimum power. Within the objectives of the present program, a bandpass of 0.410 microns to 1.2 microns was selected, which is the typical blue/red filter employed on solar cells. The filters are deposited on one side of 0.0152 cm (0.006 inch) thick Corning 0211 microsheet which has an anti-reflection coating (described in Section 5.3.2.2) on the other side. These filter covers were OCLI part number BR-SCC-410-1.2-M-C manufactured to the General Specification Guide for Solar Cells (Reference 35). Typical transmission curves for these filters are presented in Figure 2.

5.3.3 Solar Cell Assemblies and Nomenclature

Each cell used in this program was initially numbered and then evaluated at one-sun conditions. The calibrated cells were then arranged into representative groups for assembly with cover slides to form groups of cells according to the categories described in Section 5.2.2. At least 10 cells were assembled for each category to allow for breakage and cell test temperature determination, and still provide an acceptable quantity of reference cells and test cells. Particular emphasis will be placed on the statistical correlation of the data.

The covers were cemented to the cells using Dow Corning XR-63488 adhesive. This adhesive is a standard solar cell adhesive designed to bridge the difference in the indices of refraction between the materials.

To facilitate handling and description of the ten categories of cells, the following designation is adopted for this program.

X	Y	ZZ
Cover Type	Cell Type	Cell Number

where

X is the cover type as follows

1 - as received

2 - 6 mil cover, .0211 microsheet, with A/R coating

3 - 6 mil cover, .0211 microsheet, blue-red filter, A/R coating

4 - A/R coating on SiO_2 integral cover

Y is cell type

A - experimental cells

B - cells used in previous work

C - late production cells

ZZ is particular cell number

This nomenclature completely describes the cell assembly according to the requirement of this program.

5.4 TEST APPARATUS

Four basic test facilities were employed during the experimental portions of this program: (1) the OCLI one-sun test facility, (2) the carbon arc, high-intensity test facility, (3) spectral response equipment, and (4) spectrophotometric apparatus. A description of these facilities is presented in the following subsections. A complete list of equipment used on this program is provided in Table 1.

5.4.1 OCLI One-Sun Test Facility

The OCLI one-sun test facility is designed to enable one to make a comprehensive evaluation of a single solar cell at one-sun conditions. This facility is used to determine the effects of temperature and angle of incidence on solar cell performance at one-sun AME ($140 mW/cm^2$). A block diagram of the experimental apparatus is shown in Figure 3. The main items are the OCLI solar simulator and the universal solar cell test fixture. The cell fixture is mounted on a heat sinked thermoelectric cooler which provides accurate temperature control. The temperature of the cell fixture is determined by a thermocouple located in the fixture, under the test cell, and very near the cell fixture interface. The solar cell is held to the back of the test fixture by vacuum with the fixture making electrical contact with the back of the cell. The front contact is accomplished by spring loaded beryllium-copper fingers. The fixture is identical in manufacture to that shown in Figure 4.

Included as an integral part of this facility are the following calibration equipment:

a. Pyrheliometer fixture used for balancing the tungsten and xenon lights.

b. Uniformity traverse for determining the uniformity of the light over the test area.

c. The spectral fixture which is five narrow bandpass interference filters over silicon solar cells used as a coarse spectral check of the combined light source.

d. A Heliotek standard cell which is used for total intensity calibration and adjustment.

Every change of lights requires careful balancing, following the procedures established by the manufacturer. Uniformity measurements are then made to ensure proper placement of the lights and reflectors. Figure 5 presents a typical uniformity measurement of the OCLI simulator. The spectral output of the combined lamps, as shown in Figure 6, successfully meets the AIEE Solar Simulator Specification (Reference 21) in 1,000 angstrom intervals. Spectral checks were made using the interference filters periodically during each test to ensure stability of the spectral distribution. These data show a maximum deviation of ±0.2% over the entire experimental program.

The OCLI solar simulator is mounted on an index head, carefully positioned so that when the light source is aligned with each test fixture, the one-sun test plane is accurately positioned without further adjustment. Thus, once the intensity is determined using the standard cell, the solar simulator may simply be rotated to any desired test area.

I-V curves are obtained using a Spectrolab D550 electronic load system controlling a Moseley Model 7000-A x-y recorder. Accurate calibrations of short-circuit current and open-circuit voltage points on the recorder are obtained (using laboratory precision ammeters and voltmeters). The test cell temperature is obtained by placing a fine wire thermocouple on the contact of a typical cell and calibrating the base plate temperature vs cell surface temperature. All the cells of this type are then tested at the base plate temperature necessary to provide the cell surface temperature required. This procedure should be followed for each type of cell because the varying surface properties control the heat transfer from the front and back surfaces.

Angle of incidence measurements are made by rotating the cell fixture with the angle of incidence indicated by a protractor scale and pointer. The fixture is designed so that the axis of rotation runs across the face of the cell one centimeter from the contact region and so that the top contact is rotated away from the simulator. This configuration is used to minimize the variation of light intensity across the cell and to keep shadows from falling on the active cell area. The entire assembly is permanently mounted on a table, providing a totally-integrated solar cell test facility. This facility is shown in Figures 7 and 8.

5.4.2 Strong Carbon Arc Test Facility

The high-intensity test apparatus was developed primarily for this project. This experimental setup is used solely for the experimental determination of solar cell performance at high levels of insolation. This test facility is shown in Figure 9, and illustrated schematically in Figure 10. This facility employs the Strong Carbon Arc Simulator Model 75000-2 as a high-intensity light source. This simulator is a standard model modified by the substitution of a 30 hp motor generator power supply in place of the usual rectifier supply. This modification substantially reduces the amount of flicker usually associated with this type of simulator. The basic operation of the experimental tests is identical to those described in Section 5.4.1. The universal test fixture modified for high-intensity measurements, as well as some of the total intensity devices, is shown in Figure 4. The cell test fixture is identical to that employed in the OCLI facility except that particular emphasis has been placed upon minimizing series resistance to allow accurate measurement of short-circuit current at high intensities. The measurement of short-circuit current is extremely difficult due to the large generated currents at very low terminal voltage accompanying high intensity operation.

The mounting channel upon which the fixtures are located is water-cooled to facilitate fixture thermal control at high intensities. All the electrical wires are covered with highly reflective aluminum foil to prevent insulation burning. Throughout the high-intensity experimental tasks, thermal control and temperature measurement must be carefully monitored. The initial calibration consisted of establishing the most uniform test section, verifying the centerline location, determining the collimation angle, and establishing the total intensity as a function of distance from the source. A series of measurements of uniformity were performed to determine the most uniform test section. The uniformity is controlled by the focusing assembly, with the result that the narrower the collimation angle, the greater the non-uniformity. It was also observed that the more defocused the beam was, (i.e., the wider the collimation angle), the less effect the arc instability had on solar cell measurements. Thus, it was concluded that a defocused arc provided the best test conditions.

The results of typical uniformity measurements made in a plane perpendicular to the light centerline are presented in Figure 11.

The total intensity was initially determined as a function of distance from the source using four separate techniques: (1) the Heliotek standard cell, (2) the Eppley pyrheliometer, (3) the Eppley thermopile, and (4) solar cells in the cell test fixture. The results from each of these measurements is presented in Figure 12.

A good correlation of these measurements is observed except for those made with solar cells at the higher intensities. The nonlinearity of solar cells at high intensities is readily explained by examination of the functional relationship between short-circuit current and intensity. This relationship will be more fully amplified in the discussion of the results of this program.

Figure 12 was used to determine the approximate distance from the carbon arc to the test console. Essentially this curve establishes the center-line position for the one-, three-, and six-sun tests. The position for one sun was very carefully adjusted to provide a standard cell output identical to the calibrated, one-sun, short-circuit current. Great care in adjusting the fixtures at this position was required if valid comparison of the solar cell performance under the two simulators was to be accomplished.

The temperature of the cell to be tested was measured and controlled as described in the previous section. The comparison of the I-V curves from both solar simulators at one sun intensity is presented in Appendix B and shows acceptable correlation.

5.4.3 Spectral Response Facility

The spectral response of the solar cells was obtained by direct comparison with the Heliotek standard cell. The test apparatus utilizes a Nikon 35mm slide projector to shine light through narrow bandpass filters onto the test cells. The test cells are mounted on a temperature-controlled universal test fixture as described in Section 5.4.1. The standard cell is mounted on a track so that both cells are in the identical test point when measurements are taken. The spectral response is determined by a linear comparison of the short-circuit current output of the test cell, the given spectral response from the standard cell, and the short-circuit current reading from the standard cell. This facility is schematically presented in Figure 13.

The projector optics have been modified by the removal of the heat-absorbing collimator lens, thus ensuring adequate output over the required spectral range. A standard tungsten filament lamp is employed as a light source. Use of this type of source is very beneficial for spectral measurements using bandpass filters because of its relatively uniform spectral characteristics.

The filters employed in this experiment are the same size as 35 mm glass slides; hence they can be rack-mounted in the projector and measurements can be made semi-automatically. The filters were obtained from Optical Technology, Inc., with calibration curves which were verified by Philco-Ford measurements. These filters had peak transmission points at approximately 50 mμ intervals.

The short-circuit currents are read on a laboratory precision milliammeter. The temperatures of both the standard cell and the test cell are read on an L & N potentiometer. The spectral response of the standard cell used was calibrated by Spectrolab.

5.4.4 Spectrophotometric Measurement

The spectrophotometric measurements required for this project consisted of the following: (1) solar cell cover transmission as a function of wavelength, (2) reflectivity of the assembly as a function of wavelength, and (3) the total hemispherical emissivity.

The solar cell cover transmission characteristics were measured at ambient room temperature on a Perkin-Elmer Model 350 ratio-recording spectrophotometer. This instrument is capable of measuring transmittance within a spectral range of 0.185 to 2.7 microns. The transmission characteristics of the bandpass filters used for the solar cell spectral response determination were also measured on this equipment.

The reflectivity of the various assemblies was measured as a function of wavelength on the Gier-Dunkle Directional Reflectometer. This instrument is capable of measuring the relative reflectance of a material in the spectral range of 0.4 to 22 microns; by varying the sample position, orientation information may be obtained on the specular characteristics

of the sample. The measurements were made by mounting a group of identical samples to a panel such that total reflectance could be obtained. Several measurements were made near normal to account for the various surface anomalies.

The total hemispherical emissivity was determined from the same sample assemblies used with the Gier-Dunkle reflectometer. The measurements were made on the Lion Emissometer Model 25-6 with the samples at ambient temperatures. Several readings were also taken to average the surface anomalies.

SECTION 6

EXPERIMENTAL RESULTS

6.1 GENERAL

This section presents chronologically the results obtained for this experimental program. These data establish the foundation for the discussion, comparison, and analysis in Section 7. Analysis of the uncertainty associated with these data is provided in Appendix C.

6.2 ILLUMINATED SOLAR CELL CHARACTERISTICS

Every solar cell used in this program was subjected to one sun performance determination. Figures 14, 15, and 16 provide typical I-V characteristics for cell Types A, B, and C, respectively. Plotted on each figure is the power vs. voltage curve associated with the I-V curve. Surrounding each I-V curve is the maximum envelope of the data obtained for that type of solar cell.

This envelope does not indicate the uncertainty associated with each I-V curve, but reflects the sample-to-sample variation associated with each type. It is thus observed that the Type A cells (being the result of an experimental program) are illustrative of an engineering sample, while the Type B and C cells reflect some degree of lot sorting. The cell junction temperature in each case was $28^{\circ}C \pm 2^{\circ}C$. These curves were all obtained on the OCLI solar simulator test facility described in Section 5.4.1.

Table 2 presents a comprehesive summary of the results obtained on each cell tested. Included in this table are the following quantities:

a. Cell Number

b. Short Circuit Current

c. Open Circuit Voltage

d. Series Resistance

e. Maximum Power Current

f. Maximum Power Voltage

g. Power Output at Maximum Power

h. Curve Factor $C.F. = \left[\frac{Pmp}{I_{sc} \times V_{oc}} \right]$

A review of Table 2 illustrates again the larger variation in measured values associated with the unsorted Type A cells.

Following the one sun performance evaluation, I-V curves were obtained at a reduced light intensity to allow the evaluation of each cell's series resistance.

6.3 DARK FORWARD DIODE CHARACTERISTICS

The dark forward diode characteristics of the solar cells were measured using the method described in Reference 11. These curves are expected to help in defining solar cell series resistance and its effect on power output.

Typical forward diode characteristics and the test data envelope for cell Types A, B, and C, respectively, are presented in Figures 17, 18, and 19. The sign of the current and voltage axis has been adjusted to provide data

in the first quadrant. This will cause no problems if the reader is aware that throughout this program, measured voltages and currents are considered positive for each presentation of the data.

The measurements were accomplished on the OCLI solar simulator test facility, which is easily adapted to this type of measurement. The experimental uncertainties reported in Appendix C are generally applicable to these data.

6.4 DARK REVERSE DIODE CHARACTERISTICS

Figures 20, 21, and 22 present the typical dark reverse diode characteristics for cell Types A, B, and C, respectively. Again, the envelope of the test data is presented to illustrate the cell-to-cell data variations associated with this type of data.

These data were also obtained using the basic OCLI solar cell test facility. An attempt was made to maintain the cell junction temperature at 28°C; however, the large amount of power dissipation in the cell caused the cell temperature to rise rapidly. Hence, the uncertainty associated with the temperature measurement is given as approximately ±10°C.

6.5 RELATIVE SPECTRAL RESPONSE

The relative spectral response was determined for random samples from each type of solar cell. The data was obtained using the seventeen narrow bandpass interference filters. The uses of these filters and the associated equipment described in Section 5.3.3 allowed the determination of the relative spectral response by comparison with the Heliotek laboratory standard cells used in this program. The data obtained for each cell type and each filter was averaged and the resulting average spectral response was then normalized. Figures 23, 24, and 25 present the normalized relative spectral response curves for cell Types A, B, and C, respectively. Presented at each data point is a data bar indicating the cell-to-cell variation (hence the data envelope) for each type of solar cell. Also included for reference

in Figure 26 is the relative spectral response of the Heliotek standard cell used as a reference standard for these measurements.

The relative spectral response data was obtained with the junction temperatures maintained at approximately 28°C for both the standard and each particular test specimen. The uncertainty analysis presented in Appendix C reflects the expected uncertainty associated with these data.

6.6 TRANSMISSIVITY VS. WAVELENGTH

The transmissivity of selected samples of each of the three types of cover glasses was determined as a function of wavelength using the Perkin-Elmer Model 350 Spectrophotometer. Typical curves of these measurements covering the wavelength region from .3μ to 2.5μ are presented. Typical data for the fused silica cover glasses with the anti-reflective coating indicated slight improvement in ultraviolet transmission over the same data obtained for microsheet cover glasses with the anti-reflective coating. Only the microsheet cover glasses were employed in this effort. However, the fused silica data was obtained for reference. Figure 2 presents the transmission characteristics for the microsheet cover slides with the multilayer blue-red interference filter. This filter is the one most commonly used for solar cells.

Only normal incidence measurements were made in the performance of this contract. The data presented in Reference 2 provides a detailed discussion from which the angle of incidence effects can be predicted.

6.7 TOTAL SURFACE HEMISPHERICAL EMISSIVITY

Following the assembly of the solar cells and the cover slides into the ten categories to be used in this program, the cells were assembled on masking tape to provide an assembly with an area greater than one inch in diameter. These taped assemblies were then used as test samples with the Lion Emissometer to determine the total surface hemispherical emissivity. The results are then expected to be typical of a solar cell assembly, including the

uncovered contact area. The data obtained for measurements of each of the ten categories is presented in Table 3 and illustrates the expected improvement which occurs as a result of the cover slide.

6.8 REFLECTIVITY VS. WAVELENGTH

The tabular data presented in Table 4 provides the reflectivity data taken with the Gier Dunkel Reflectometer. The data was taken on randomly selected samples for each test category. These measurements were made in the integrating sphere with the samples slightly off axis. The uncertainty associated with this data is rather large ($\sim$ 15%) and is illustrated by the sizeable deviations between samples from the same test category.

6.9 SOLAR CELL CHARACTERISTICS AT VARIOUS ANGLES OF INCIDENCE

Selected random samples of the solar cell assemblies were tested at one sun AMZ (140 mW/cm^2) conditions with the cell junction at 28 $\pm$ 1^{o}C at various angles of incidence. The normal incidence curves, thus provided one sun performance calibration curves for final comparisons. I-V curves were obtained for several samples of each of the ten categories employed in this program.

The Figures 27 through 36 present typical data for each of the ten categories. A review and analysis of these data, as well as various comparisons, is presented in the discussions of the test results located in Section 7 of this report.

These data were obtained on the OCLI solar simulator test facility and the measurements have an associated uncertainty as described in Appendix C. The considerations of the edge effects will be discussed in the evaluation and analysis of these data.

6.10 SOLAR CELL CHARACTERISTICS AT SPECIFIC TEMPERATURES

I-V curves were obtained on random samples of each cell category for specific cell junction temperatures covering the range from 28°C to 150°C. These data are presented in Figures 37 through 46, and are in a format similar to the data on angle-of-incidence. These data allow determination of the temperature coefficients which will also be discussed in the analysis of the data.

These data were obtained on the OCLI solar simulator with an experimental uncertainty as analyzed for this facility in Appendix B.

6.11 HIGH INTENSITY MEASUREMENTS

Theoretical predictions of the equilibrium temperatures were performed using the spectrophotometric data combined with the approach described in Appendix A. The calculations were performed for each test category assuming the cells to be bonded to, but thermally insulated from, a spinning spacecraft. Certain experimental limitations prohibited testing some of the theoretical temperatures. Temperatures less than 15°C caused condensation to occur on the solar cell, and since the test requirements were not substantially below this value, testing in an inert atmosphere was not warranted. Hence, temperature requirements below 15°C were not imposed. Similarly, temperatures in excess of the solder-melting temperature were not imposed. Table 5 illustrates the calculated equilibrium temperatures and the corresponding test temperatures.

I-V curves were obtained on selected samples from each category at particular angles-of-incidence. These measurements were performed at three specific simulator intensities using the Strong Carbon Arc Solar Simulator.

The test sections were established at specific distances from the base of the carbon arc with the intent of having the solar intensities equal to one, three, and six times the solar intensity at air mass zero. Careful evaluation showed the intensity at the selected test planes to be 1.0, 2.98 and 7.6 suns.

The uncertainty associated with the measurement of the mean solar intensity at each test plane is estimated to be about ±3 percent.

Figures 47 through 56 show data for a typical cell in each of the ten test categories at one sun intensity; Figures 57 through 66 present the data for three suns; and Figures 67 through 76 present the data obtained at 7.6 suns. These figures present the I-V characteristics at various angles of incidence at the specific controlled cell temperatures as recorded on each figure.

6.12 ONE SUN RECALIBRATION CURVES

I-V characteristic curves were obtained on all cells used in this experimental program following the high intensity tests. These data were compared to that obtained in the earlier phases of this effort to ascertain any possible degradation resulting from exposure to either the elevated intensities or from the elevated temperatures. No effects were observed and the comparison showed consistency throughout. These data also provided a useful reference for the solar cell configurations tested in this program.

SECTION 7

ANALYSIS AND DISCUSSION

7.1 GENERAL

This section discusses, analyzes, and compares the results presented in Section 6. The objective of this section is to evaluate the test results and to study the effects of temperature, angle of incidence, and solar intensity on the performance of a solar cell subjected to these conditions.

Three types of solar cells were employed in this experimental program. Types A and B were nominally 1 x 2cm cells. Type C were nominally 2 x 2cm cells. Comparison of the performance parameters of these cells required establishment of the applicable area comparison criteria. Two such criteria are generally used: (1) active cell area, and (2) total cell area. Active cell area is generally used to establish junction performance comparisons, while comparison of cells based upon total cell area reflects, more generally, the "practical engineering approach" of energy conversion per unit surface area. Therefore, the total cell area method, which allows comparisons simply by dividing the current axis of the Type C 2 x 2cm cells by a factor of 2, will be employed throughout the following discussions.

For reference and comparison, the active areas of each type of cell were determined by enlarging photographs of each type of cell, on mylar, and integrating the respective active areas. The results showed that the active area of Type A, B, and C cells was ~ 1.637 cm^2, 1.715 cm^2, and 3.672 cm^2, respectively. Employing the total area criteria for comparison shows a slight area advantage on the 2 x 2 cm cell; however, subsequent discussions will illustrate the advantages of type A cell at high

isolations that substantially outweigh this slight disadvantage.

Another problem tending to complicate the comparisons of these three types of cells is the fact that Type A cells were received with integral covers. These covers were of poor quality and showed significant areas of delamination and stress cracking. Figure 77 is a 60X photomicrograph showing a section of a Type A cell. This photo shows significant areas of delamination, as well as major cracking over the area of the contact.

To comply with the contract, ten cells were sent to Optical Coating Laboratory, Inc. for deposition of antireflection coatings on the front surface.

The integral covers appeared to remain intact and the cells did not show any detrimental effects as a result of the antireflective coating process. It was observed, however, that temperature cycling, specifically during the high intensity tests, caused the delaminated areas to increase, indicating very poor adhesion between the cover and the cell.

7.2 BASIC CELL COMPARISON

7.2.1 Spectral Response

The data presented in Section 6.4 (Figures 23 through 26) illustrate typical silicon solar cell spectral response curves. The spectral response for Type A cells, as reported in Reference 4, peaked at approximately 7000 Å while typical blue-shifted solar cells have a peak relative spectral response which occurs at approximately 8000 Å. The reasons for the 1000 Å shift were not ascertained, but it was believed to be caused by the stresses induced in the cells by the application of the integral quartz cover glass. Reference 4 also stated that the presence of such a stress was evidenced by the fact that the cells were slightly bowed after the cover glass application. This stress would tend to distort the silicon lattice, causing a decrease in minority carrier lifetime, with a con-

sequent decrease in the red response of the cells. The tremendous cracks observed on these cells and the fact that, when received, very little bowing was evidenced, seems to indicate that the above referenced stresses had been relaxed through the cracking and delamination. The measurement of the relative spectral response of these cells during this program indicated a peak at 8200 Å; and, the discrepancy in reported results is substantiated by the above discussion. Figure 78 illustrates the discrepancy between reported results of the respective relative spectral response measurements. The relative spectral response curves obtained for all three cell types compare favorably with typical silicon solar cells. It is concluded that internal stresses had caused the spectral shift reported for the Type A cells and that the cracking and delamination had sufficiently relaxed the internal stresses that the relative spectral response had again become that expected of a typical silicon solar cell.

7.2.2 Temperature Effects on Solar Cell Performance

The temperature coefficients for the three basic parameters (short circuit current, open circuit voltage, and maximum power) were obtained from the data reported in Section 6.9. This data was extrapolated to $0^{\circ}C$ and normalized to this value for comparison. Figure 79 presents the normalized open circuit voltage as a function of temperature and Figure 80 presents the normalized maximum power as a function of temperature. The data gave a short circuit temperature coefficient of +.05ma/$^{\circ}C$ for Type A cells, +.04ma/$^{\circ}C$ for Type B cells, and .05ma/$^{\circ}C$ for Type C cells. Figure 79 illustrates the corresponding percentage increase over the extrapolated zero degrees centigrate reference. All three cells had an open circuit voltage temperature coefficient of approximately -.002 volts $^{\circ}C$ as shown in Figure 80.

Figure 81 shows the percentage decrease in power as a function of temperature and the corresponding advantage of the Type A cells over the others. At $140^{\circ}C$ the Type C cell produced 11 milliwatts/cm^2 while the

Type A cell produced only 10 milliwatts/cm^2. Above this temperature the Type A cells show a definite advantage.

The projected advantage of the Type A cells at elevated temperatures is further evidenced by the consideration of the temperature coefficient of the short circuit current, and the open circuit voltage.

7.2.3 Angle of Incidence Effects on Solar Cell Performance

Figures 82, 83, and 84 present the normalized correlation of short circuit current, open circuit voltage, and maximum power as a function of angle of incidence from the one sun basic cell data. Figure 82 confirms the trends reported in Reference 2 that the short circuit current tends to fall very slightly below the curve for the cosine of the angle.

Attempts were made to evaluate the I-V characteristics of several cells at an angle of incidence of 90^o. Theoretically, the light should not strike the solar cell when the incident light is parallel to the cell; however, three factors should be considered; (1) reflected and stray light, (2) edge effects of the cover, and (3) edge effects of the cell. An elementary experimental evaluation of these effects showed that the majority of the generated power resulted from the second and third consideration rather than from the first. The stray light is minimized by painting the possible reflecting surfaces with a flat black paint and by performing the experiments in a dimly lit room which is also painted flat black.

The cover appears to contribute significantly to the edge effects since solar cells without coverslips showed less edge effects at the inclination angle of 90^o. Additionally, when the edge was blocked, the I-V curve at 90^o was essentially eliminated. While this output is only a small percentage of the output at normal incidence, studies of solar cell performance at very high angles of incidence must consider the optical and photovoltaic edge effects. Similar results were also obtained from angle

of incidence measurements using the carbon arc at elevated light intensities.

Power subsystem designers attempting to utilize oriented arrays at very high angles of inclination must consider the possibility of edge effects not only for power generation design but also for thermal control. This factor is extremely important at very high intensities (~ 25 suns).

The comparison of open circuit voltage normalized to $0^{o}C$ for all three cell types as a function of angle of incidence provided data so consistent that the differences were indistinguishable. Figure 83 illustrates the correlation of open circuit voltage vs. angle of incidence obtained from the basic cell data.

Figure 84 presents the normalized peak power vs. angle of incidence for the three types of bare solar cells. The deviations between these curves can be partly attributed to the experimental uncertainty associated with the determination of the maximum power point. It is observed, however, that the maximum power point on the one sun case can be closely approximated by the cosine curve substantiating the assumptions used in the thermal analysis presented in Appendix A. The one sun normal incidence power generated for Type A was approximately 8.5 mw/cm^2, Type B ~ 11 mw/cm^2, and Type C ~14 mw/cm^2. Considering the differences in absolute power, the correlation given in Figure 84 is very good.

7.2.4 Dark Diode Characteristics

The dark diode forward characteristics and the photovoltaic output (translated to $I_I = I + I_L$) are compared in Figures 85, 86, and 87. The associated effects are completely described in Reference 11. Adjunct to that presentation, review of the diode equation and the two techniques of measurements allows an alternate method for evaluation of the effects of series resistance. The difference between the diode forward characteristic and the photovoltaic output characteristic is primarily attributed to

the fact that the voltage drop across the lumped series resistance is in the opposite direction. Thus, the voltage difference, between the diode forward characteristic and the translated photovoltaic characteristic at a current corresponding to the open circuit voltage, can be related to the series resistance; the larger the difference the larger the series resistance.

It is observed, however, that the three methods of obtaining the I-V characteristics discussed in Reference 11 do give different results. Wolf and Rauschenbach concluded that whenever the performance of a solar cell as a photovoltaic energy converter is concerned, the use of the photovoltaic output characteristics is required. The problems associated with measuring accurately the series resistance preclude the use of the other methods.

The dark reverse diode characteristics of solar cells are primarily used for solar array shadow and failure analysis; however, they are very important for the output evaluation of solar arrays where boom shadows can possibly fall on the array. The dark reverse diode characteristics also allow a first order comparison to the illuminated reverse characteristics, the value of which will be presented in the discussion of these results. These rather large variations are typical of all solar cells and are to be expected from basic diode technology. The solar cell is a poor diode and the nature of the manufacture of the solar cells suggest rather large cell-to-cell variations.

7.2.5 Heat Transfer Surface Properties

The total hemispherical surface emissivity and solar absorptivity were determined from analysis and evaluation of the spectrophotometric measurements. The reflectance data were combined and compared to the transmittance measurements to provide a "best estimate" of the solar absorptivity as a function of wavelength for each sample. The reflectance data varied from sample to sample more than was expected. It was felt that the

coverslide transmittance modified for ultra violet absorption provided a much better approximation to the absorptance as a function of wavelength than did the Gier - Dunkel reflectivity measurements. The largest discrepancies in the Gier - Dunkel measurements were associated with the Type A cells. It appeared that the largest disagreements between samples had some connection with the stress cracks and delamination on the integral covers.

The absorptance data was combined with the solar spectrum to evaluate the solar absorptivity for each sample. The values of solar absorptivity used in the equilibrium temperature calculations are presented in Table 5.

The measurements of the total hemispherical surface emissivity were compared for each sample with the same type of covers. It was observed that cells having microsheet cover slides all seem to have a surface emissivity of 0.80. This value appears to be lower than expected; however, these measurements do have an experimental uncertainty of about 5 to 10%. The data is very consistent and hence the values reported in Table 5 were employed in the equilibrium temperature tests.

7.3 HIGH INTENSITY ANALYSIS

7.3.1 Solar Simulator Evaluation

Prior to performance of the high intensity tests, a detailed calibration of the carbon arc simulator was performed. The first part of this calibration was to compare solar cell output resulting from exposure to the carbon arc to the results from the OCLI experimental program. The intensity at the test plane was carefully adjusted so that the resulting short circuit current from the Heliotek Standard Cell was equivalent to the air mass zero calibration.

Selected samples were tested at 28°C and the one sun intensity. The solar cell performances agreed, within the experimental uncertainty, with

the data obtained from the OCLI solar simulator. Correlation of the one sun data for each of the ten categories agreed very closely to the normalized curves reported in Section 7.2 of this report. A detailed comparison of the two solar simulators used in this program is presented in Appendix C. Included in this appendix are typical I-V curves which illustrate the correlation of the data obtained from the two simulators. The analysis and comparison of these two simulators indicated that while the carbon arc is not the best solar simulator it is an acceptable test vehicle for evaluating solar cell performance at high insolations.

7.3.2 Theoretical Predictions of Equilibrium Temperatures

Following the comparison of the two light sources at one sun intensity, a theoretical analysis was conducted to determine the approximate equilibrium temperatures for a solar cell bonded to, but thermally insulated from, the spacecraft. The analysis presented in Appendix A was used to calculate the temperatures for each of the ten samples at one, three and six suns for the following boundary conditions: (1) nonrotating, no power generated, (2) rotating, no power generated, and (3) rotating at maximum power. Table 6 shows the relative effect of considering the temperature reduction caused by these various parameters. The temperatures calculated for the cells rotating at maximum power conditions became the test objectives for the respective insolation levels. As reported in Section 6.11 physical limitations prohibited the attainment of the temperature extremes. The actual test temperatures (listed in Table 5 and on the I-V curves) provided test temperatures within the range of interest. The actual cell temperatures did not differ significantly from the theoretical requirements. Hence, the data obtained from this experimental program are sufficient to indicate the combined effects of intensity, temperature, and angle of incidence upon solar cell performance.

7.3.3 High Intensity Tests

A preliminary mapping of total intensity versus distance from the carbon arc was performed to establish location of the test facility. The test apparatus was then positioned at specific distances from the simulator for each test. The intent was to provide test intensities of approximately one, three, and six solar constants. Evaluation of the light intensities at each of the three selected test planes showed the intensities to be 1.0, 2.98, and 7.6 solar constants. These values were obtained by several means; but the two best results were obtained using the light generated current and the average of the short circuit currents of the standard cell through the seventeen interference filters. The correlation of total intensity versus distance is included with the comparison of the OCLI and Strong Carbon Arc simulators found in Appendix B.

Figures 88 through 97 present a comparison of the normal incidence I-V curves for each of the ten categories at the test temperatures for the three test intensities (1, 3, 7.6 suns). A comparison of the curve shapes indicates the substantial improvement in power per unit area at high solar intensities with silicon solar cells designed for low series resistance. The analysis of these curves substantiates the low series resistance reported for the Type A cells. These data also show the limitations associated with the use of standard production cells having higher internal series resistances. In spite of the substandard integral cover slides on the Type A cells, their power output per unit area proved to be greatly superior at the 7.6 sun intensity.

The data reported for these tests were predicted very closely from the one sun test. It must be observed, however, that both temperature and intensity variations must be accounted for. If both are evaluated, proper adjustment of the axes provides very good agreement with actual test data. It must be remembered that the light generated current and not the short circuit current is a multiple of intensity (modified by temperature effects) and that the light generated current generally occurs at a negative bias. It is only fortuitous that the light generated current is equal to the short circuit current at the lower insolation levels.

Examination of the short circuit current as a function of intensity and temperature illustrates that as long as the translation does not approach the knee of the curve, the results are fair; however, the short circuit current can be lower at six suns than at three suns if the series resistance is large (very rounded knee). Additionally, invoking the cosine relationship between intensity and angle of incidence, it is observed that the data for equal incident intensities agree within 3 percent. Continued checking of this relationship established great confidence in the data reported.

The measurement of short circuit current is the most severe problem associated with the experimental determination of solar cell performance at high solar intensities. It is observed from the data for high temperatures and high intensities that the solar cell is capable of generating suprisingly large currents at rather low voltages. Detailed analysis of the electrical relationships show that the current measuring devices must have internal resistance less than .01 Ω to meet the requirements of this program. For example, currents of .75 amps (I_{sc} from Figure 107) produces a voltage drop of .0075 volts across a .01 Ω which might cause approximately a 2 percent error in the short circuit current. It is

observed that when shunts of this resistance are employed, care must be given to the connections, lead temperature, and resistance measurement. The care exercised in this program is illustrated in Figure 4, by observing the double battery grounding straps used for solar cell connecting ends. In addition, the electrical contacts were periodically checked by soldering the lead wires directly to the cells. Because of the techniques utilized, the data reported are expected to be as accurate as indicated in the error analysis presented in Appendix B. The problems also indicate additional justification for determining the negative bias portion of each I-V curve.

7.4 ONE SUN PERFORMANCE RE-EVALUATION

Following the exposure to the high intensity tests, all physically intact cells used in this program were re-evaluated to determine possible performance degradation. These tests consisted of obtaining one sun performance curves and comparing them to the first performance curve obtained for each specific sample. The results of these performance evaluations illustrated that no cell degradation had occurred because of the exposure to the high intensities.

It was concluded that the only degradation occurred as a result of the melting of the solder on the solder dipped cells which made it difficult to insure electrical contact in the test fixture. However, when care was taken to insure cell contact, no degradation in performance was observed.

SECTION 8

CONCLUDING REMARKS

8.1 GENERAL

The results of this experimental program again definitely illustrated the adverse effects of high series resistance on solar cell performance at high temperatures and high insolations. This was shown by the improvement in relative performance of the solar cells specifically designed for this type of application. In the temperature range considered, low base resistivity is directly relatable to low series resistance; however, the susceptibility to radiation damage is also increased with lower base resistivity. Thus, without considering radiation damage effects, it is concluded that the series resistance should be minimized through careful cell design.

Examination and evaluation of the data obtained from this program illustrates that the solar cell performance at up to seven suns can be estimated from the basic diode equation. Initial evaluation of the lumped parameter model tends to support its use throughout the range of temperatures and intensities considered herein. With high temperatures and insolations, short circuit current is no longer equivalent to light generated current. At these conditions it is more informative to measure light generated current as well as short circuit current to provide definitive cell characteristic data. Programs requiring the measurement of solar cell performance at high intensities should include the measurement of light generated current for reference.

Temperature effects on performance were comparable for all cells tested (short circuit current ≈ 0.05 ma/^{o}C and open circuit ≈ -0.002 volts/^{o}C). These coefficients are typical of silicon solar cell technology. The advantage of the Type A cells is attributed to the sharper knee which provides higher maximum power output at high temperatures and intensities. The

sharpness of the knee is inversely proportional to internal series resistance and for that reason supports the above conclusions.

The angle of incidence studies illustrated that performance at high angles of incidence can be predicted from basic considerations of incidence solar intensity up to an incidence angle of approximately 75°. At angles of incidence greater than 75° edge effects may become increasingly important. These effects could cause sizeable uncertainties in predicting solar array performance where very high angles of incidence are employed, if the edges of the cell are exposed.

The measurement of relative spectral response provided data for all three types of cells which was characteristic of silicon solar cells. These data were in direct disagreement with the measurements made by the manufacturer of the experimental type A cell. The manufacturer's conclusions were verified that internal stresses had caused the spectral shift reported for those cells. Cracking and delamination had sufficiently relaxed the internal stresses yielding relative spectral response curves consistent with those expected for typical silicon solar cells.

It was also observed that the Type A cells used in this program were an experimental production lot and illustrated much more spread in the data than was obtained for the Type B and Type C cells. This fact must be considered when reviewing the data presented herein.

Calculated equilibrium temperatures exceeded $180^{\circ}C$ for a few test categories. It is thus concluded that solderless contacts should be considered for future high intensity tests.

The performance re-evaluation tests showed that solar cells can be exposed to high temperature ($\sim 170^{\circ}C$) and high insolations (~ 7 suns) for a short time without apparent degradation in overall performance. This fact validates the reported data,and final degradation results can only be obtained after much longer exposures than were encountered in this experimental program.

The results of this program illustrate the advantage of employing solar cells of specific design for near sun missions. The maximum power output can definitely be optimized for missions where high insolations are encountered.

Finally, the difficulty in accurately measuring short circuit current illustrates the problems to be encountered in rotating equilibrium experiments, it is recommended that for such experiments, groups of cells be tested in submodule configurations rather than as single cells.

8.2 RECOMMENDATIONS

The conclusions obtained from this program provide specific recommendations concerning future investigations of solar cell performance applicable to near sun missions.

Study of short circuit current indicates the need for additional testing at intensities ranging from 6 to 25 suns to extend the investigation of solar cell performance parameters. It is also suggested that extensive computerized parametric studies be made of the high intensity data, examining the parameters of the diode equation to provide basic insight into solar cell performance at these extreme conditions.

As a result of the calculated equilibrium temperatures for spinning solar cells it is also recommended that solderless attachment techniques such as thermal compression bonding be examined.

SECTION 9

LIST OF REFERENCES

1. Cobb, M. W.; Cummings, W. S.; and Fairbanks, J. W.; "The Feasibility of a Programmed Heat Shield for Solar Cell Performance Control", Philco WDL-TR-2623, October 15, 1965.

2. Briggs, D. C., "Experimental Study of Coatings for Temperature Control of Solar Cells", Philco WDL-TR-2949, June 6, 1966.

3. Foster, J. V.; Wilbur, A. C.; Briggs, D. C.; and Friedlander, S.; "Silicon Solar Cells for Near Sun Missions", Sixth Photovoltaic Specialists Conference, Cocoa Beach, Florida, March 28-30, 1967.

4. Friedlander, S.; and Rolik, G. P.; "Silicon Solar Cells for Near Sun Missions", Electro-Optical Systems, Inc., Final Report on Contract NAS 2-3613.

5. Chapin, D. M., et. al., J. Appl. Phys. 25, 676 (1954).

6. Pfann, W.; and van Roosbroeck, W.; J. Appl. Phys. 25, 1422 (1954).

7. Prince, M. B., "Silicon Solar Energy Converters", J. Applied Phys. 26, 534 (1955).

8. Rappaport, P., RCA Rev., 20, September 1959.

9. Evans, W.; and Menetry, W. R.; Energy Conversion Systems Reference Handbook, Vol. 5, "Direct Solar Conversion", WADD Technical Report 60-699, September 1960.

10. Wysocki, J. J., "The Effect of Series Resistance on Photovoltaic Solar Energy Conversion", RCA Review, March 1961.

11. Wolf, M.; and Rauschenback, H.; "Series Resistance Effects on Solar Cell Measurements", Advanced Energy Conversion 3, 455-479, Pergamon Press, 1963.

12. Berman, P. A., "High Efficiency Silicon Solar Cells", Final Report on Contract DA-36-0-39-SC-90777, Heliotek Corporation, July 1964.

13. Runyon, W. R., Silicon Semiconductor Technology, McGraw-Hill Book Company, 1965.

14. Picciano, W. T., Private Communication.

15. Berman, P.; and Ralph, E. L.; "Improved Solar Cells for Use in Concentrated Sunlight", 18th Annual Power Sources Conference, Atlantic City, New Jersey, 19-21 May 1964.

16. Wysocki, J. J.; Toferski, J. J.; and Rappaport, P.; "Research on Photovoltaic Converters, Procedures of the 14th Annual Power Sources Conference, V. S. Army Signal Res. and Dev. Lab, Ft. Monmouth, New Jersey, 1960.

17. Shockley, W., Electrons and Holes in Semiconductors. Van Nostrand, New York, 1950.

18. Watson, R. H., "Equivalent Circuit Characteristics of the Solar Cell", Presented at the 1960 Pacific General Meeting of the AIEE at San Diego, California, August 11, 1960.

19. Wolf, M.; and Rauschenbach, H.; "Series Resistance Effects on Solar Cell Measurements", 1961 Pacific General Meeting of the AIEE, Salt Lake City, Utah, August 23-25, 1961.

20. Johnson, F. S., Satellite Environment Handbook, Stanford University Press, 1961.

21. Hamilton, R. C., "AIEE Photovoltaic Solar Simulator Specifications", Proceedings of the Solar Working Group Conference, NASA Auditorium, Washington, D. C., February 1962.

22. Thekalkara, M. P.; "The Solar Constant and the Spectral Distribution of Solar Radiant Flux". Solar Energy, Vol. 9, No. 1, 1965.

23. Stair, R.; Schneider, W. E.; et al: "Some Developments in Improved Methods for the Measurement of the Spectral Irradiances of Solar Simulators," NASA CR-201, April 1965.

24. Gibson, D. W.; and Winard, J.: "Studies of the Spectral Energy Distribution of Different Light Sources in Connection with Solar Simulation." Proceedings of the Institute of Environmental Sciences, 1962.

25. Gummel, H. K.; and Smits, F. M.; "Evaluation of Solar Cells by Means of Spectral Analysis," The Bell System Technical Journal, May 1964.

26. Morrison, G.: "Calibration of TI Primary Intensity Standards (Solar Cells)," Texas Instruments, Inc. SC 1584, Oct. 15, 1967.

27. Broder, J. D.; Kantz, H.; Mandelkorn, J.; Schwartz, L.; and Ulman, R.: "Solar Cell Performance at High Temperatures." Paper Presented at Fourth Photovoltaic Specialists Conference at Lewis Research Center, Cleveland, Ohio, Aug. 1964.

28. Thelen, A.: "The Use of Vacuum Deposited Coatings to Improve the Conversion Efficiency of Silicon Solar Cells in Space," Progress in Astronautics and Rocketry, Vol. 3, Academic Press, New York, New York, 1962.

29. Thelen, A.: "Multilayer Filters with Wide Transmittance Bands," Journal of the Optical Society of America, Vol. 53, No. 11, 1963.

30. Ralph, E. L.; and Wolf, M.: "Effects of Antireflection Coatings and Coverglass on Silicon Solar Cell Performance," Presented at the Photovoltaic Specialists Conference, Cleveland, Ohio, Aug. 1964.

31. Sears, F. W.: "Optics," Addison Wesley Press, Inc., 1949.

32. McAdams, W. H.: "Heat Transmission," Third Edition, McGraw-Hill Book Company, Inc., 1954.

33. Walsh, J. W. T.: "Photometry," Constable and Company, Ltd., Second Edition, 1953.

34. Sandstrom, J. D.; and Castle, E. F.: "Solar Simulation," JPL - Test Engineering, August 1967.

35. General Specification Guide for Solar Cell Covers; Optical Coating Laboratory, Inc., January 1, 1966.

36. Kline, S.J. and McClintock, F.A.,"The Description of Uncertainties in Single Sample Experiments," Mechanics Engineering, January 1953.

TABLE 1

LIST OF TEST EQUIPMENT

1. Optical Coating Laboratory, Incorporated, Solar Simulator Model 30, Serial 5.

2. NJE Power Supply, 10-80 V.D.C., 0-30 Amp., Model TRM 80-30.

3. United Systems Corporation, Digital D.C. Voltmeter Model 201R10K, Serial 10225C, Calibrated 1-23-67.

4. United Systems Corporation, Digital D.C. Voltmeter Model 201R10K, Serial 10226C, Calibrated 1-23-67.

5. Spectrolab, Electronic Load Model D-550, Serial 5936.

6. Moseley, X-Y Recorder Model 7000A, Serial 624-00824, Calibrated 2-23-67.

7. Moseley, X-Y Recorder Model 7000A, Serial T15-01047, Calibrated 8-23-67.

8. Leeds & Northrup, Thermocouple Switch, 4 each Model 8248-16.

9. Kepco, Regulated D. C. Power Supply, 0-12 V, 0-100 A, Model KO 12-100M, Serial C-64 147

10. Kepco, Regulated D.C. Power Supply, 0-70 V, 0-20 A, Model KO-70-20M, Serial C-37593, Calibrated 11-22-66

11. Kepco, Regulated D.C. Power Supply, 0-7.5 V, 0-2 A, Model ABC 7.5-2M, Serial E-27412, Calibrated 3-6-67.

TABLE 1 (Continued)

12. Kepco, Regulated D.C. Power Supply, 0-75 V, 0-8 A, Model SM-75-8M, Serial C-29959, Calibrated 1-11-67.

13. Superior Electric Company, Stabiline Voltage Regulator Model EMK 4105R, Serial 74, Calibrated 11-1-66.

14. Leeds & Northrup, Temperature Potentiometer Model 8693, Serial 1721955, Calibrated 6-28-67.

15. Leeds & Northrup, Temperature Potentiometer Model 8693, Serial 1688711, Calibrated 10-4-67.

16. Leeds & Northrup, Temperature Potentiometer Model 8693, Serial 1721963, Calibrated 6-28-67.

17. Weston, Laboratory Standard D.C. Milliampmeter Model 931, Serial 7142, Calibrated 4-11-67.

18. Weston, Laboratory Standard D.C. Milliampmeter Model 931, Serial 70684, Calibrated 4-11-67.

19. Weston, Laboratory Standard D.C. Milliampmeter Model 931, Serial 74865, Calibrated 6-28-67.

20. Weston, Laboratory Standard D.C. Milliampmeter Model 931, Serial 74864, Calibrated 10-16-67.

21. Weston, Laboratory Standard D.C. Milliampmeter Model 931, Serial 65245, Calibrated 3-17-67.

22. Weston, Laboratory Standard D.C. Voltmeter Model 622, Serial 32460, Calibrated 7-26-67.

TABLE 1 (Continued)

23. Rustrak Instrument Company, Strip Chart Recorder Model 88, Serial 16529

24. Rustrak Instrument Company, Strip Chart Recorder Model 88, Serial 16528

25. John Fluke Mfg. Company, A.C./D.C. Differential Voltmeter Model 883 A, Serial 1319, Calibrated 6-27-67.

26. Electro Scientific Industries, Potentiometer Voltmeter-Bridge, Model 300 PVB, Serial 736029, Calibrated 8-31-67.

27. General Radio, 1 Ohm Shunt $\pm$ 0.1%, Model 500A

28. Strong Electric Company, Arcomatic Automatic Reflection Arc Lamp, Model 75000-2, Serial 54943

29. Strong Electric Company, Heat Exchanger Model 23518-8, Serial 23153.

30. Hertner Electric Company, Transverter Projection Arc Rheostat, Model HD-X-203

31. Transverter, Motor-Generator Unit, 90 V, 165 A, Model HK-165/330, Serial 3403-306.

32. Helipot, Precision Potentiometer Laboratory Model T-10-A, Serial S-1.

33. Duo-Seal, Vacuum Pump Model 1400, Serial 89871

34. Duo-Seal, Vacuum Pump Model 1400, Serial 34436-0

35. Nikkormat, Automatic Slide Projector (Modified) Model GC-1, Serial 13049.

TABLE 1 (Continued)

36. OT1, Narrow Band-Pass Interference Filters (17 Each), 40-1200 Milli Micrms

37. Heliotek Standard Solar Cell, Serial 170

38. Heliotek Standard Solar Cell, Serial 1090

39. The Epply Laboratories, Inc. 180 Degree Pyrheliometer (Calibration 8-65 millivolts/cal cm^{-2} min^{-1}) Model 50, Serial 4311.

40. The Epply Laboratory, Inc., Thermopile.

41. Variac, Autotransformer Model W5MT3

42. Perkin-Elmer, Spectrophotometer Model 350

43. Gier Dunkle Instrument, Source Transfer Optical System Model STOS-4, Serial 116.

44. Lion Research Corporation, Emissometer Model 25-6.

TABLE 2

BARE SOLAR CELL DATA SUMMARY

CELL TEMPERATURE = $28^0 \pm 1^0C$

SOLAR INTENSITY = $140 mW/cm^2$

CELL NO.	I_{sc}	V_{oc}	R_s	I_{mp}	V_{mp}	P_{mp}	CF
	MA	VOLTS	Ω	MA	VOLTS	MW	
A-1	41.2	0.570	1.1	37.0	0.480	17.8	0.756
A-2	39.0	0.568	1.3	35.0	0.482	16.9	0.762
A-3	35.5	0.554	0.9	32.0	0.455	14.6	0.740
A-4	39.0	0.566	0.4	34.1	0.470	16.0	0.726
A-5	38.0	0.563	0.6	34.3	0.469	16.1	0.752
A-6	38.0	0.562	0.6	34.2	0.469	16.0	0.751
A-7	39.9	0.570	1.1	36.6	0.476	17.4	0.766
A-8	34.5	0.554	1.5	31.1	0.456	14.2	0.792
A-9	45.0	0.568	1.4	40.6	0.475	19.3	0.755
A-10	39.0	0.567	1.0	35.6	0.475		
A-11	45.1	0.572	2.3	42.0	0.473	19.9	0.770
A-12	41.0	0.564	0.6	37.0	0.468	17.3	0.749
A-13	39.5	0.567	0.5	35.2	0.470	16.5	0.739
A-14	45.0	0.573	0.2	41.0	0.480	19.7	0.763
A-15	45.0	0.573	5.4	35.5	0.475		
A-16	40.0	0.569	0.3	35.5	0.475	16.9	0.741
A-17	42.2	0.574	3.4	38.3	0.475	18.2	0.751
A-18	37.0	0.563	0.2	34.0	0.470	16.0	0.767
A-19	43.8	0.574	0.3	40.1	0.480	19.2	0.766
A-20	44.9	0.572	0.6	40.7	0.477	19.4	0.756
A-21	43.0	0.566	0.2	39.0	0.460	17.9	0.737
A-22	40.0	0.569	0.3	36.2	0.470	17.0	0.748
A-23	34.5	0.562	<0.1	31.5	0.460	14.5	0.747
A-24	39.3	0.565	0.2	36.0	0.470	16.9	0.762
A-25	39.0	0.568	1.2	36.0	0.475	17.1	0.772
A-26	36.0	0.555	0.4	32.5	0.450	14.6	0.732
A-27	39.5	0.561	0.5	35.5	0.460	16.3	0.737
A-28	40.6	0.560	0.6	36.9	0.465	17.2	0.755
A-29	44.5	0.571	0.3	40.5	0.475	19.2	0.757
A-30	39.0	0.571	0.3	36.0	0.475	17.1	0.768
A-31	37.3	0.570	0.4	33.7	0.475	16.0	0.753
A-32	32.4	0.555	<0.1	28.7	0.450	12.9	0.719
A-33	47.3	0.576	0.3	43.3	0.480	20.8	0.763
A-34	36.8	0.557	0.7	38.4	0.455	17.5	0.852
A-35	37.3	0.562	0.4	33.5	0.465	15.6	0.743
A-36	41.9	0.573	0.4	37.2	0.480	17.9	0.744
A-37	37.0	0.571	0.4	38.8	0.480	18.6	0.882
A-38	34.3	0.559	0.5	30.6	0.460	14.1	0.734
A-39	39.5	0.566	1.3	35.5	0.470	16.7	0.746
A-40	40.9	0.567	0.8	37.3	0.475	17.1	0.764
B-1	68.0	0.525	0.8	57.0	0.410	23.4	0.655
B-2	71.8	0.533	1.5	58.5	0.400	23.4	0.612
B-3	70.0	0.535	0.9	57.9	0.415	24.0	0.642
B-4	68.4	0.531	1.2	56.2	0.410	23.0	0.634
B-5	68.5	0.534	1.2	58.0	0.415	24.1	0.658
B-6	70.1	0.533	0.4	57.8	0.410	24.0	0.634
B-7	68.5	0.533	0.8	56.0	0.415	23.2	0.637
B-8	71.9	0.529	1.0	58.0	0.405	23.5	0.618
B-9	68.5	0.534	0.5	56.0	0.410	23.0	0.628
B-10	70.8	0.523	1.1	57.0	0.395	22.5	0.608
C-1	150.0	0.557	0.4	135.5	0.430	58.3	0.697
C-2	148.1	0.555	0.6	134.5	0.430	57.8	0.704
C-3	149.2	0.557	0.6	135.0	0.430	58.1	0.699
C-4	148.1	0.552	0.6	134.5	0.430	57.8	0.707
C-5	147.1	0.548	0.4	135.5	0.425	57.6	0.714
C-6	148.5	0.558	0.5	134.0	0.435	58.3	0.704
C-7	148.4	0.558	0.5	134.0	0.437	58.6	0.707
C-8	148.3	0.550	0.5	135.5	0.430	58.3	0.714
C-9	146.7	0.553	0.6	134.0	0.435	58.3	0.719
C-10	148.0	0.549	0.5	134.5	0.435	58.5	0.720
C-11	148.8	0.553	0.5	135.0	0.435	58.7	0.718
C-12	149.5	0.555	0.6	134.5	0.430	57.8	0.697
C-13	146.8	0.554	0.6	133.0	0.440	58.5	0.720
C-14	148.0	0.555	0.6	133.5	0.430	57.4	0.699
C-15	147.5	0.554	0.6	134.0	0.435	58.3	0.713

TABLE 3

TOTAL SURFACE HEMISPHERICAL EMISSIVITY

OF SOLAR CELL ASSEMBLIES

	CELL TYPE	METER READING	EMISSIVITY
1A	As Received	.84 - .855	.705 - .725
2A	6 Mil Cover A/R Coating	.92 - .93	.805 - .825
3A	Blue/Red Filter	.87 - .89	.74 - .765
4A	OCLI A/R Coating	.815 - .825	.685 - .69
1B	As Received	.755 - .76	.628 - .63
2B	6 Mil Cover A/R Coating	.91 - .92	.79 - .805
3B	Blue/Red Filter	.89 - .92	.76 - .805
1C	As Received	.515 - .525	.425 - .43
2C	6 Mil Cover A/R Coating	.91 - .92	.79 - .805
3C	Blue/Red Filter	.89 - .91	.74 - .79

TABLE 4

SOLAR CELL ASSEMBLY, RELUCTANCE VS. WAVELENGTH

WAVELENGTH MICRONS	MEASURED REFLECTANCE BY CELL TYPE									
	1A	2A	3A	4A	1B	2B	3B	1C	2C	3C
.296	25.0	4.0	5.0	25.0	36.5	4.0	4.0	12.5	4.0	4.0
.330	27.5	20.0	55.0	29.5	32.0	18.5	57.5	22.0	17.0	57.0
.335	31.0	23.0	81.0	33.5	32.0	22.0	85.5	31.5	24.0	86.0
.377	29.0	21.8	78.0	35.0	30.0	21.5	96.5	31.5	26.0	96.0
.400	27.5	21.0	70.0	36.0	24.5	19.0	87.0	27.0	24.0	89.0
.415	26.5	20.5	25.5	36.0	21.5	18.0	31.0	23.5	21.0	40.0
.430	25.5	21.5	21.5	34.5	19.0	17.5	18.5	21.5	19.5	21.0
.444	24.5	20.5	22.5	35.0	17.6	16.5	18.0	19.5	17.0	16.5
.457	24.5	20.0	21.0	33.0	16.5	16.0	14.5	17.5	15.5	14.5
.470	23.0	18.0	19.5	33.0	16.0	15.0	14.0	15.0	14.0	13.0
.483	22.5	20.5	22.0	31.5	15.0	15.0	15.0	13.0	13.0	13.0
.497	22.5	18.5	20.5	30.5	14.0	14.5	14.0	11.5	12.0	12.0
.511	22.0	18.0	19.0	30.5	13.0	14.5	13.5	10.5	11.5	13.0
.526	22.0	19.5	18.5	30.5	12.5	14.5	13.5	8.5	10.0	11.5
.540	21.5	16.5	18.5	30.0	12.0	14.0	13.0	7.5	9.5	10.5
.554	22.0	18.5	18.0	28.5	11.5	13.5	13.0	7.0	8.5	10.5
.569	21.0	19.0	18.0	30.0	11.0	13.0	11.5	6.5	9.0	10.0
.584	22.0	17.0	18.0	28.5	11.0	13.0	13.0	5.5	8.0	10.5
.599	21.0	19.0	19.0	28.0	10.5	12.5	11.0	5.0	8.0	10.5
.615	21.5	18.5	21.0	27.5	10.5	12.0	12.5	5.0	8.0	11.5
.630	22.5	17.0	18.0	27.5	10.5	12.0	11.0	5.0	8.0	11.0
.648	21.0	15.0	18.5	27.0	10.0	12.0	11.5	5.0	9.0	11.0
.664	21.5	16.5	20.5	26.0	10.5	11.5	13.0	5.0	9.0	12.5
.683	21.5	15.5	22.5	26.5	10.5	12.0	17.5	5.5	9.5	16.0
.703	21.0	15.5	20.0	28.5	11.0	12.5	16.5	6.5	9.0	17.0
.722	22.0	16.0	20.0	28.5	11.0	12.0	14.0	65.0	9.5	15.0
.743	22.0	16.0	20.0	29.0	11.0	11.5	12.0	7.5	9.5	13.0
.766	22.0	16.0	18.5	30.5	11.5	12.0	12.0	7.5	10.0	12.5
.789	22.0	16.5	20.0	30.5	12.0	12.0	13.0	8.5	10.5	13.0
.815	21.5	14.5	17.5	29.5	12.0	11.0	11.0	8.5	11.0	13.5
.842	21.5	15.5	17.0	30.0	12.0	11.0	11.0	9.0	11.5	14.0
.870	21.5	16.5	19.0	30.5	12.5	11.0	12.0	10.0	12.0	15.0
.899	21.0	14.5	19.0	31.0	12.5	11.0	12.0	10.5	12.5	16.0
.932	21.0	16.0	20.0	30.0	13.0	11.5	13.0	11.5	13.0	17.0
.967	21.0	16.5	21.5	32.0	14.0	11.5	15.0	12.5	14.0	19.0
1.002	22.0	17.0	23.0	35.0	15.0	12.0	14.5	15.5	17.0	22.0
1.043	24.0	19.5	25.5	38.0	15.0	12.0	15.0	18.5	19.5	24.0
1.085	25.0	22.0	28.0	40.0	15.5	12.5	18.0	23.0	23.5	30.5
1.133	26.5	22.5	35.0	40.0	16.0	12.0	20.0	24.0	25.5	32.5
1.185	26.0	23.5	69.5	42.5	16.5	13.0	72.0	26.0	27.0	68.0
1.240	27.5	25.0	80.0	43.0	16.5	13.0	94.0	27.5	27.5	91.5
1.302	27.5	26.5	82.0	44.0	17.5	12.5	97.0	28.5	28.0	96.5
1.380	28.5	27.0	83.5	44.5	18.5	13.0	97.0	31.0	29.0	97.0
1.470	31.5	26.5	80.0	44.0	18.5	13.5	13.5	92.5	29.5	93.0
1.580	30.5	28.5	38.0	43.0	18.5	14.0	42.5	32.5	30.0	56.0
1.713	29.0	26.5	41.0	43.5	19.5	14.0	94.5	33.5	31.0	43.0
1.895	33.0	26.5	29.0	43.5	20.0	14.0	16.0	37.0	33.5	35.5
2.160	29.5	25.0	32.5	42.0	20.0	14.5	24.5	38.5	33.5	40.0
2.610	26.5	16.5	25.0	35.0	18.5	13.0	19.5	32.0	30.5	36.0

TABLE 5

CALIBRATE MAXIMUM EQUILIBRIUM TEMPERATURES & CORRESPONDING TEST TEMPERATURES

CELL TYPE		α	ϵ	T_1	$T^*_{1_A}$	T_3	$T^*_{3_A}$	T_6	$T^*_{6_A}$
1A	As received	.65	.70	12	16	106	106	182	182
2A	6 Mil Cover A/R Coating	.82	.80	20	20	117	117	194	194
3A	Blue/Red Filter	.60	.80	-4	16	85	85	157	157
4A	OCLI A/R Coating	.65	.70	12	16	107	107	183	183
1B	As received	.80	.63	35	35	139	134	221	180
2B	6 Mil Cover A/R Coating	.82	.80	18	18	116	116	194	180
3B	Blue/Red Filter	.60	.80	-8	16	82	86	156	156
1C	As received	.80	.43	65	65	182	180	221	180
2C	6 Mil Cover A/R Coating	.82	.80	16	16	114	114	194	180
3C	Blue/Red Filter	.60	.80	-10	16	79	79	154	154

T_1 = One Sun Temperature (^oC)

T_3 = Three Sun Temperature (^oC)

T_6 = Six Sun Temperature (^oC)

α = Determined from data

ϵ = Determined from data in Table 3

* = Actual Test Temperature

TABLE 6

COMPARISON OF CALCULATED EQUILIBRIUM TEMPERATURES

(TEMPERATURES IN ^{o}C)

TYPE CELL	T_{01}	T_{03}	T_{06}	T_{R01}	T_{R03}	T_{R06}	TEST REQUIREMENTS		
							T_{RMP1}	T_{RMP3}	T_{RMP6}
1A	115	238	336	19	111	184	12	106	182
2A	126	251	351	26	121	195	20	117	194
3A	95	211	305	04	91	160	-4	85	157
4A	116	238	336	19	111	184	12	107	183
1B	147	280	385	43	143	221	35	139	221
2B	126	251	351	26	121	195	18	116	194
3B	95	211	305	04	91	160	-8	82	156
1C	189	336	451	74	185	271	65	182	221
2C	126	251	351	26	121	195	16	114	194
3C	95	211	305	04	91	160	-10	79	154

Subscripts

0 - No Power - Non-rotating

RMP - Maximum Power - Rotating

RO - No Power - Non-rotating

1,3,6 - Corresponding to solar intensities

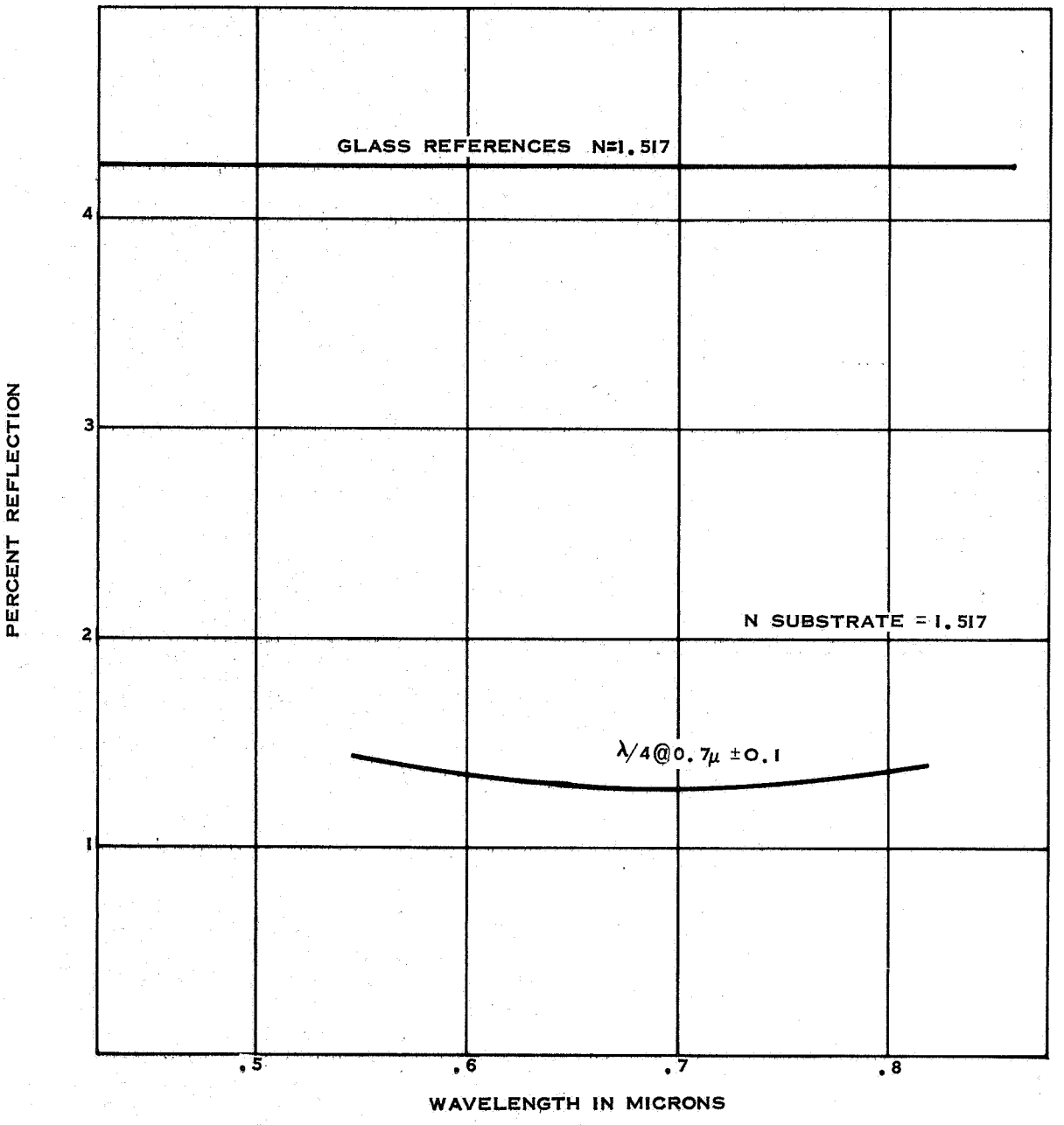

Figure 1 Characteristics of Anti-reflection Coatings

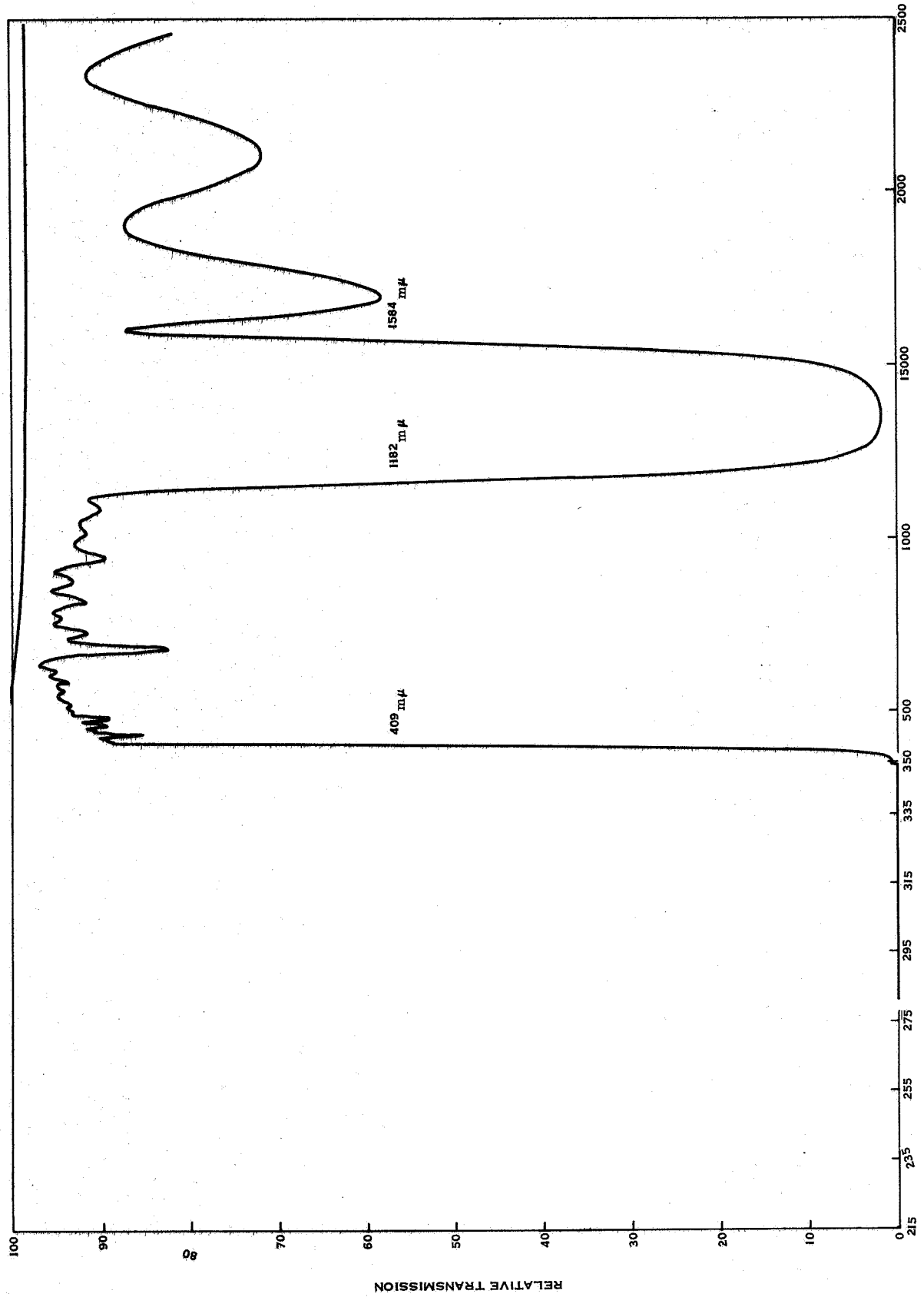

Figure 2 Transmission of Blue-Red Filters

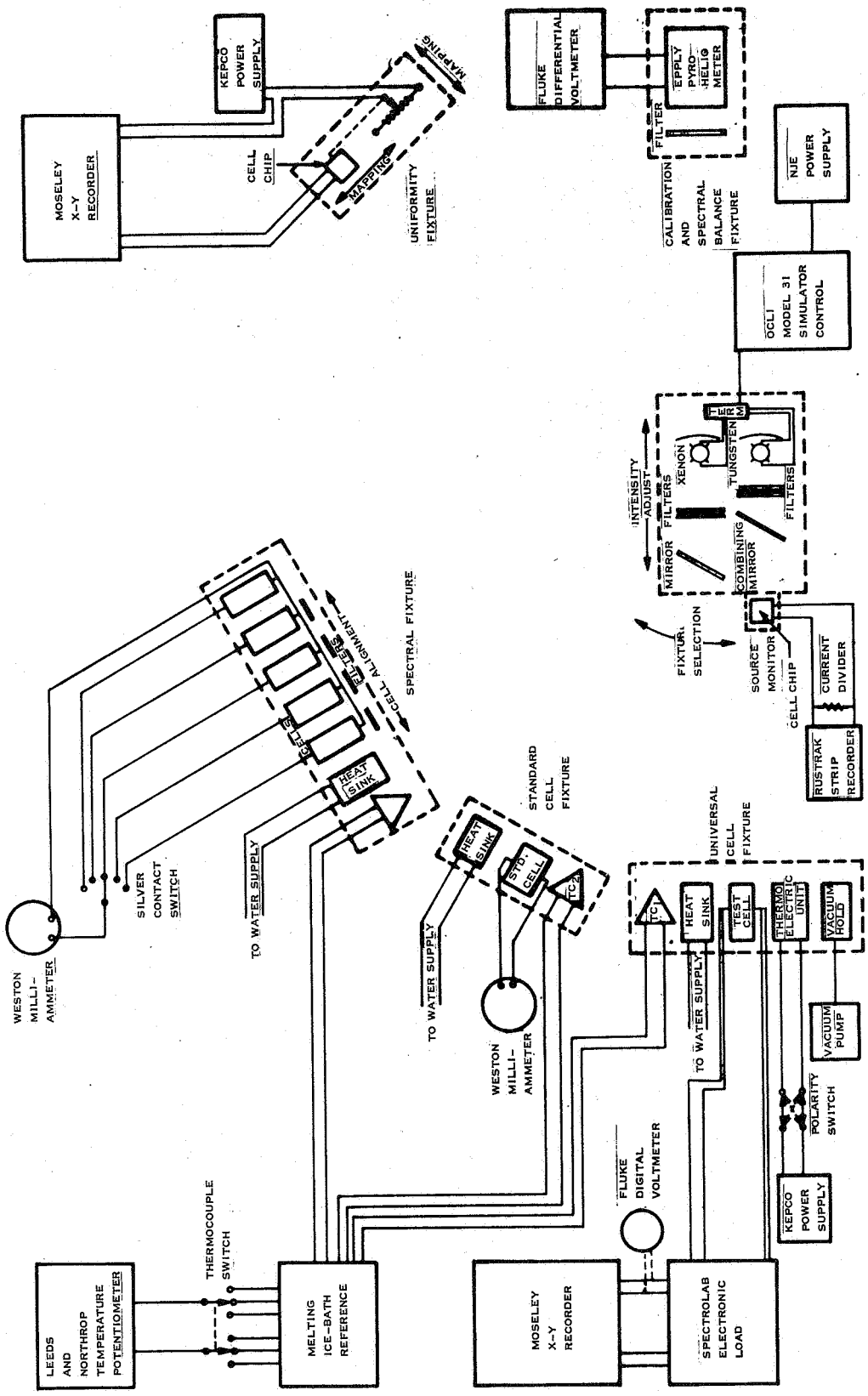

Figure 3 Block Diagram of OCLI Solar Simulator Test Facility

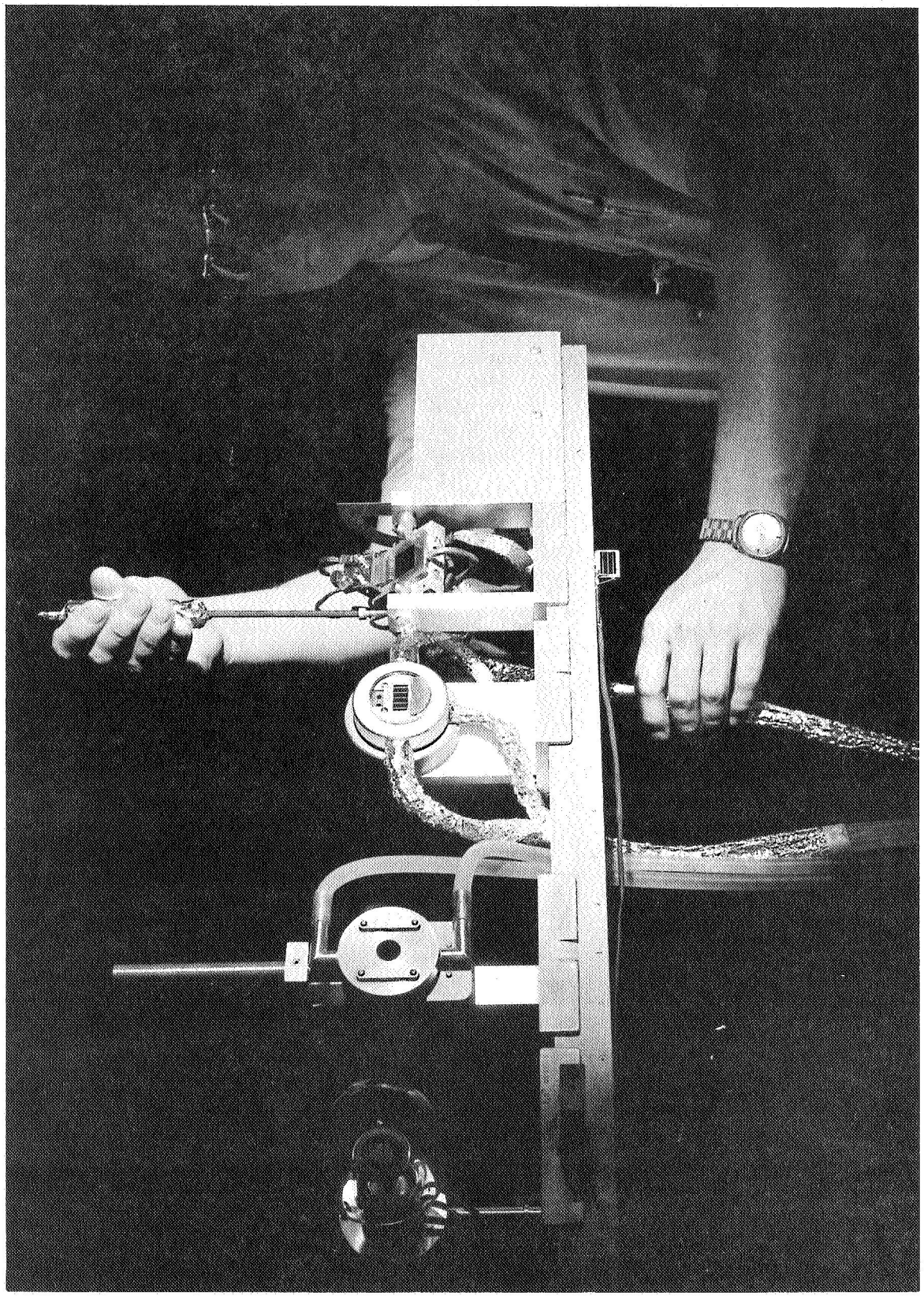

Figure 4 Solar Cell Test Figures

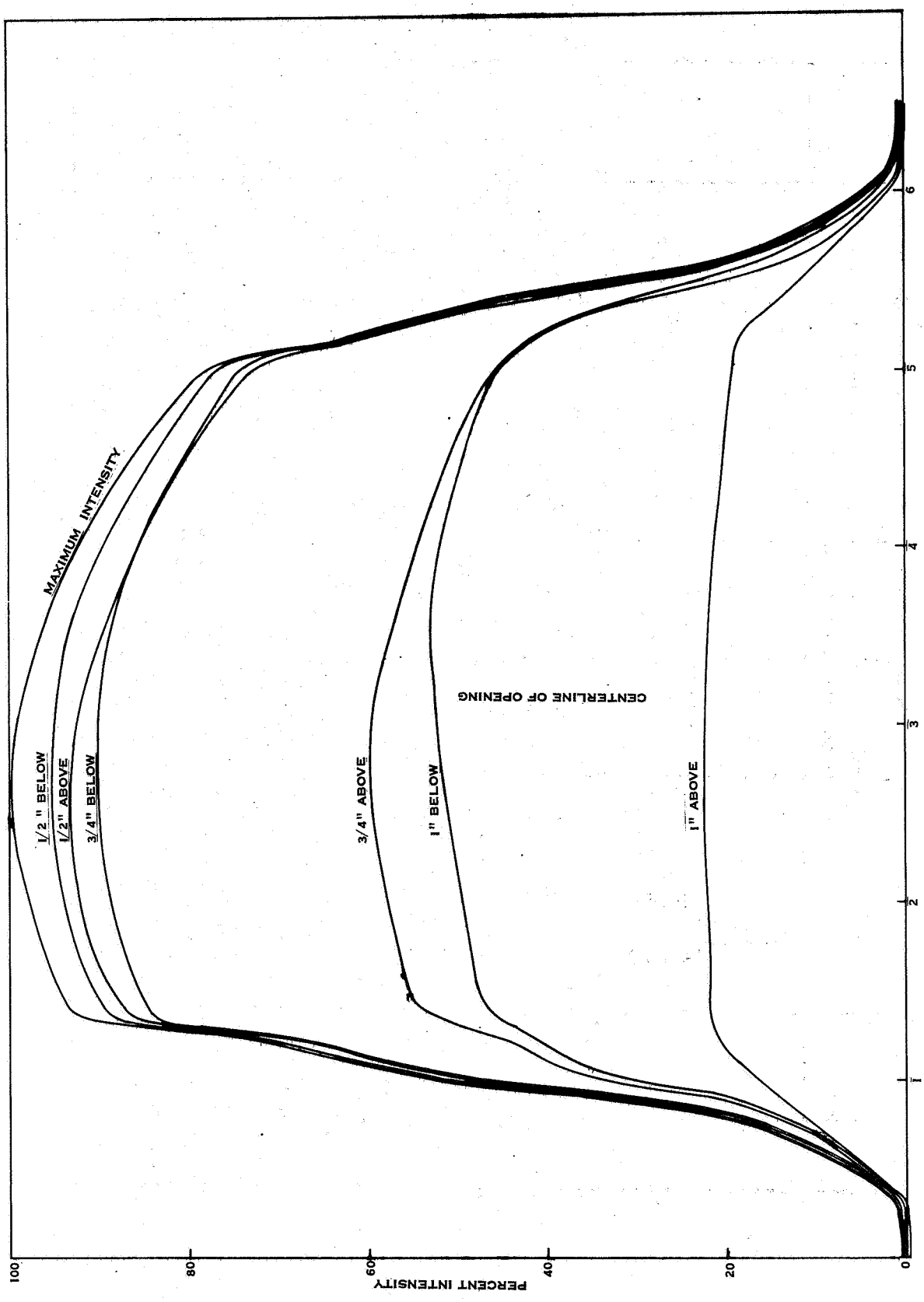

Figure 5 Typical Uniformity Measurement of OCLI Solar Simulator

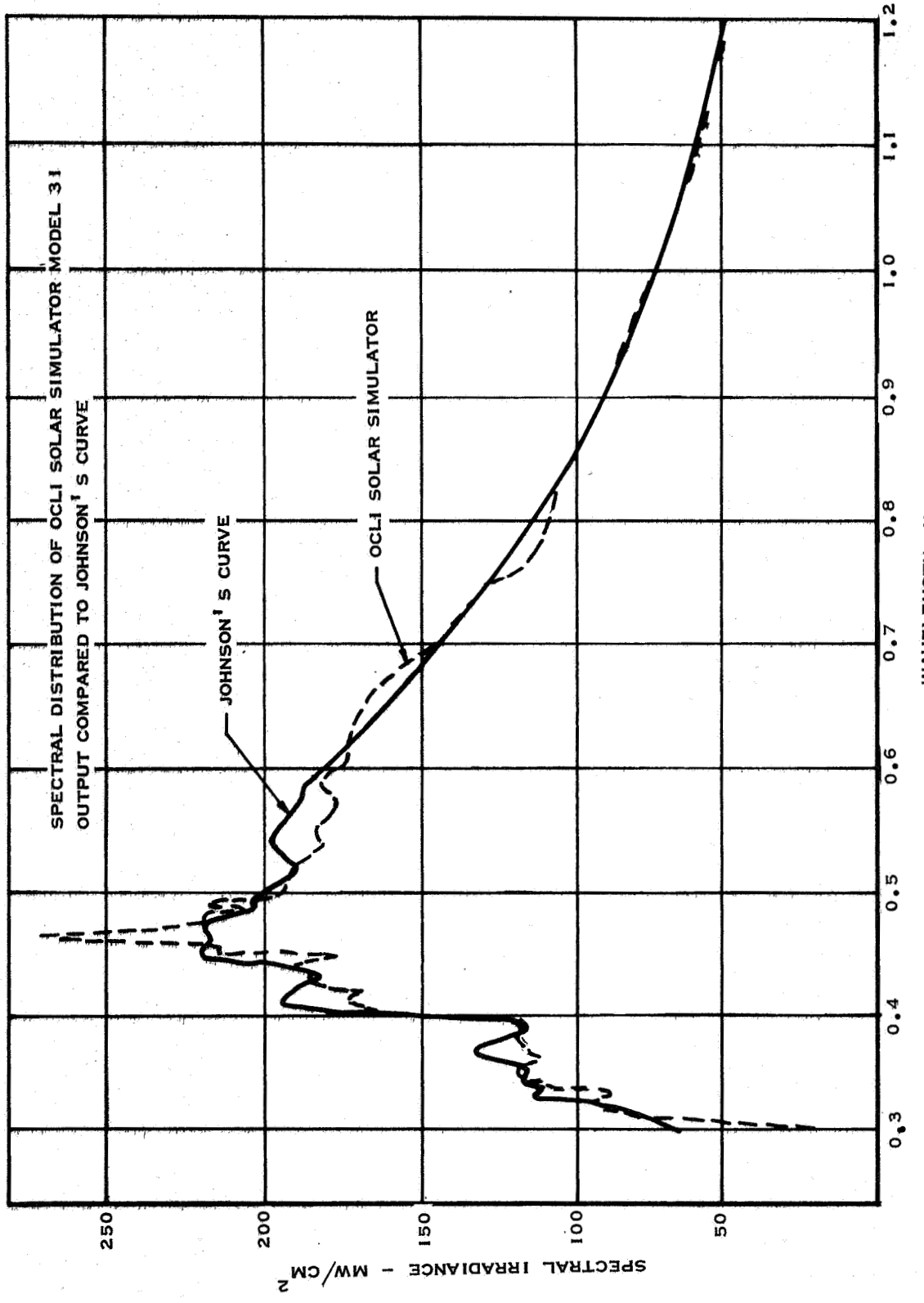

Figure 6 Spectral Output of OCLI Solar Simulator

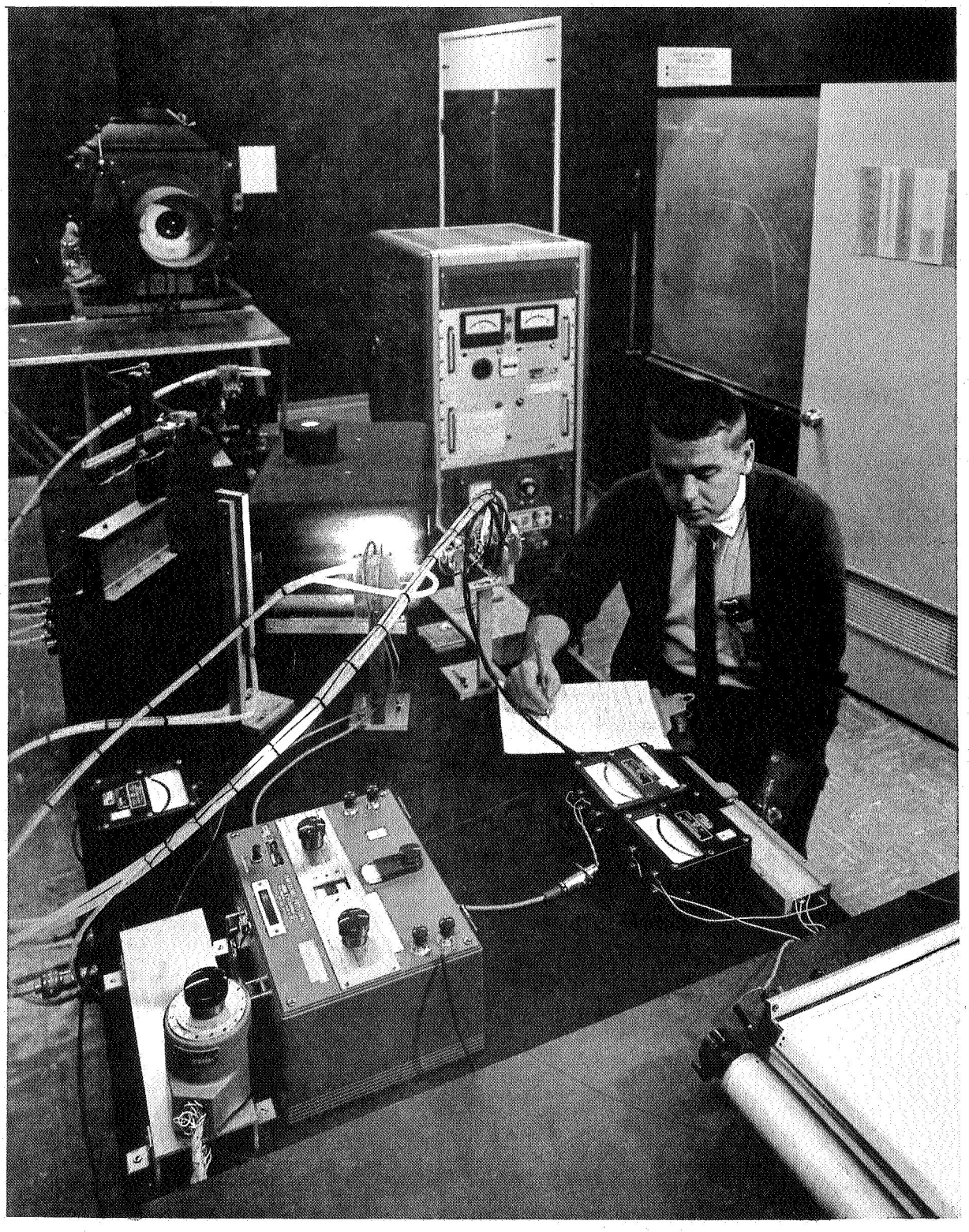

Figure 7 Solar Cell Evaluation Area

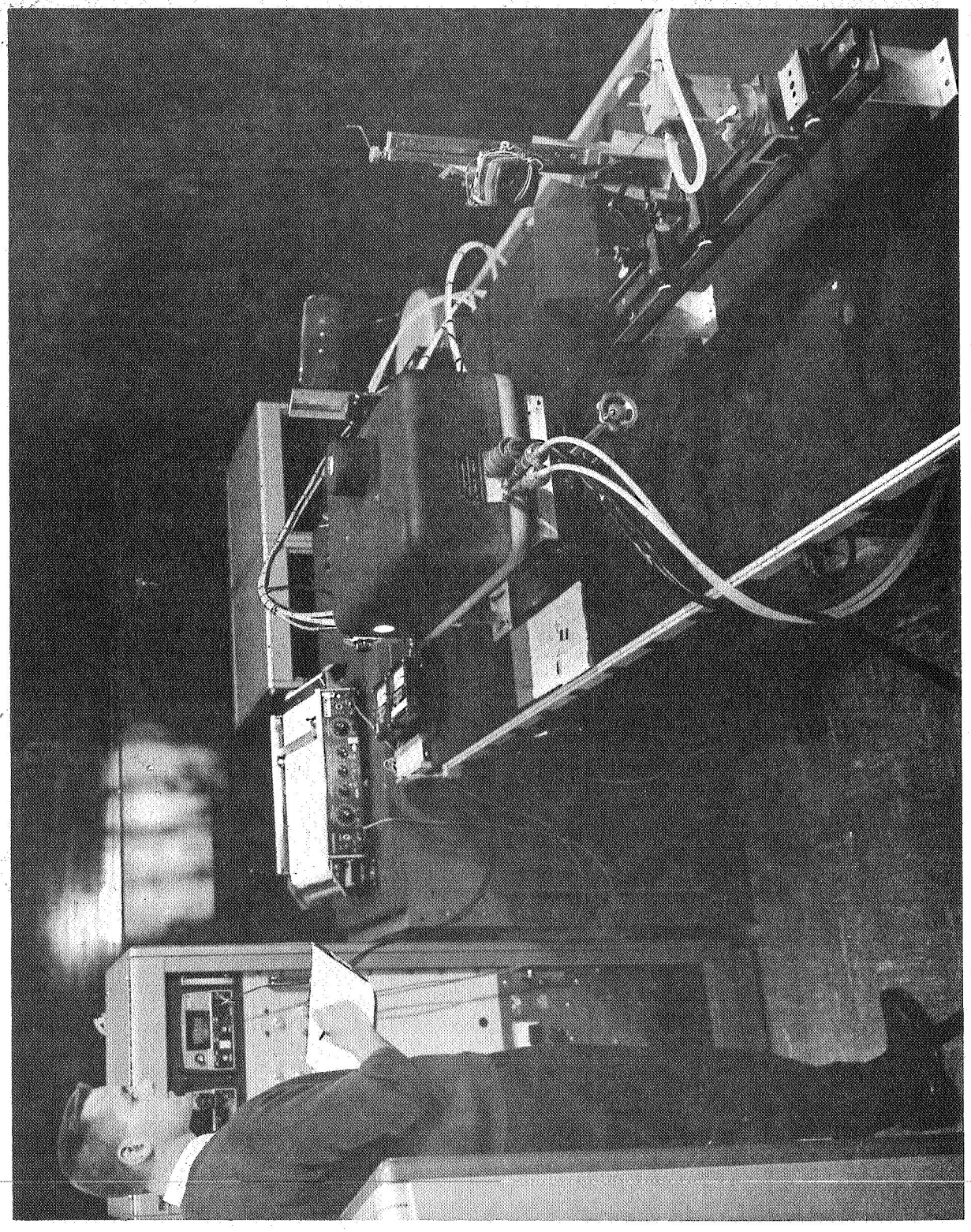

Figure 8 Solar Cell Performance Instrumentation

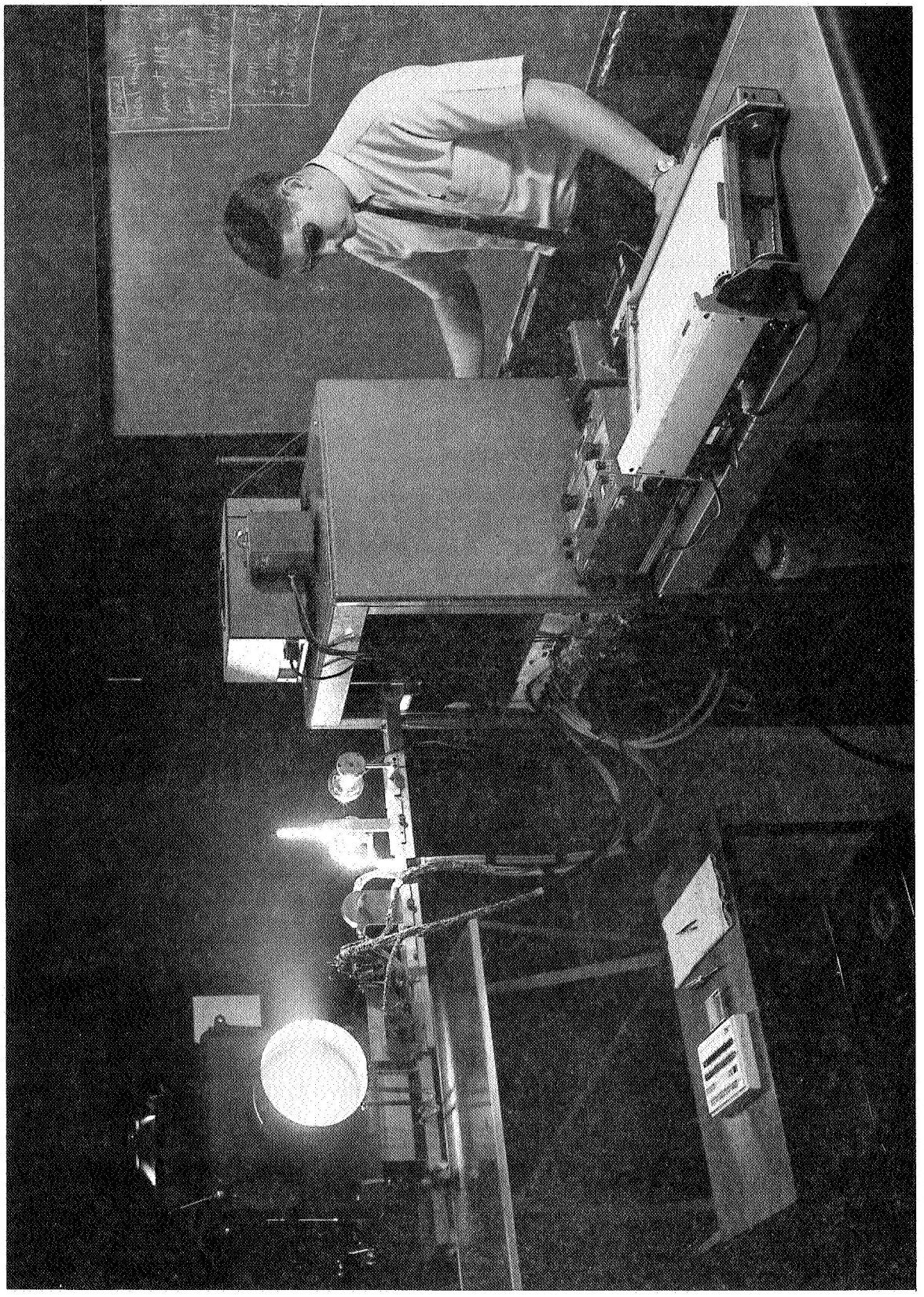

Figure 9 Carbon Arc Test Facility

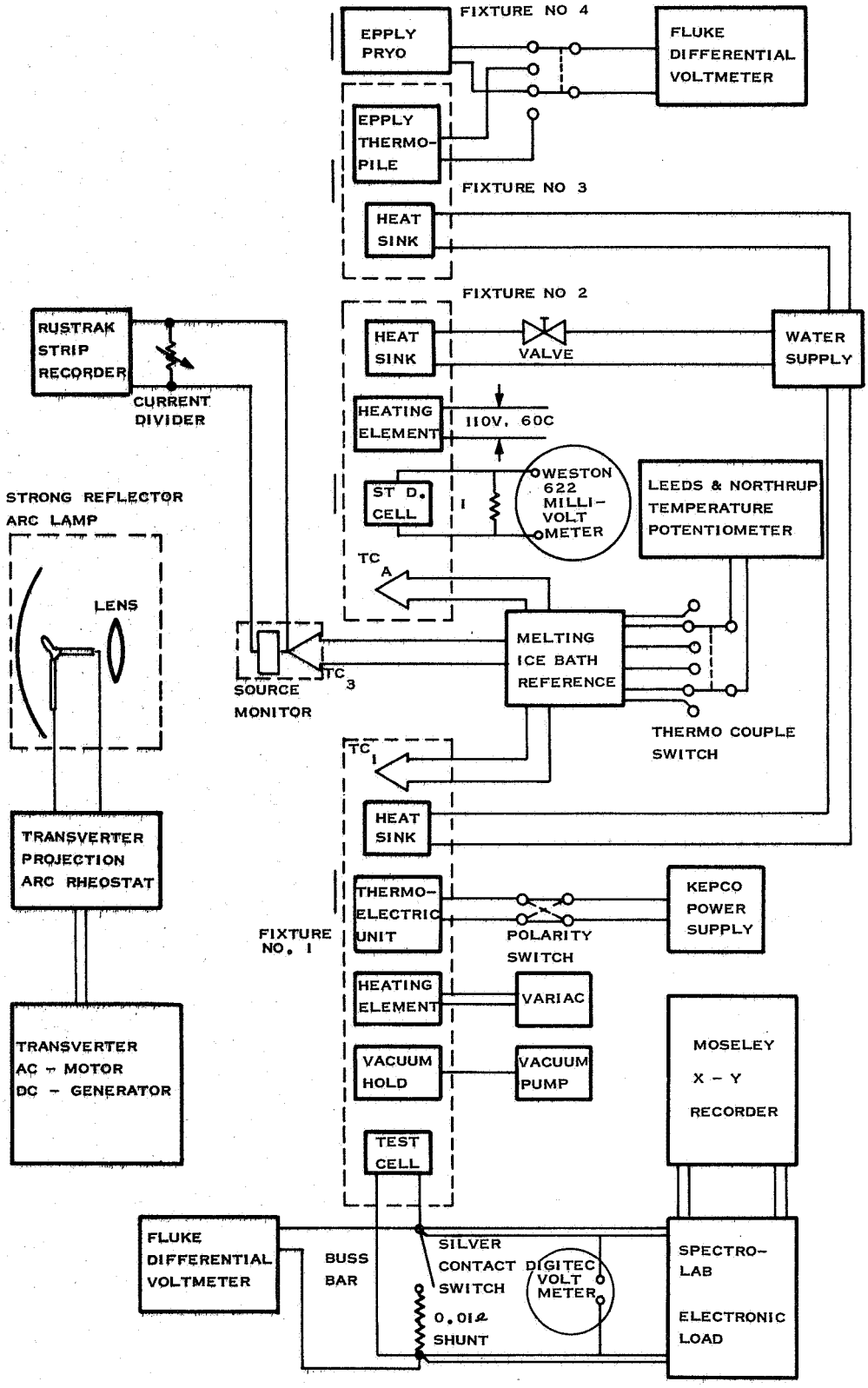

Figure 10 Block Diagram of Carbon Arc Test Facility

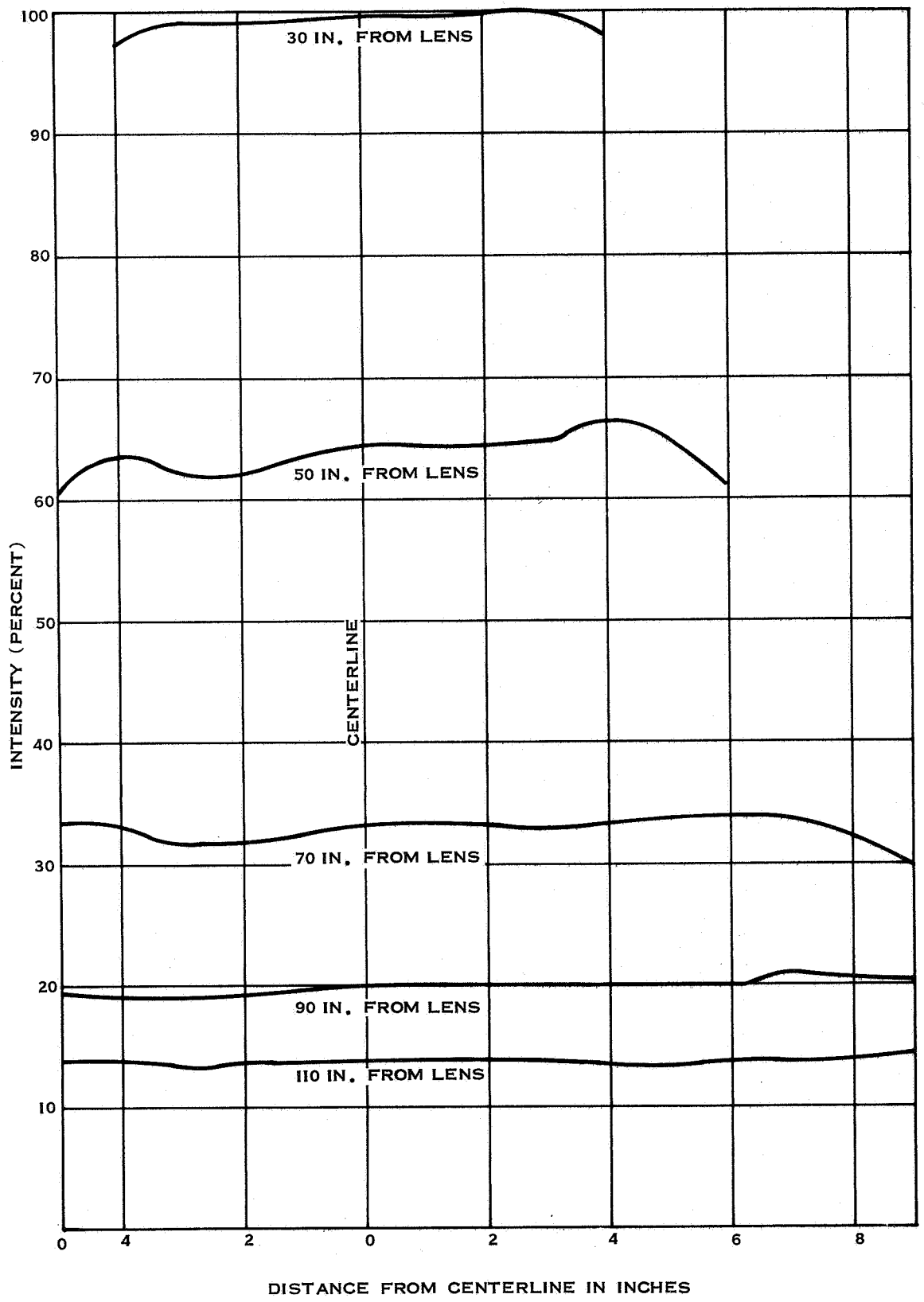

Figure 11 Uniformity Measurement of Carbon Arc Test Facility

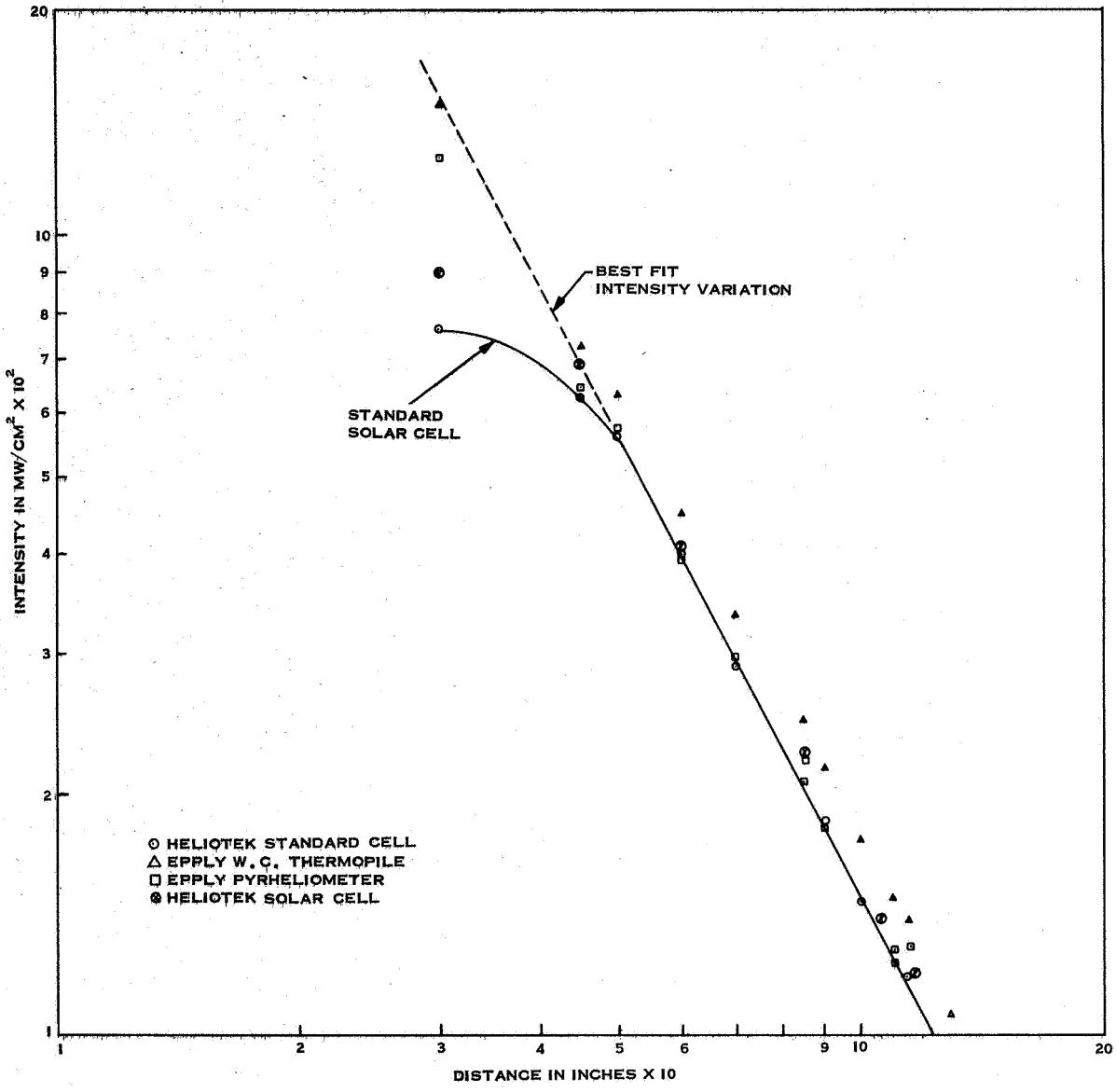

Figure 12 Intensity as a Function of Distance (Carbon Arc)

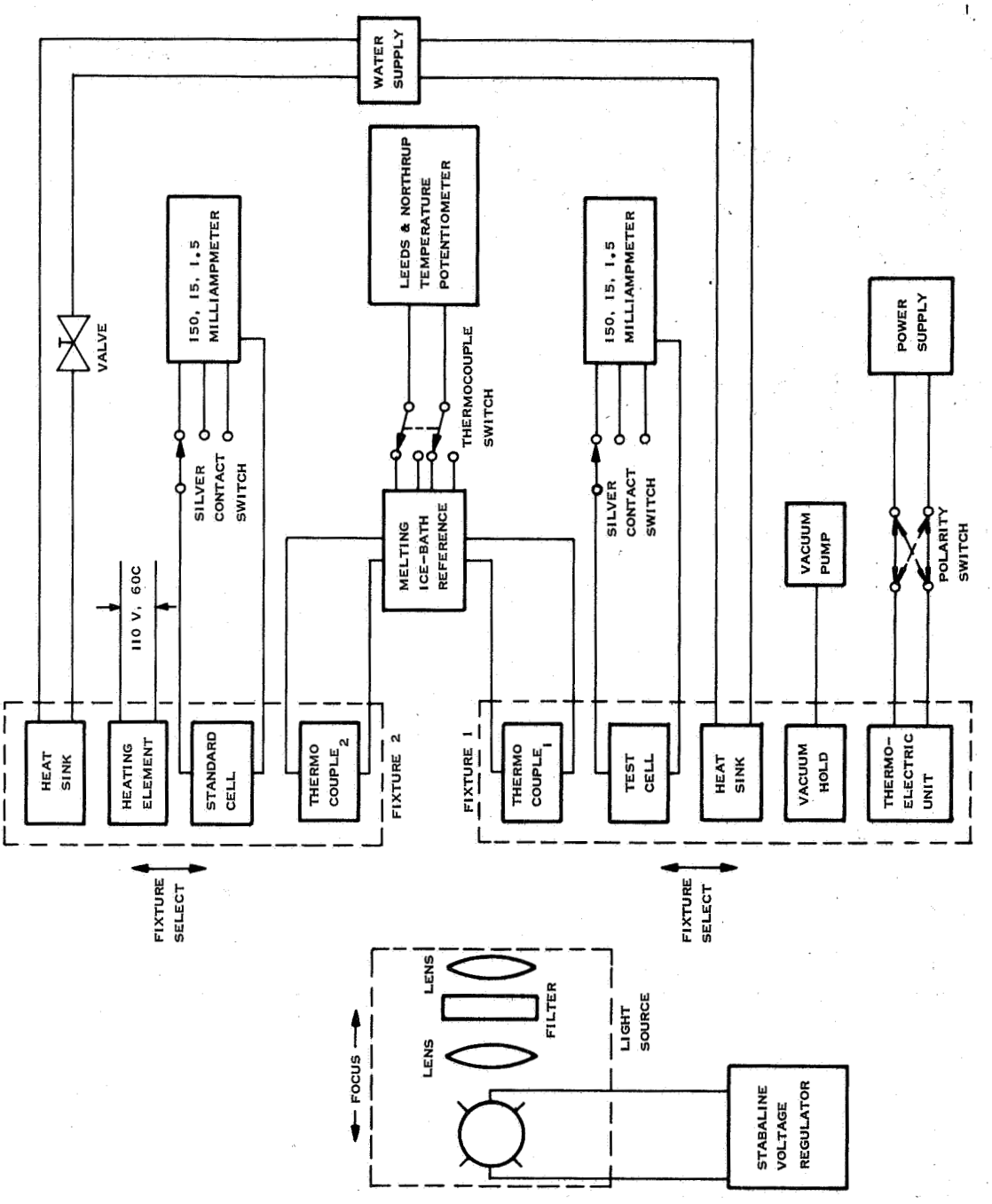

Figure 13 Spectral Response Test Facility Block Diagram

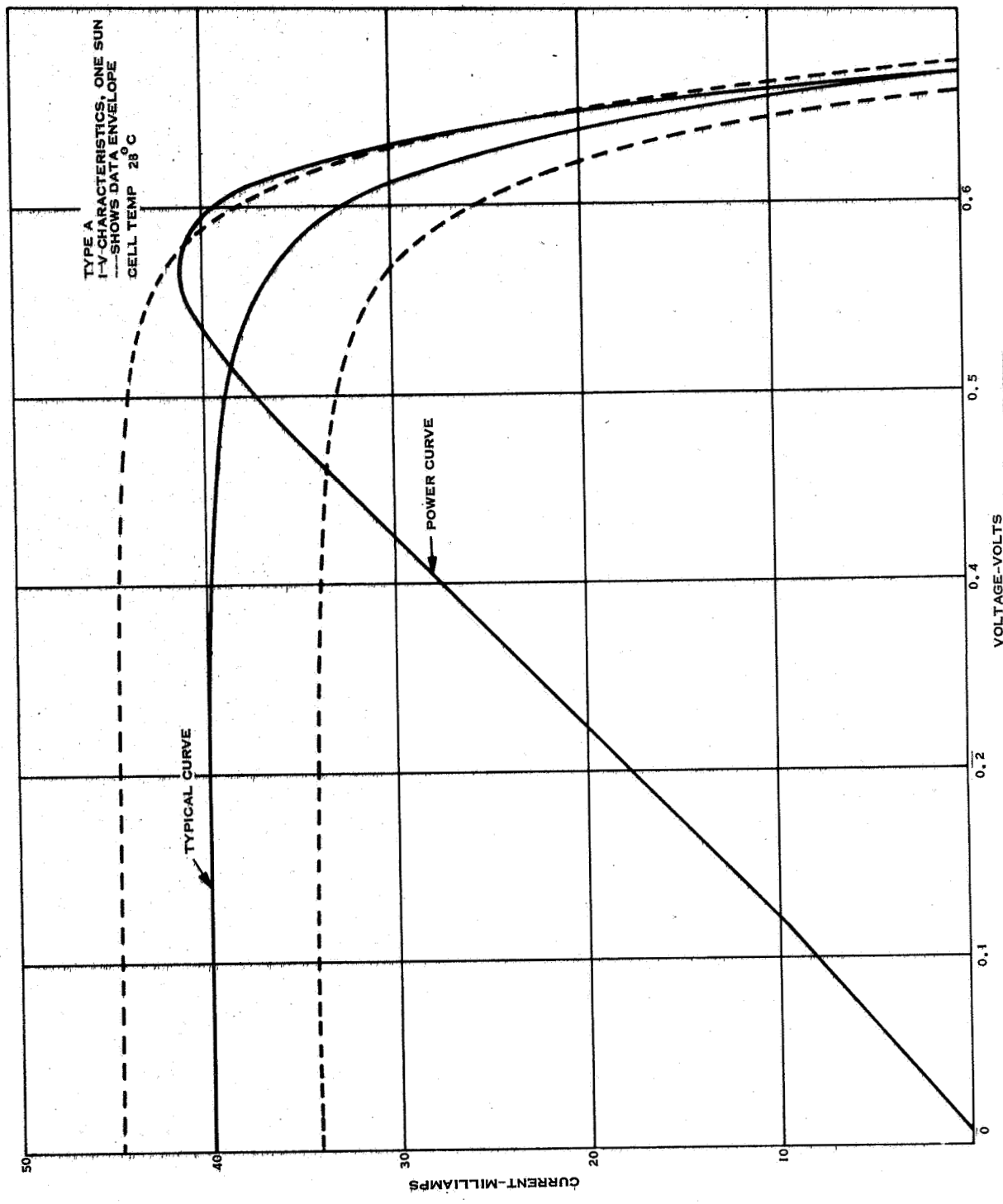

Figure 14 One Sun I-V Characteristics Cell Type A

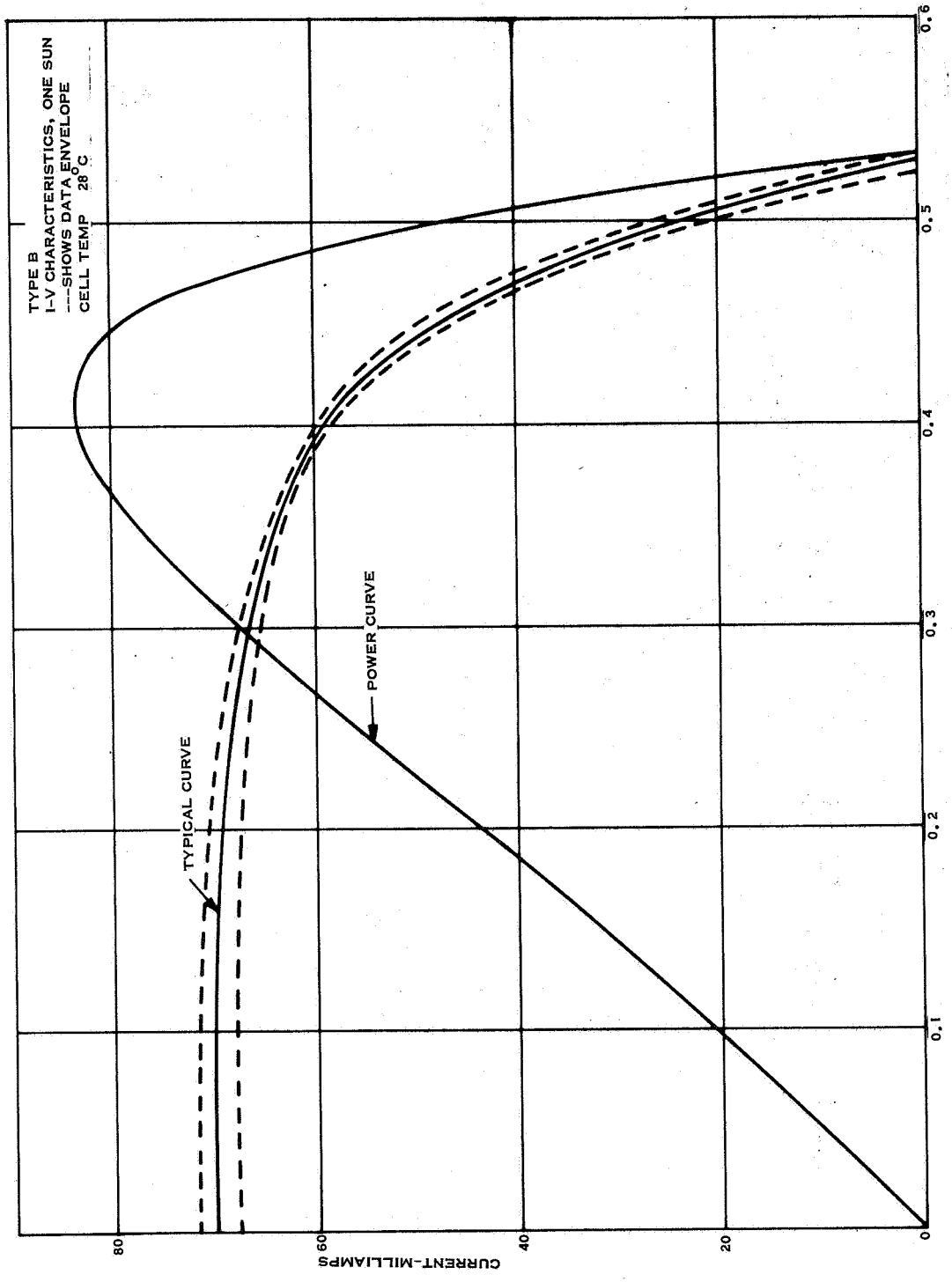

Figure 15 One Sun I-V Characteristics Cell Type B

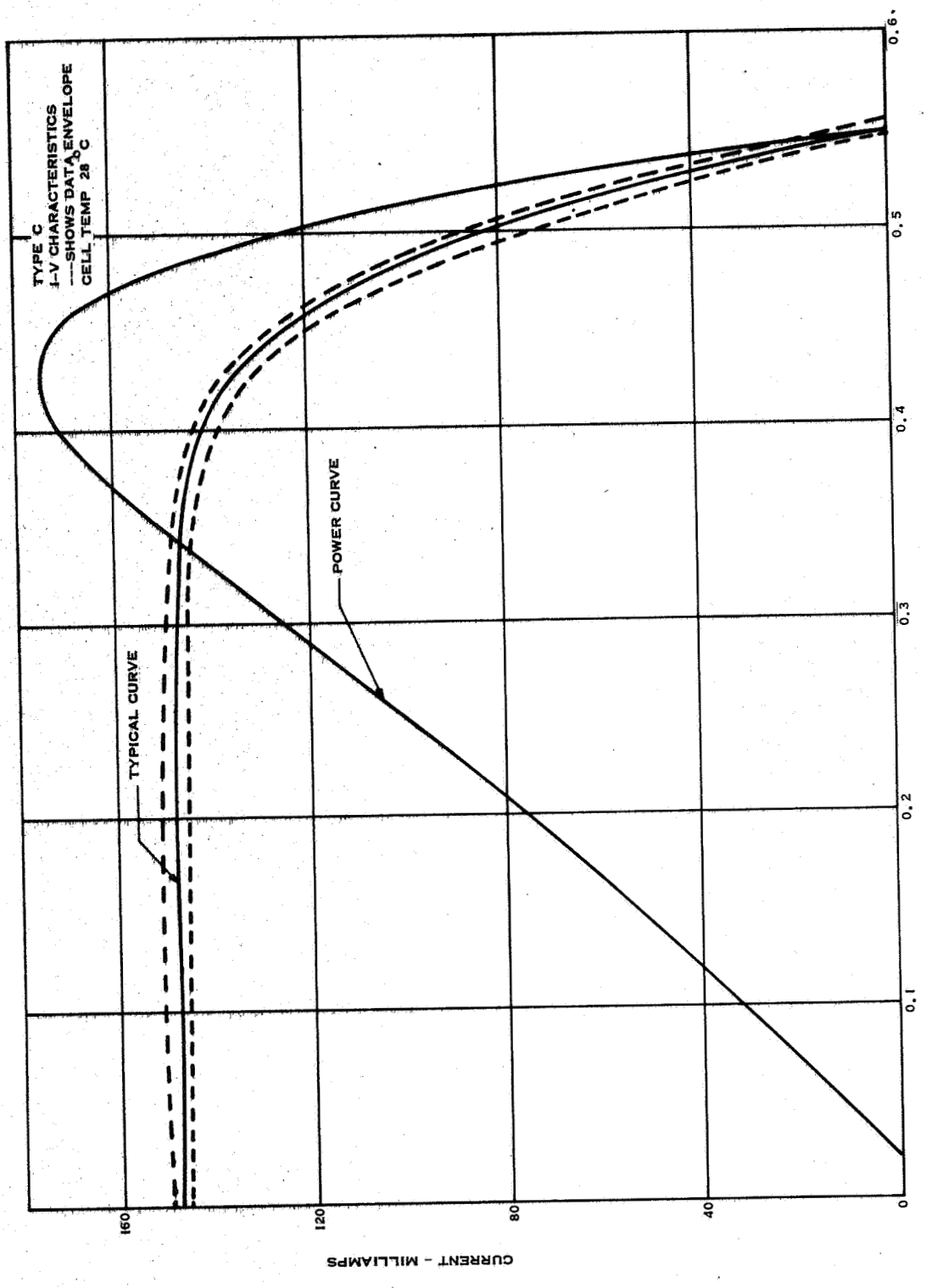

Figure 16 One Sun I-V Characteristics Cell Type C

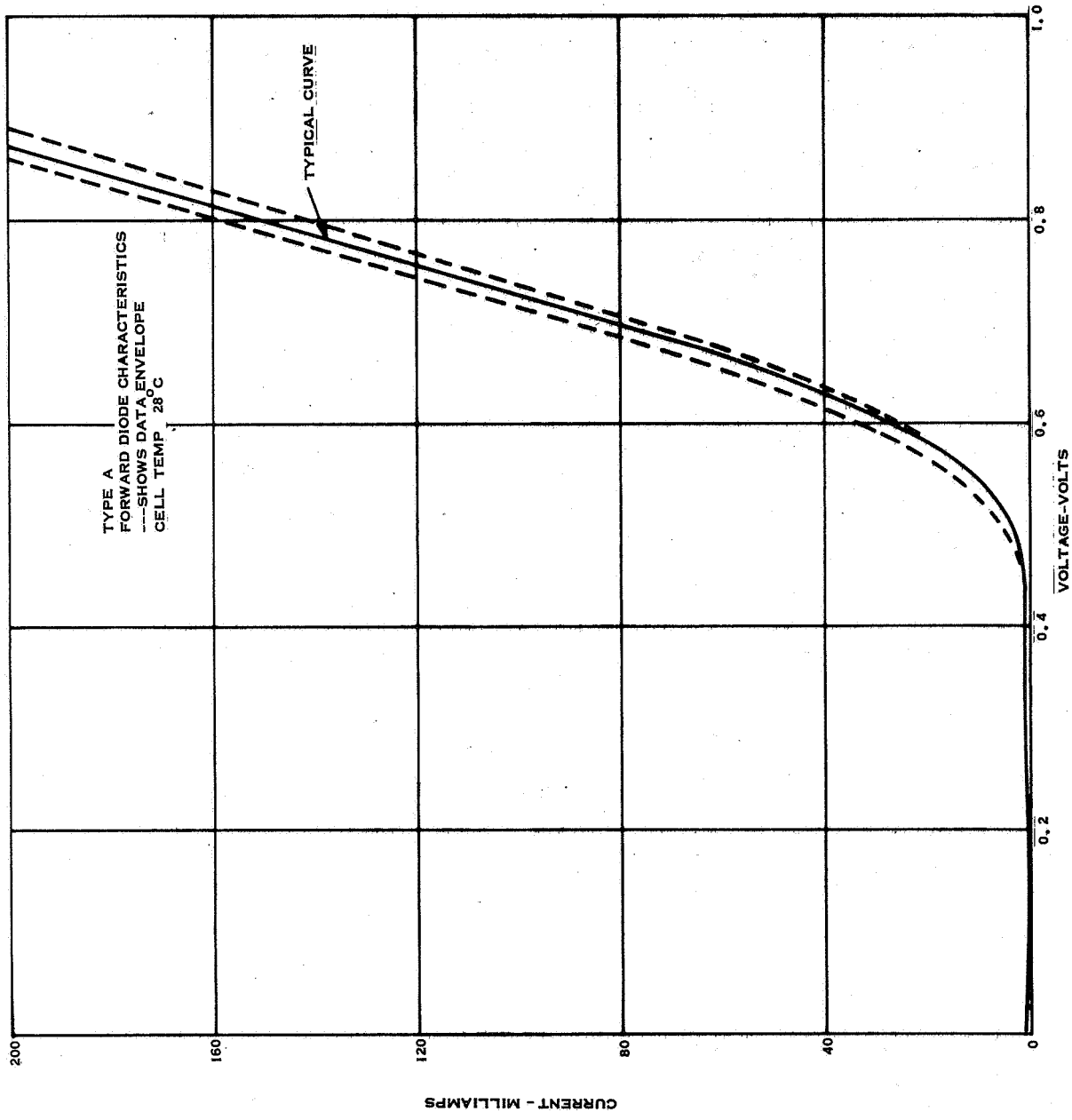

Figure 17 Dark Forward Diode Characteristics Cell Type A

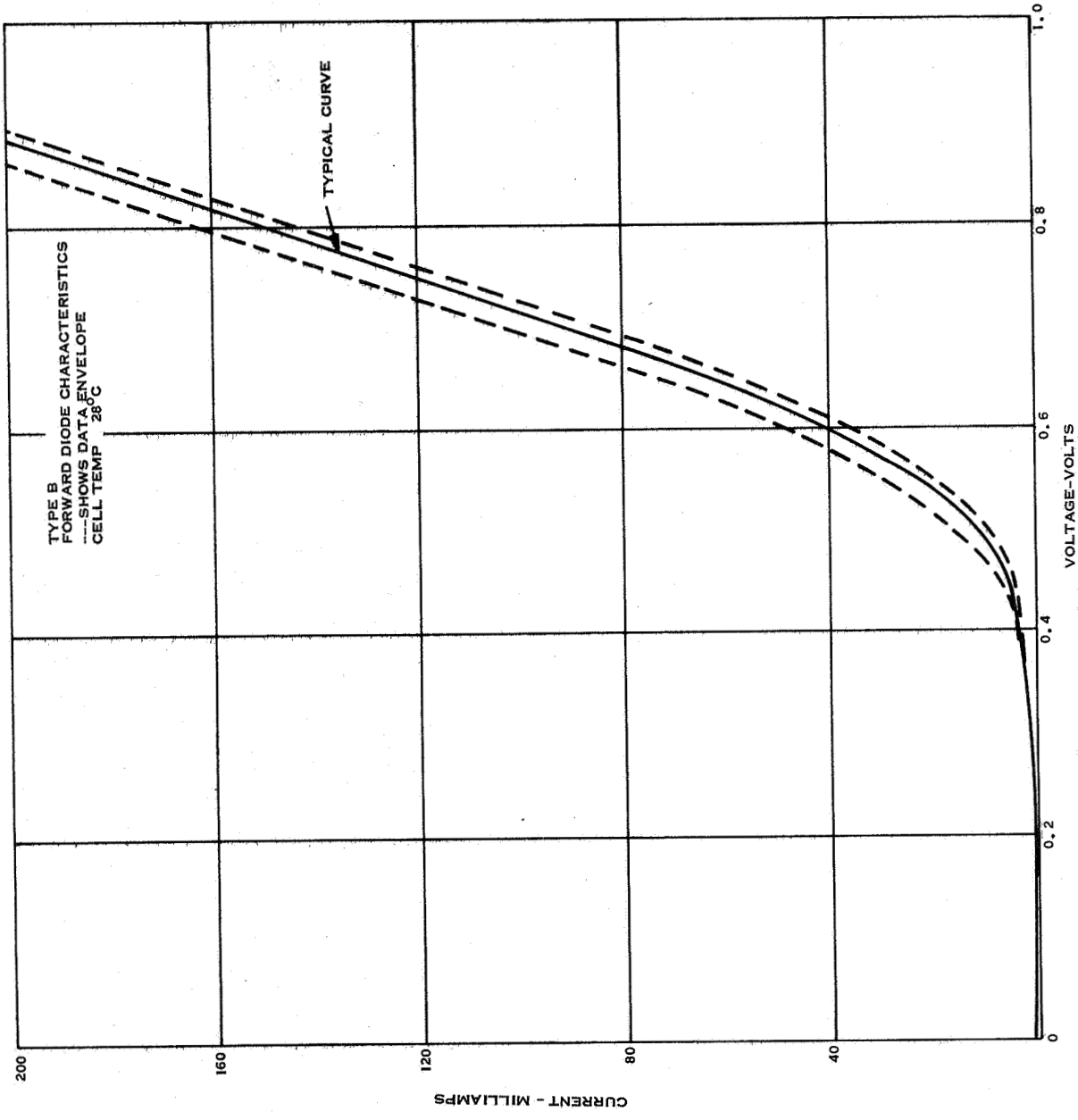

Figure 18 Dark Forward Diode Characteristics Cell Type B

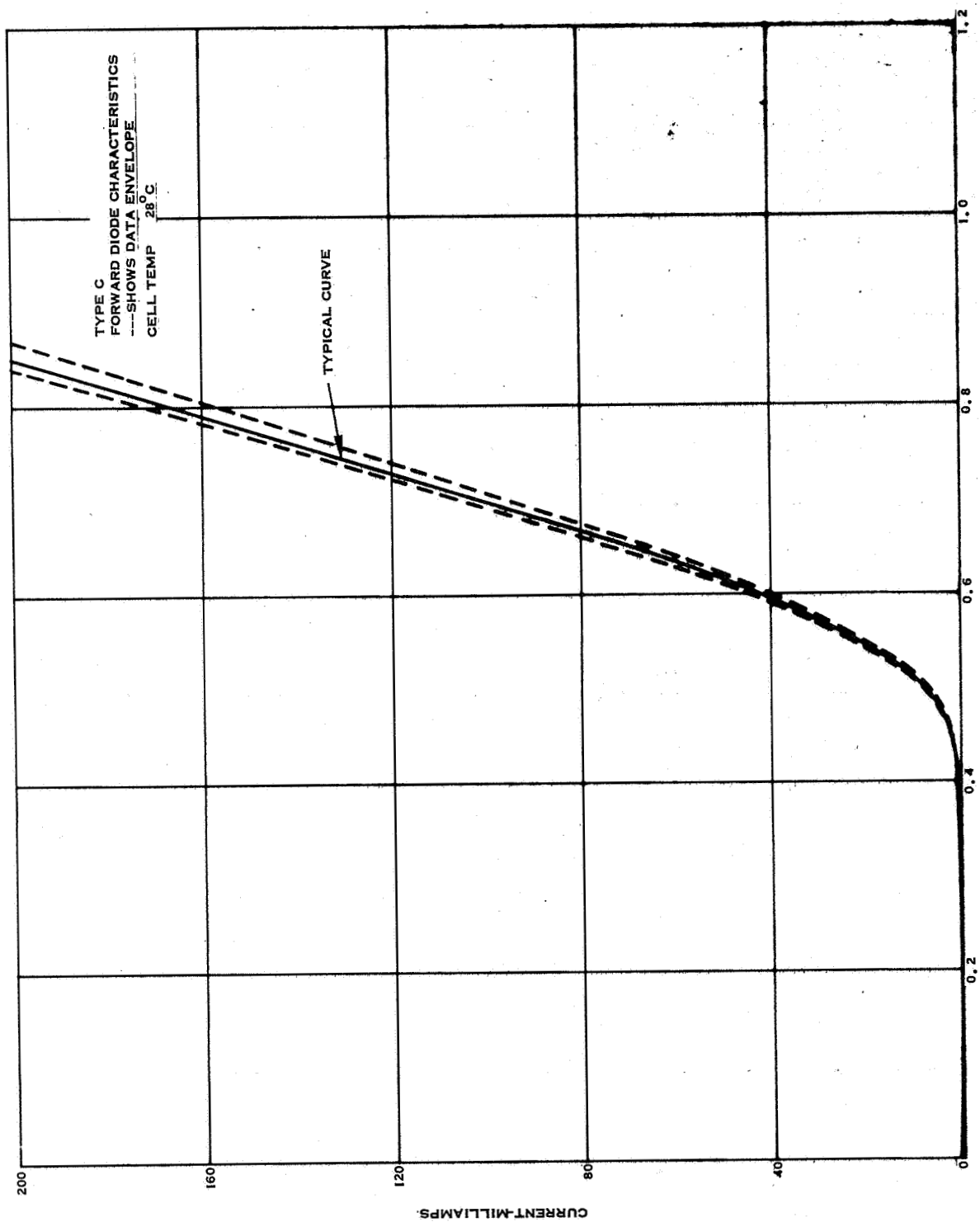

Figure 19 Dark Forward Diode Characteristics Cell Type C

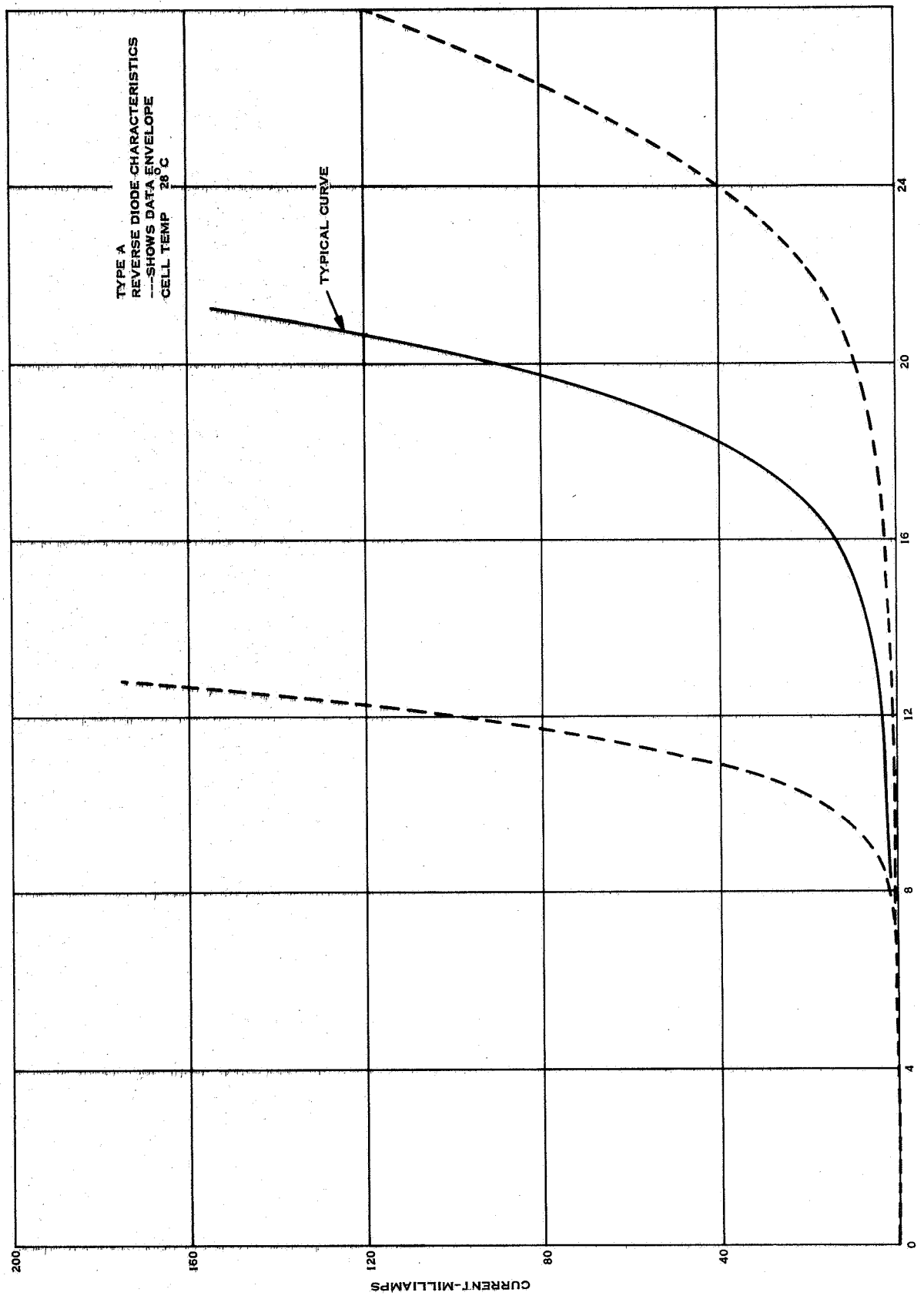

Figure 20 Dark Reverse Diode Characteristics Cell Type A

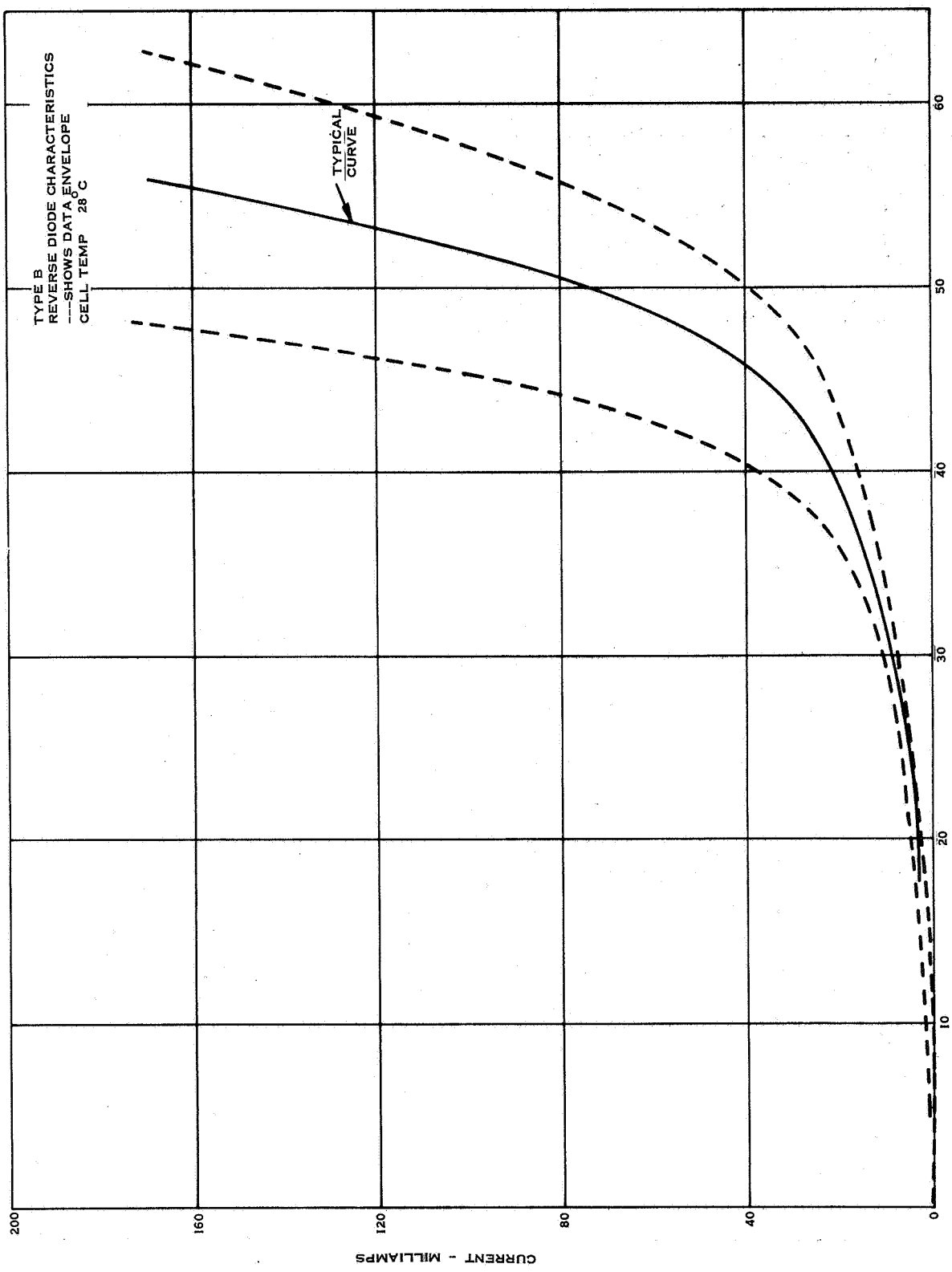

Figure 21 Dark Reverse Diode Characteristics Cell Type B

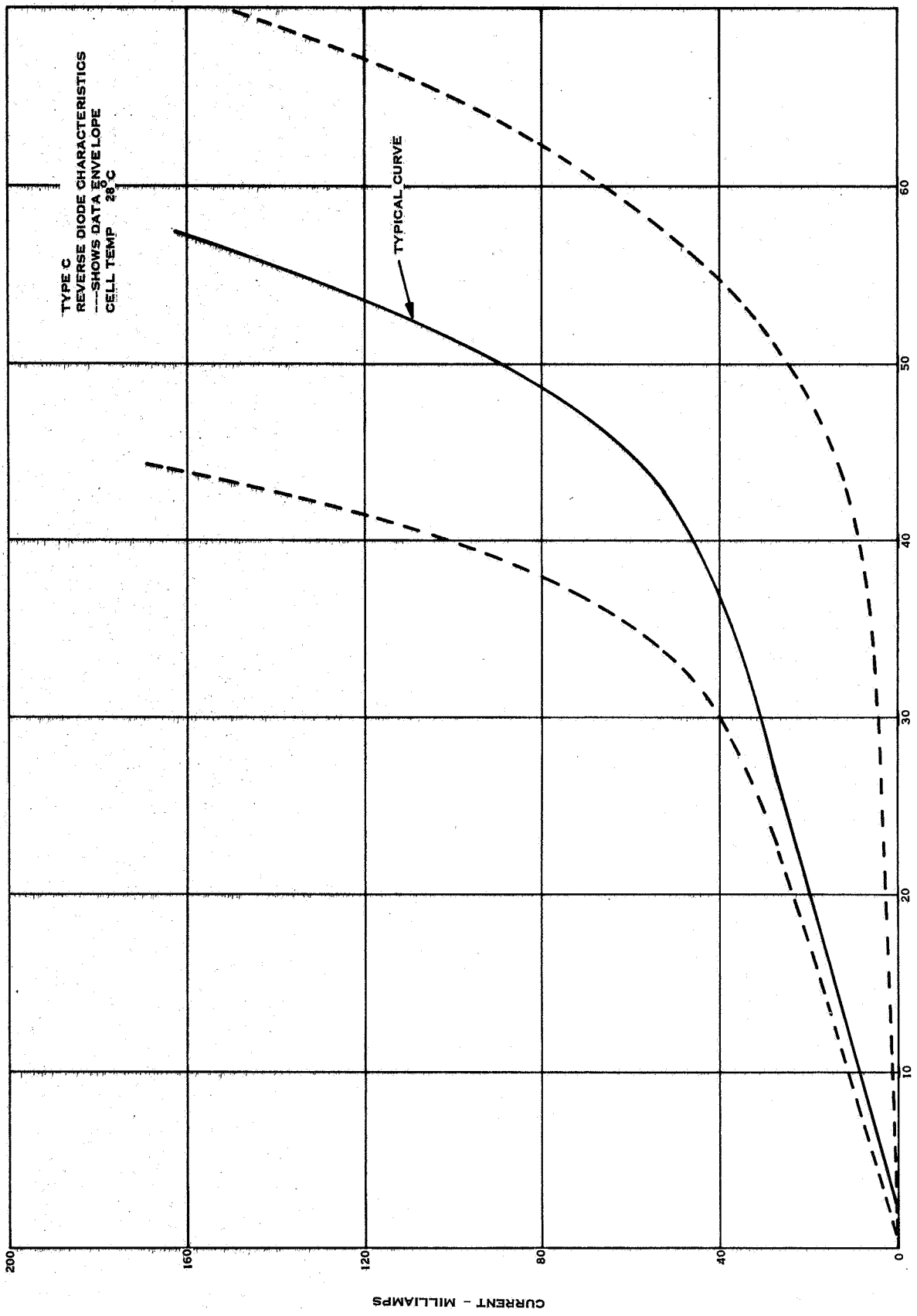

Figure 22 Dark Reverse Diode Characteristics Cell Type C

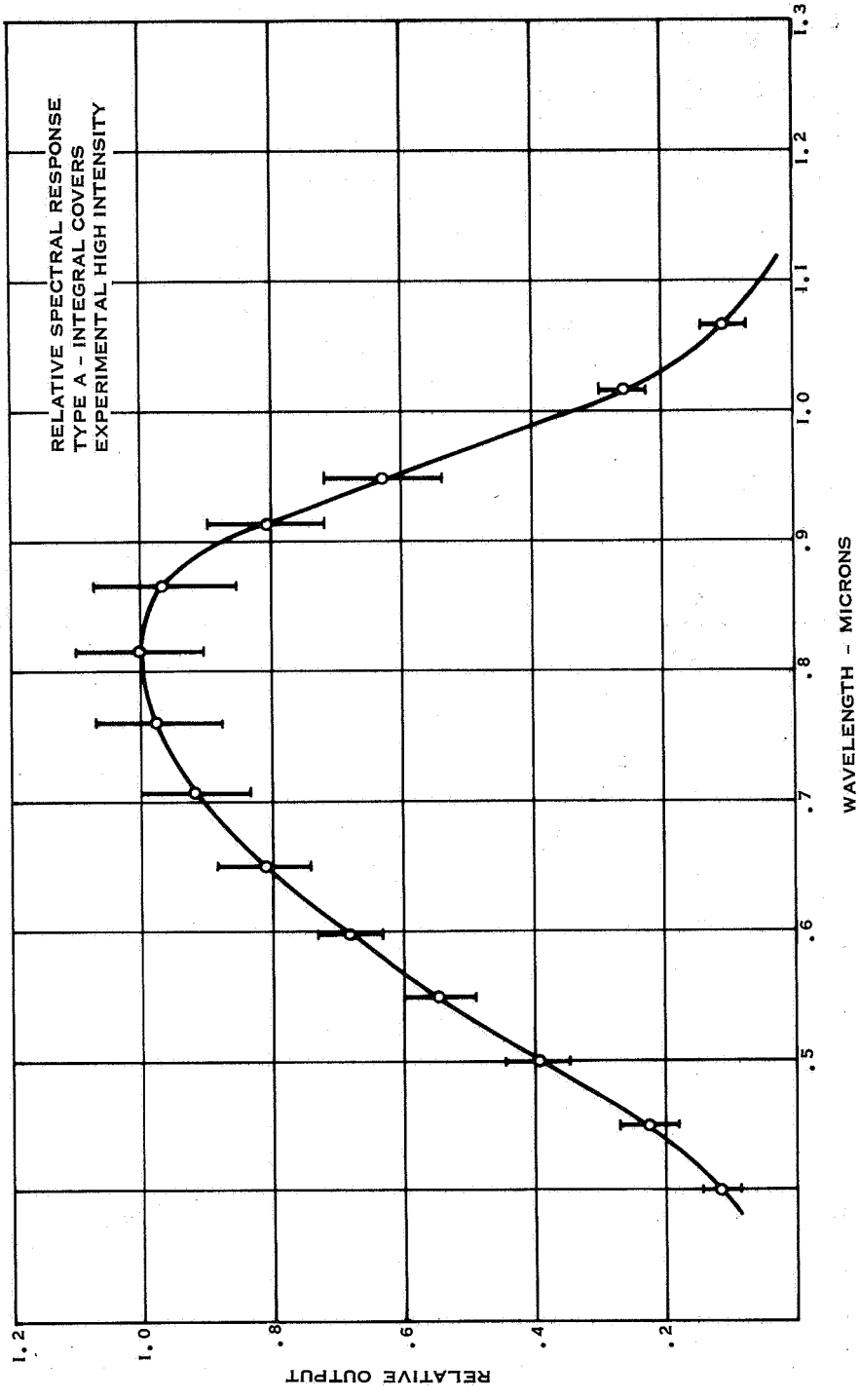

Figure 23 Relative Spectral Response Cell Type A

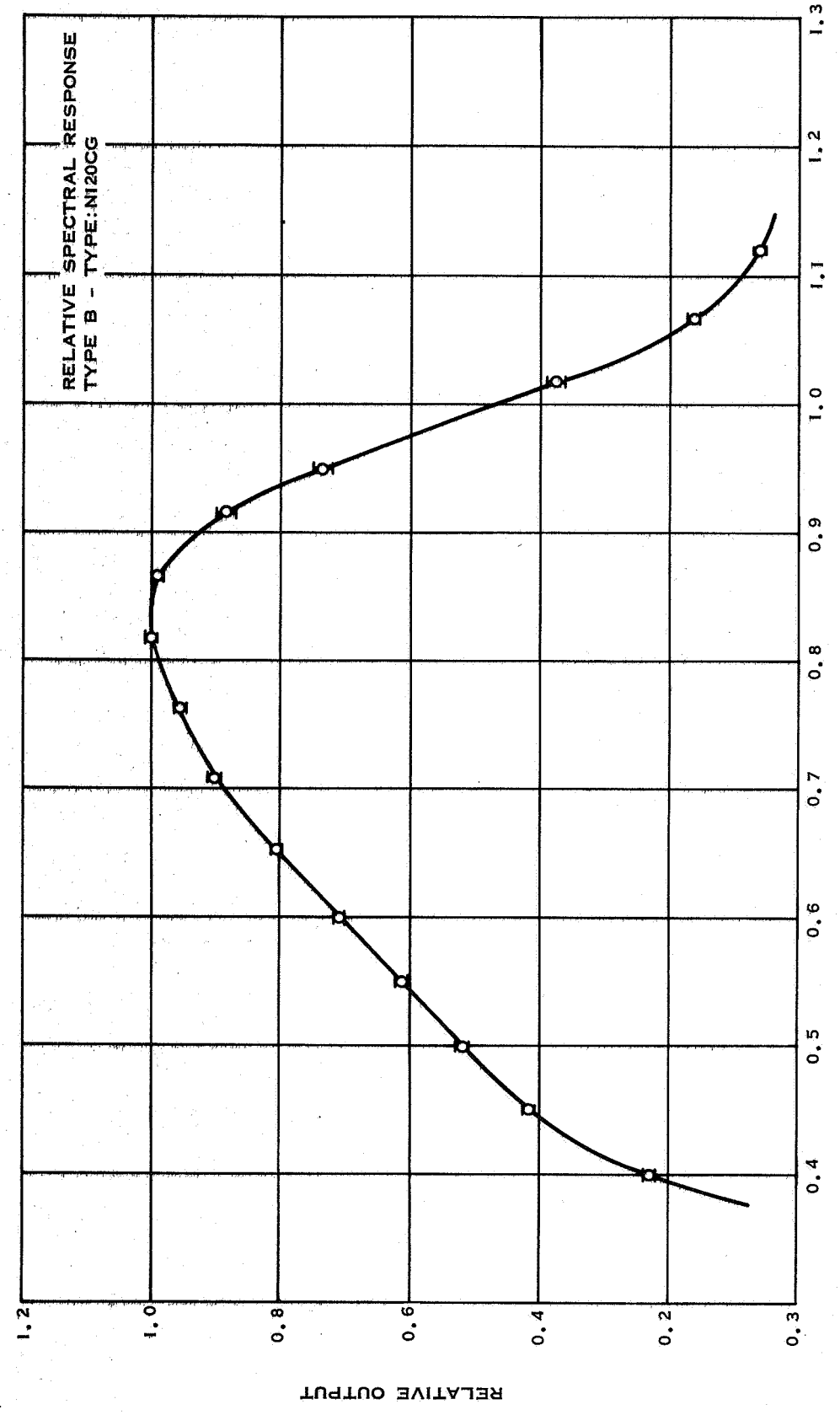

Figure 24 Relative Spectral Response Cell Type B

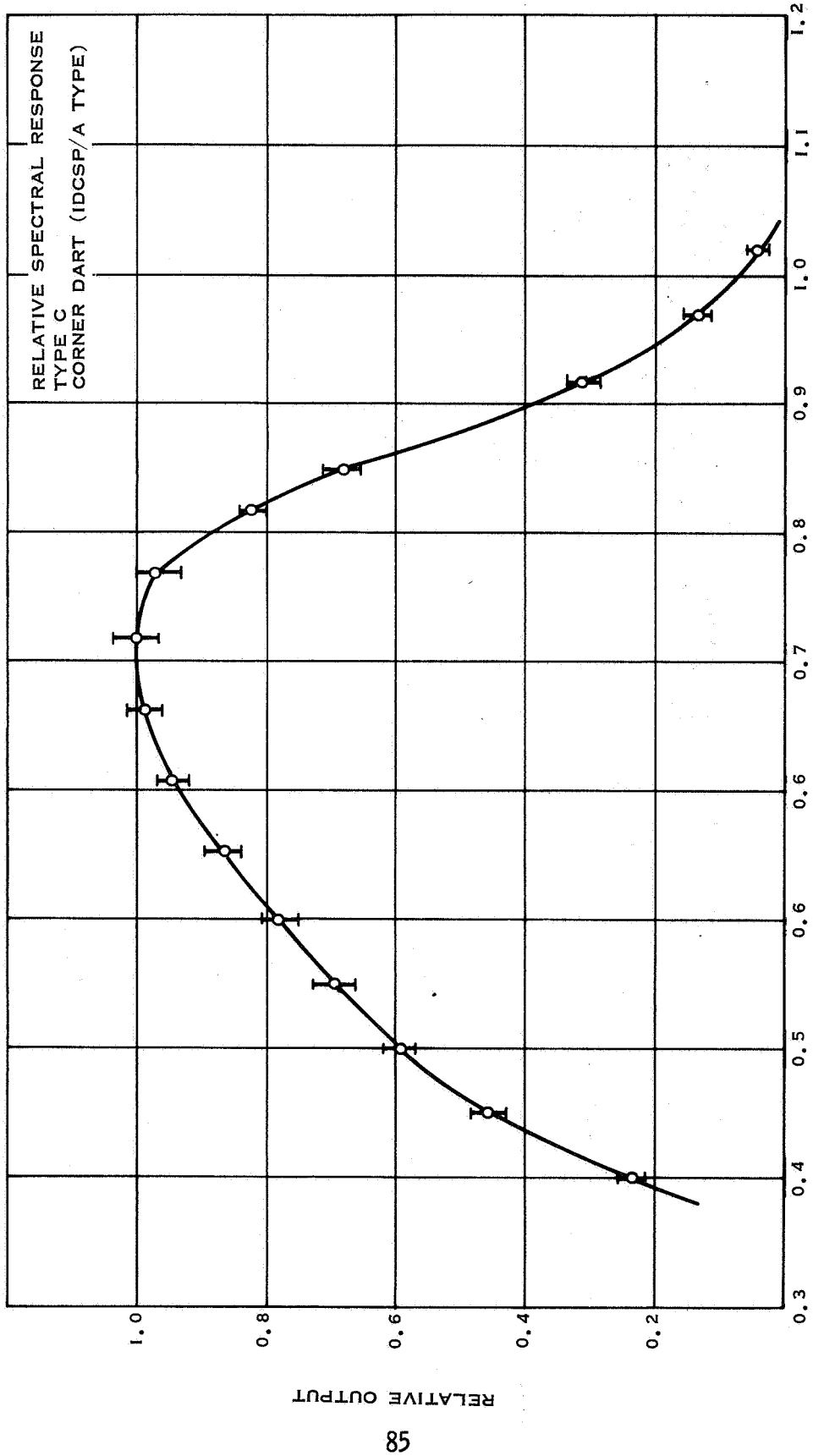

Figure 25 Relative Spectral Response Cell Type C

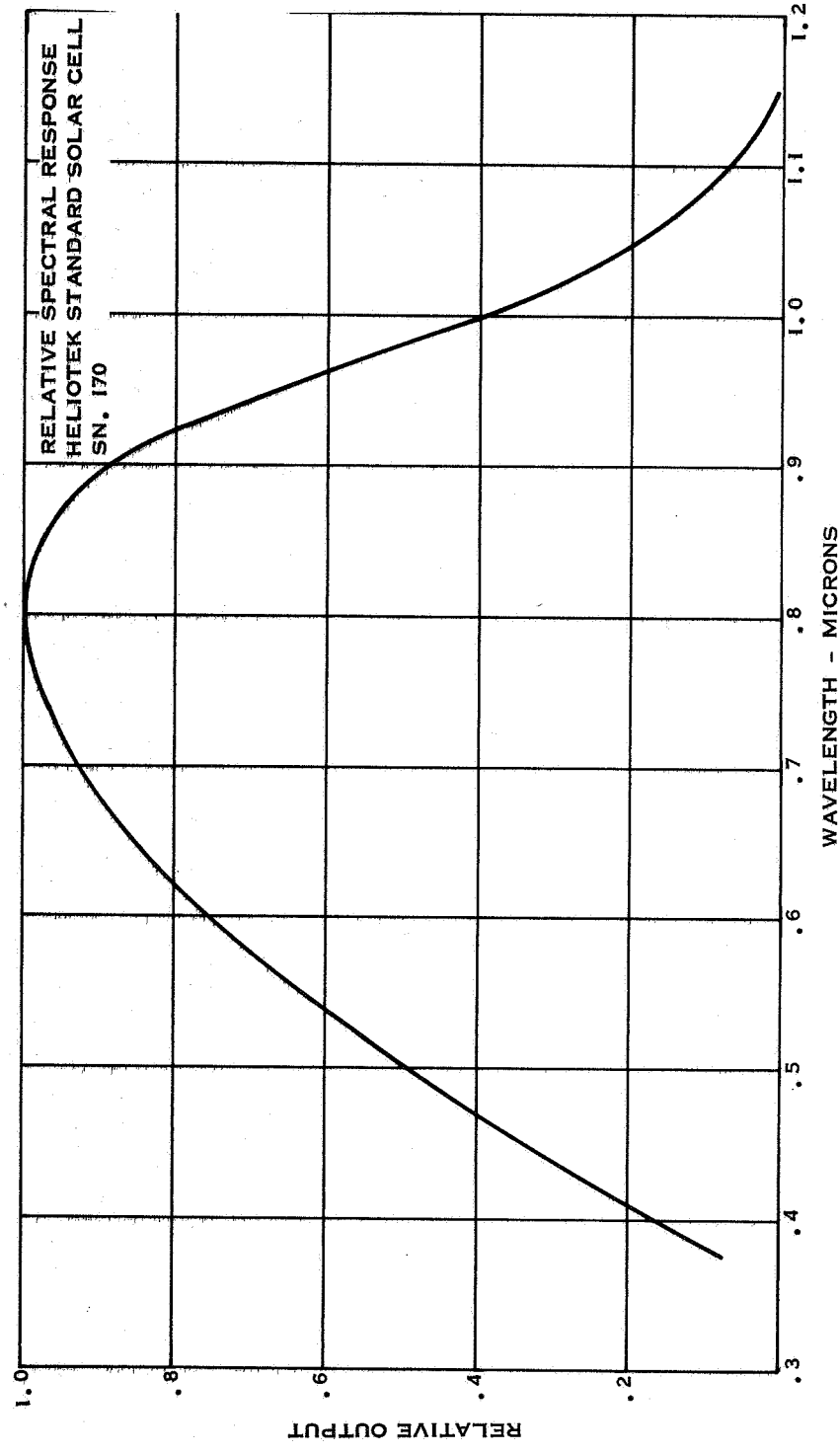

Figure 26 Relative Spectral Response Heliotek Standard Cell

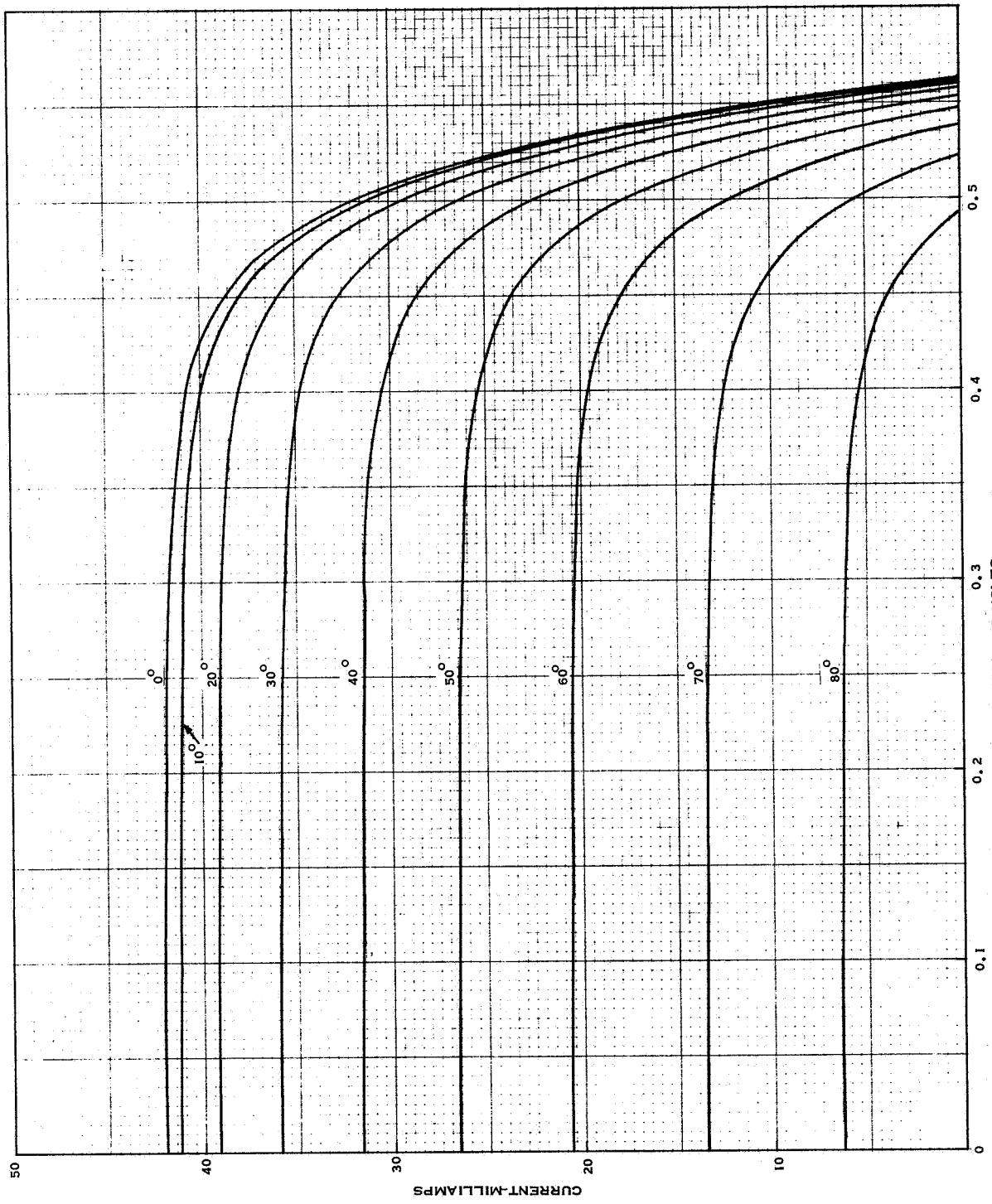

Figure 27 OCLI One Sun Angle of Incidence Characteristics Cell Type 1A

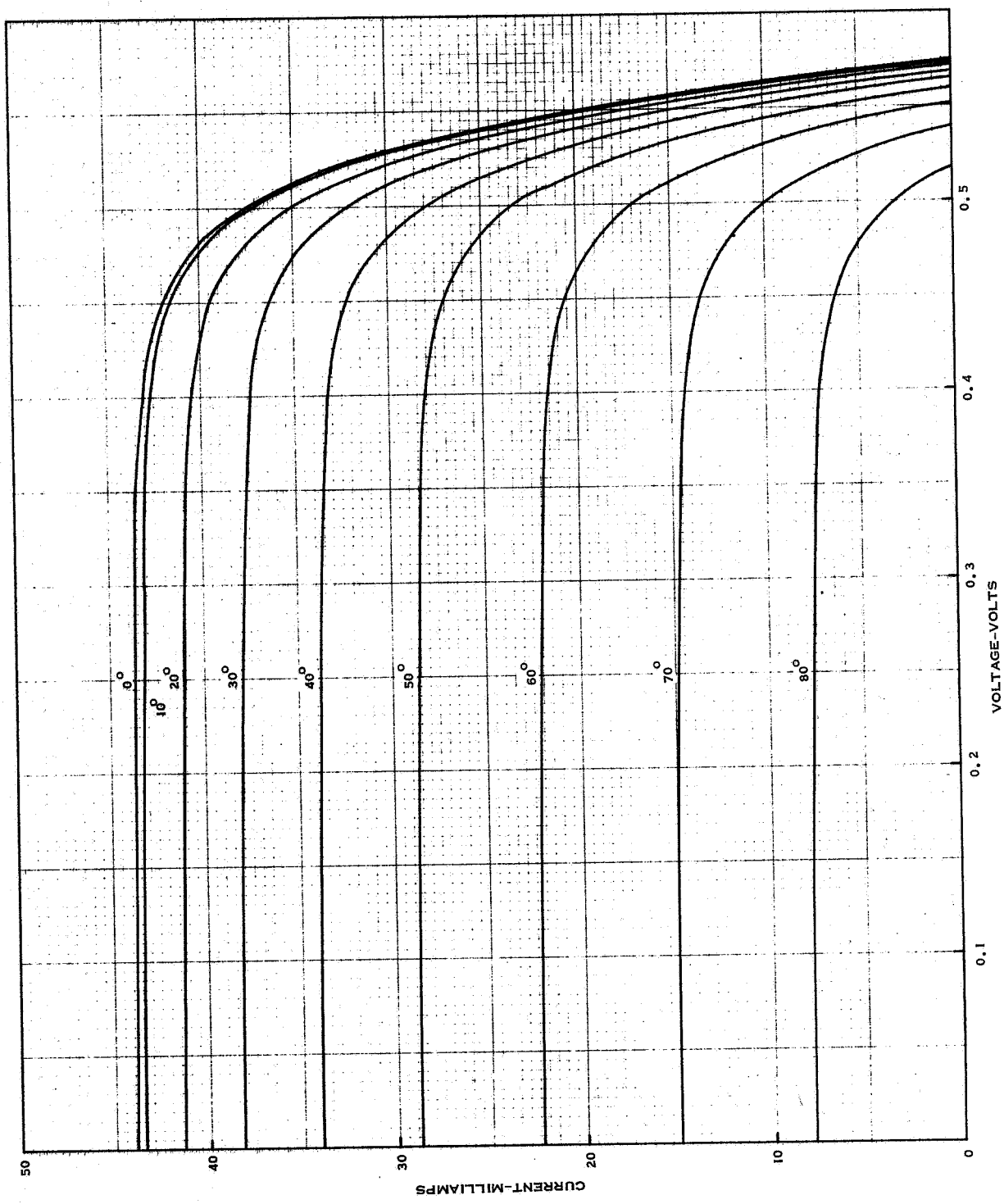

Figure 28 OCLI One Sun Angle of Incidence Characteristics Cell Type 2A

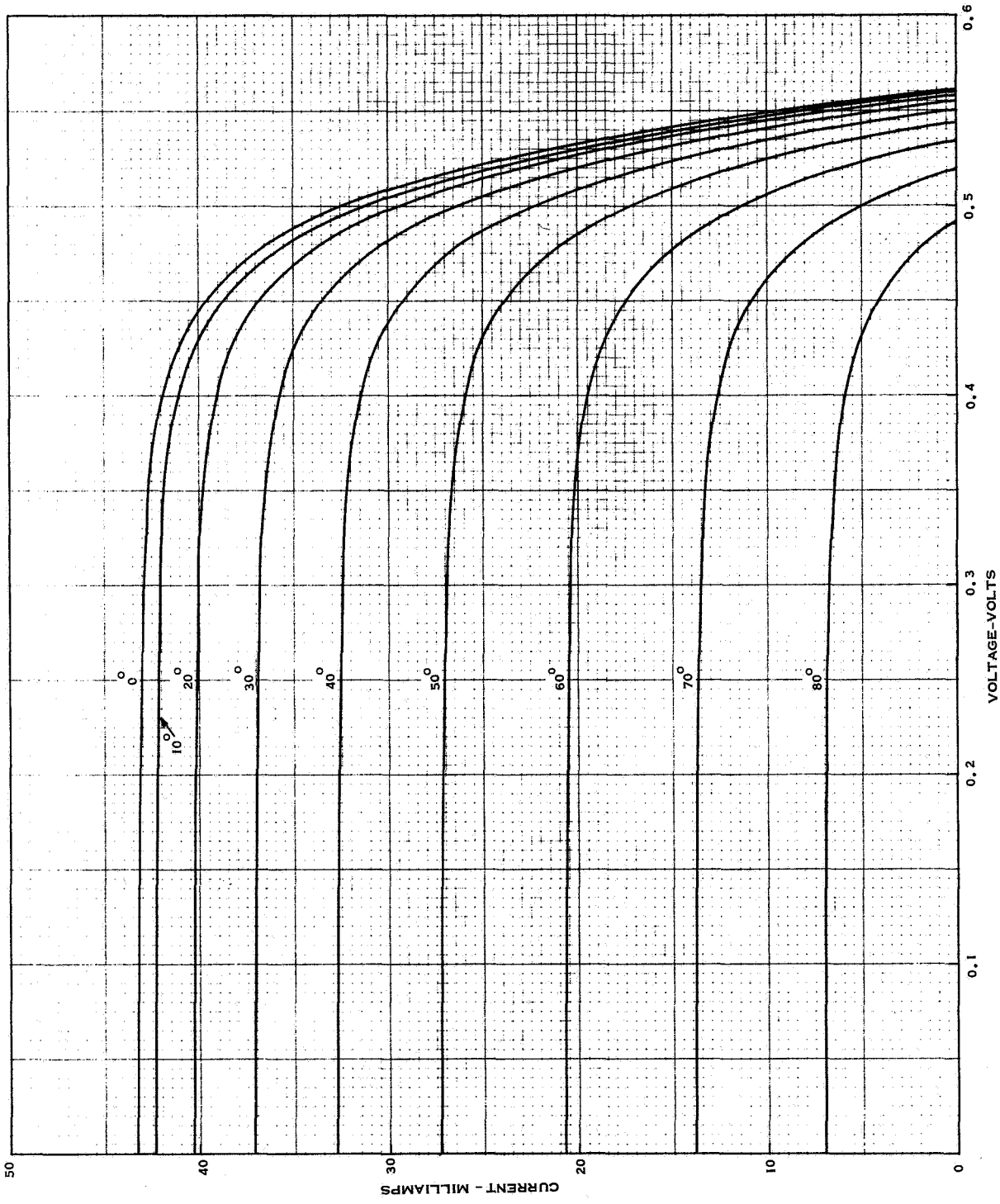

Figure 29 OCLI One Sun Angle of Incidence Characteristics Cell Type 3A

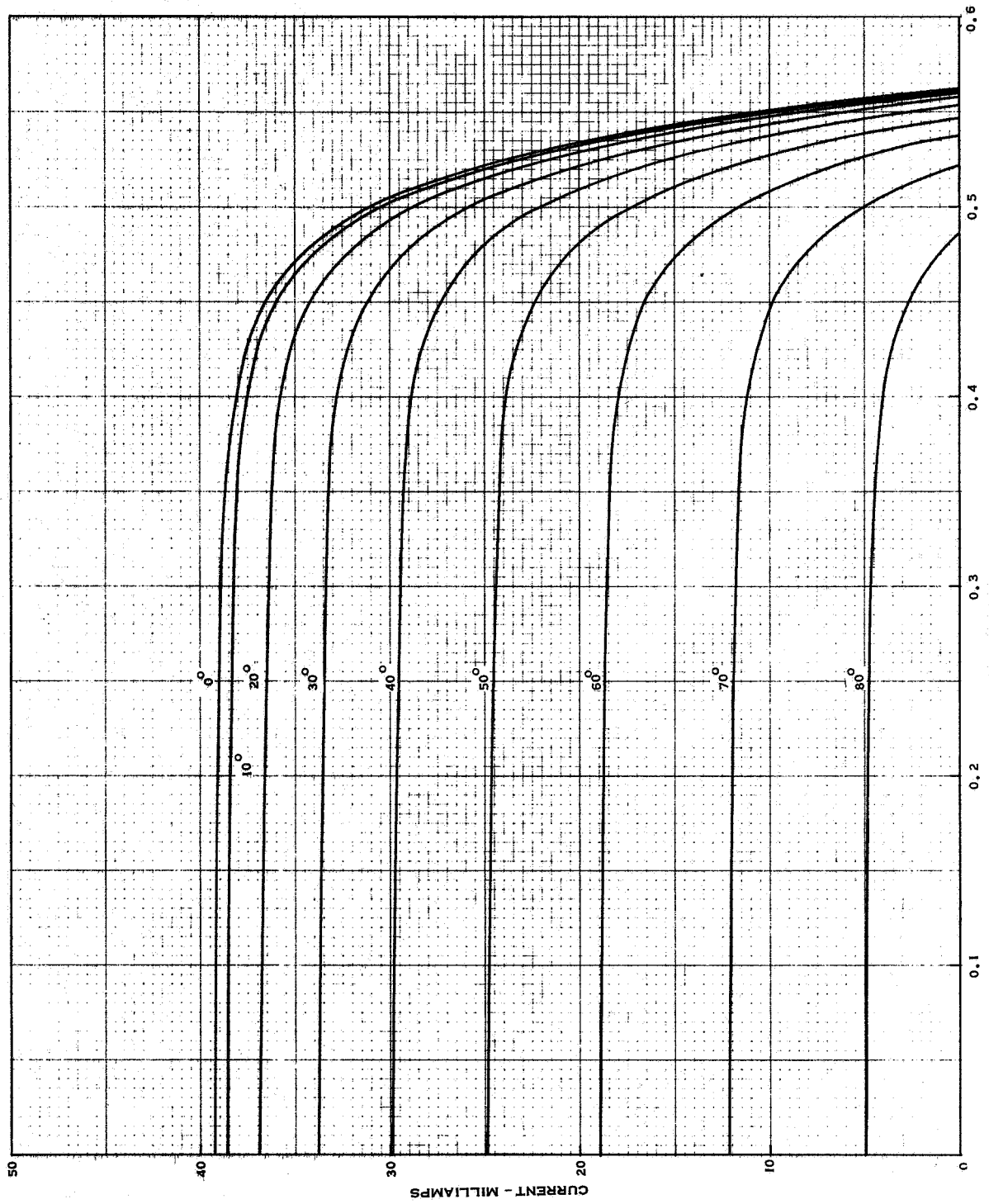

Figure 30 OCLI One Sun Angle of Incidence Characteristics Cell Type 4A

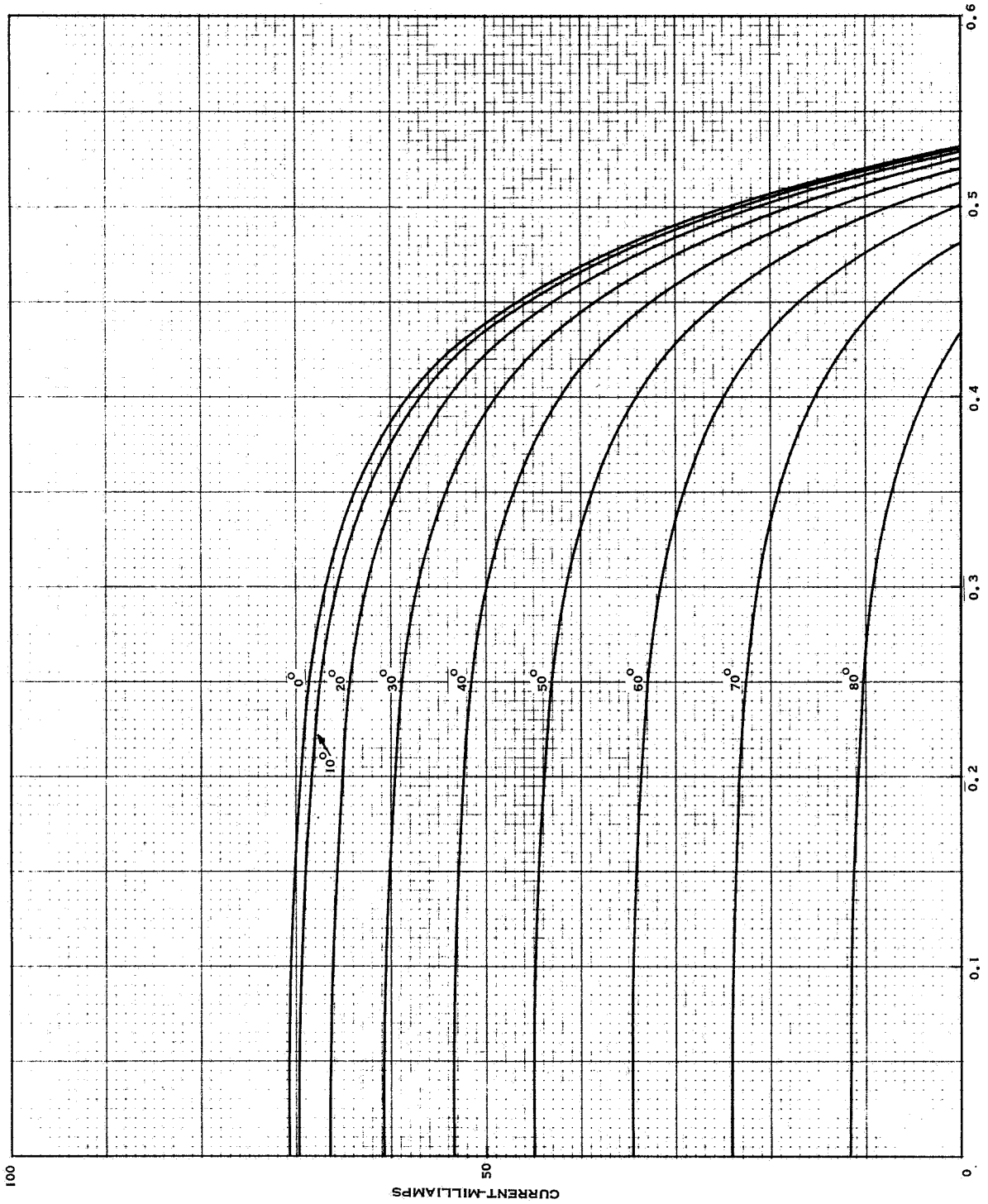

Figure 31 OCLI One Sun Angle of Incidence Characteristics Cell Type 1B

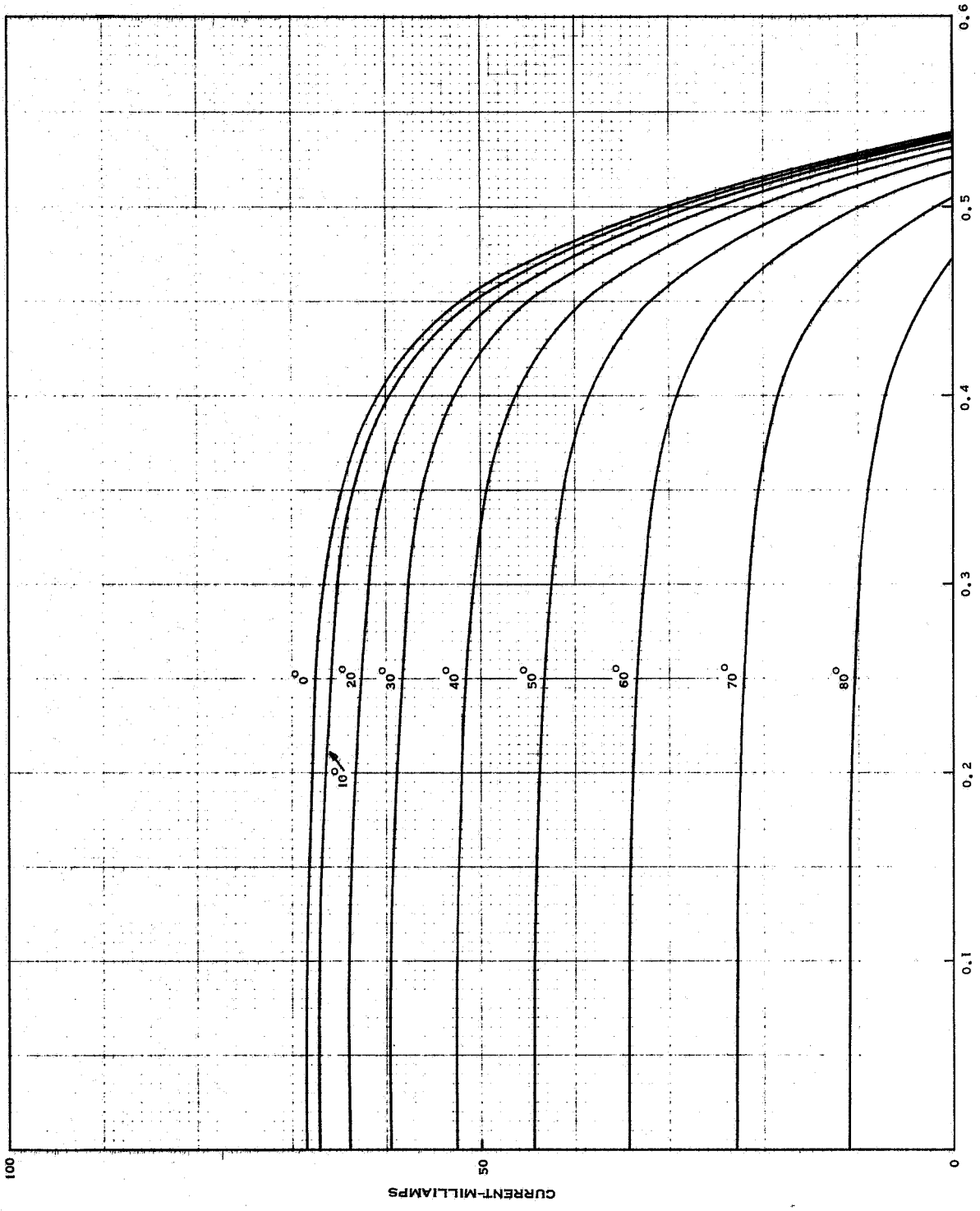

Figure 32 OCLI One Sun Angle of Incidence Characteristics Cell Type 2B

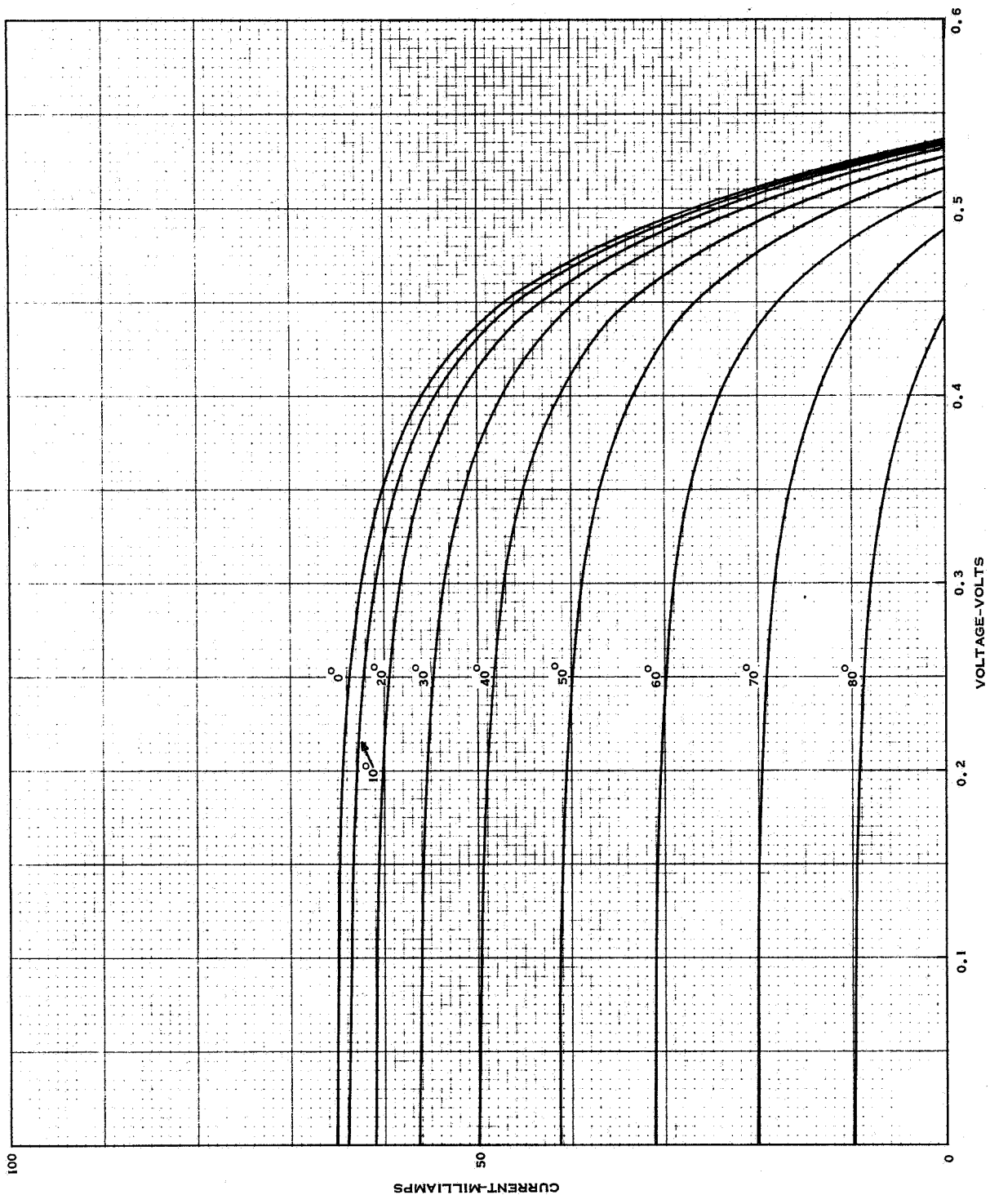

Figure 33 OCLI One Sun Angle of Incidence Characteristics Cell Type 3B

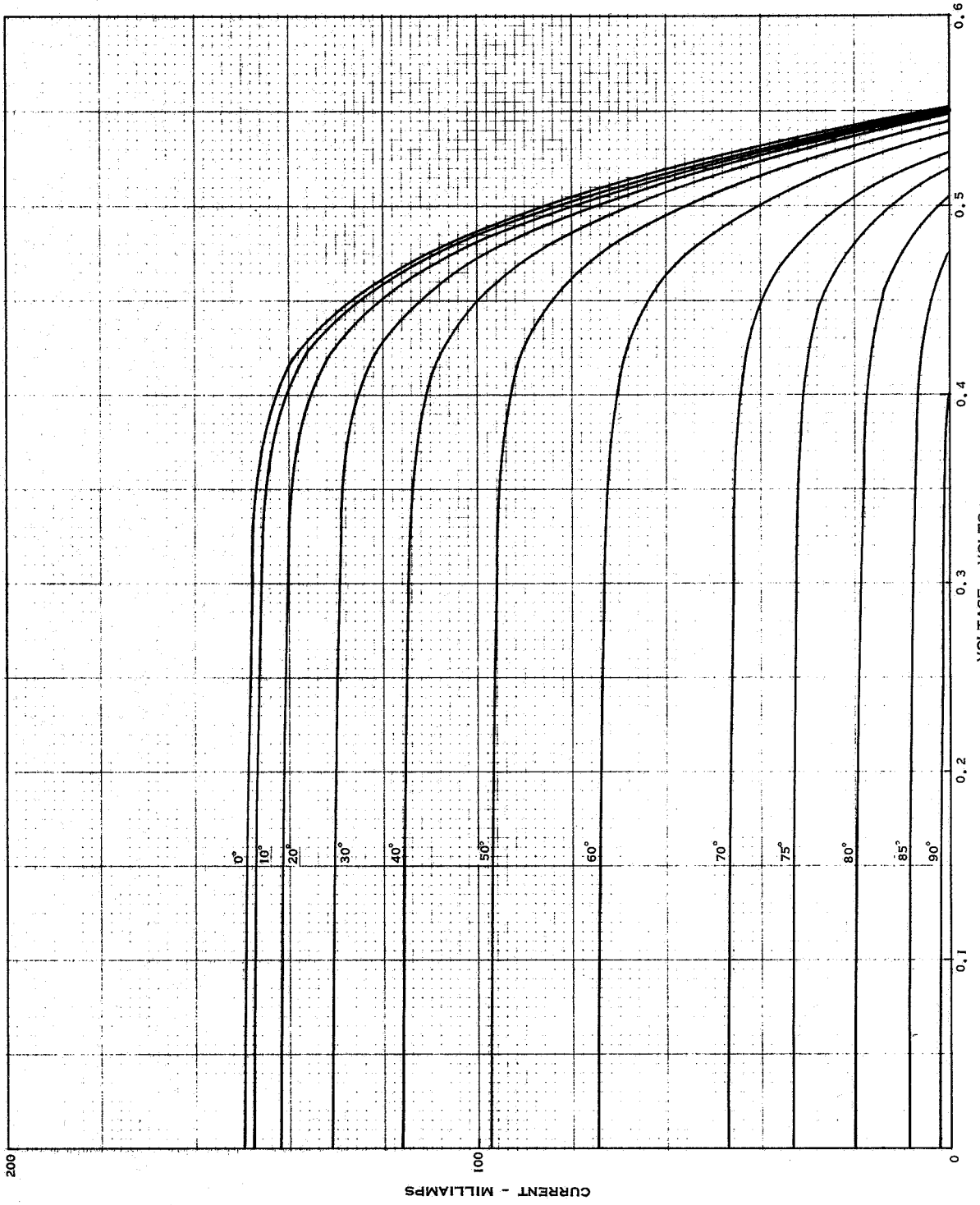

Figure 34 OCLI One Sun Angle of Incidence Characteristics Cell Type IC

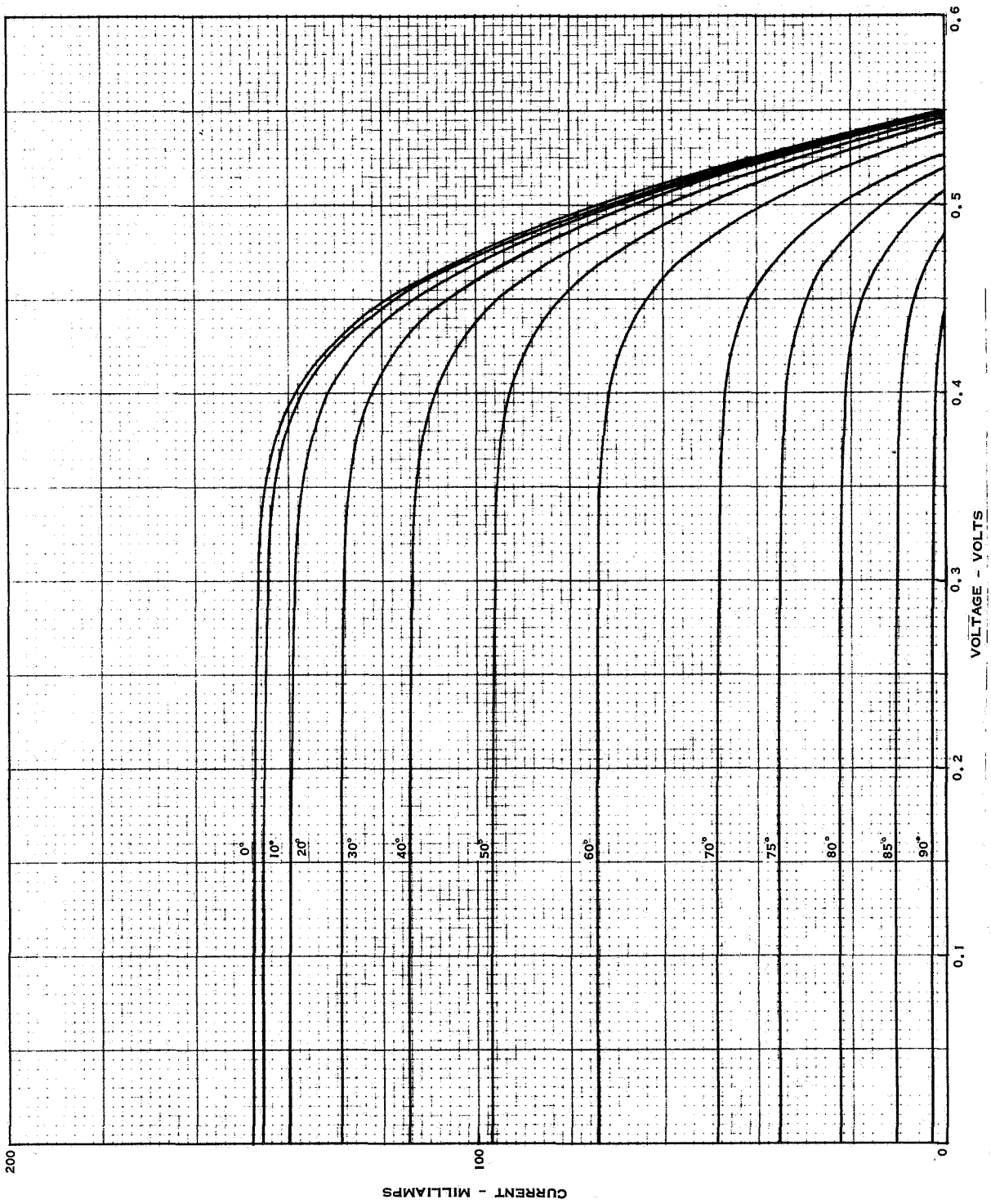

Figure 35 OCLI One Sun Angle of Incidence Characteristics Cell Type 2C

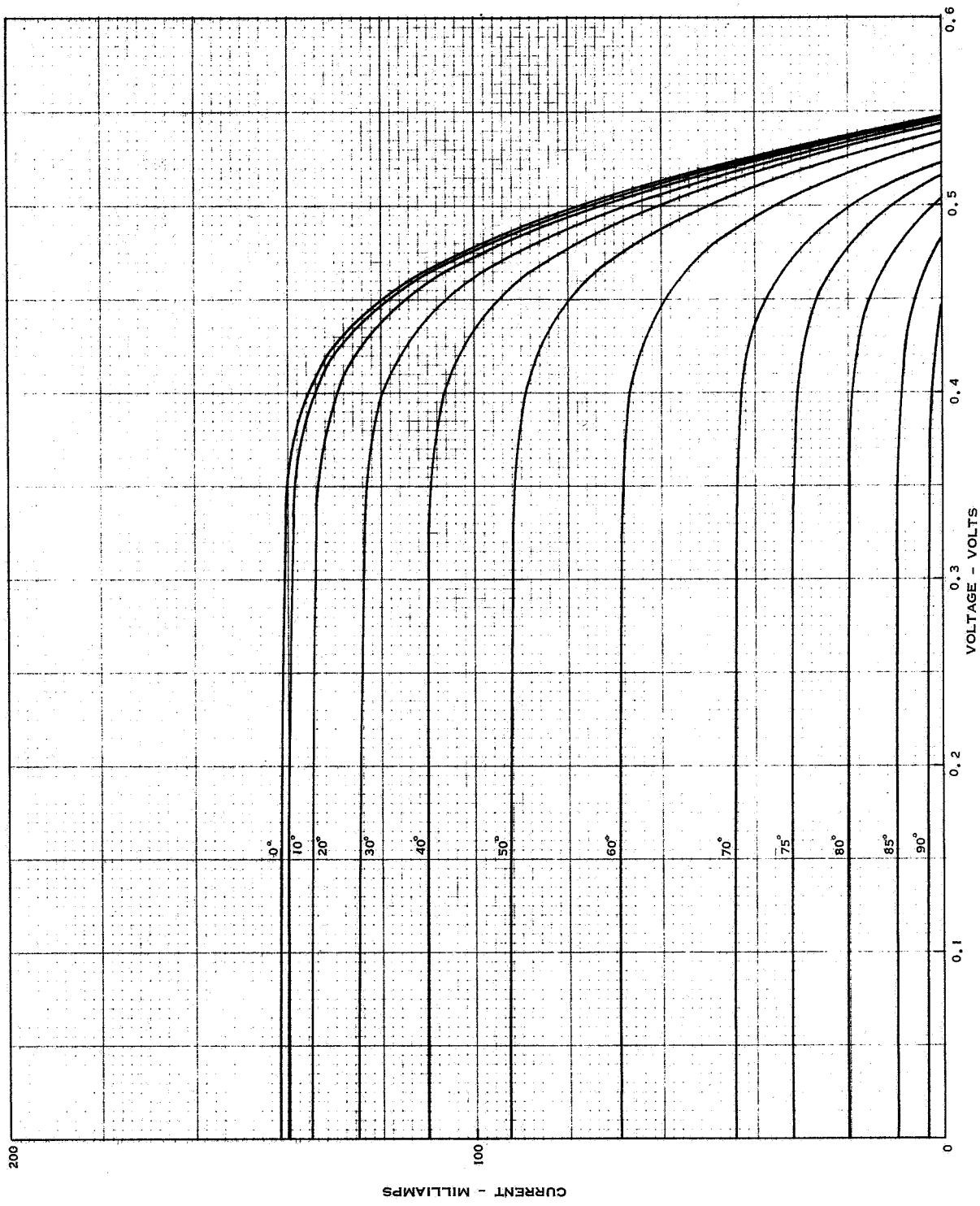

Figure 36 OCLI One Sun Angle of Incidence Characteristics Cell Type 3C

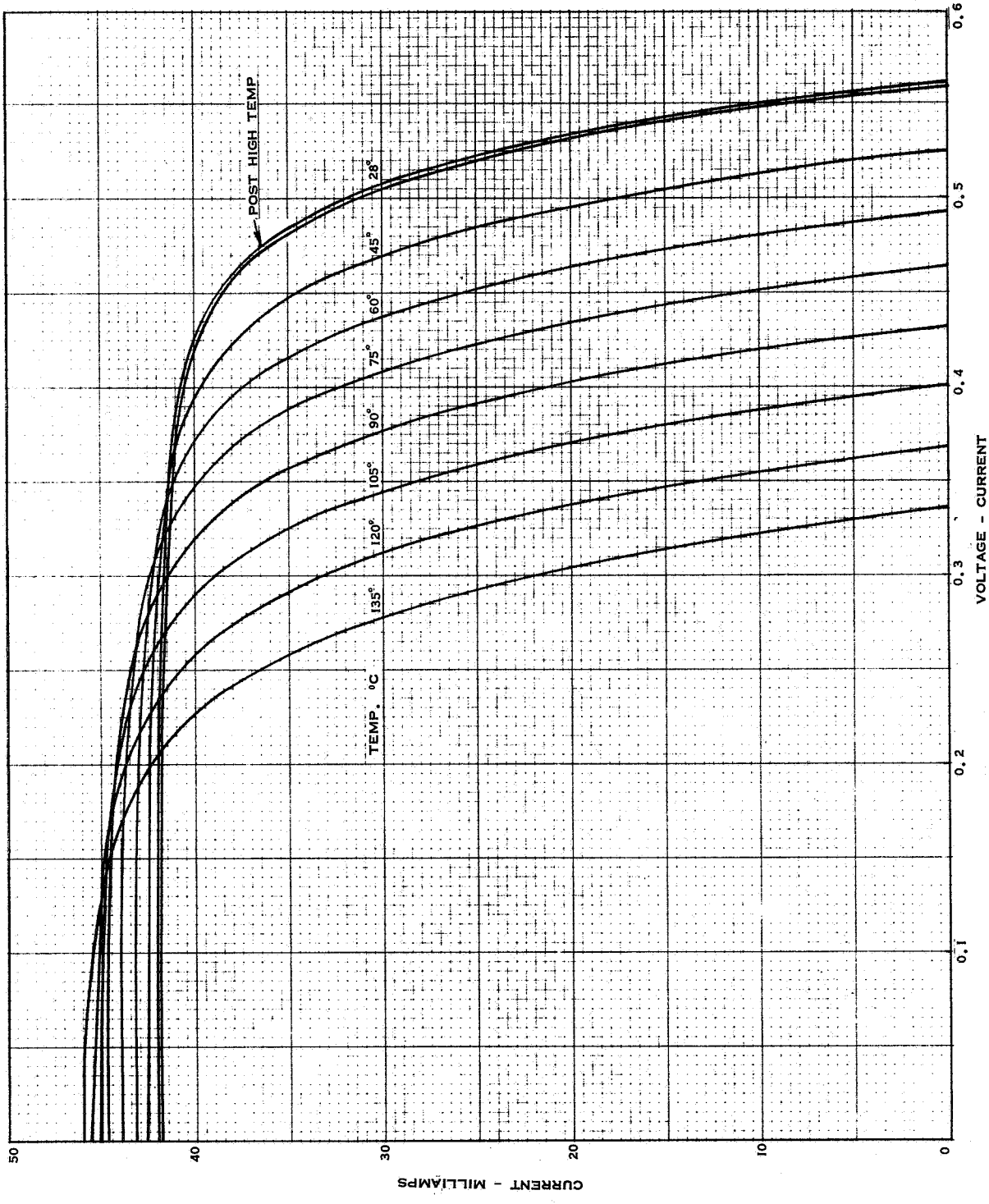

Figure 37 I-V Characteristics as a Function of Temperature Cell Type 1A

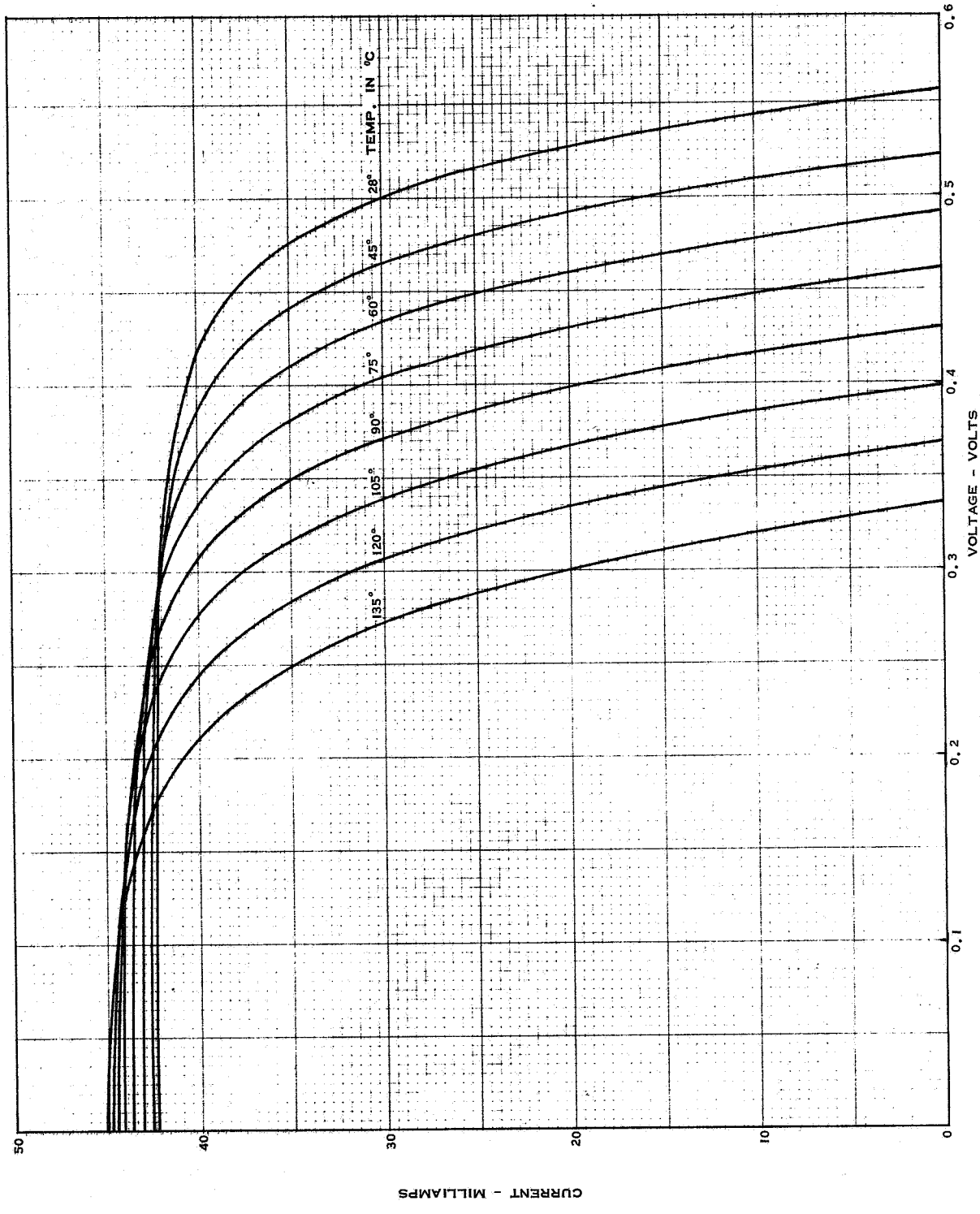

Figure 38 I-V Characteristics as a Function of Temperature Cell Type 2A

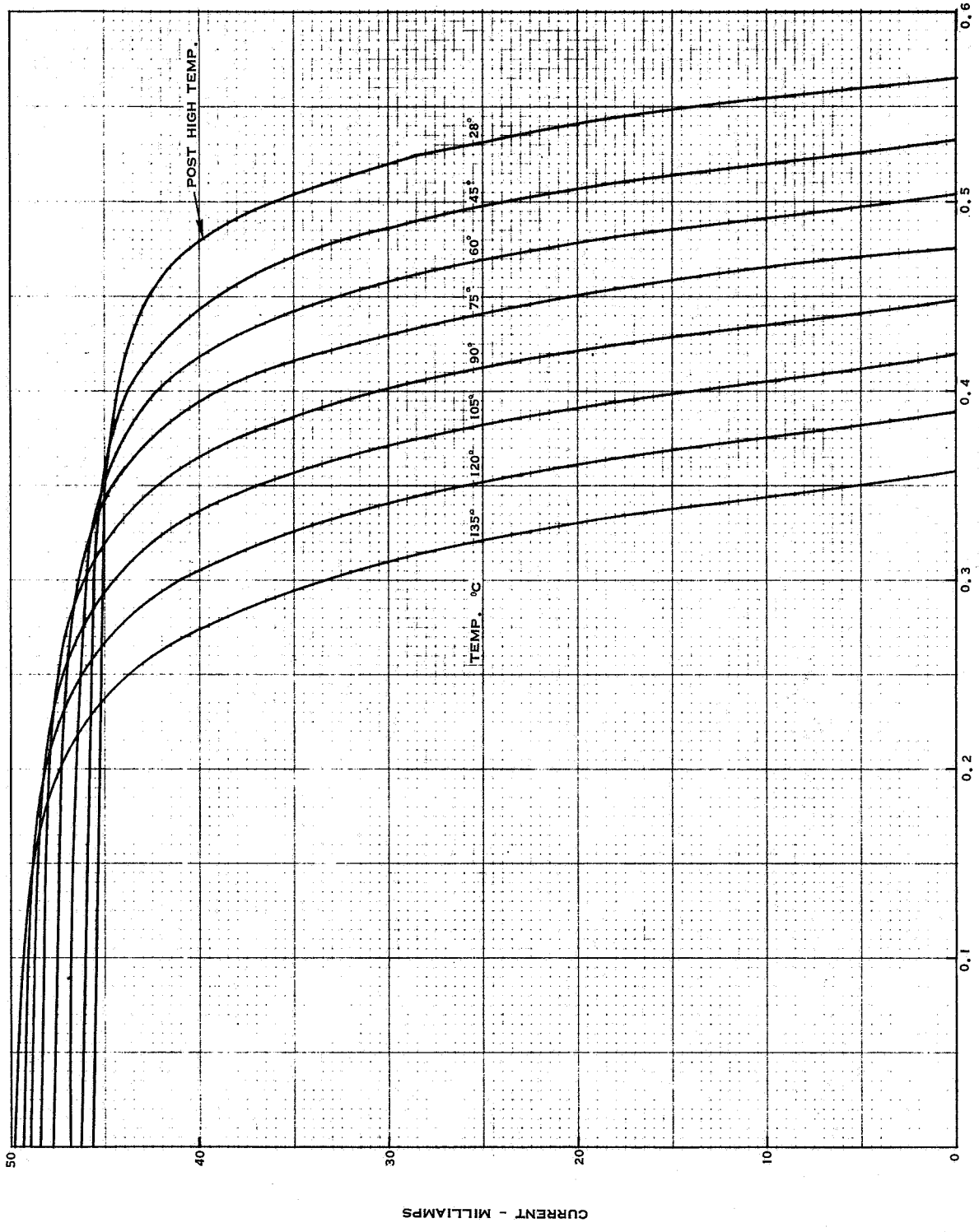

Figure 39 I-V Characteristics as a Function of Temperature Cell Type 3A

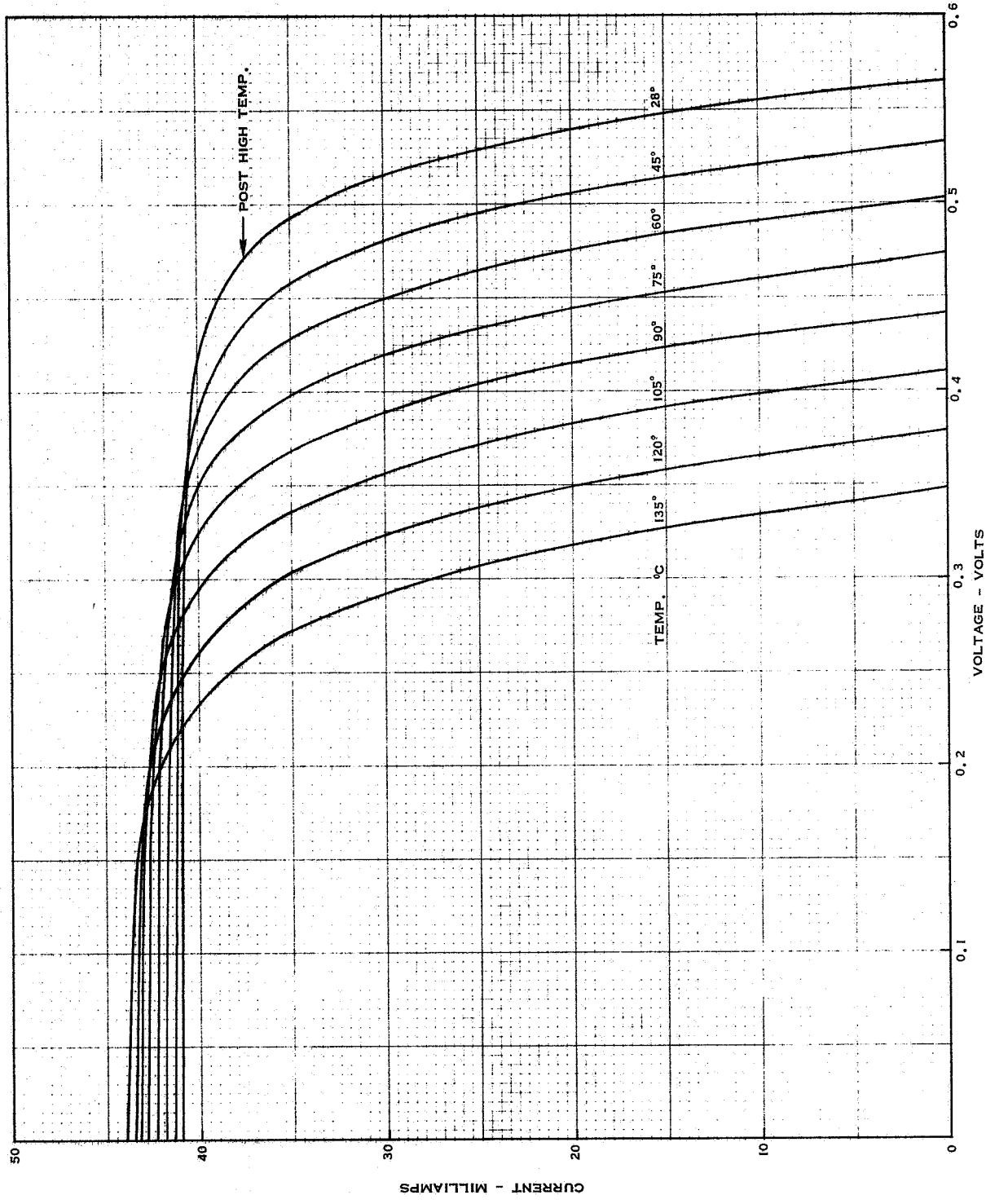

Figure 40 I-V Characteristics as a Function of Temperature Cell Type 4A

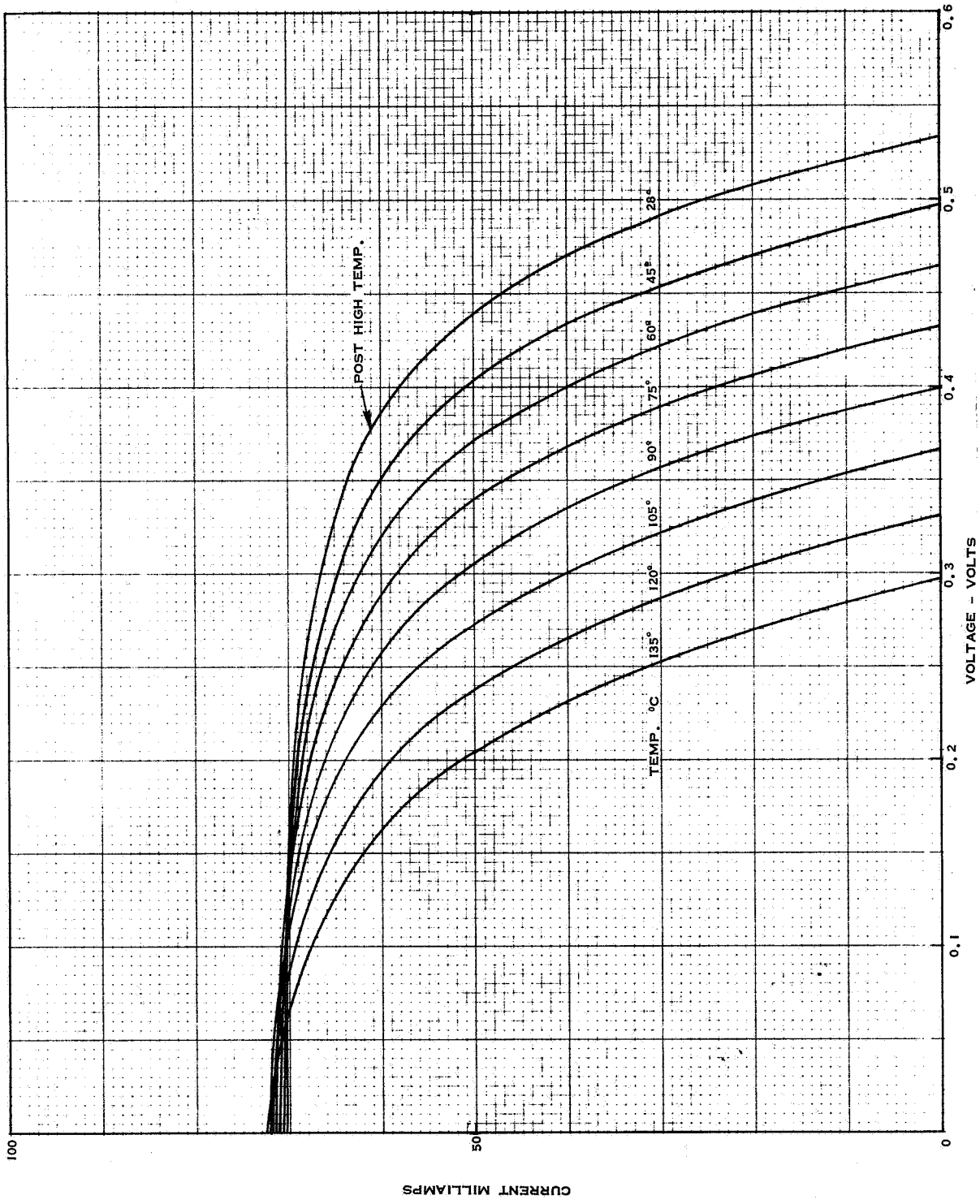

Figure 41 I-V Characteristics as a Function of Temperature Cell Type 1B

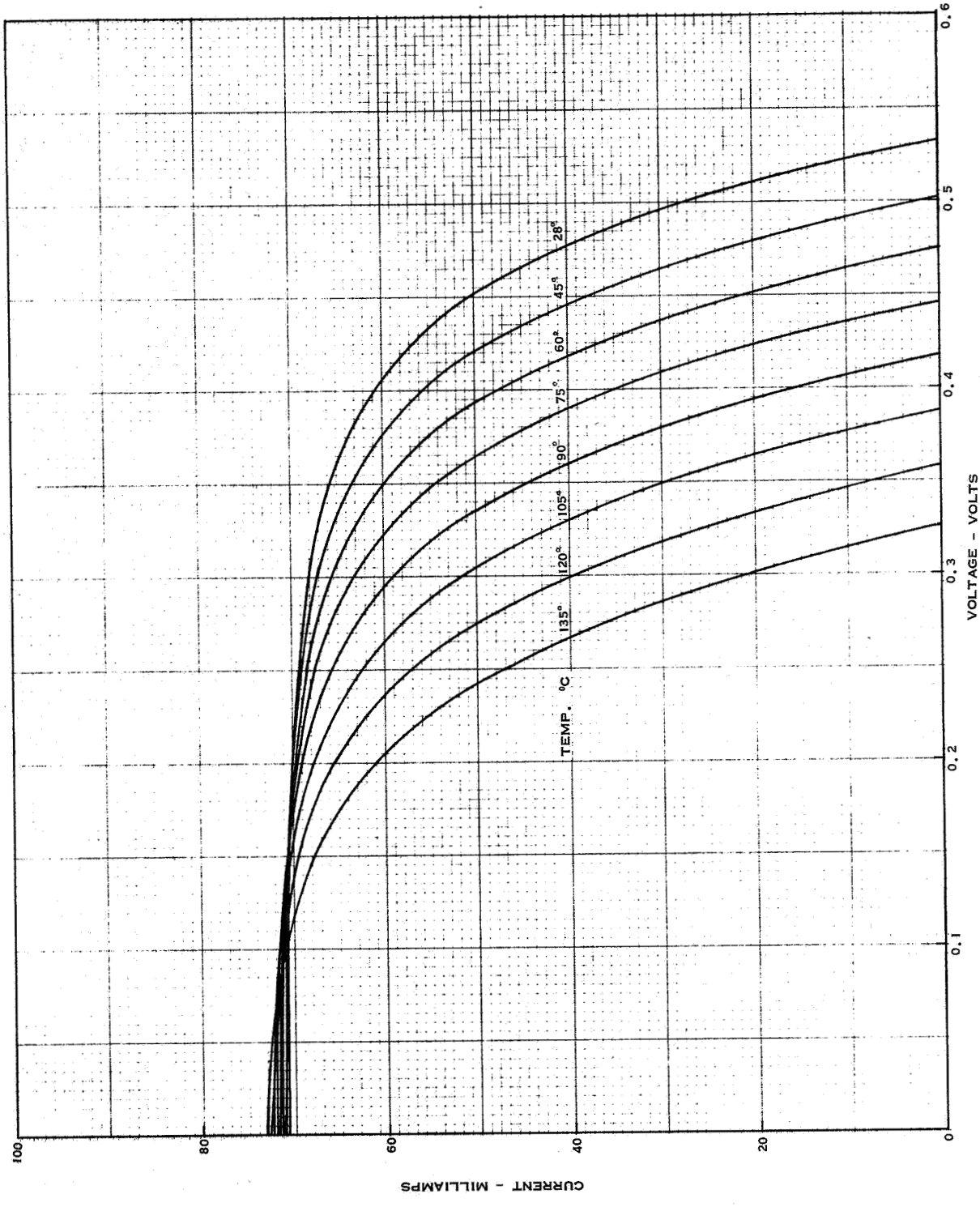

Figure 42 I-V Characteristics as a Function of Temperature Cell Type 2B

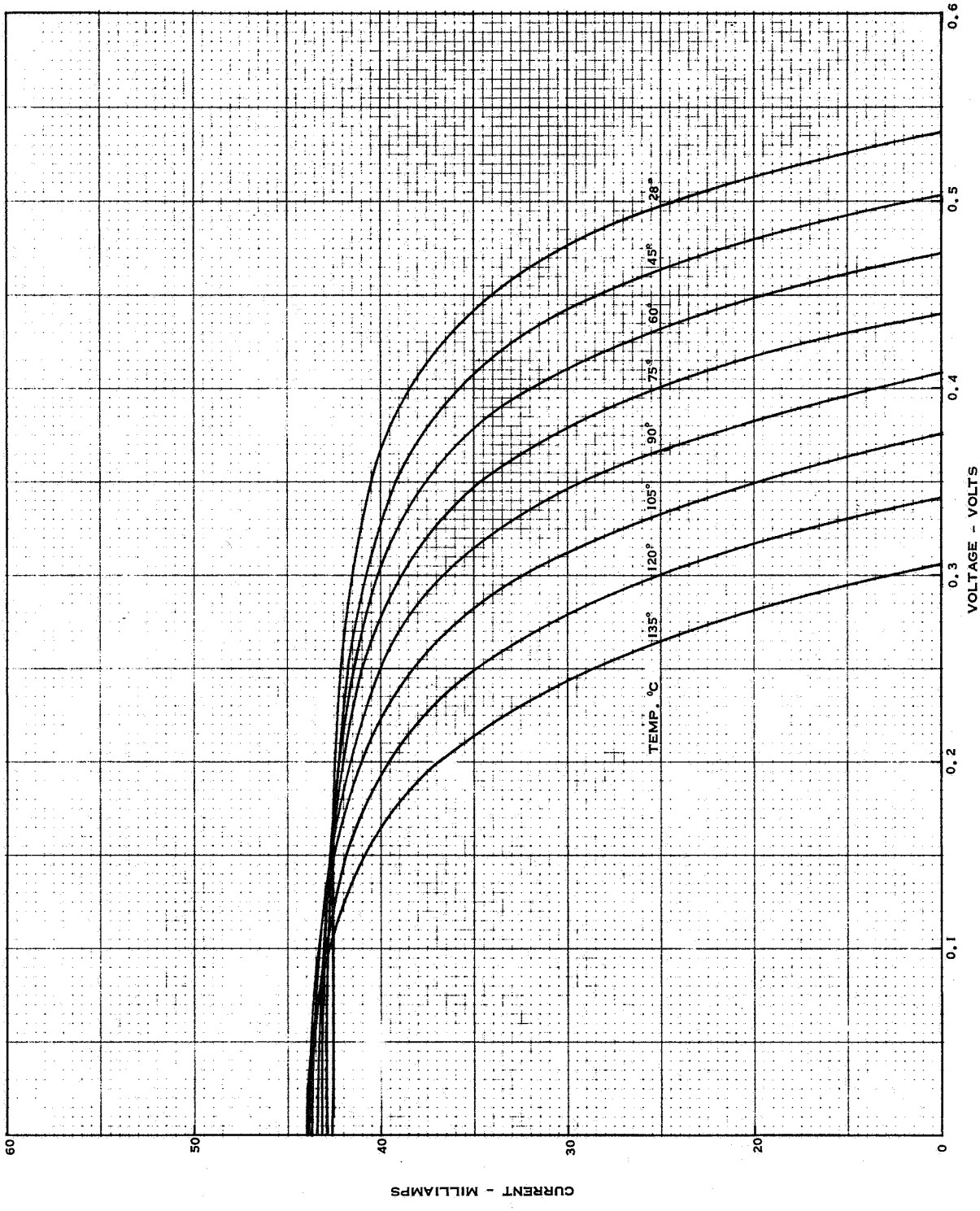

Figure 43 Characteristics as a Function of Temperature Cell Type 3B

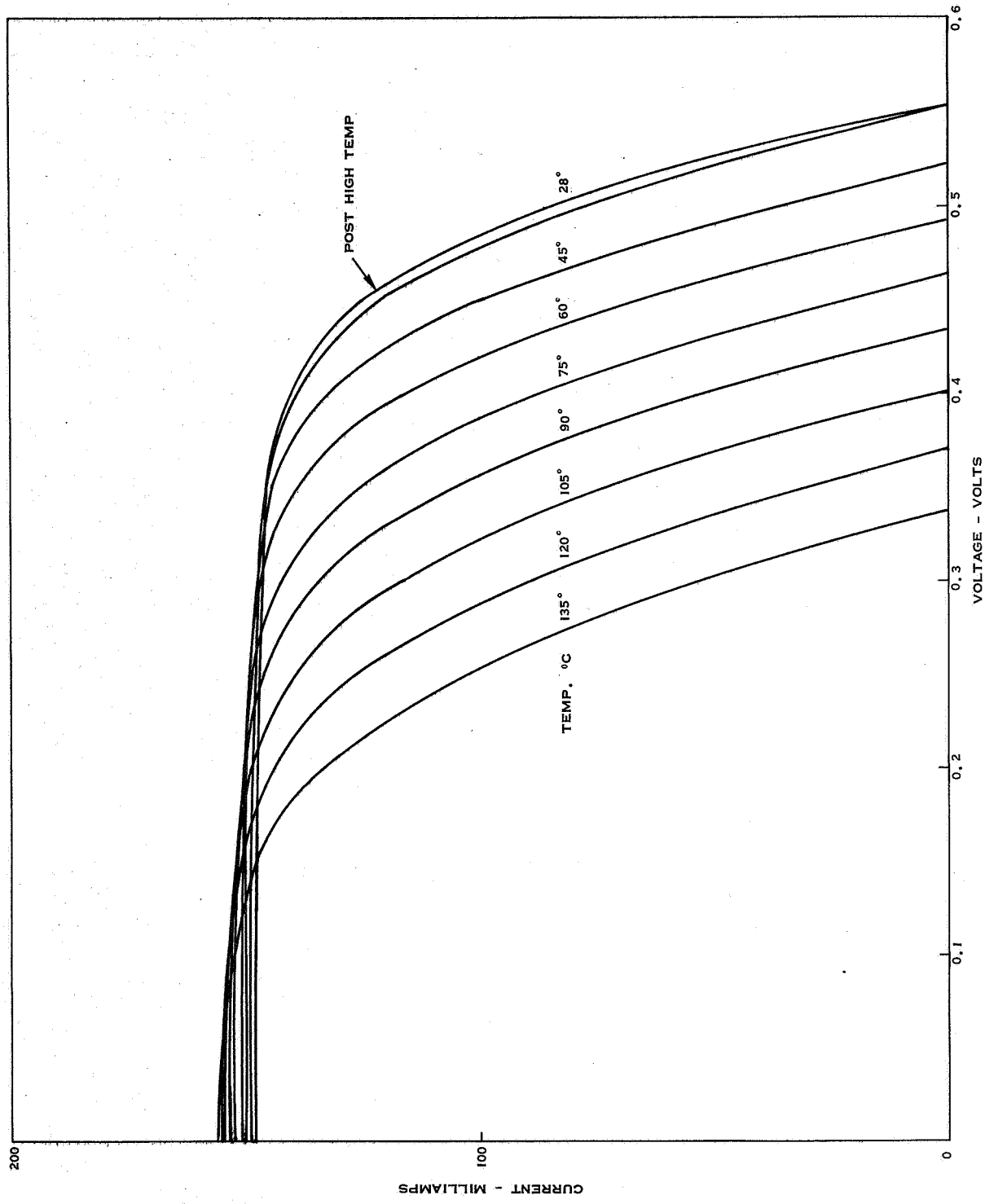

Figure 44 I-V Characteristics as a Function of Temperature Cell Type 1C

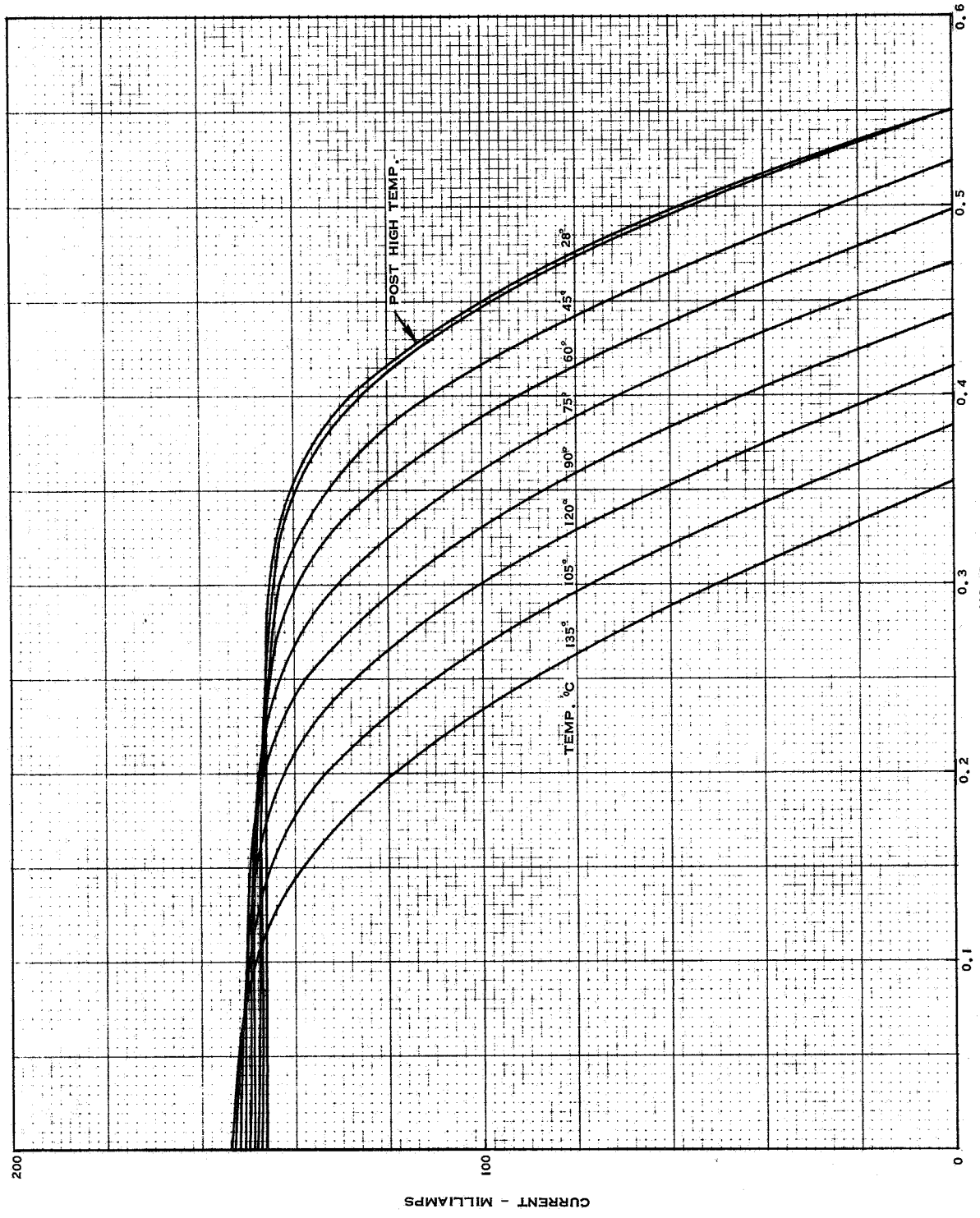

Figure 45 I-V Characteristics as a Function of Temperature Cell Type 2C

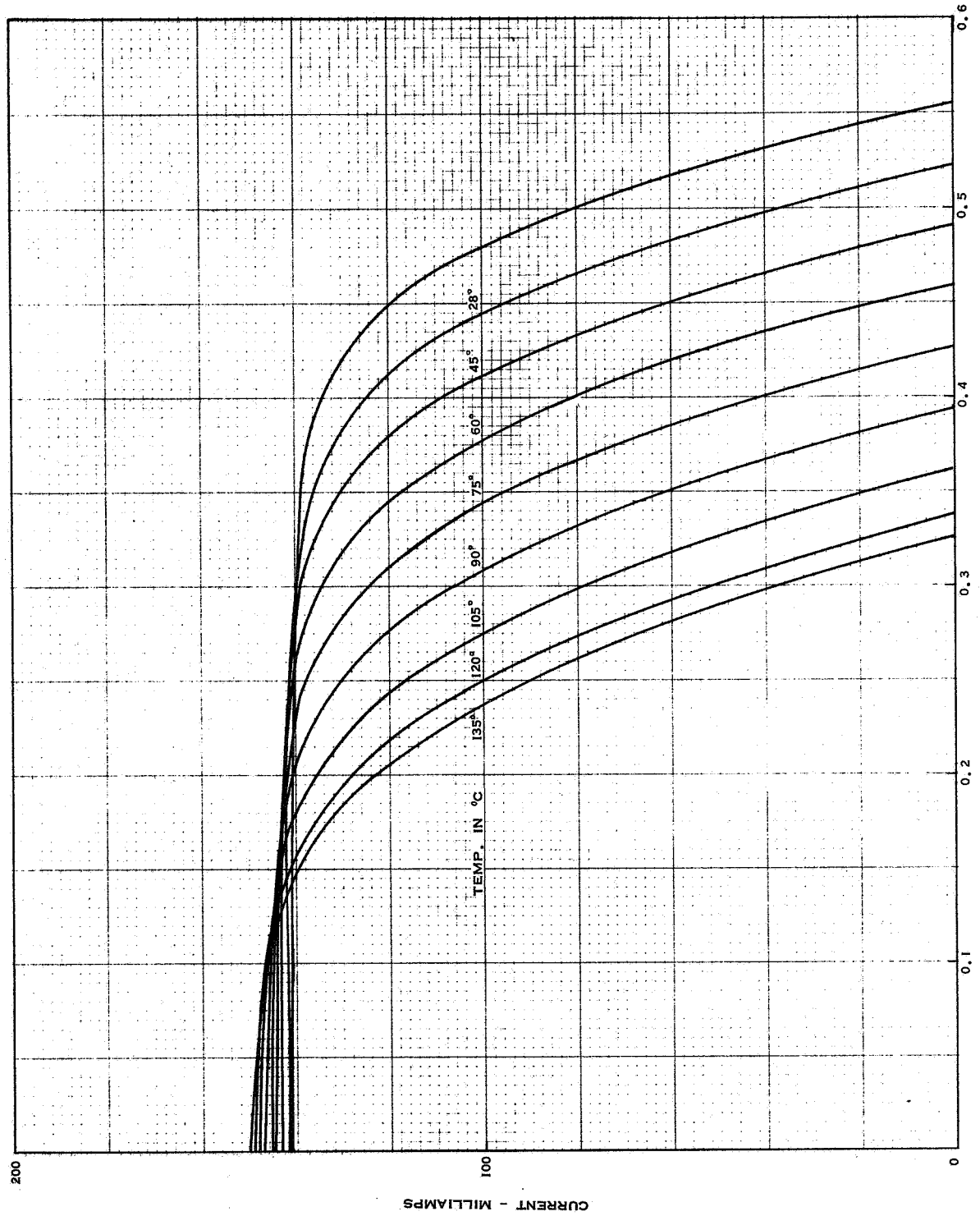

Figure 46 I-V Characteristics as a Function of Temperature Cell Type 3C

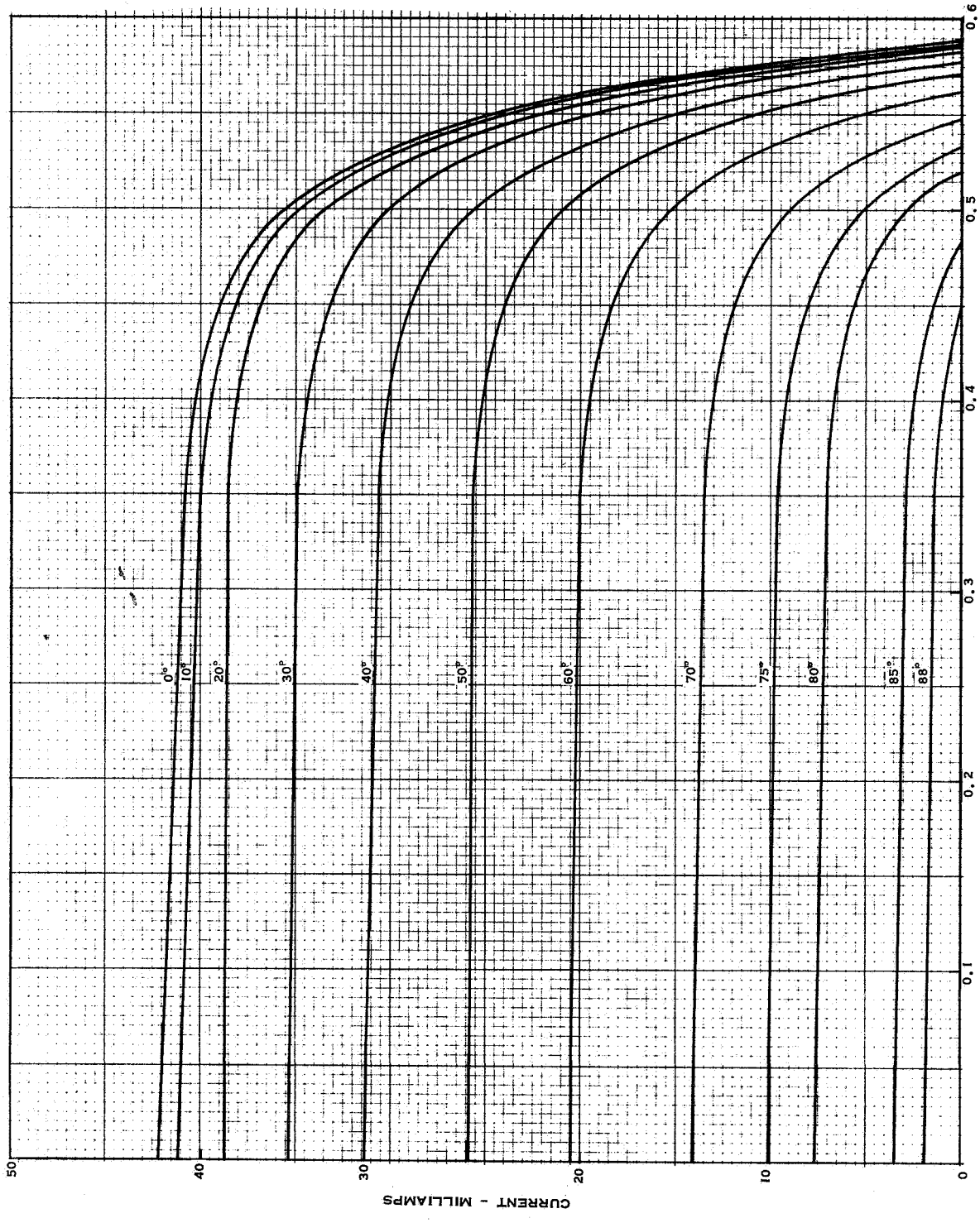

Figure 47 Carbon Arc One Sun I-V Characteristics Cell Type 1A at Various Angles of Incidence

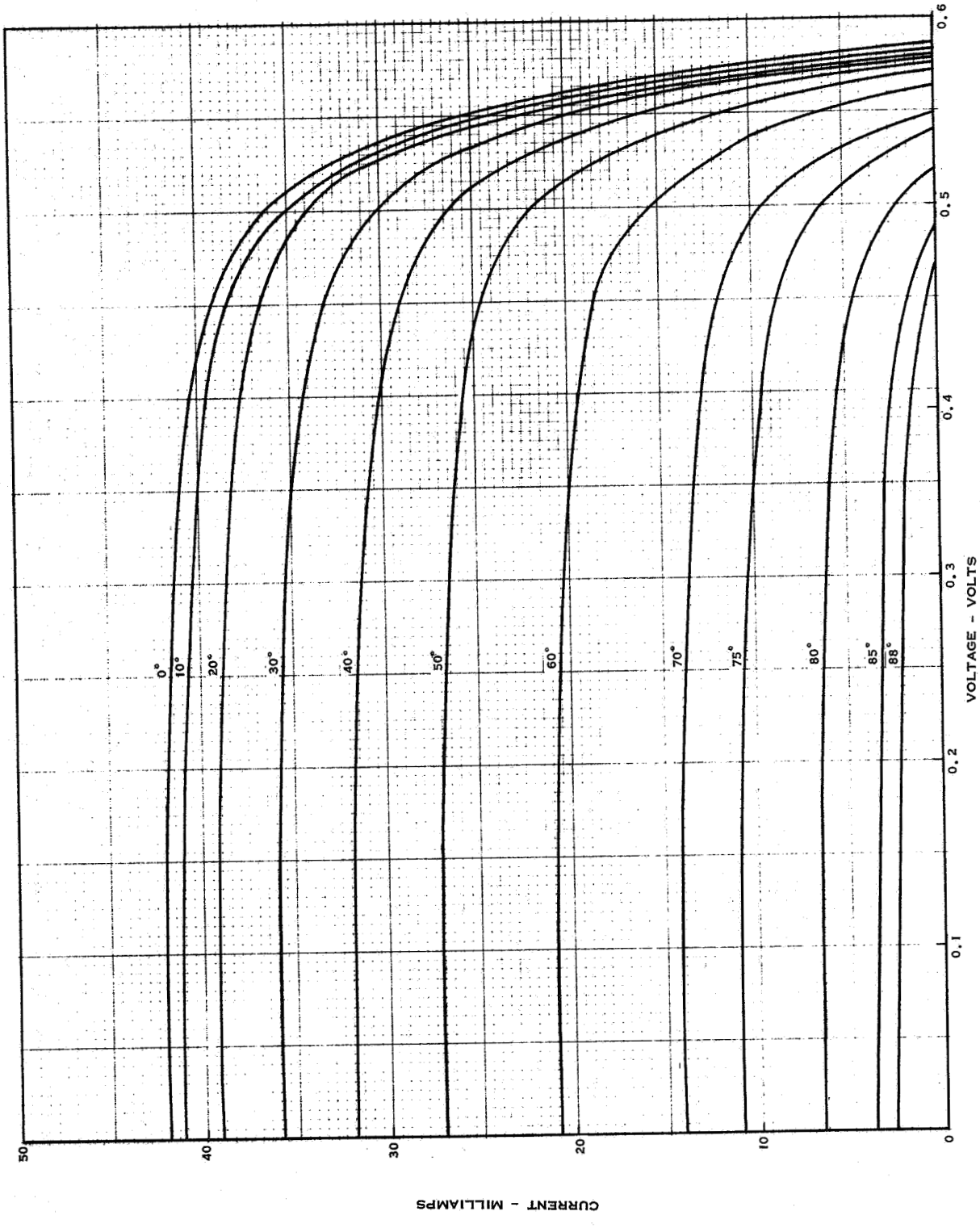

Figure 48 Carbon Arc One Sun I-V Characteristics Cell Type 2A at Various Angles of Incidence

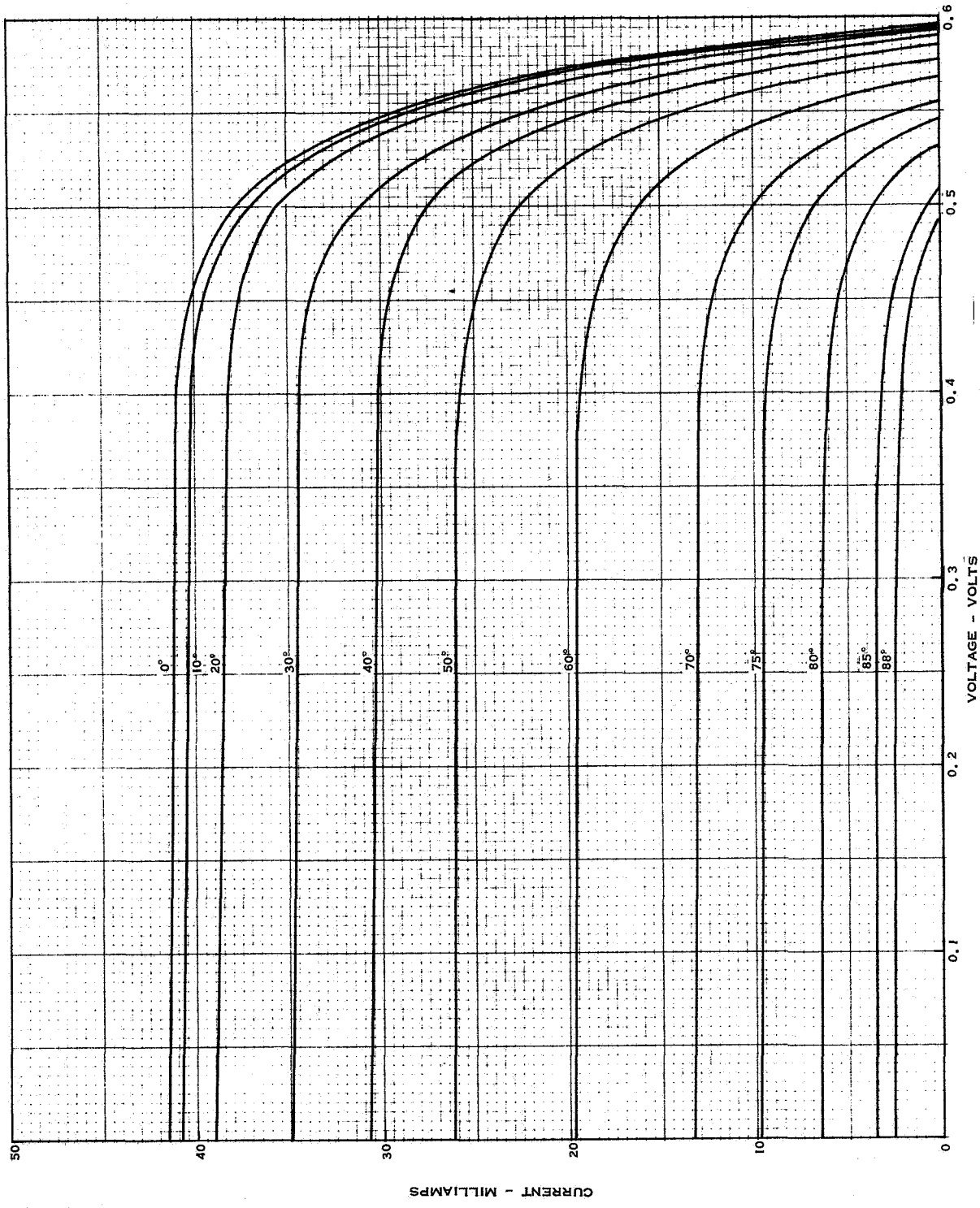

Figure 49 Carbon Arc One Sun I-V Characteristics Cell Type 3A at Various Angles of Incidence

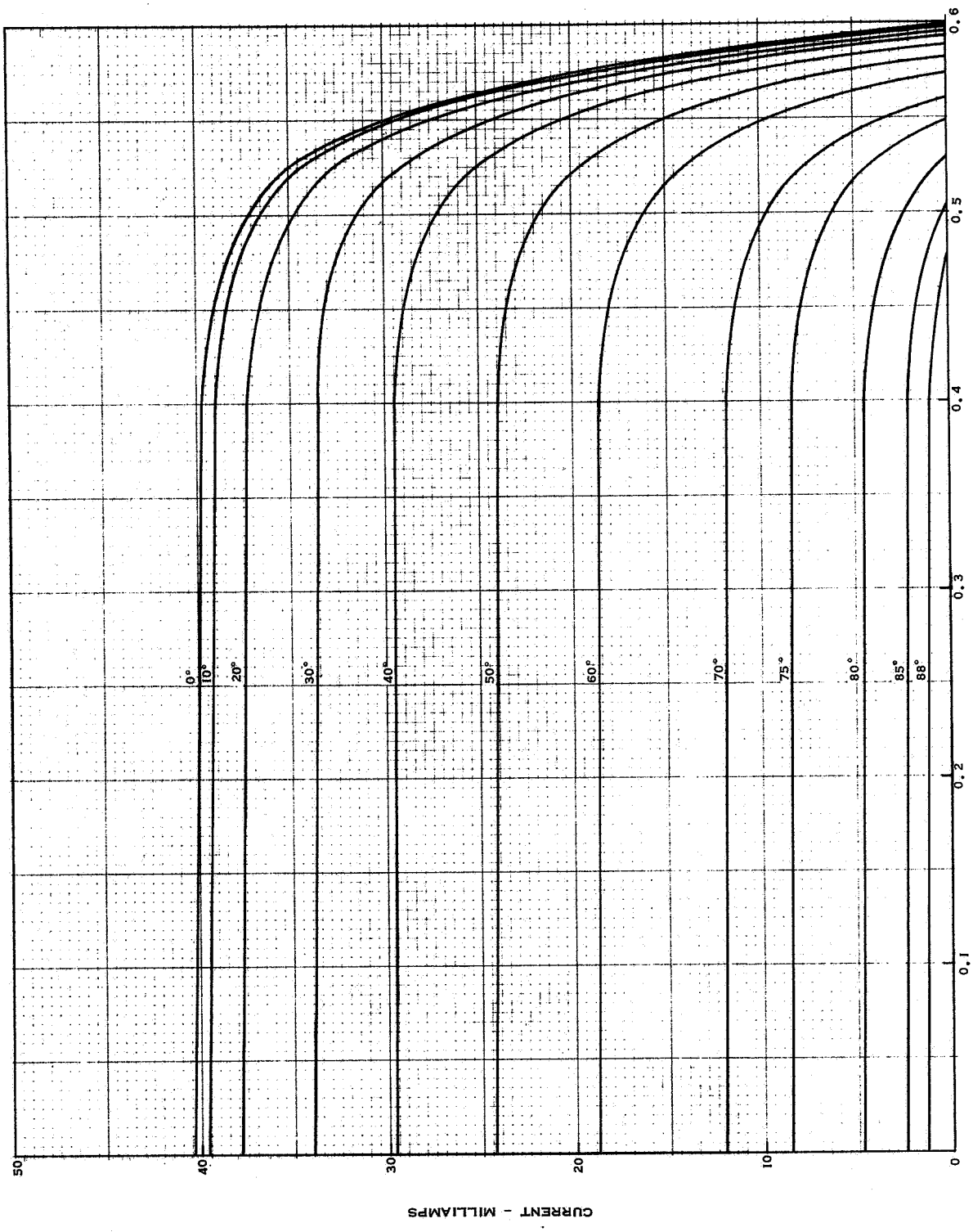

Figure 50 Carbon Arc One Sun I-V Characteristics Cell Type 4A at Various Angles of Incidence

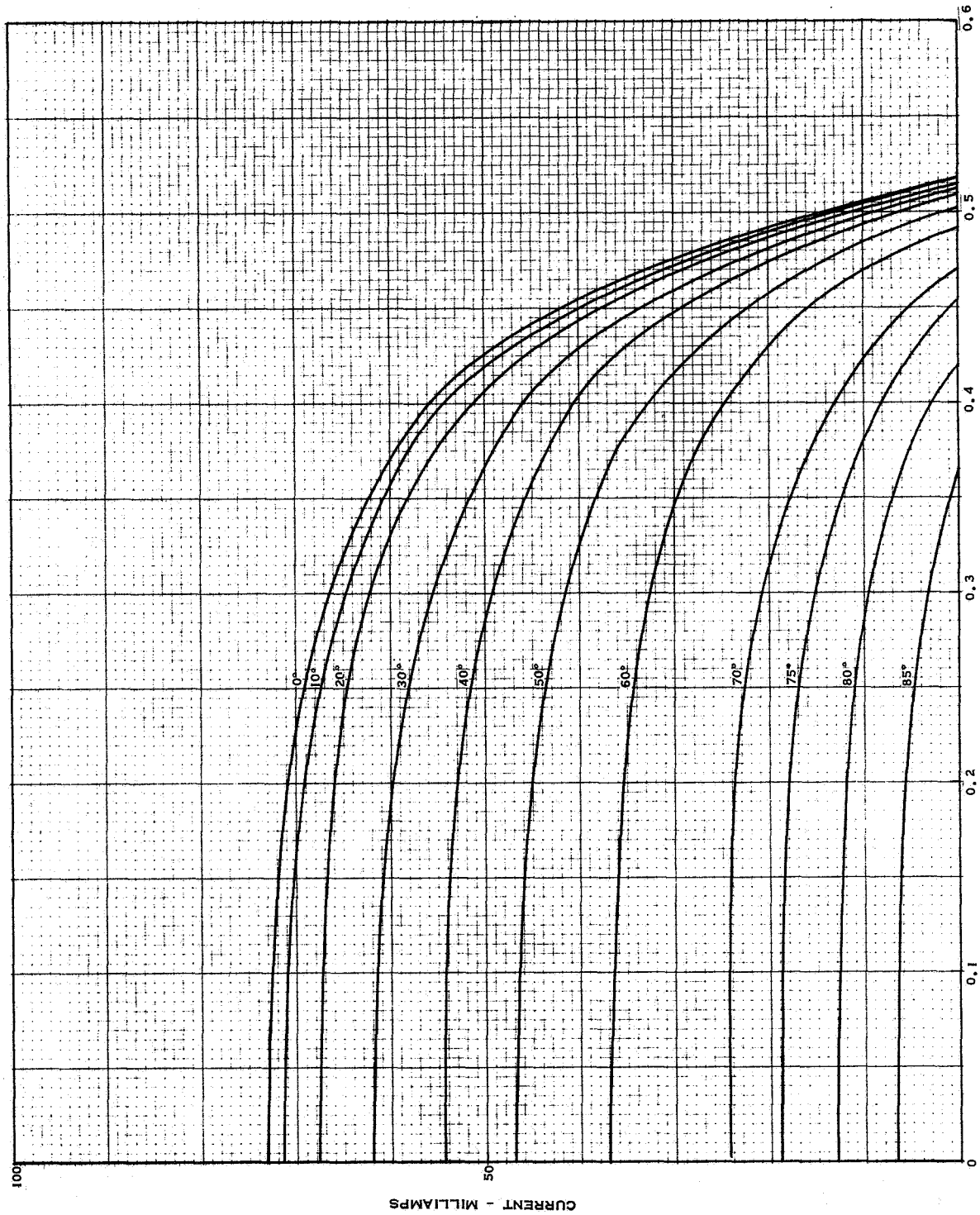

Figure 51 Carbon Arc One Sun I-V Characteristics Cell Type 1B at Various Angles of Incidence

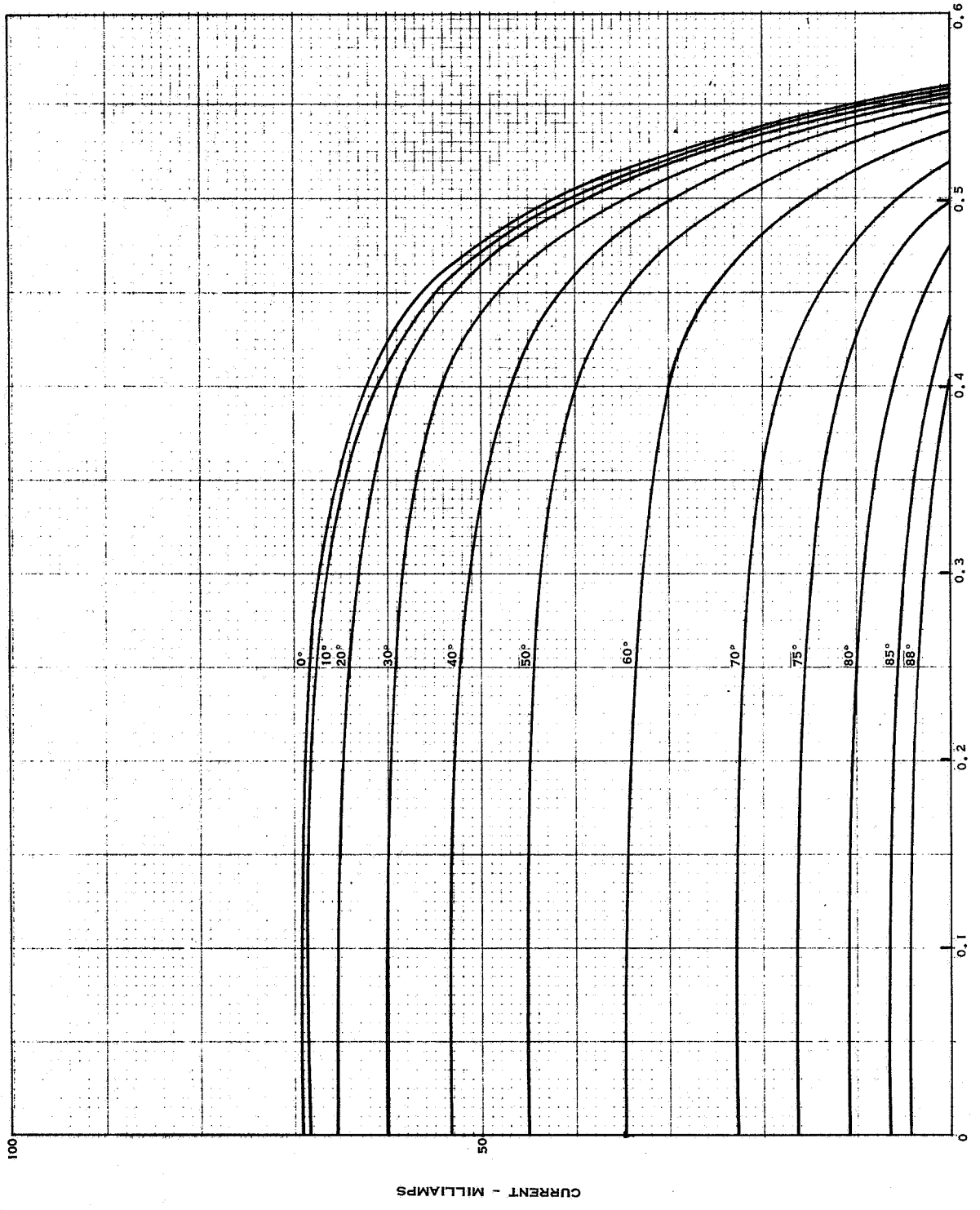

Figure 52 Carbon Arc One Sun I-V Characteristics Cell Type 2B at Various Angles of Incidence

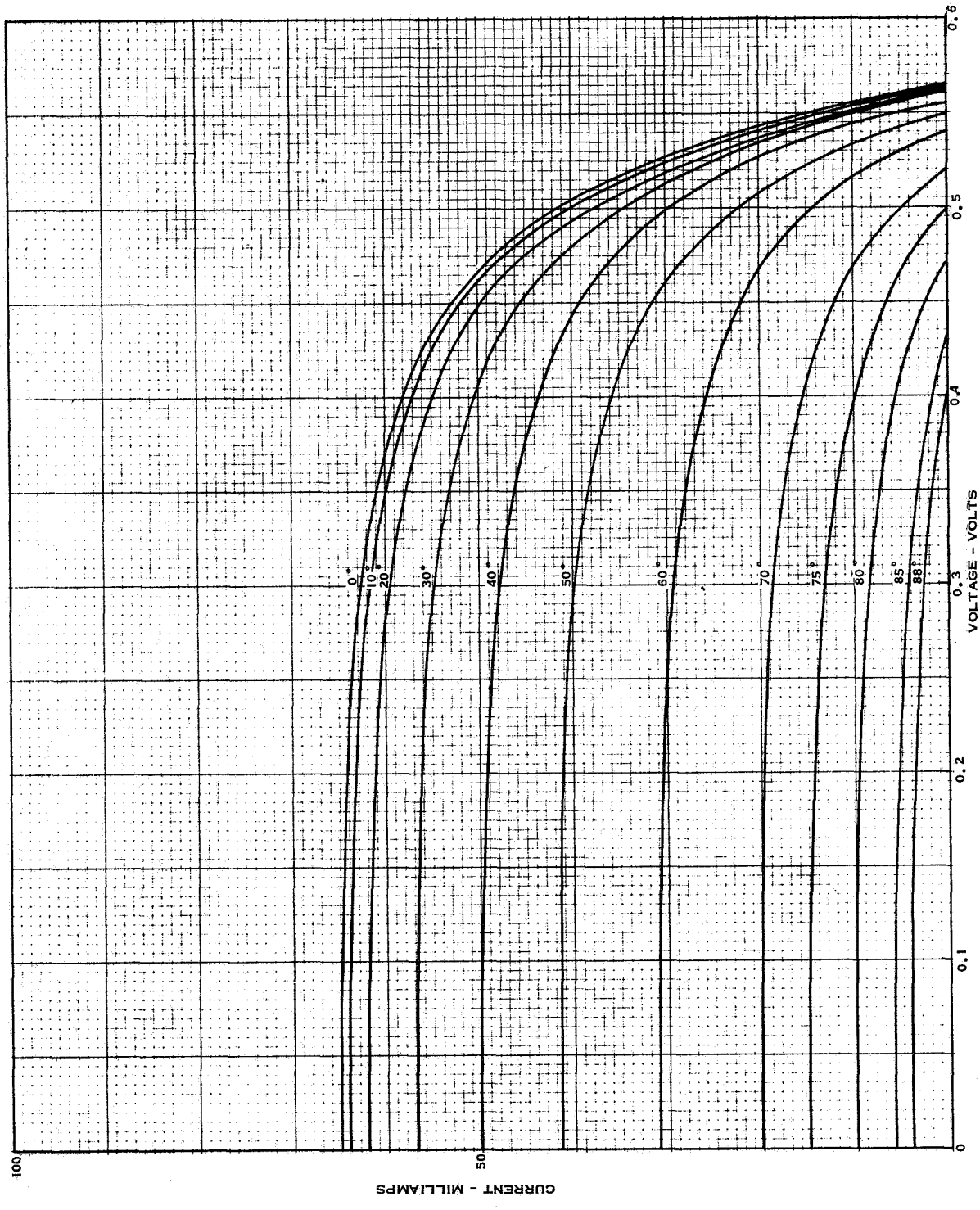

Figure 53 Carbon Arc One Sun I-V Characteristics Cell Type 3B at Various Angles of Incidence

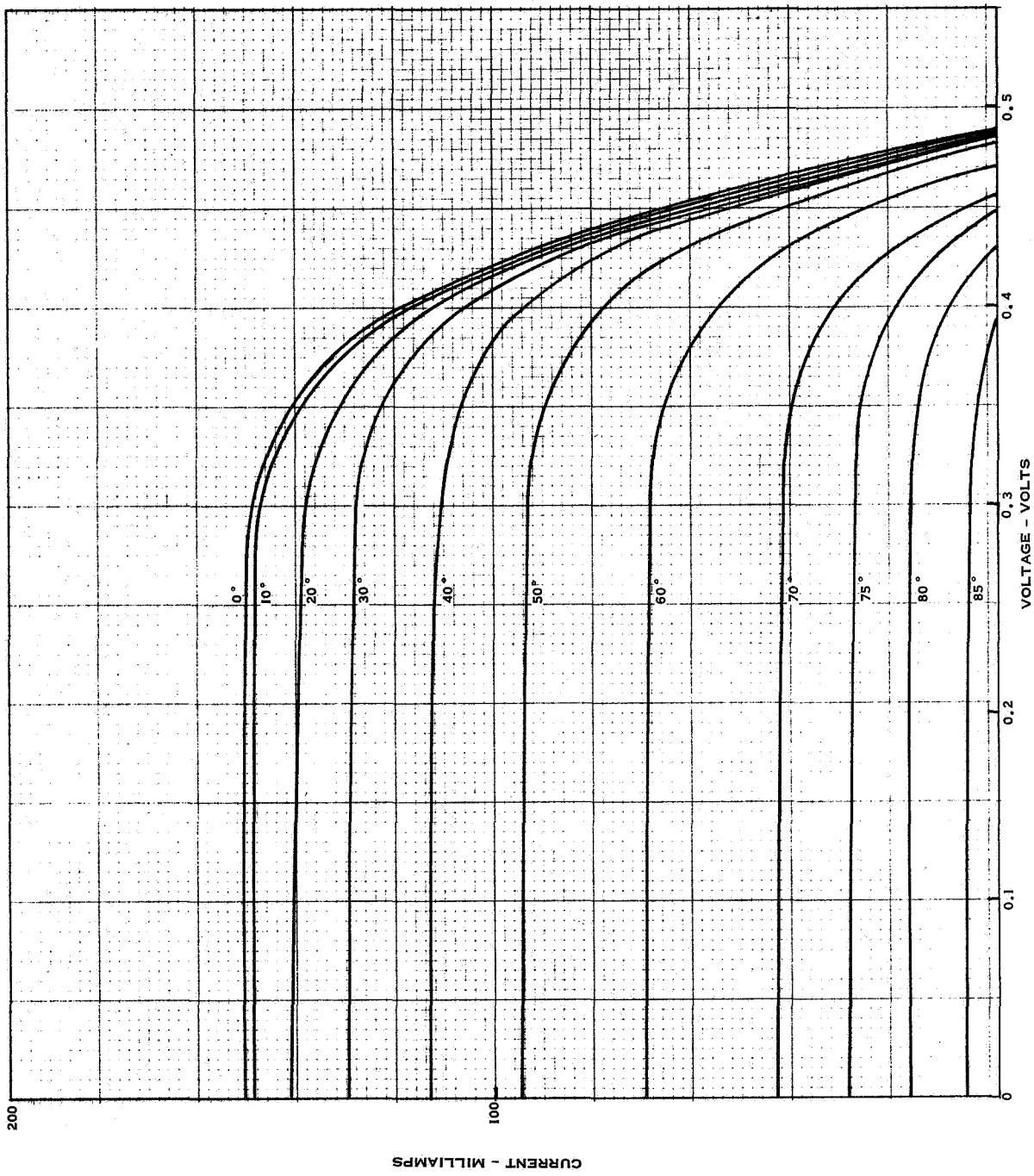

Figure 54 Carbon Arc One Sun I-V Characteristics Cell Type 1C at Various Angles of Incidence

Figure 54 Carbon Arc One Sun I-V Characteristics Cell Type IC at Various Angles of Incidence

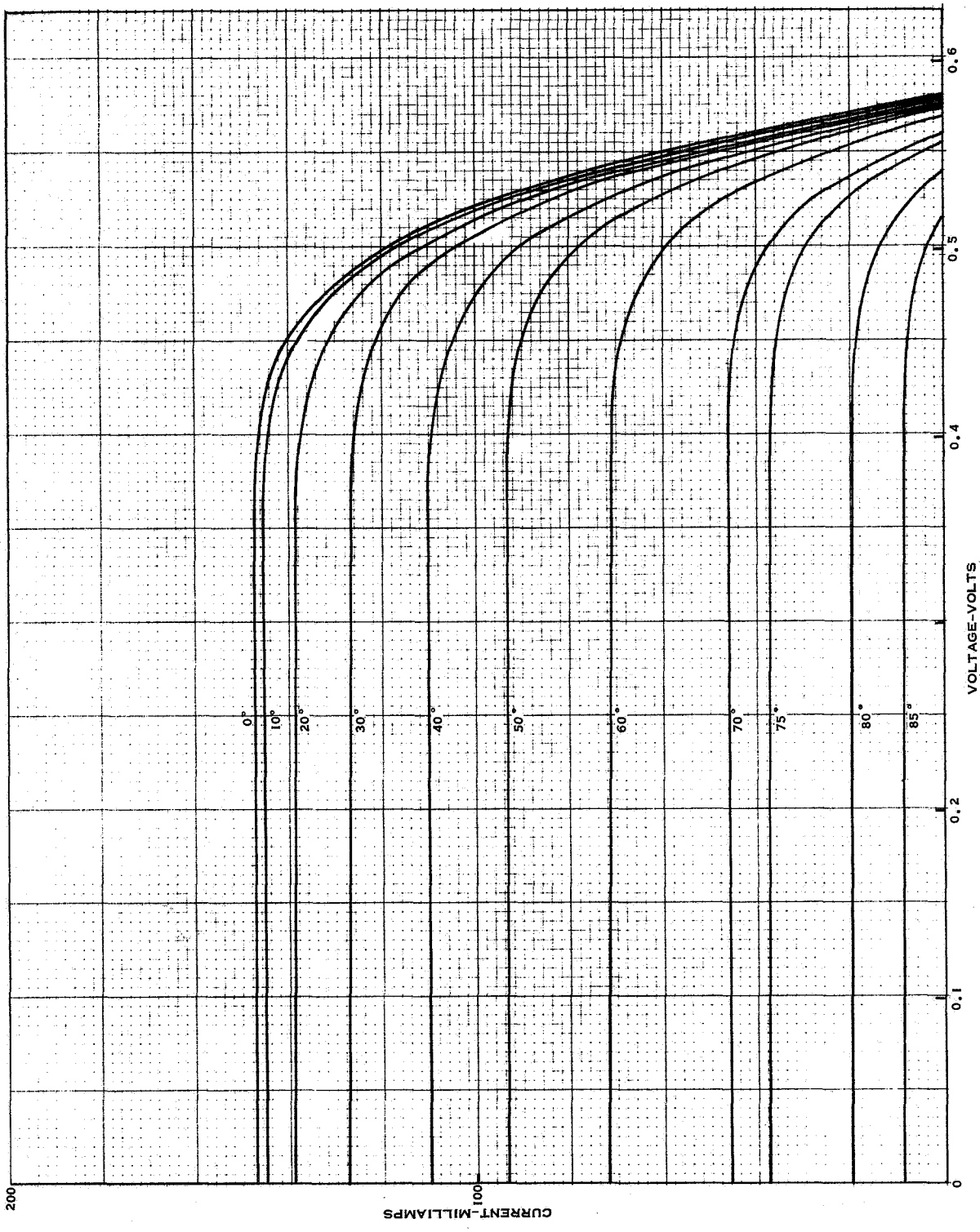

Figure 55 Carbon Arc One Sun I-V Characteristics Cell Type 2C at Various Angles of Incidence

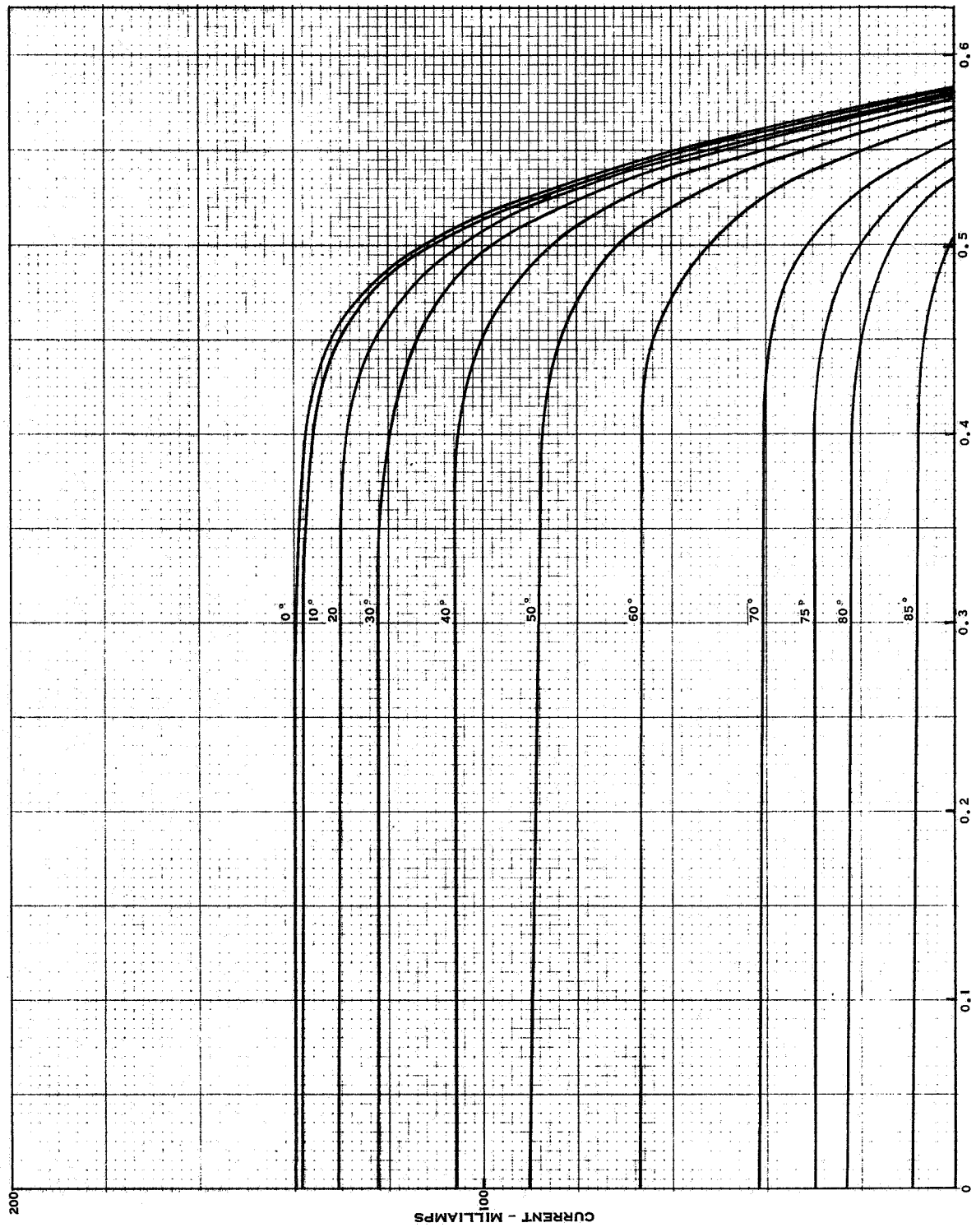

Figure 56 Carbon Arc One Sun I-V Characteristics Cell Type 3C at Various Angles of Incidence

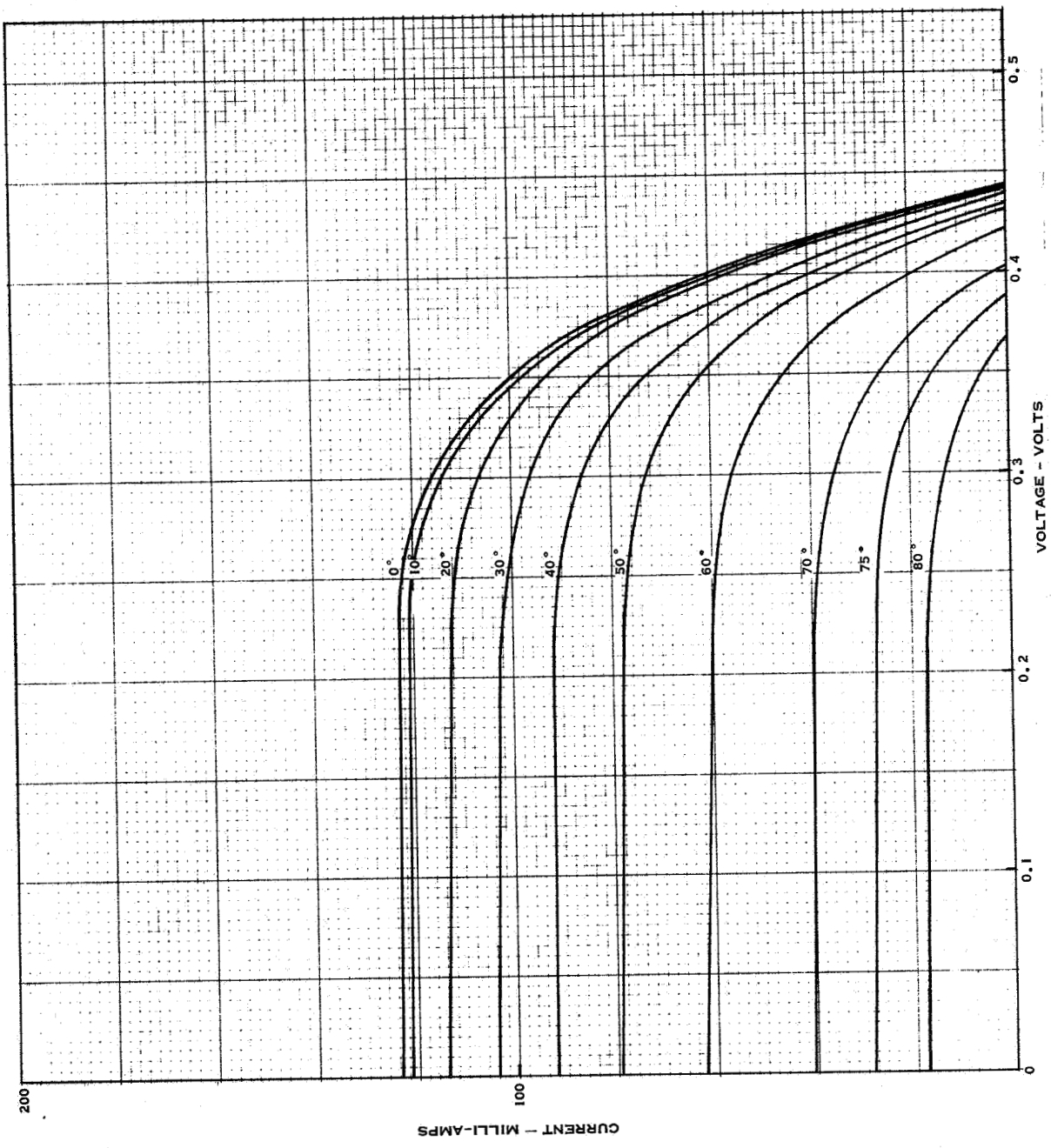

Figure 57 Carbon Arc Three Sun I-V Characteristics Cell Type 1A at Various Angles of Incidence

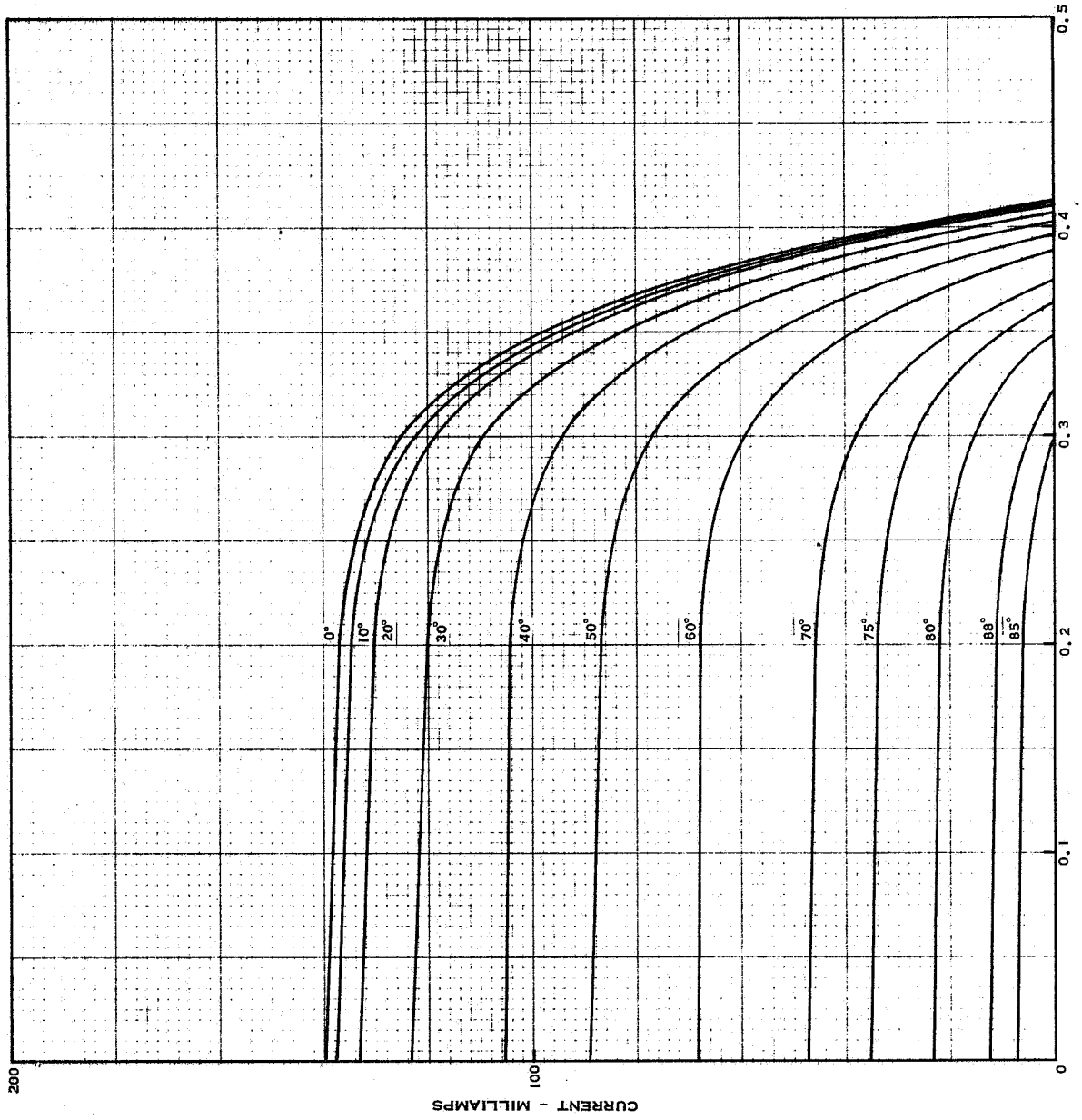

Figure 58 Carbon Arc Three Sun I-V Characteristics Cell Type 2A at Various Angles of Incidence

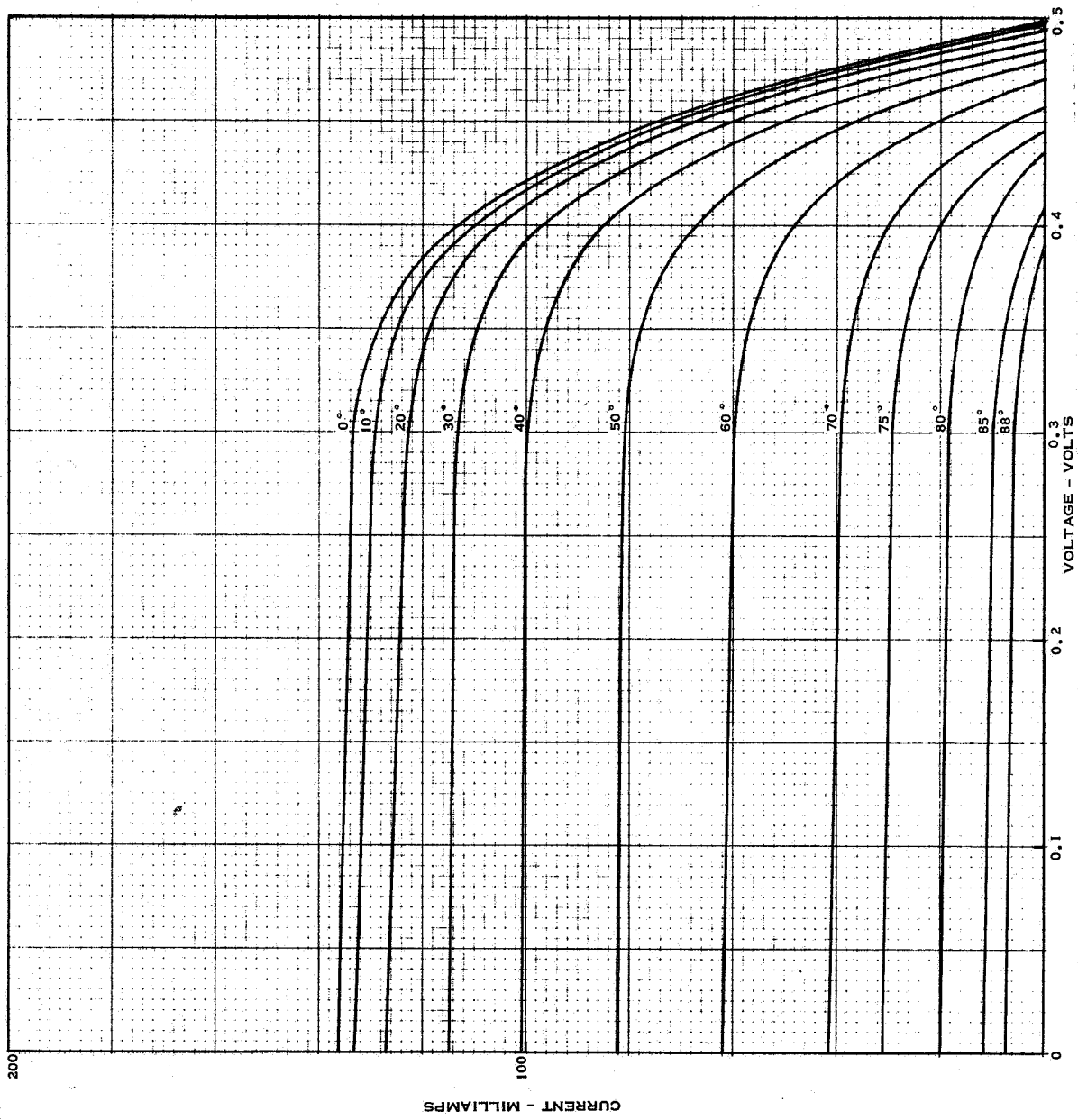

Figure 59 Carbon Arc Three Sun I-V Characteristics Cell Type 3A at Various Angles of Incidence

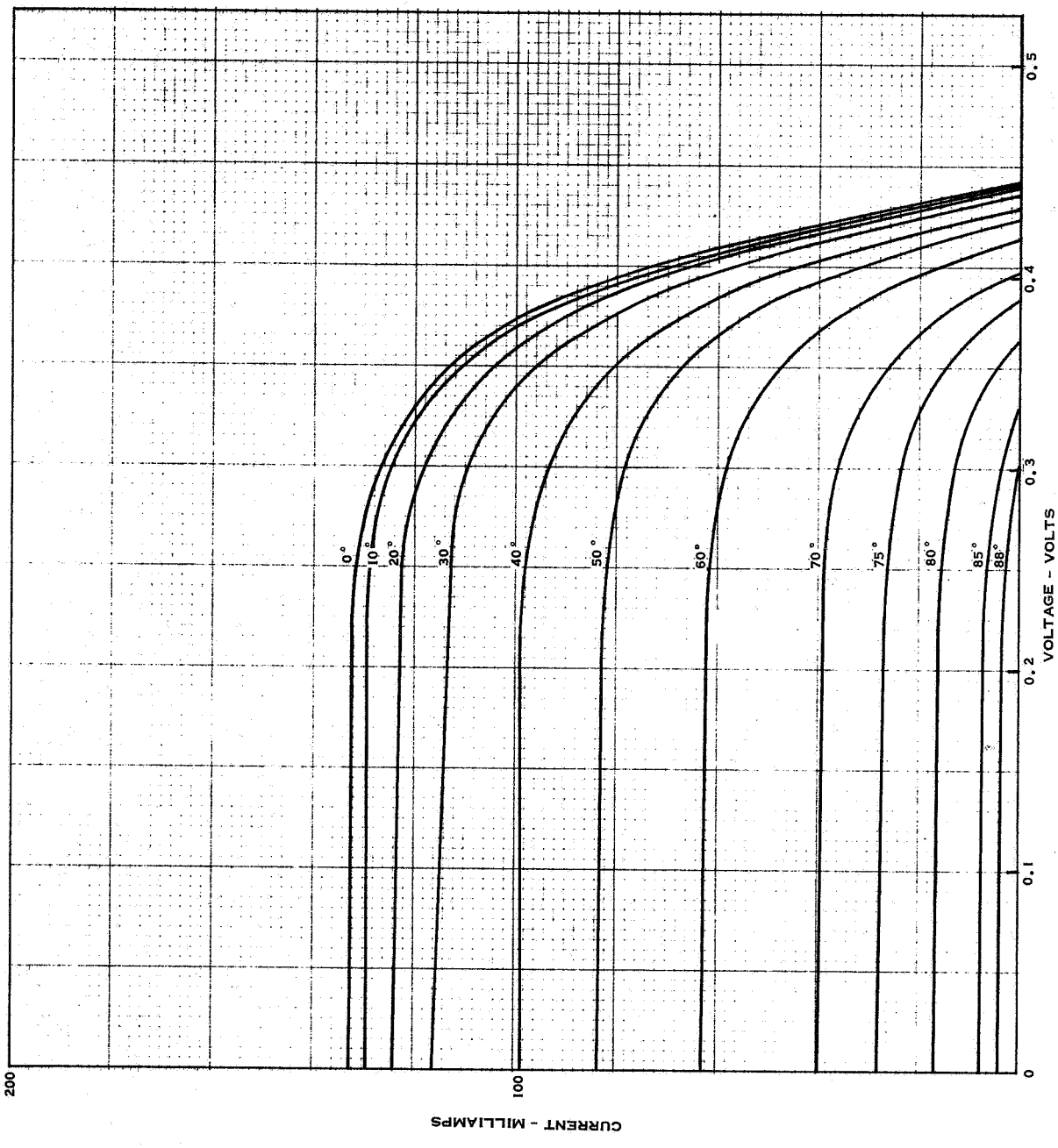

Figure 60 Carbon Arc Three Sun I-V Characteristics Cell Type 4A at Various Angles of Incidence

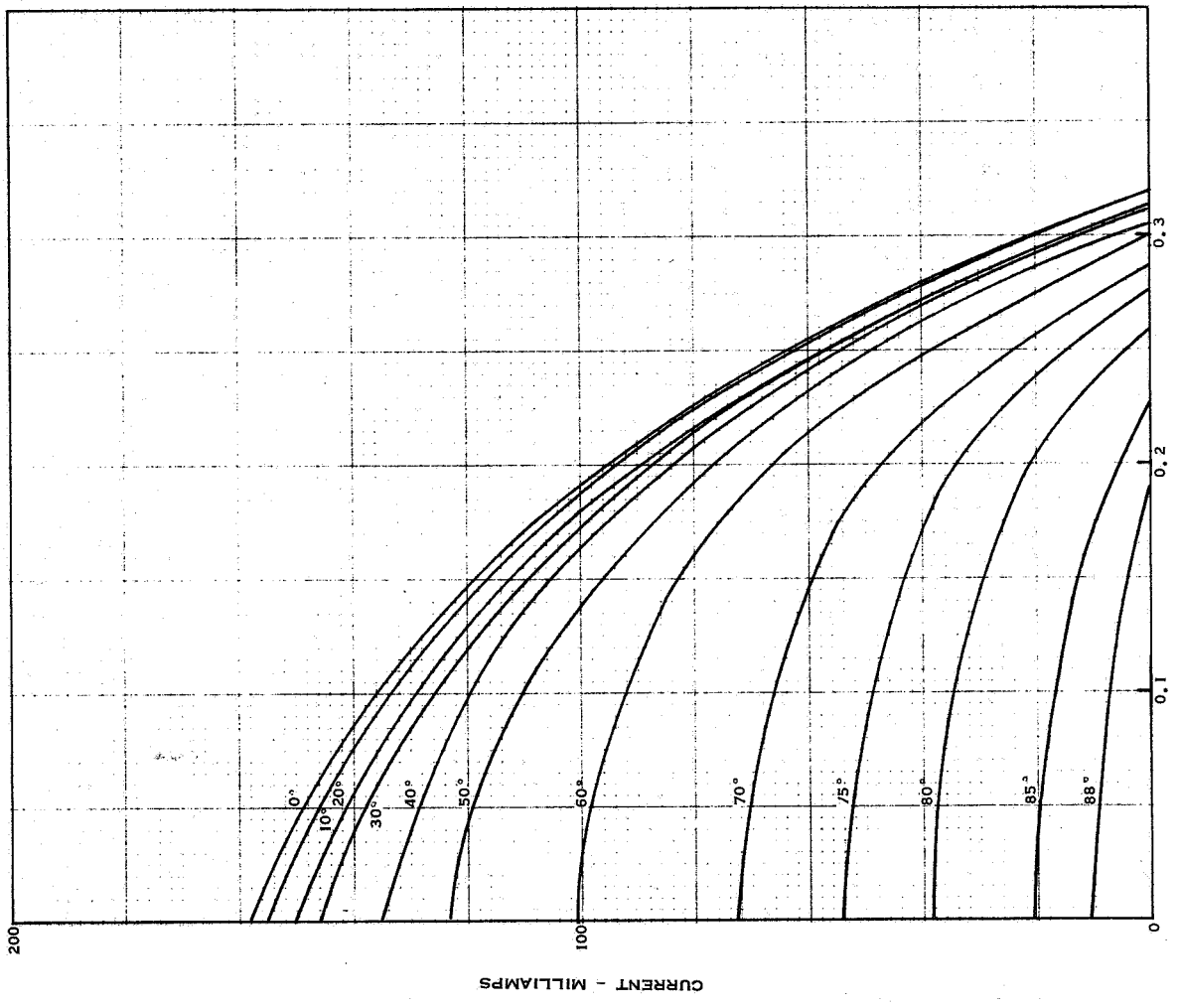

Figure 61 Carbon Arc Three Sun I-V Characteristics Cell Type 1B at Various Angles of Incidence

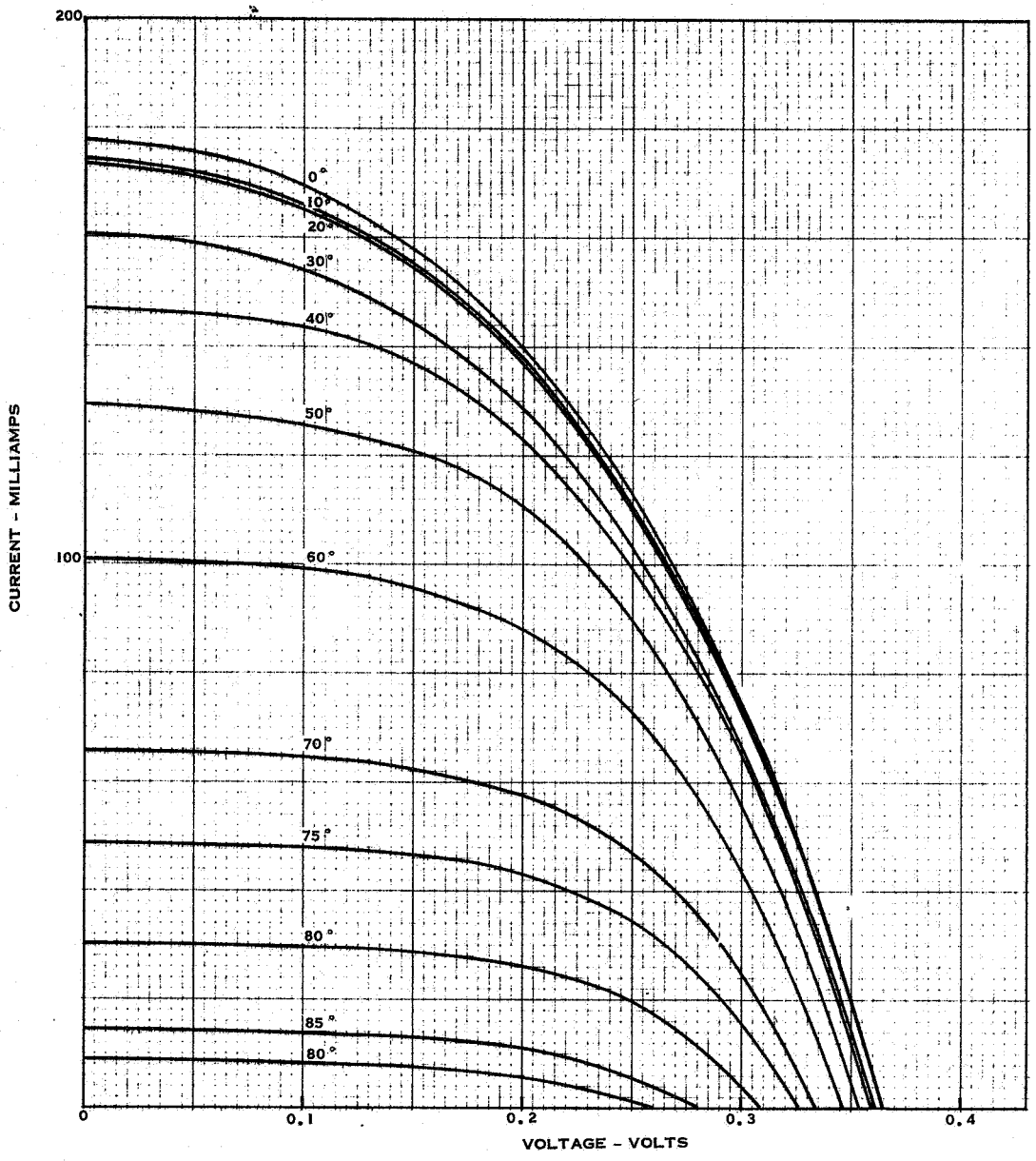

Figure 62 Carbon Arc Three Sun I-V Characteristics Cell Type 2B at Various Angles of Incidence

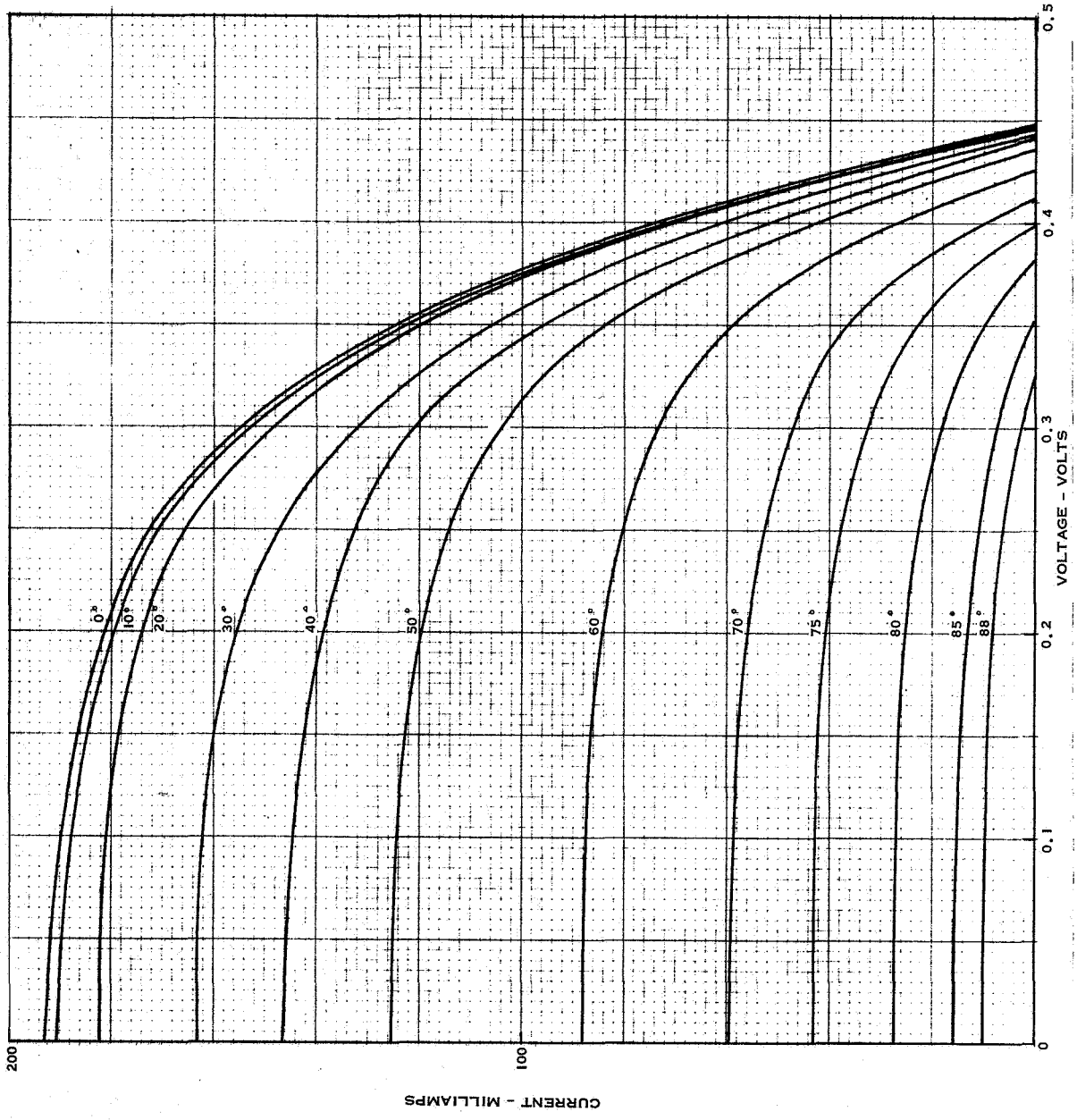

Figure 63 Carbon Arc Three Sun I-V Characteristics Cell Type 3B at Various Angles of Incidence

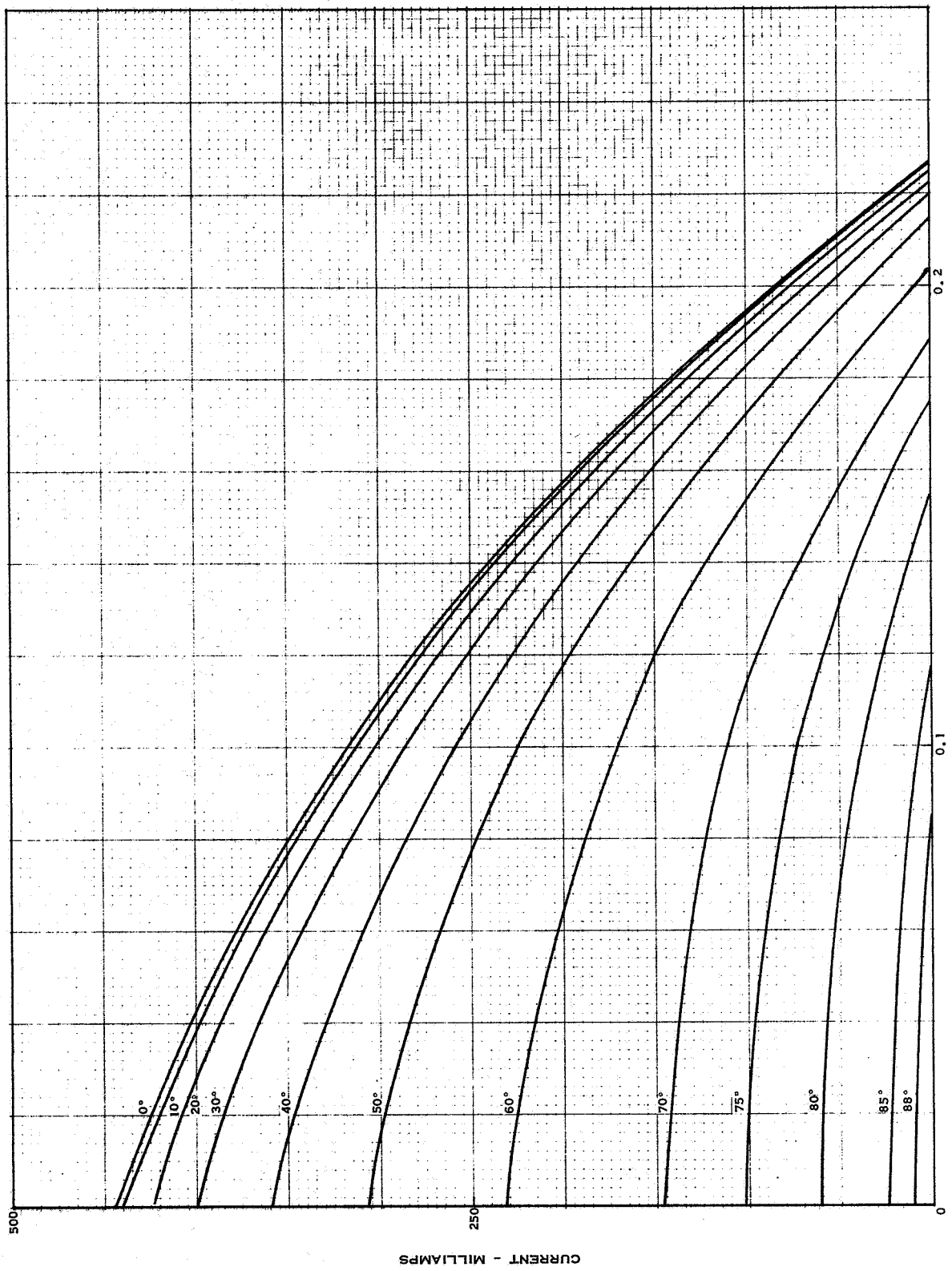

Figure 64 Carbon Arc Three Sun I-V Characteristics Cell Type 1C at Various Angles of Incidence

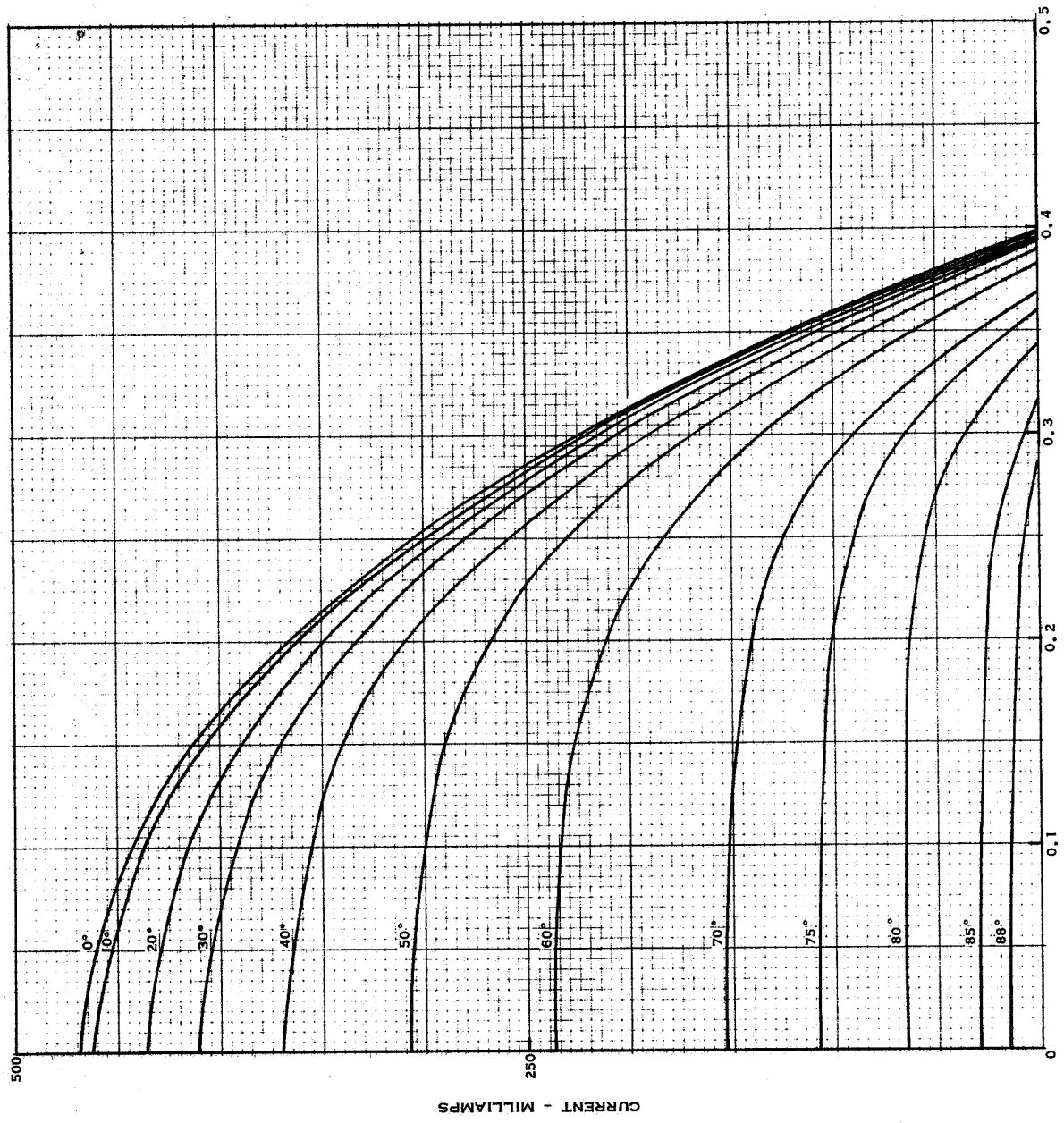

Figure 65 Carbon Arc Three Sun I-V Characteristics Cell Type 2C at Various Angles of Incidence

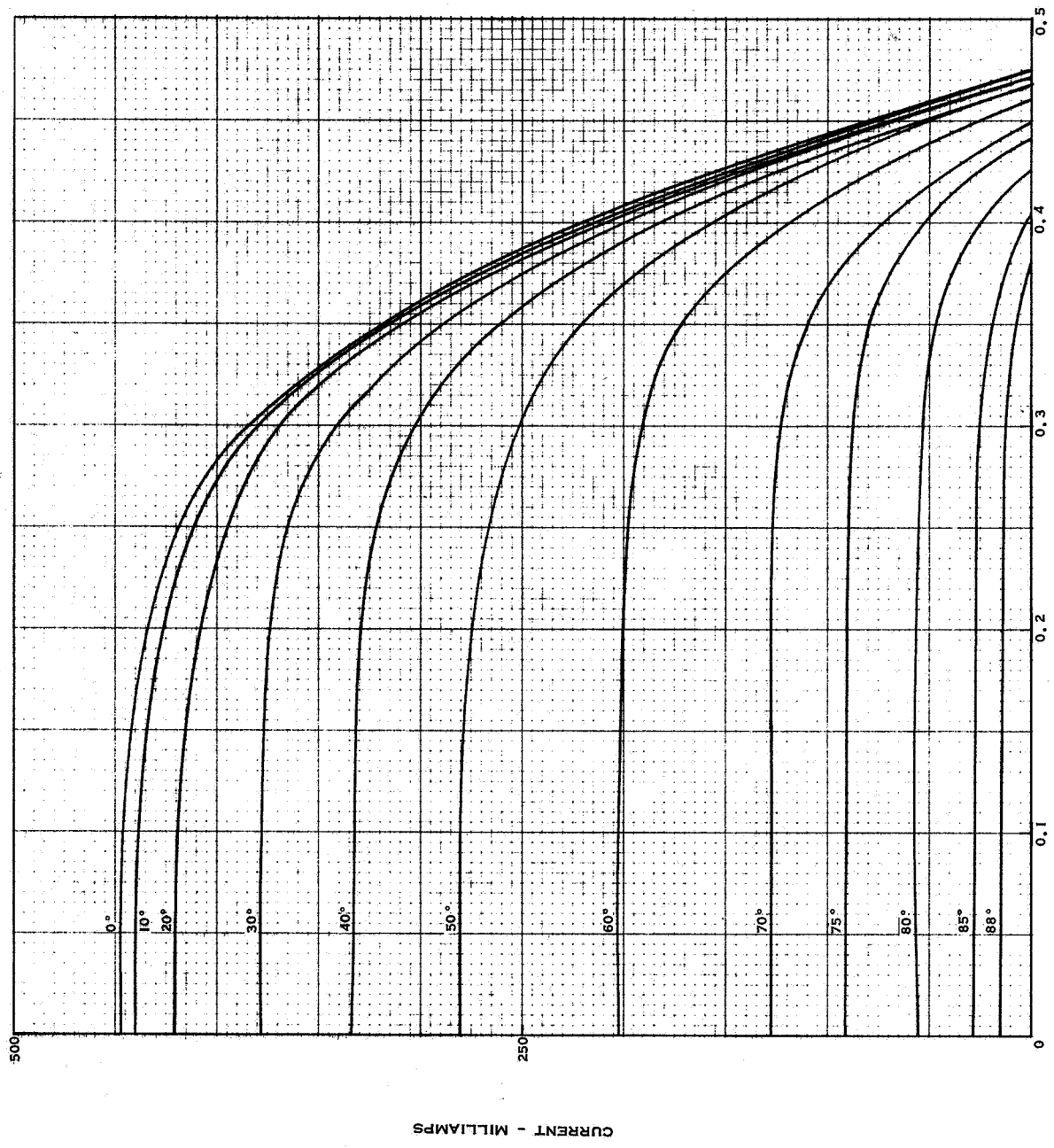

Figure 66 Carbon Arc Three Sun I-V Characteristics Cell Type 3C at Various Angles of Incidence

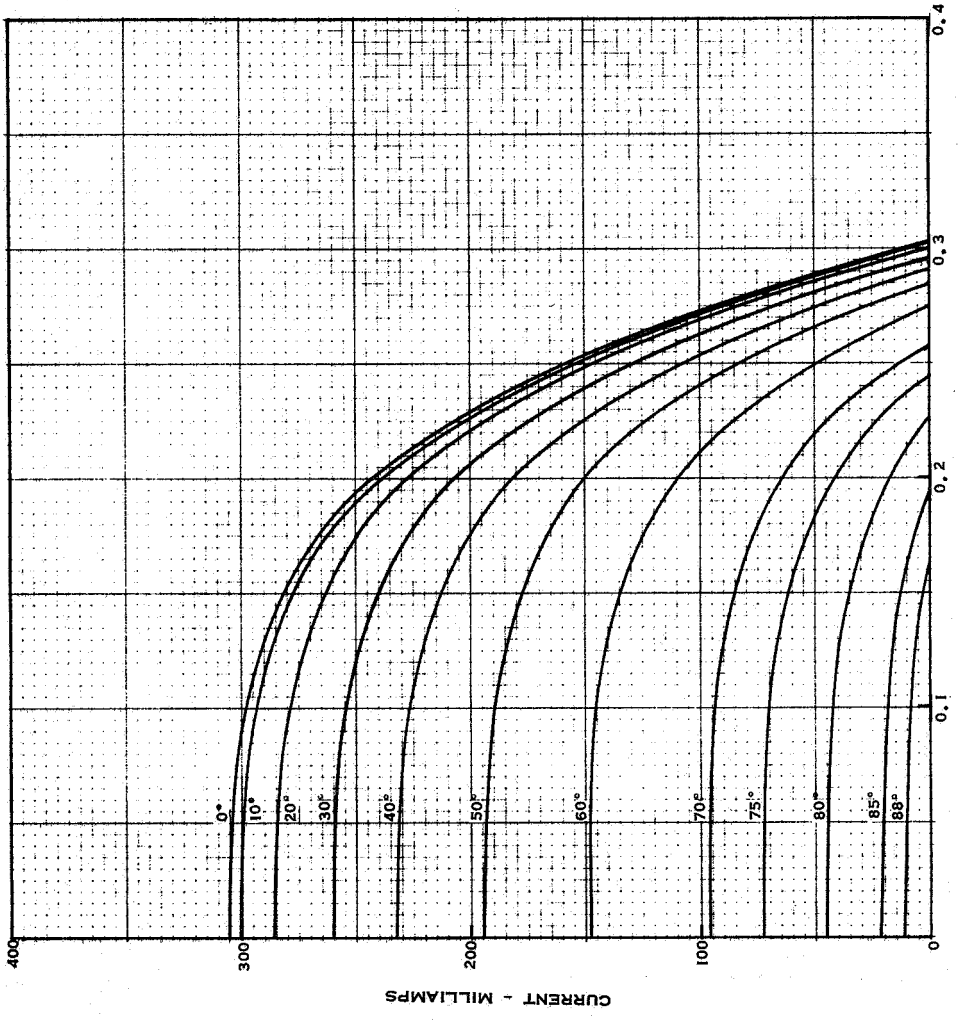

Figure 67 Cabron Arc 7.6 Sun I-V Characteristics Cell Type 1A at Various Angles of Incidence

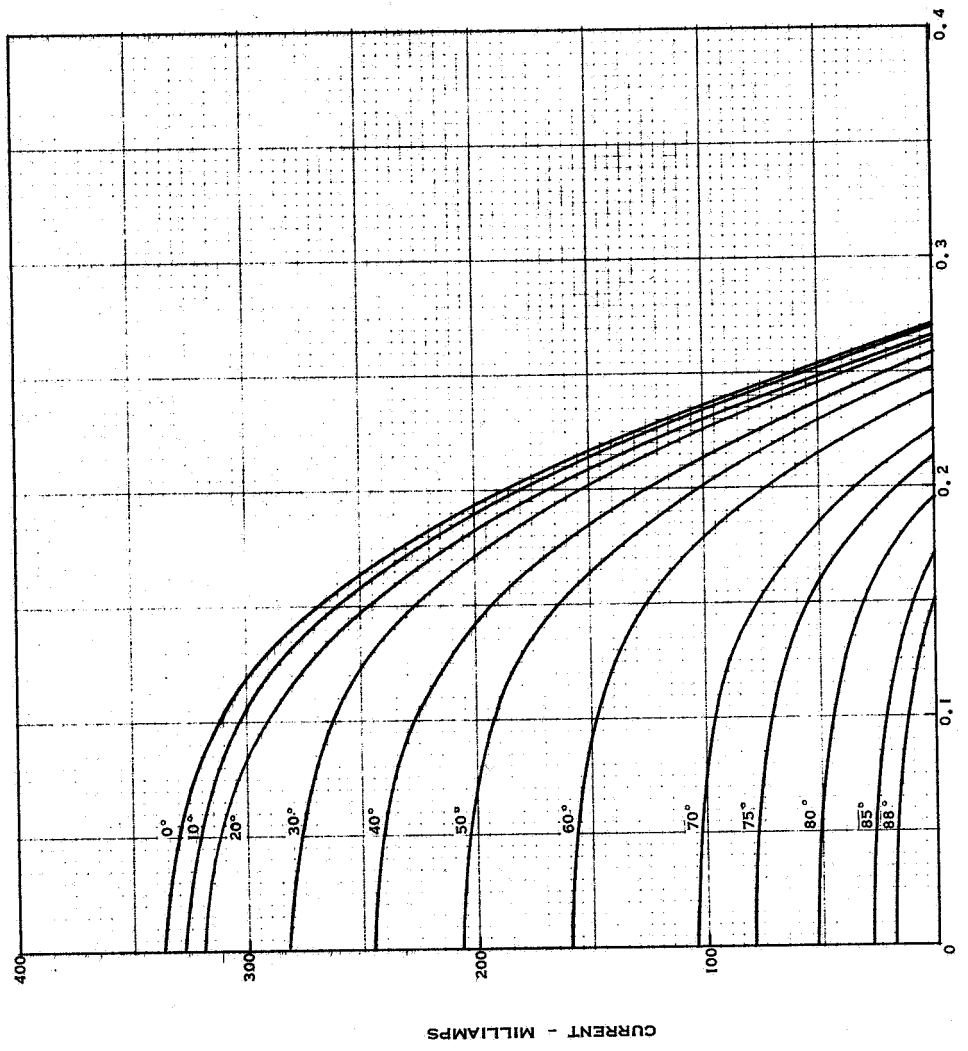

Figure 68 Carbon Arc 7.6 Sun I-V Characteristics Cell Type 2A at Various Angles of Incidence

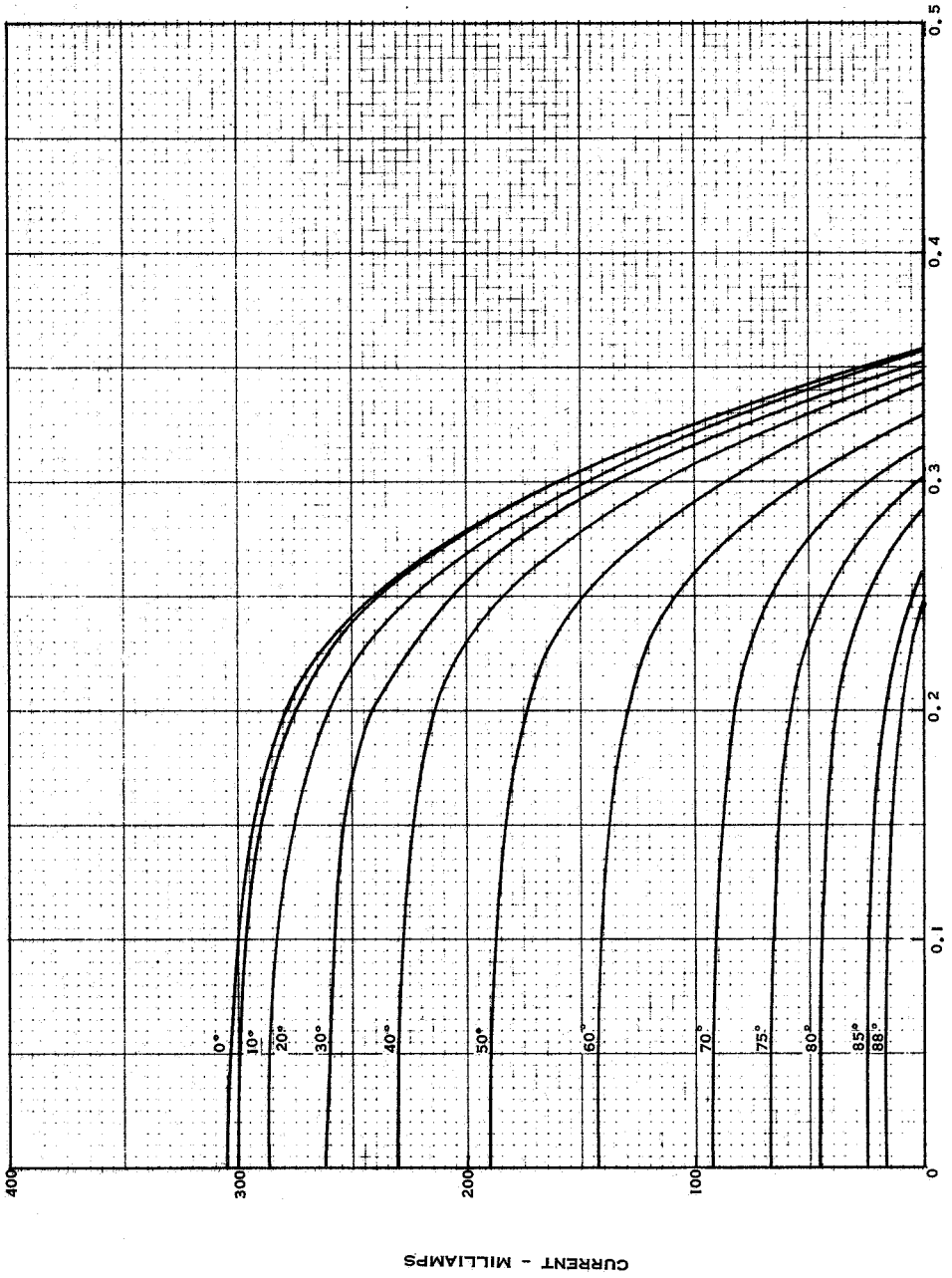

Figure 69 Carbon Arc 7.6 Sun I-V Characteristics Cell Type 3A at Various Angles of Incidence

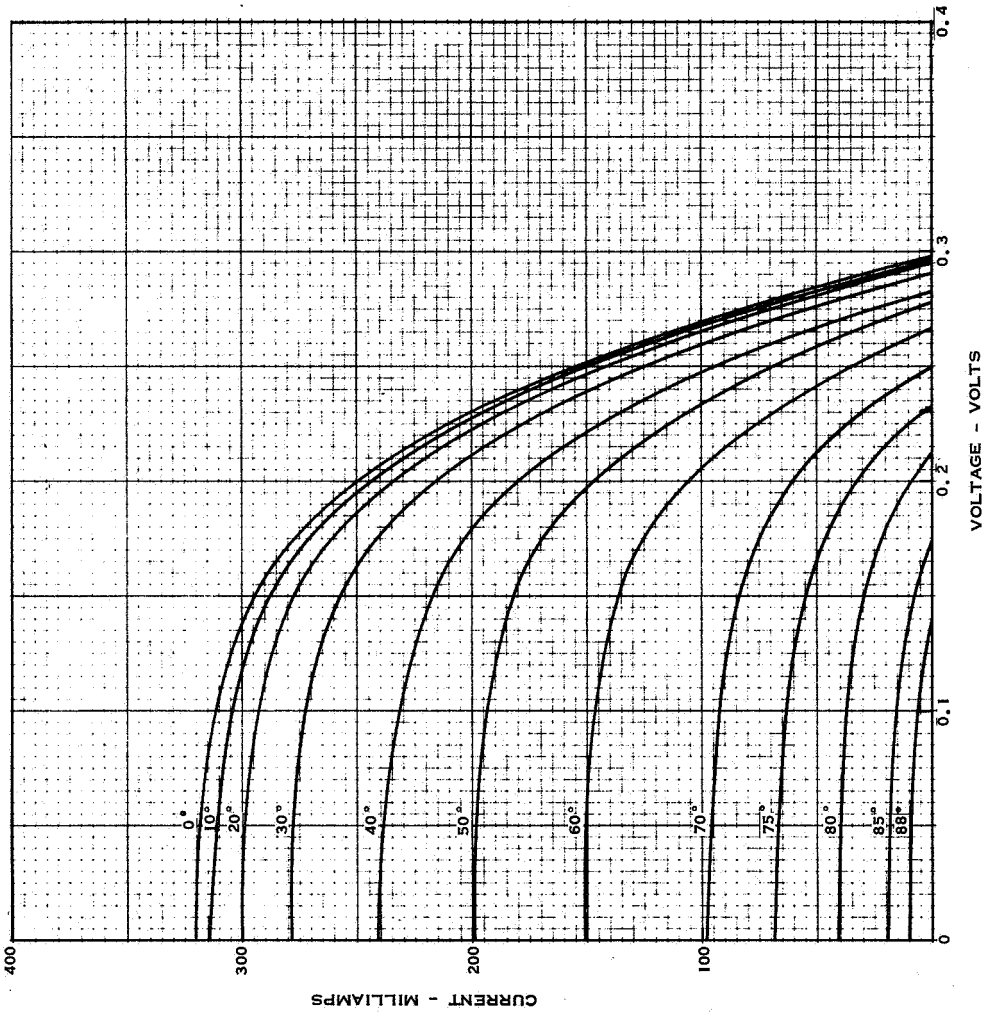

Figure 70 Carbon Arc 7.6 Sun I-V Characteristics Cell Type 4A at Various Angles of Incidence

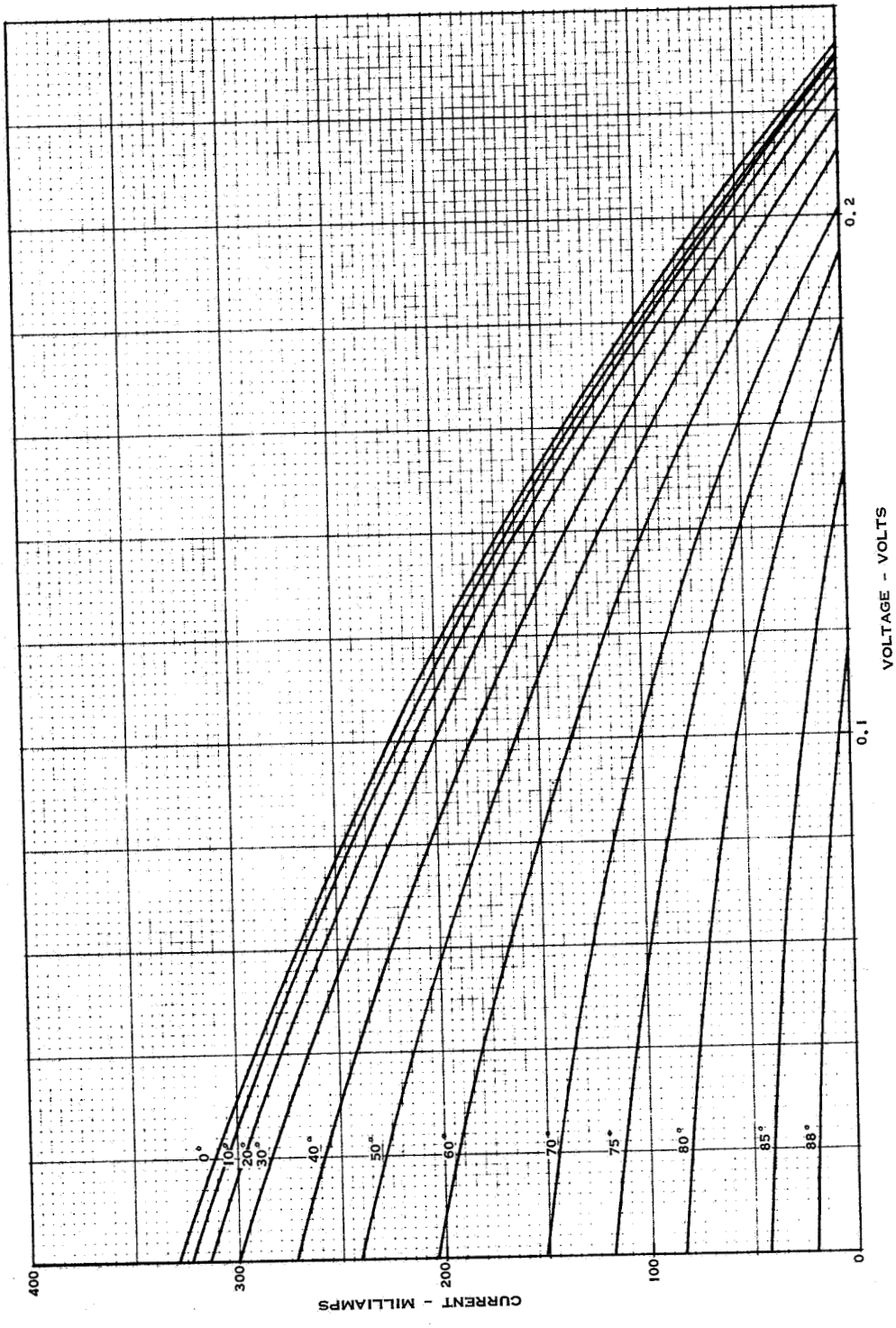

Figure 71 Carbon Arc 7.6 Sun I-V Characteristics Cell Type 1B at Various Angles of Incidence

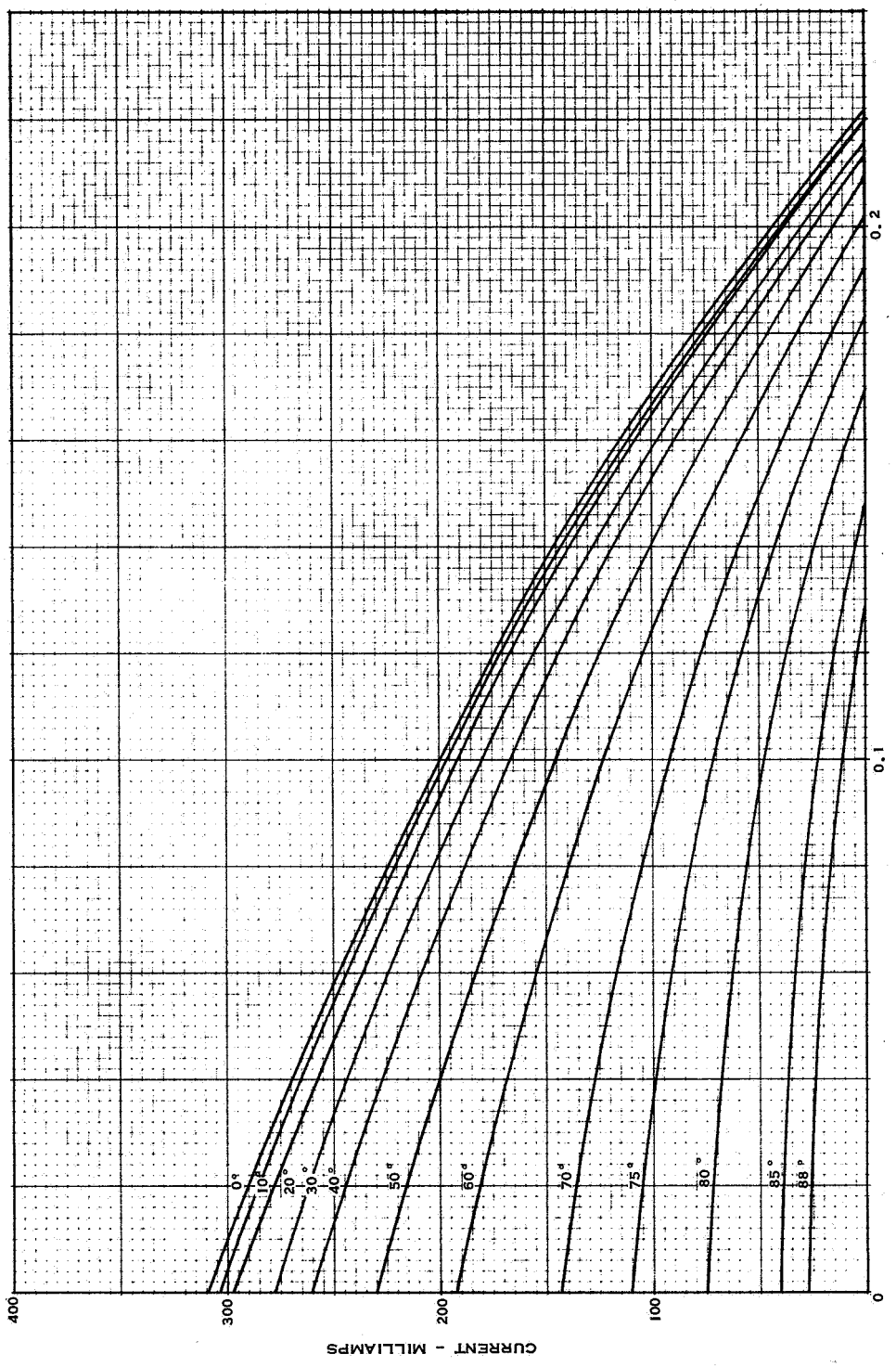

Figure 72 Carbon Arc 7.6 Sun I-V Characteristics Cell Type 2B at Various Angles of Incidence

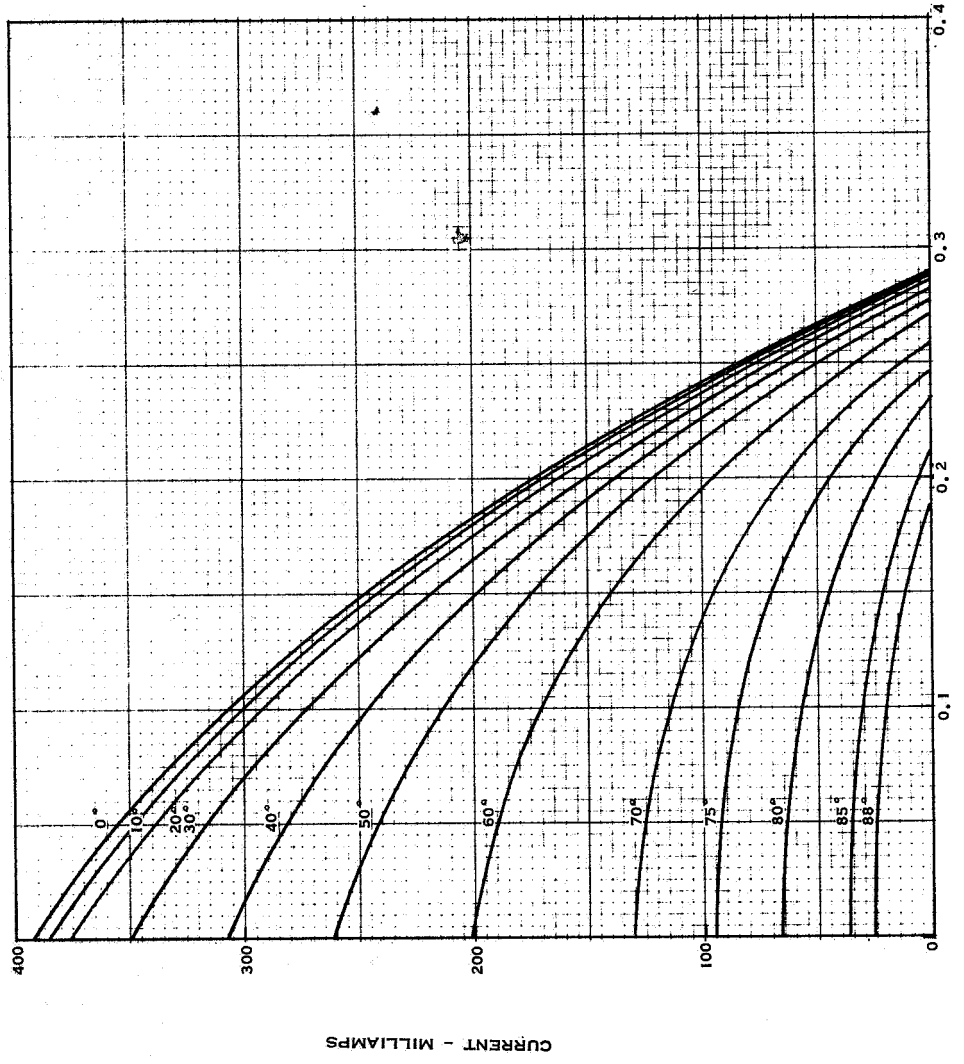

Figure 73 Carbon Arc 7.6 Sun I-V Characteristics Cell Type 3B at Various Angles of Incidence

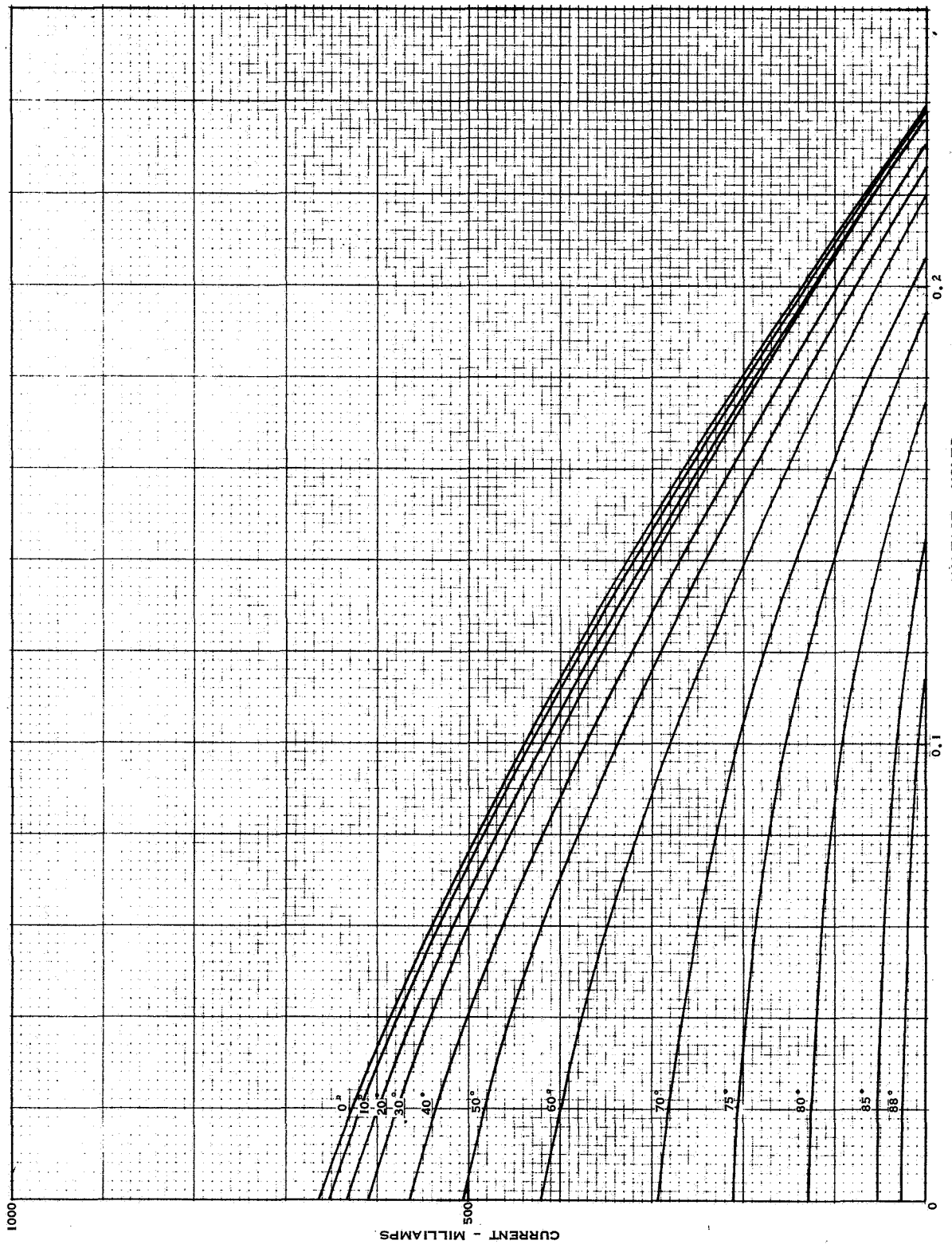

Figure 74 Carbon Arc 7.6 Sun I-V Characteristics Cell Type 1C at Various Angles of Incidence

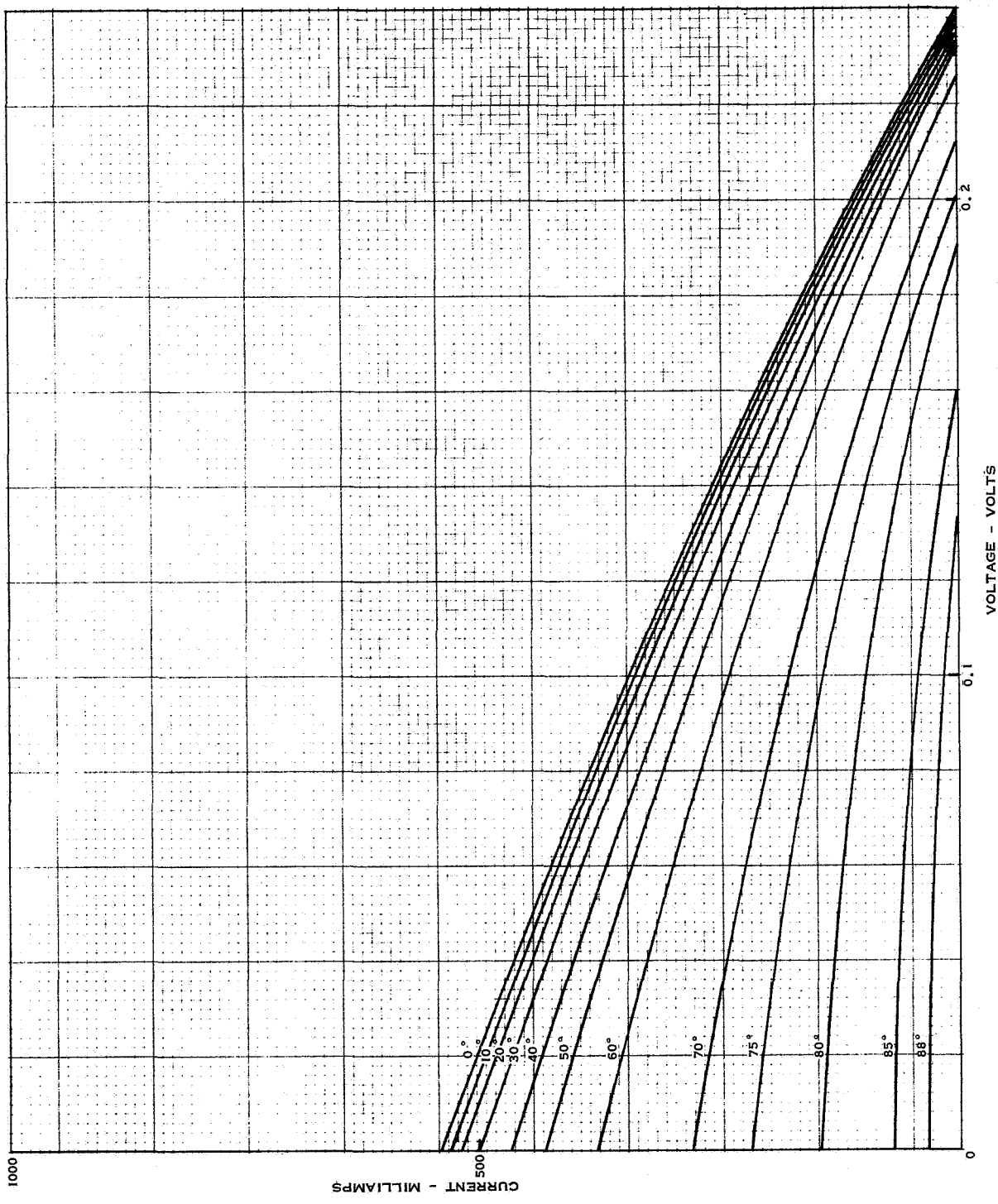

Figure 75 Carbon Arc 7.6 Sun I-V Characteristics Cell Type 2C at Various Angles of Incidence

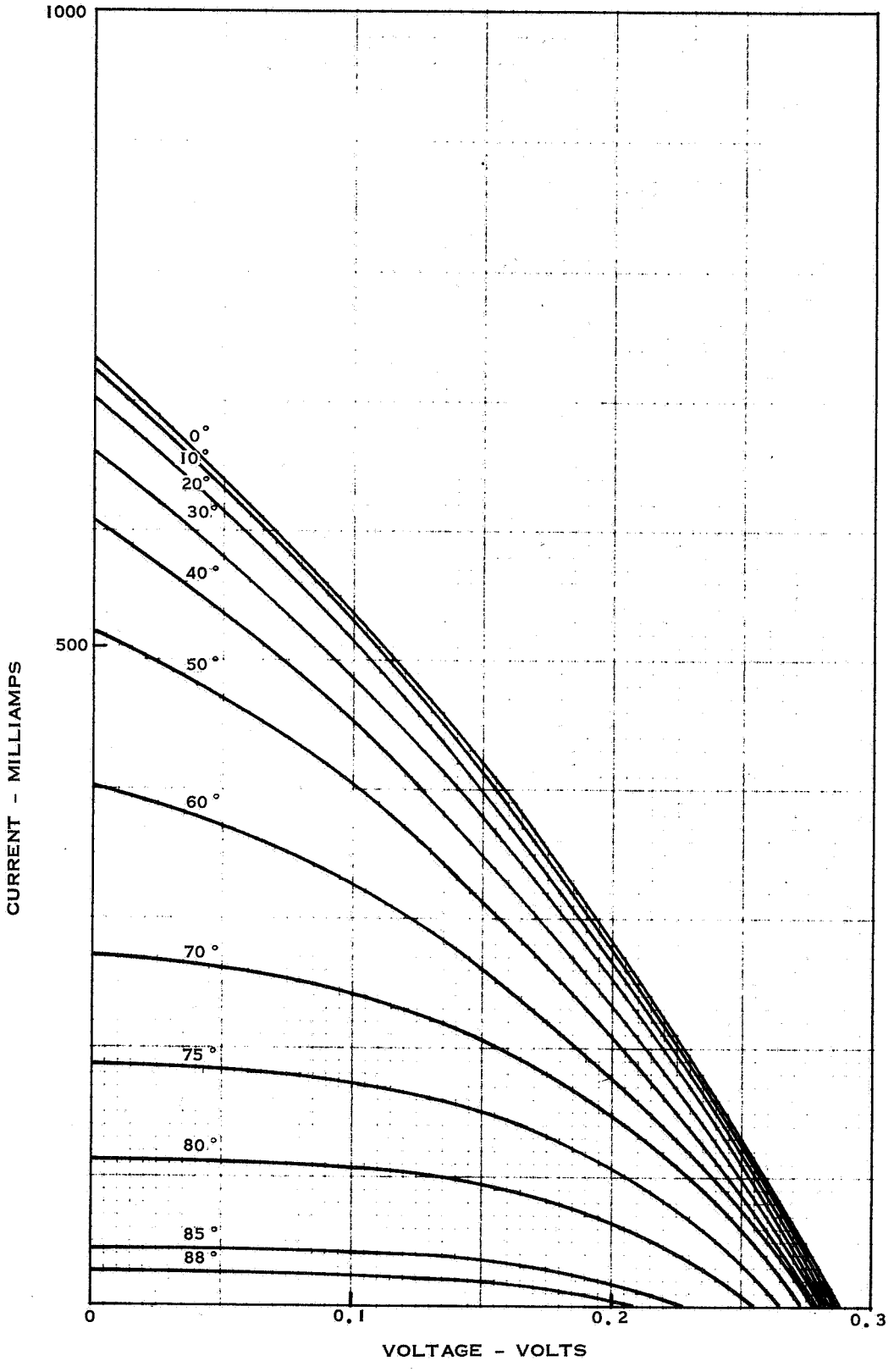

Figure 76 Carbon Arc 7.6 Sun I-V Characteristics Cell Type 3C at Various Angles of Incidence

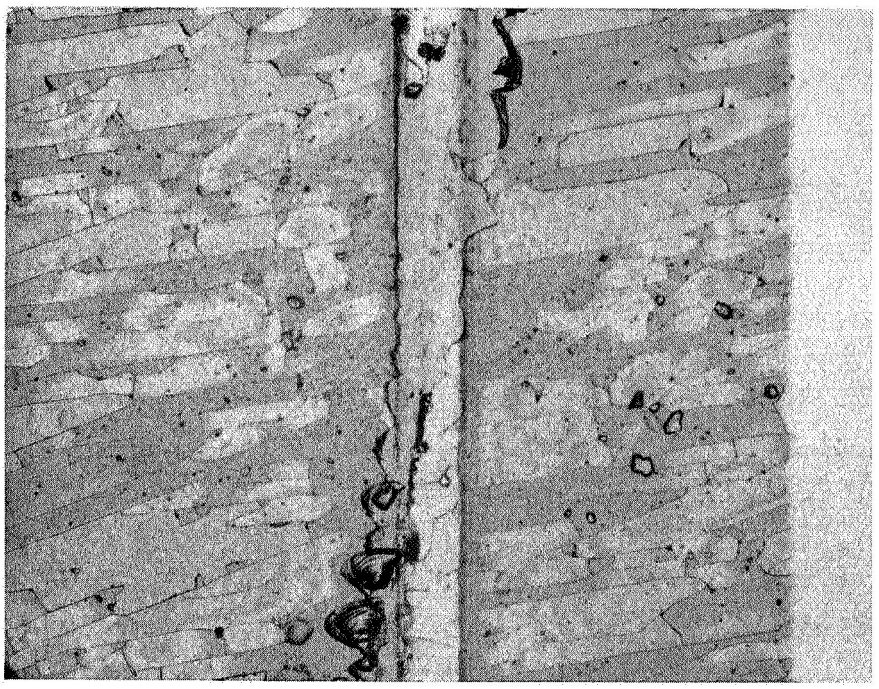

Figure 77 60X Photomicrograph of Cell Type A

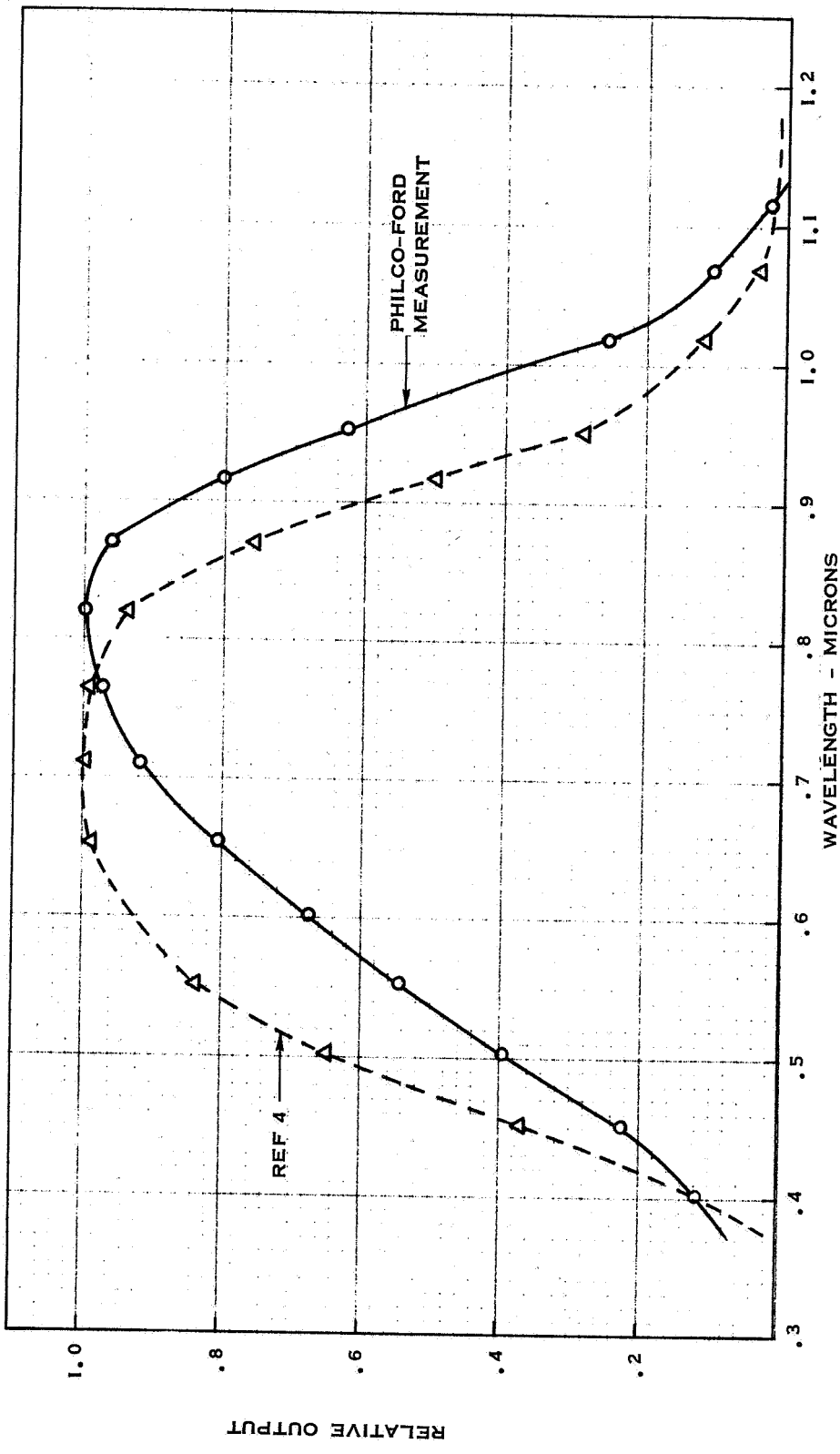

Figure 78 Comparison of Spectral Response Cell Type A

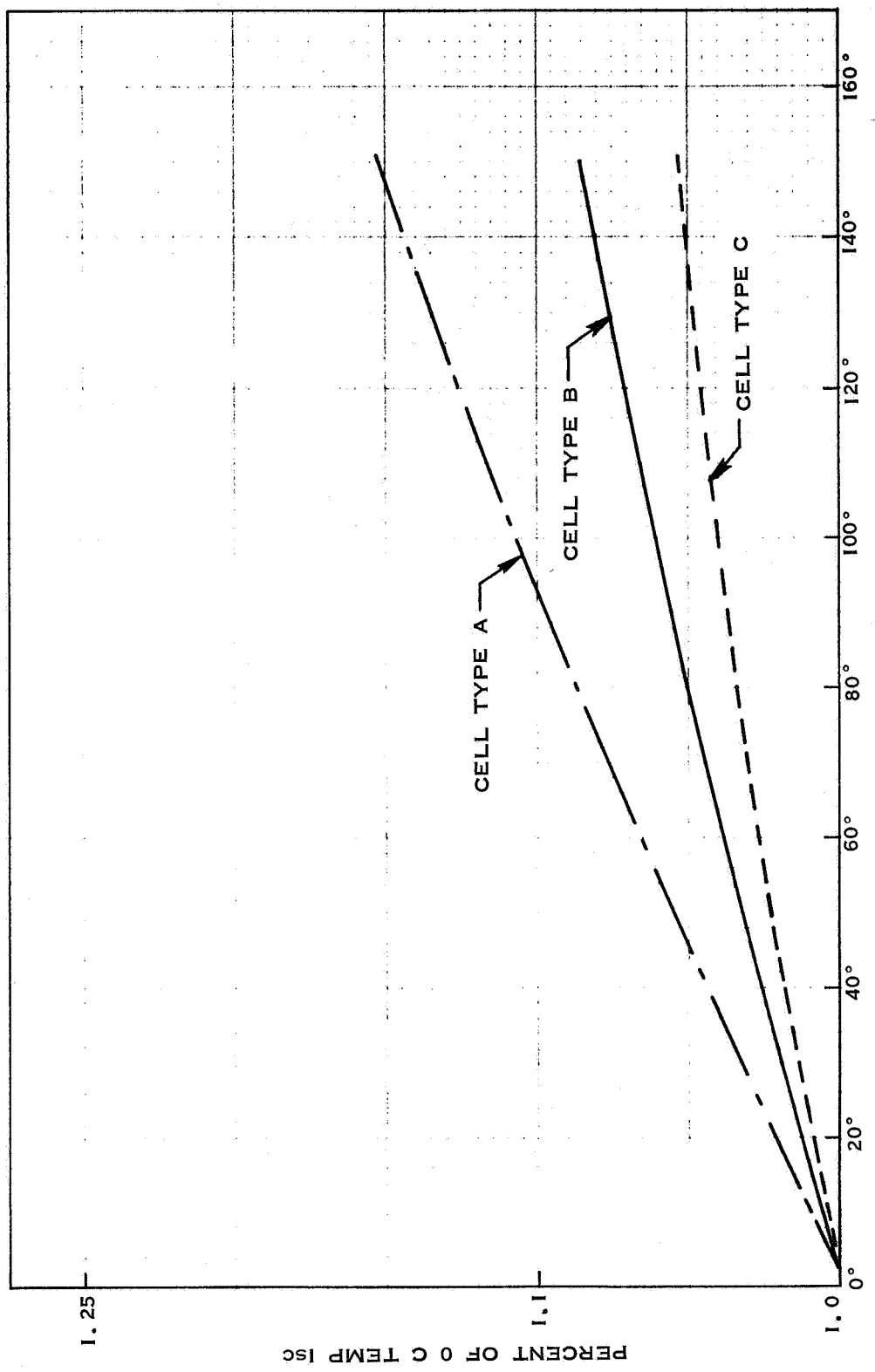

Figure 79 Normalized Short Circuit Current Versus Temperature

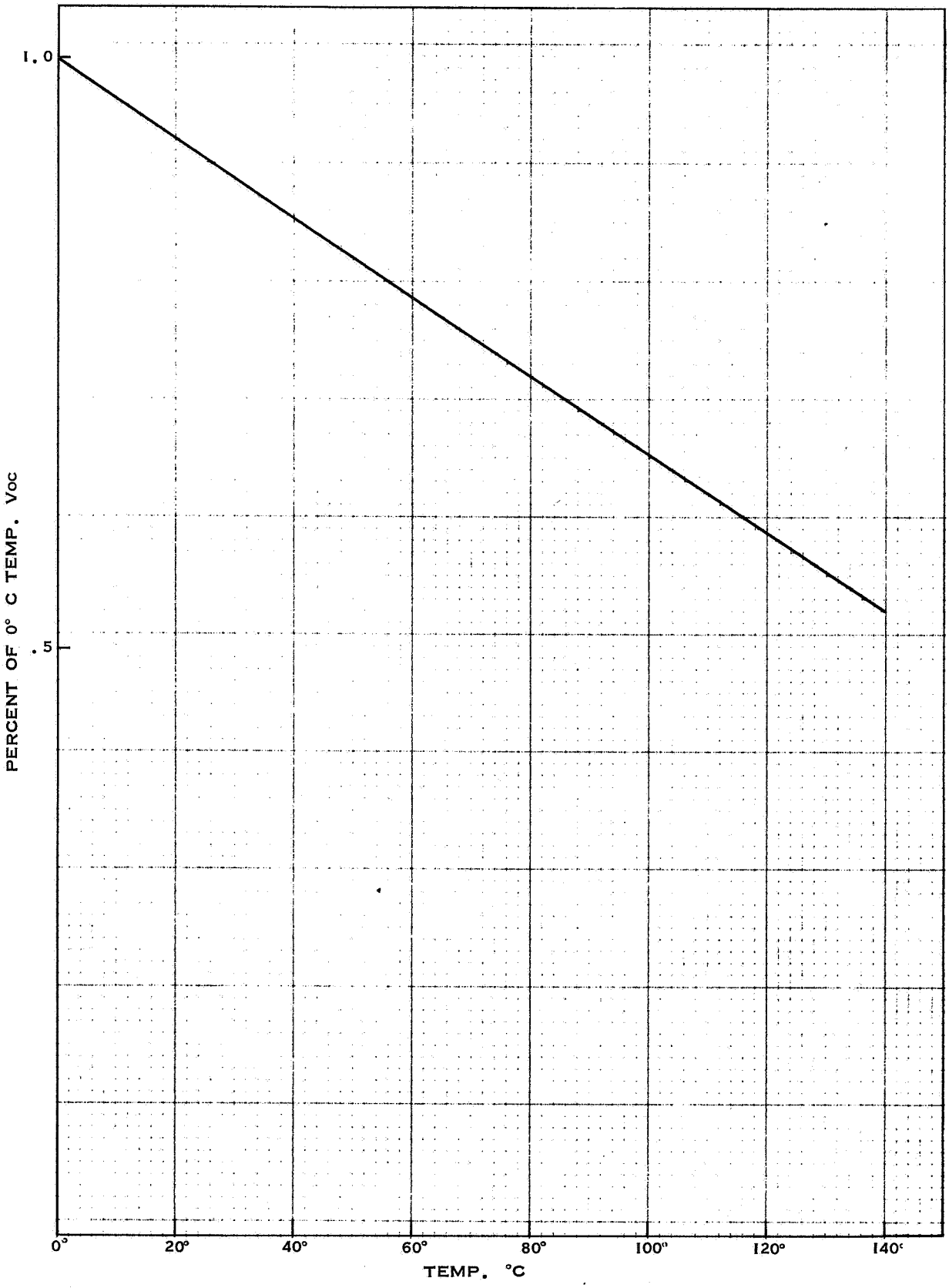

Figure 80 Normalized Open Circuit Voltage versus Temperature

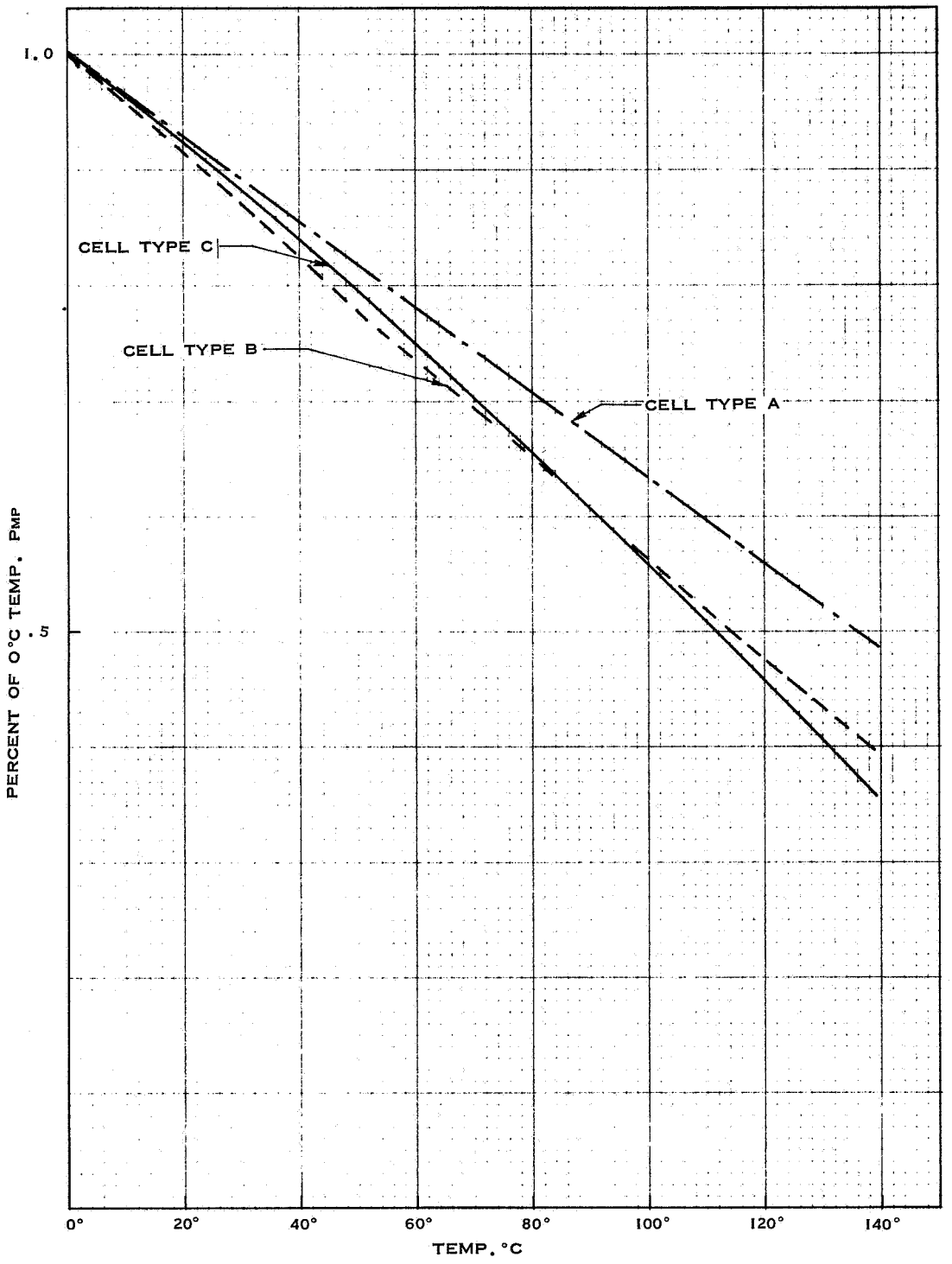

Figure 81 Normalized Max Power versus Temperature

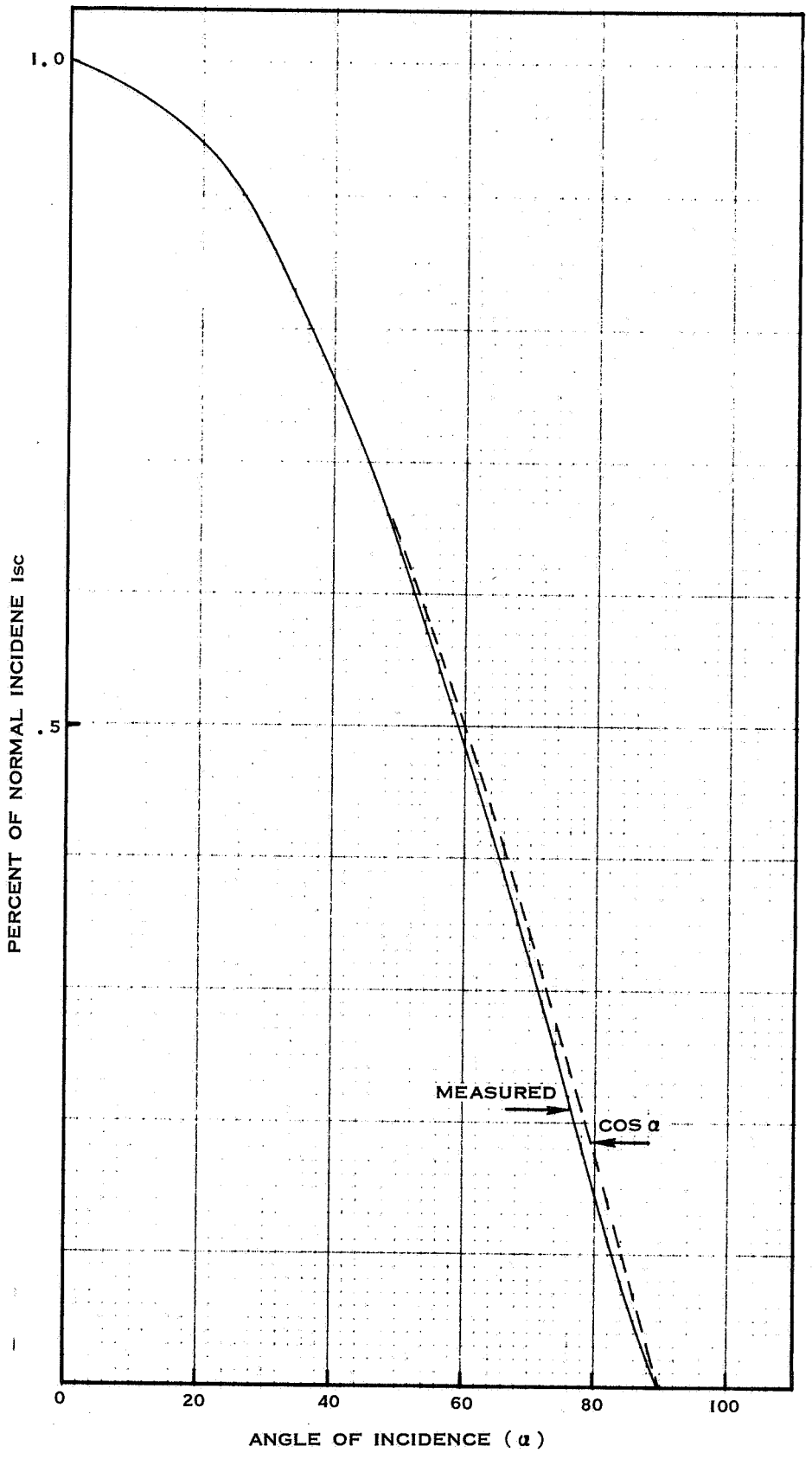

Figure 82 Normalized Short Circuit Current versus Angle of Incidence

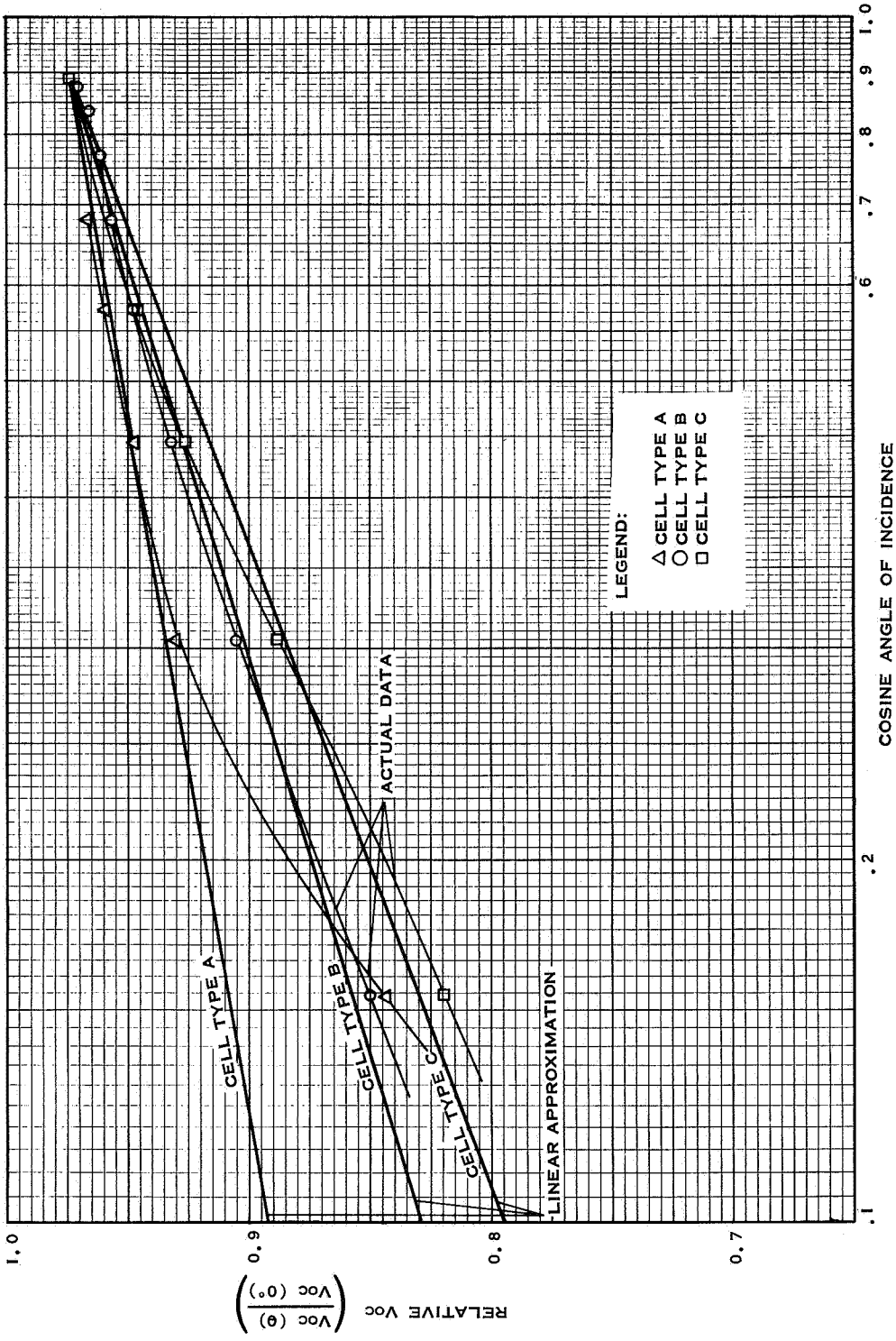

Figure 83 Normalized Open Circuit Voltage versus Angle of Incidence

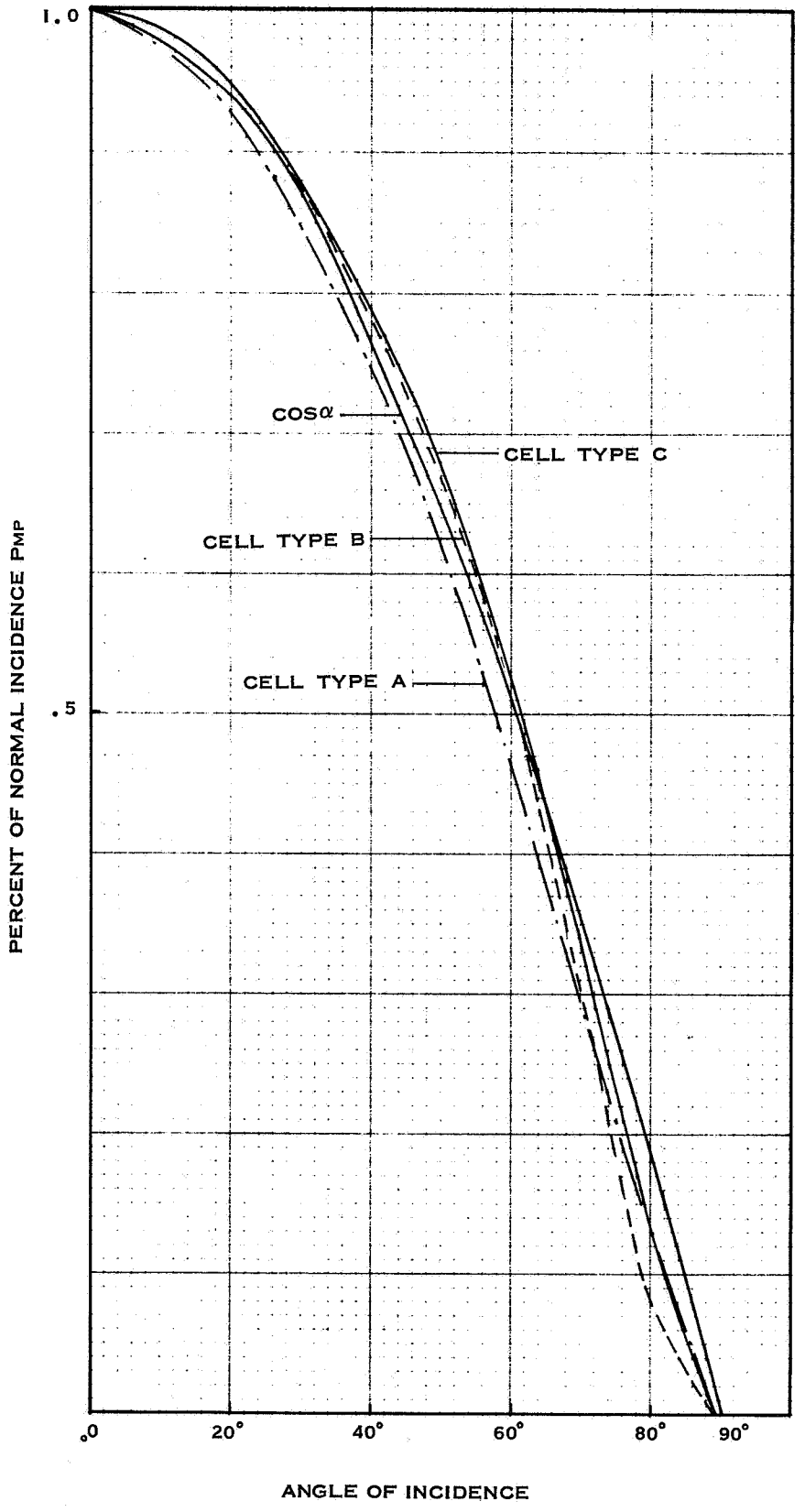

Figure 84 Normalized Max Power Versus Angle of Incidence

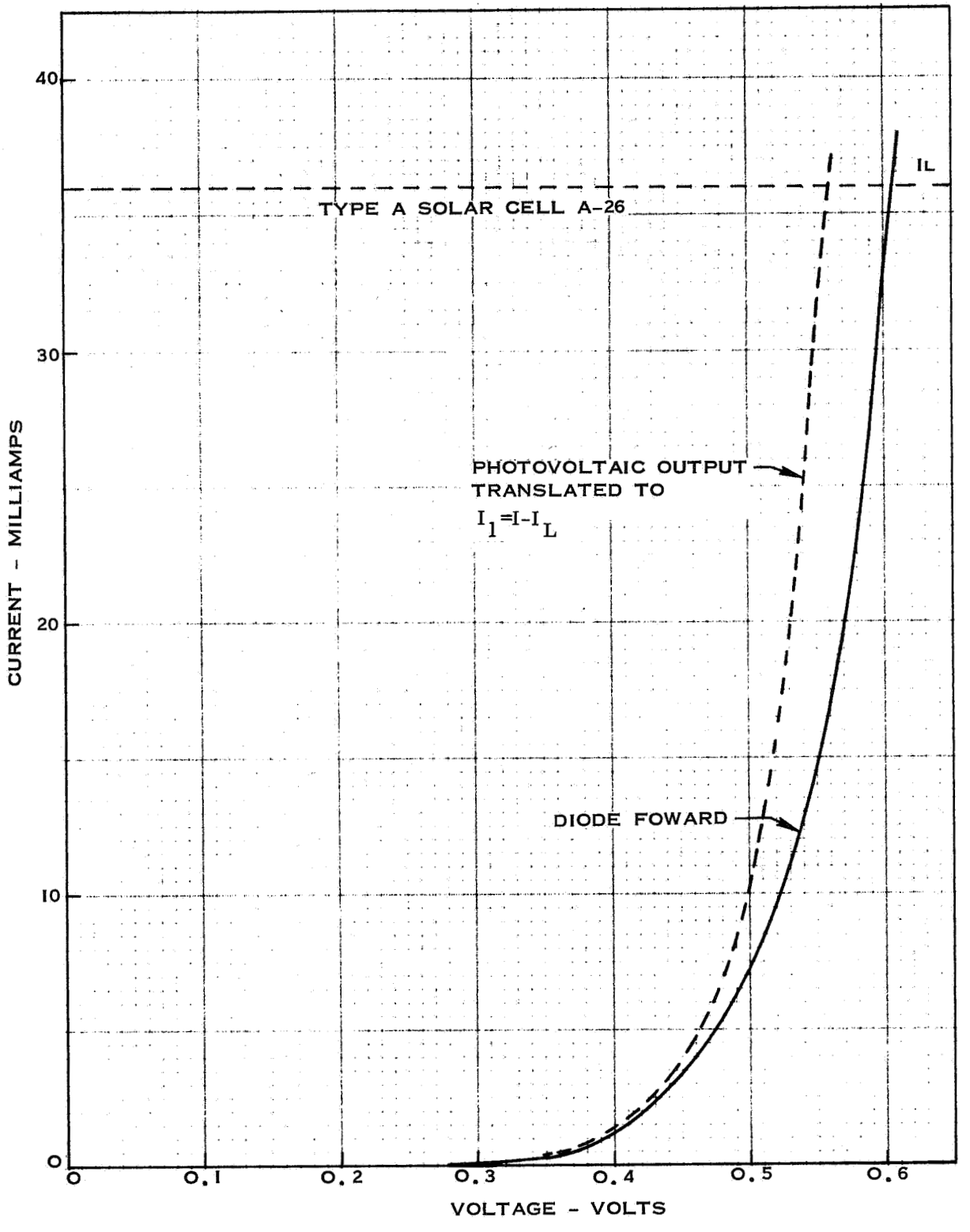

Figure 85 Comparison of Dark Forward Diodes & Photovoltaic Output Cell Type A

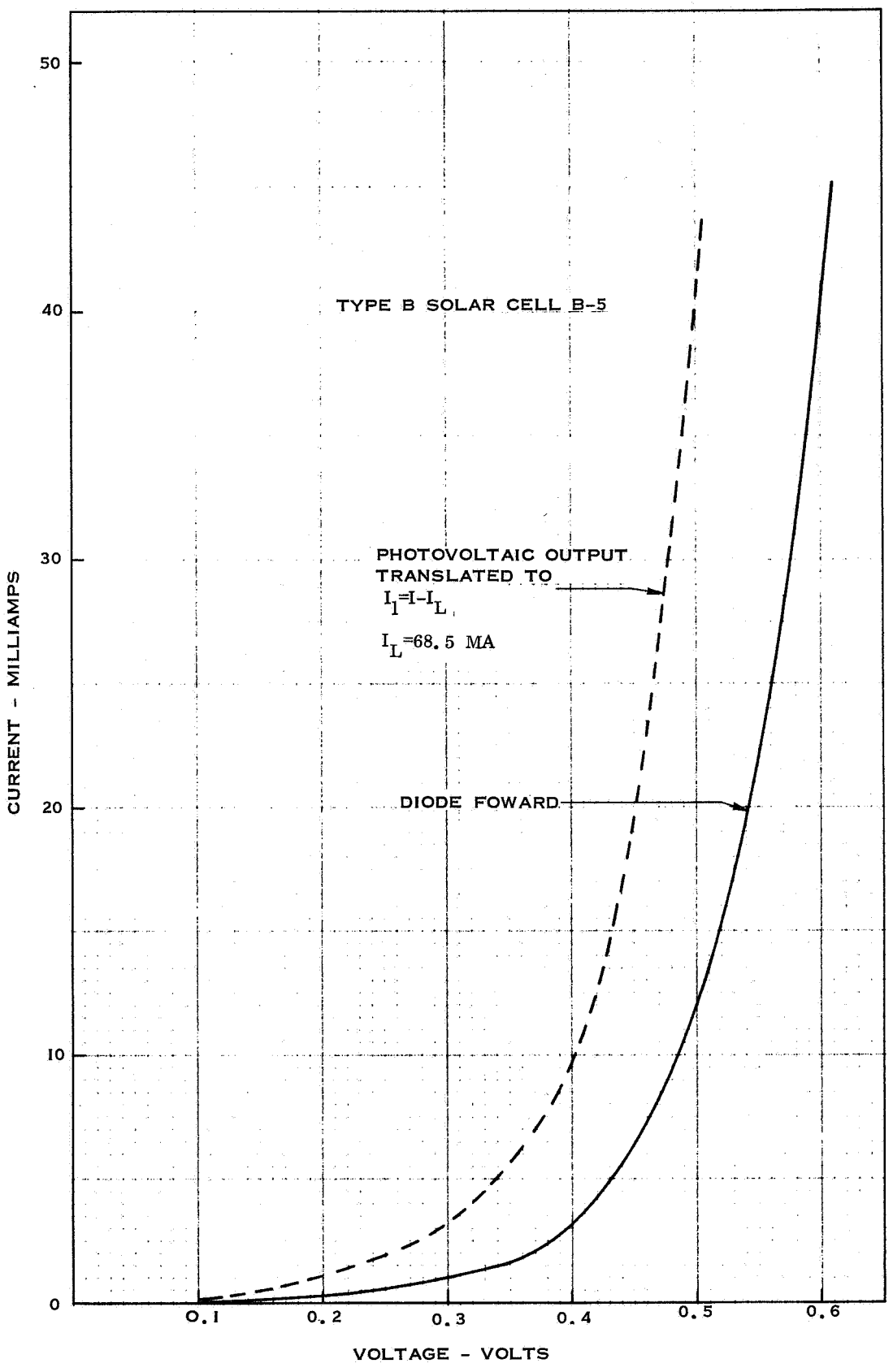

Figure 86 Comparison of Dark Forward Diodes & Photovoltaic Output Cell Type B

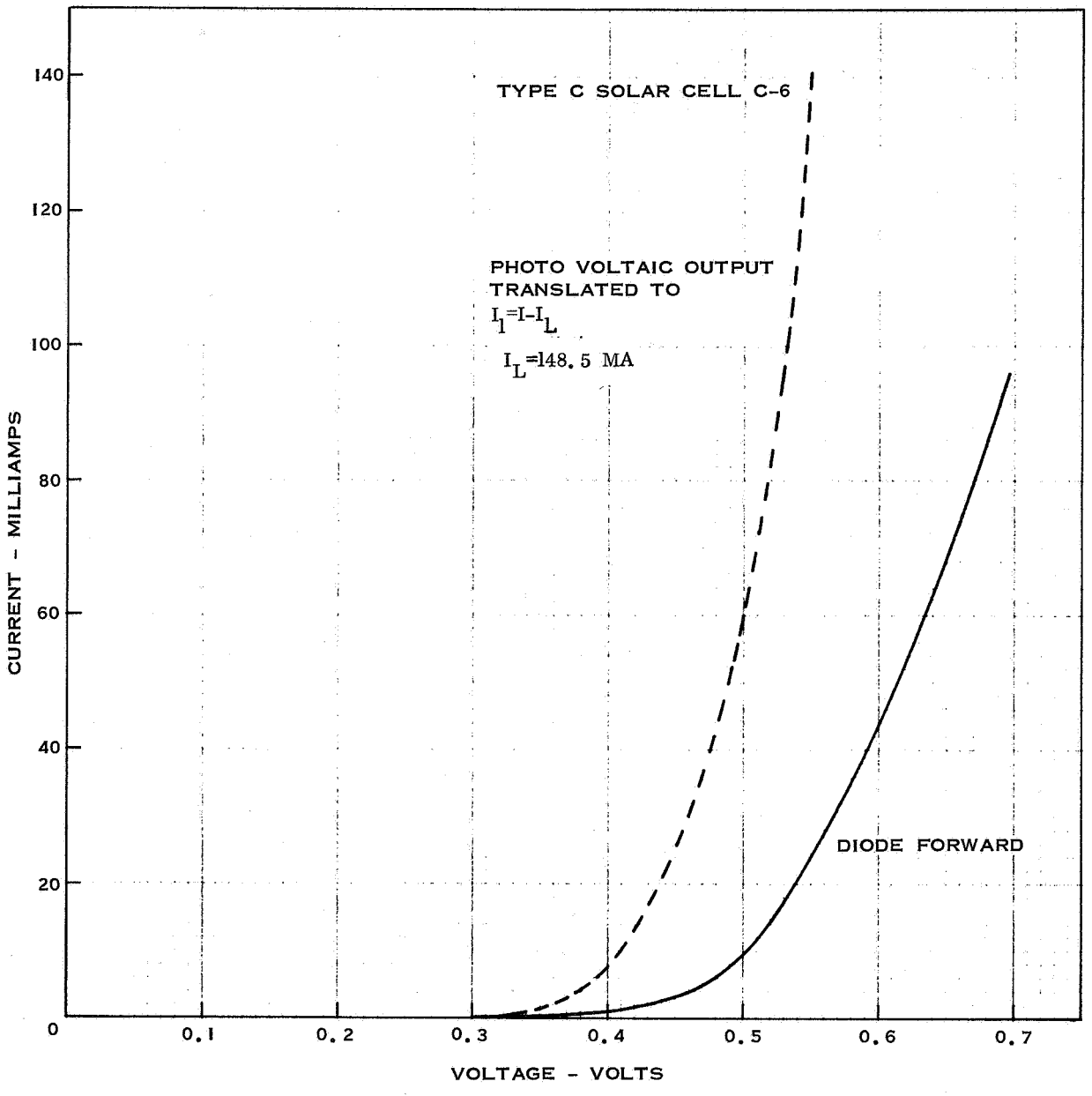

Figure 87 Comparison of Dark Forward Diodes & Photovoltaic Output Cell Type C

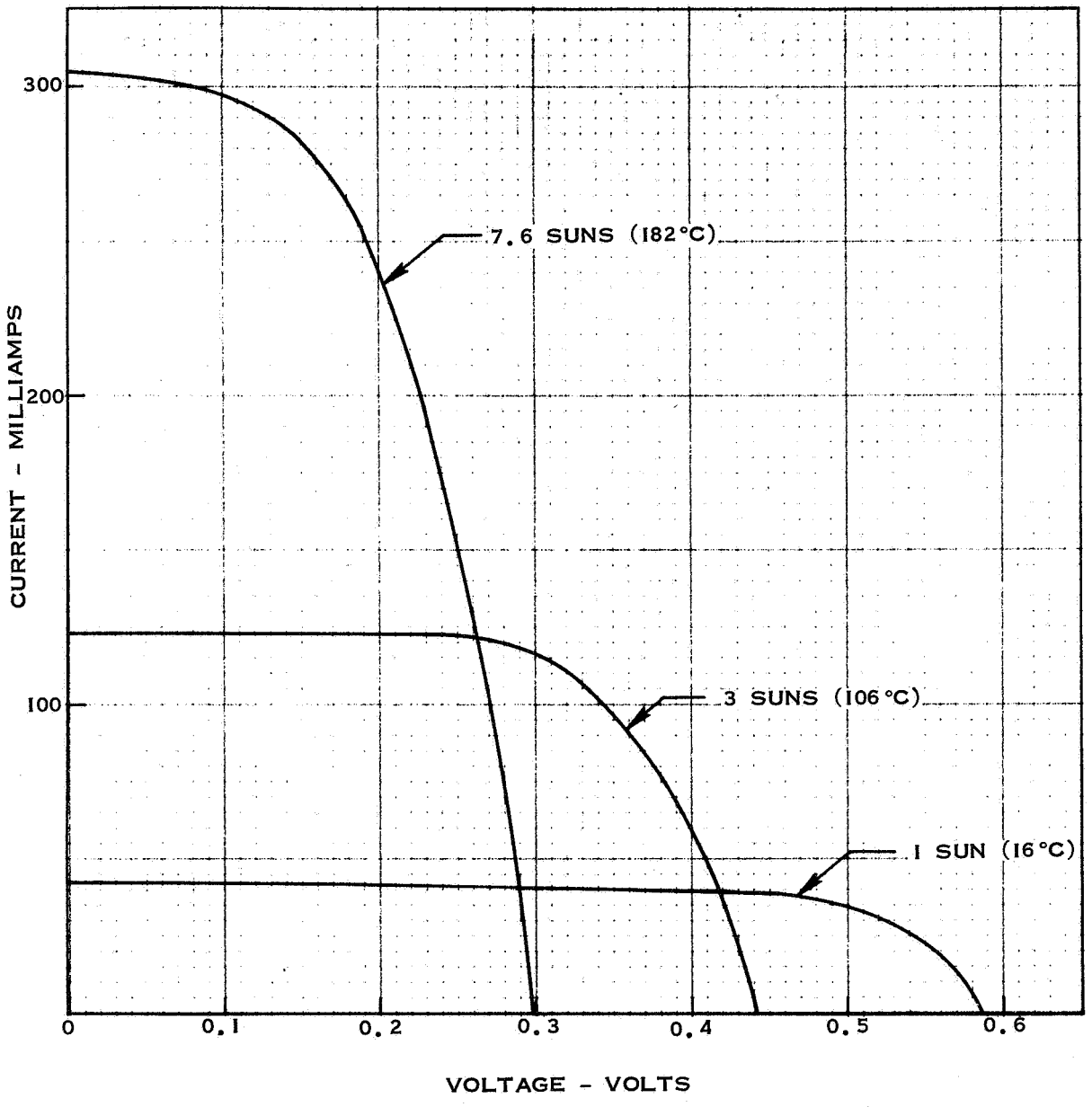

Figure 88 High Intensity Normal Incidence Comparison 1A

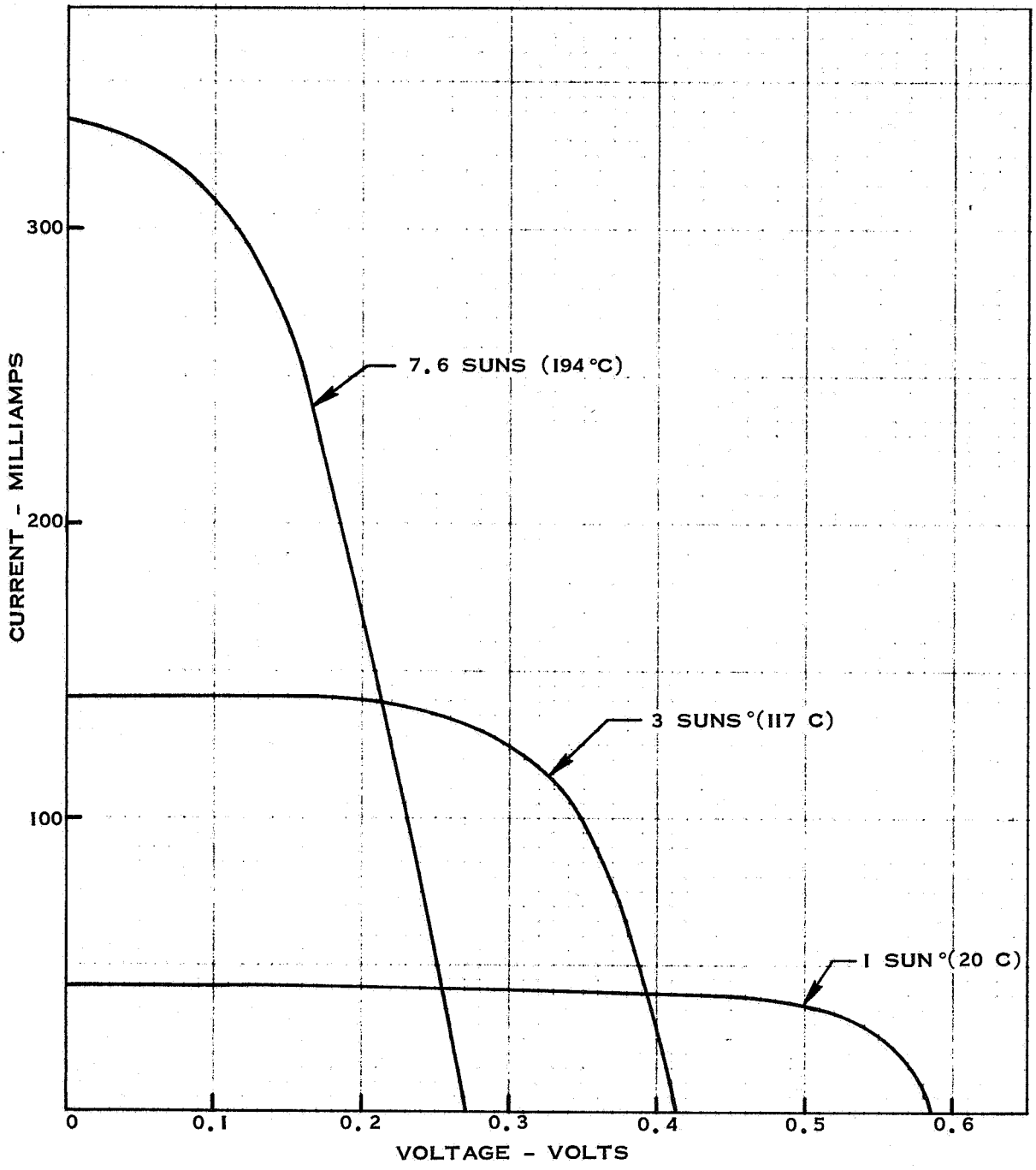

Figure 89 High Intensity Normal Incidence Comparison 2A

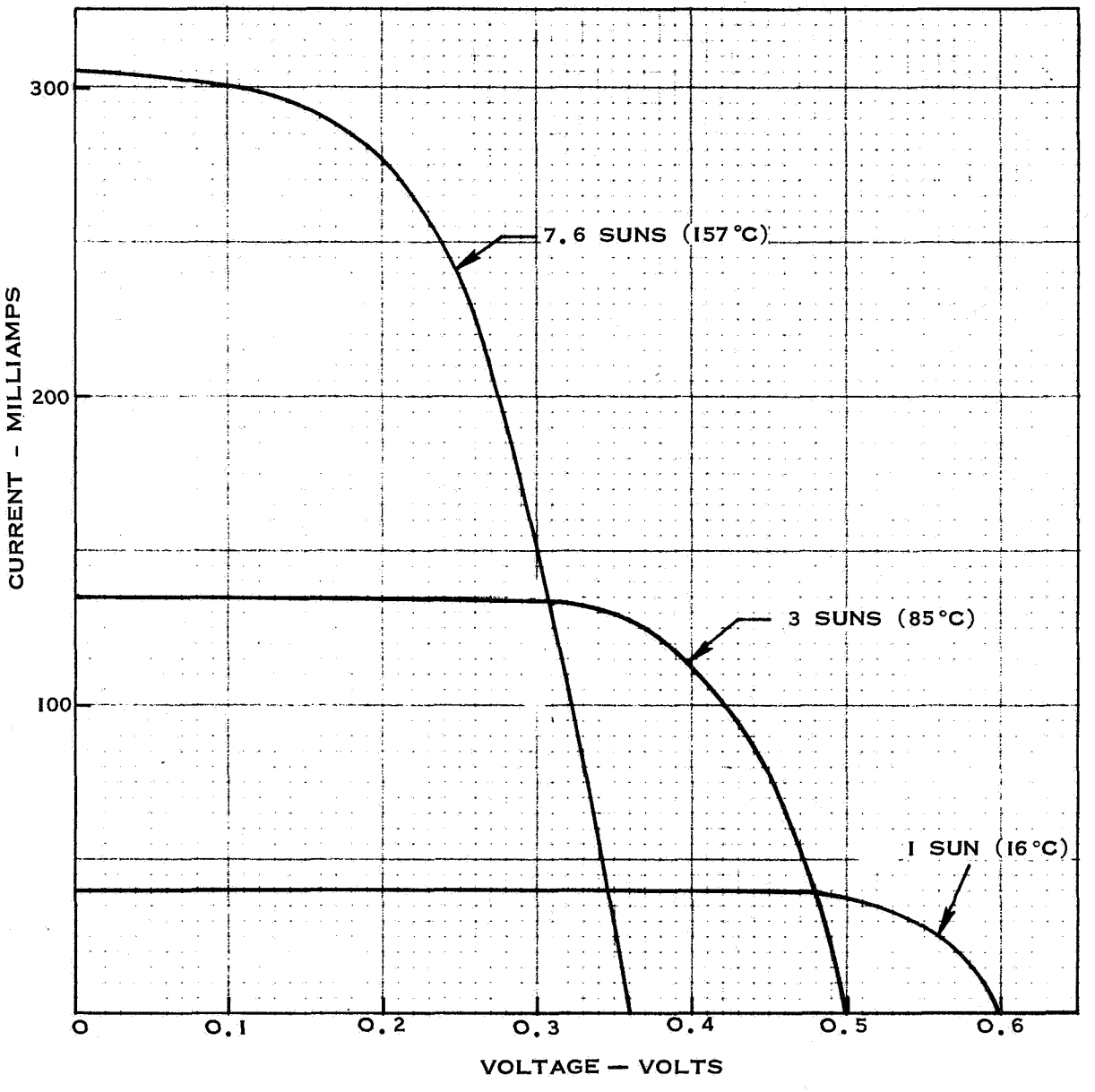

Figure 90 High Intensity Normal Incidence Comparison 3A

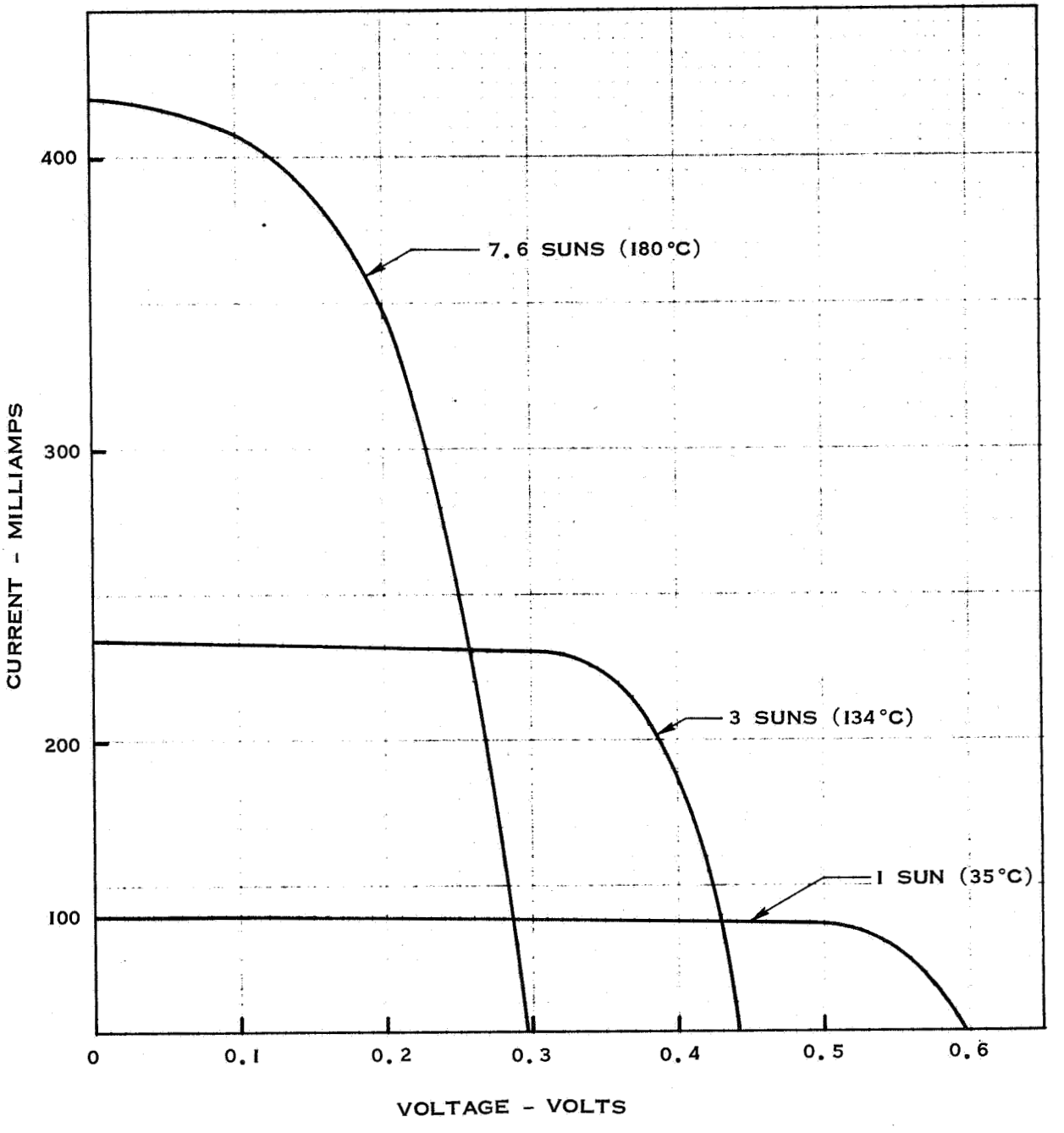

Figure 91 High Intensity Normal Incidence Comparison 4A

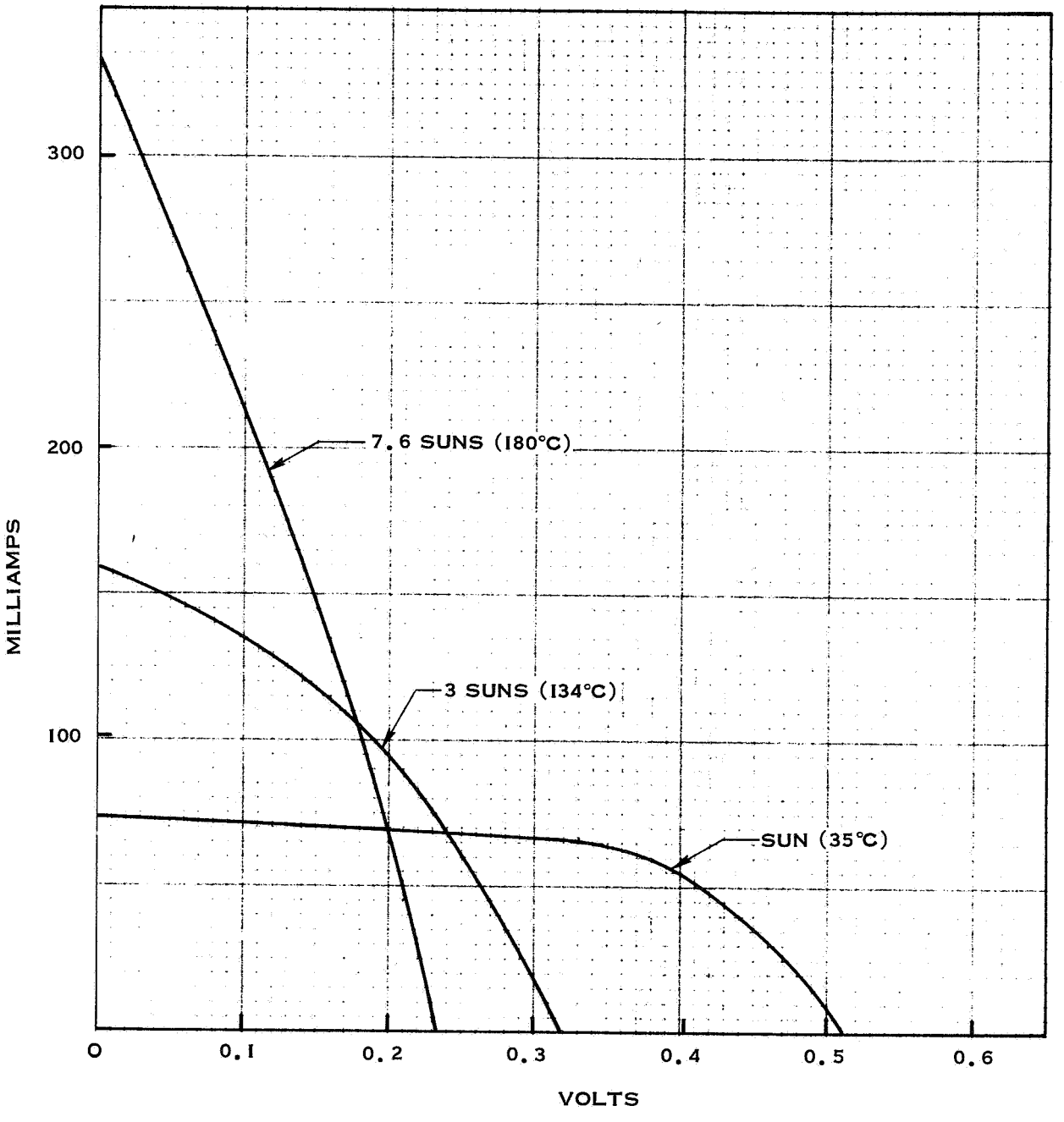

Figure 92 High Intensity Normal Incidence Comparison 1B

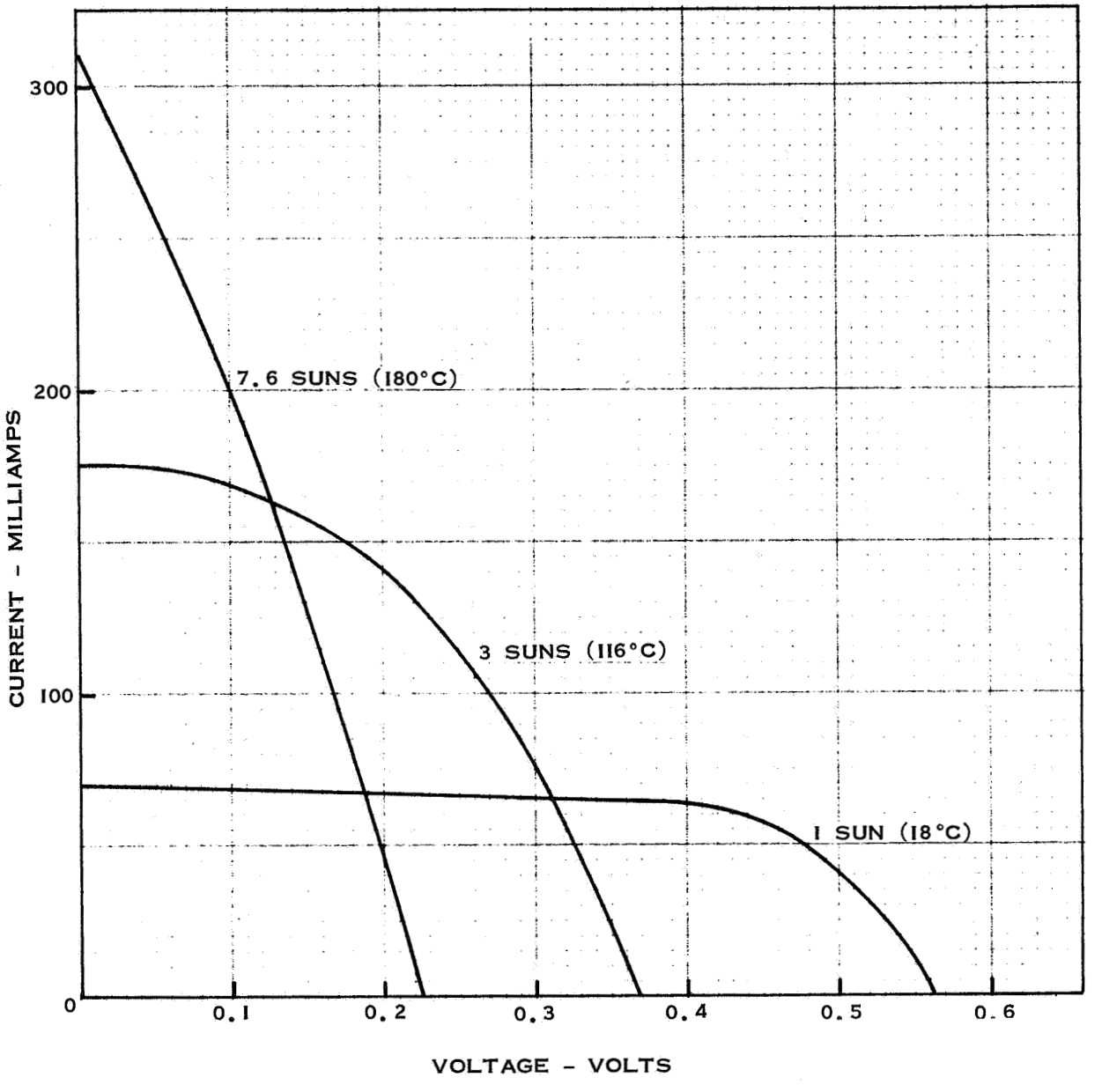

Figure 93 High Intensity Normal Incidence Comparison 2B

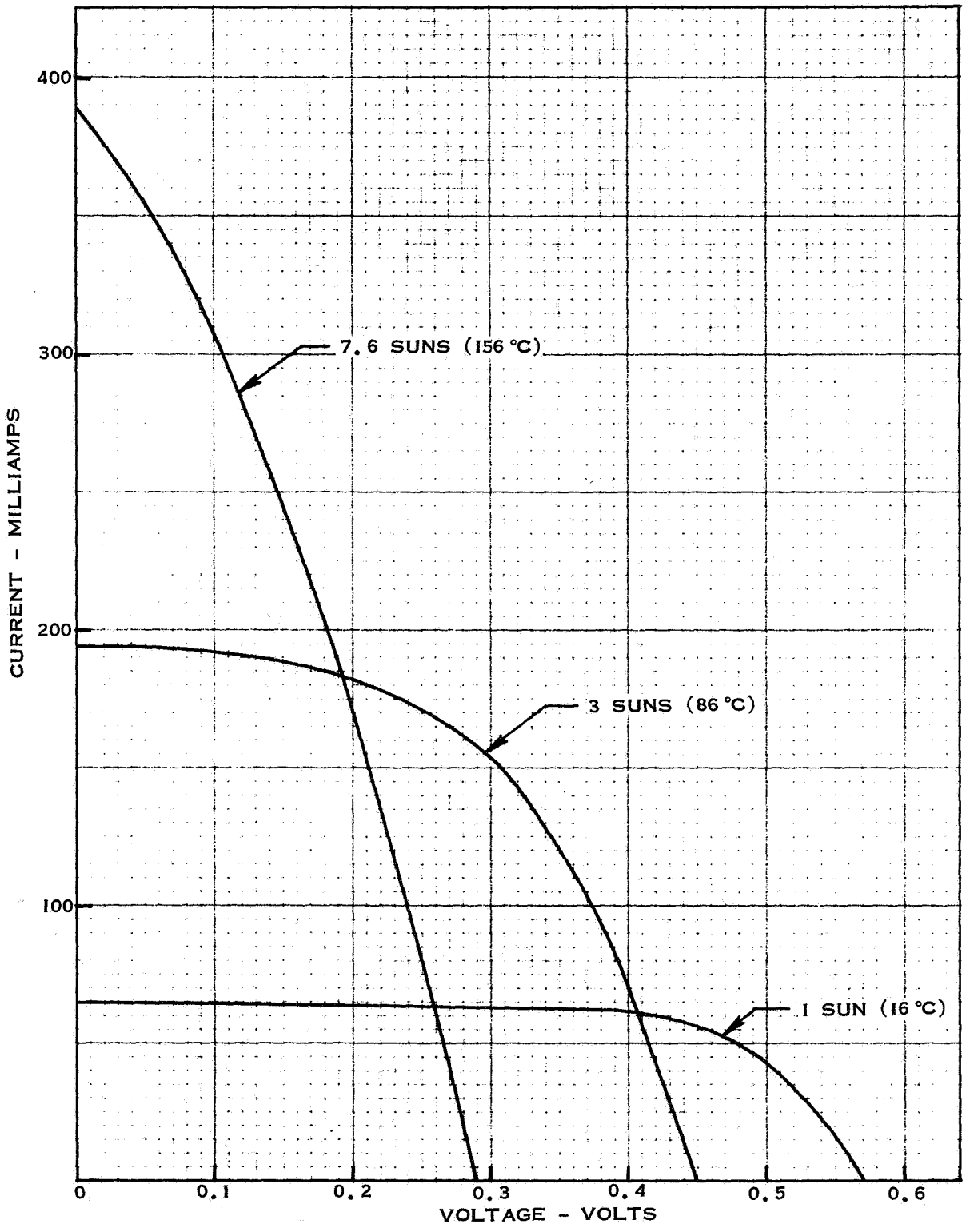

Figure 94 High Intensity Normal Incidence Comparison 3B

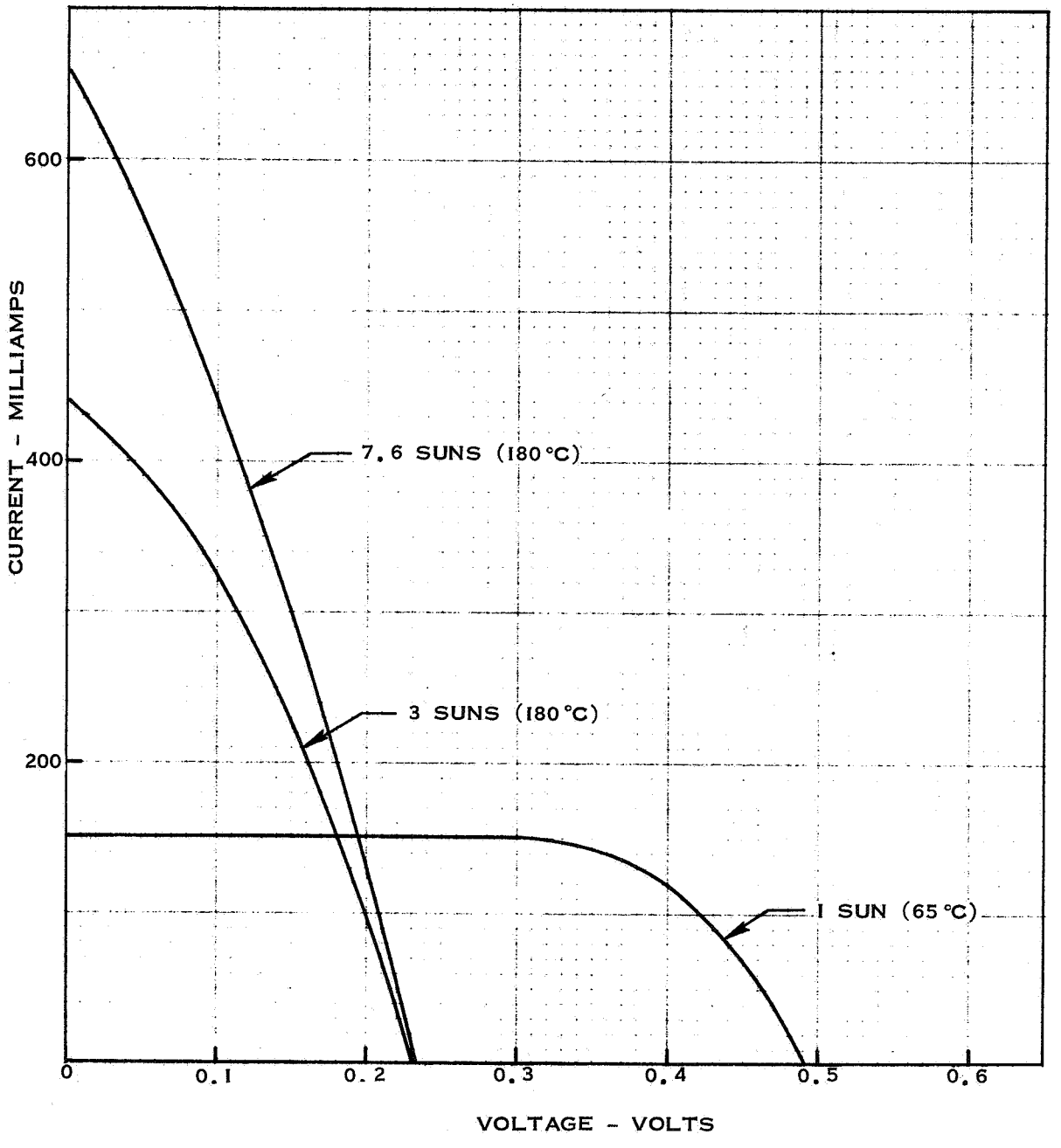

Figure 95 High Intensity Normal Incidence Comparison 1C

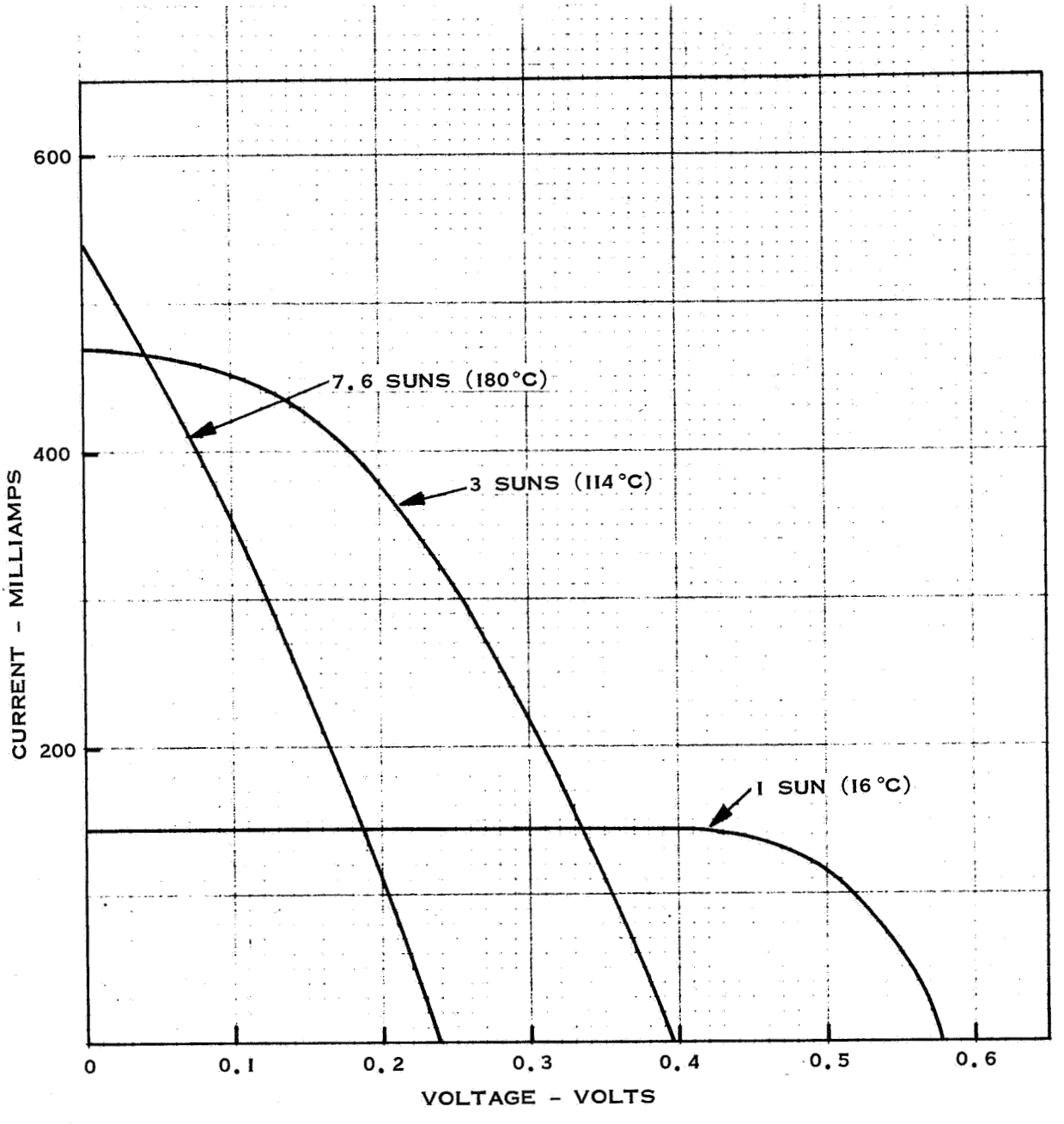

Figure 96 High Intensity Normal Incidence Comparison 2C

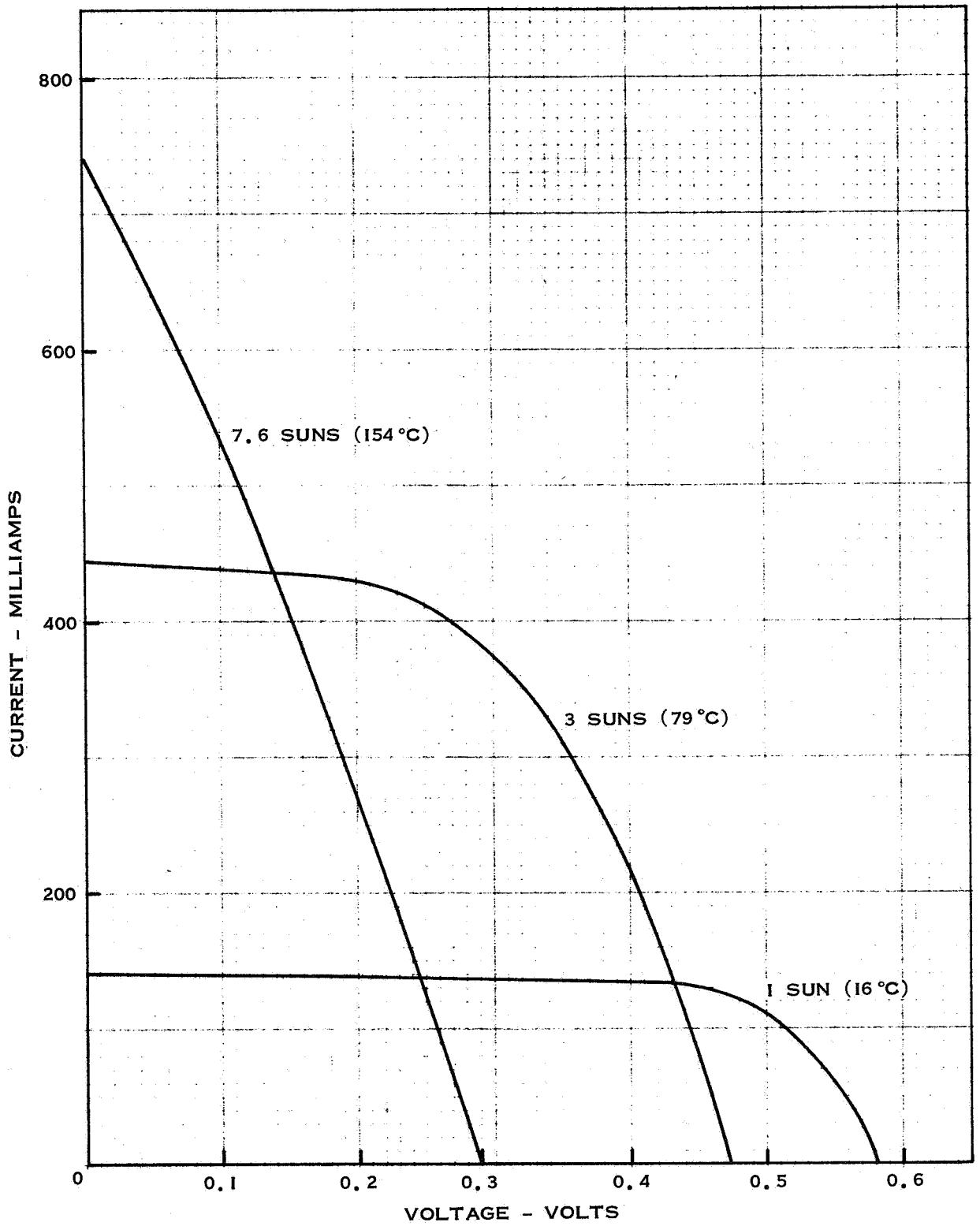

Figure 97 High Intensity Normal Incidence Comparison 3C

APPENDIX A

THEORETICAL THERMAL ANALYSIS OF A SINGLE SOLAR CELL

APPENDIX A

THEORETICAL THERMAL ANALYSIS OF A SINGLE SOLAR CELL

This appendix describes the method employed for solar cell thermal analysis used in this project. A single cell is considered bonded to but insulated from a rotating surface such that heat transfer can occur only across the face of the assembly. The assembly considered is presented below.

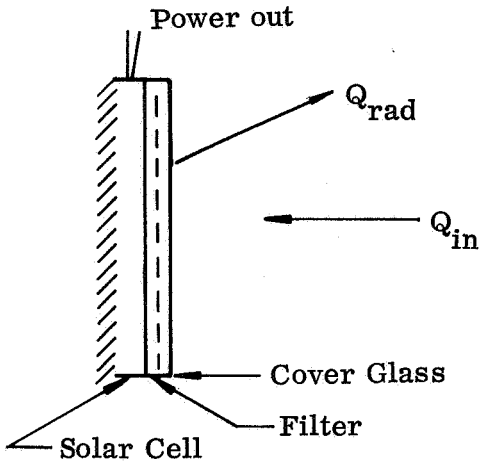

The fixture is assumed to be at constant temperature and quasi-steady state. The basic energy balance can now be characterized by the following general equation:

$$Q_{ave_{in}} - Q_{ave_{rad}} - P_{ave_{out}} = 0 \qquad \text{(A-1)}$$

Each term of equation (A-1) is now expanded individually in an effort to establish the specific equation.

The average energy into a rotating system irradiated on one side only can be expressed as:

$$Q_{ave} = \frac{\alpha Q_{in} \int_o^{\pi} \cos\theta d\theta}{2\pi} \qquad \text{(A-2)}$$

where

θ = angle of incidence

Q_{in} = incident heat rate (normal)

Q_{ave} = average heat rate per cycle rotation

α = absorptivity

Simplifying equation (A-2)

$$Q_{ave} = \frac{\alpha Q_{in}}{\pi} \qquad \text{(A-3)}$$

But

$$\alpha = \frac{\int_o^{\infty} \alpha_\lambda S_\lambda^* d\lambda}{\int_o^{\infty} S_\lambda^* \, d\lambda} \qquad \text{(A-4)}$$

where

α_λ = absorptivity as a function of wavelength

S_λ^* = relative solar intensity as a function of wavelength

S = solar constant

Thus

$$Q_{ave} = \frac{S \int_o^{\infty} \alpha_\lambda S^* d\lambda}{\pi \int_o^{\infty} S^* d\lambda} \qquad \text{(A-5)}$$

The only heat transfer from the cell occurs as a result of radiation from the front surface to absolute zero space (neglecting minor effect from heavenly bodies). Thus the average energy loss by heat transfer is given

$$Q_{ave_{rad}} = \epsilon \sigma T^4 \qquad \text{(A-6)}$$

where

ϵ = total hemispherical emissivity
σ = Stephan Boltzmann constant
T = Assembly surface temperature

The electrical power generated has the effect of reducing the assembly mean temperature. It is to be noted that the power generated by the solar cell is a function of the load resistance and that the power is zero both at short circuit current and open circuit voltage conditions. Thus the maximum reduction cell temperature occurs at the maximum power point. The power generated at maximum power can be approximated by:

$$P = \frac{Q_{in} \int_o^{\pi} \cos\theta d\theta}{2\pi} \eta_S \eta_T \eta_F \qquad \text{(A-7)}$$

or

$$P = \frac{S}{\pi} \eta_S \eta_T \eta_F \qquad \text{(A-8)}$$

Where the following quantities are defined

η_S = Solar Conversion Efficiency
η_T = Temperature efficiency
η_F = Filter efficiency .

Following the development by Fairbanks (Reference 1)

$$\eta_T \approx 1 - .00545\ (T - 301^{\circ}K) \qquad \text{(A-9)}$$

$$\eta_F = \frac{\int_{\lambda}^{\lambda_2} \tau_\lambda\, r_\lambda^* S_\lambda^*\, d\lambda}{\int_o^\infty r_\lambda^*\, S_\lambda^*\, d\lambda} \qquad \text{(A-10)}$$

and observing that

$\eta_s \approx$ to the conversion efficiency ($\sim .10$ for 10% efficient solar cells)

Thus combining

$$\frac{S}{\pi}\ \frac{\int_o^\infty \alpha_\lambda S_\lambda^* d\lambda}{\int_o^\infty S_\lambda^*\, d\lambda} - \epsilon\,\sigma\,T^4 - \frac{\delta}{\pi}\,\eta_S[1-.00545(T-301^{\circ}K)]\ \frac{\int_{\lambda}^{\lambda_2} \tau_\lambda\, r_\lambda^*\, S_\lambda^* d\lambda}{\int_o^\infty r_\lambda^*\, S_\lambda^* d\lambda}$$

$$= 0 \qquad \text{(A-11)}$$

However it is obvious that at either open circuit voltage or short circuit current the energy balance is given by:

$$\frac{S}{\pi}\ \frac{\int_o^\infty \alpha_\lambda\, S_\lambda^*\, d\lambda}{\int_o^\infty S_\lambda^*\, d\lambda} - \epsilon\,\sigma\,T^4 = 0 \qquad \text{(A-12)}$$

Now let

$$\alpha_{eff} = \frac{\int_o^\infty \alpha_\lambda\, S_\lambda^*\, d\lambda}{\int_o^\infty S_\lambda^*\, d\lambda} \qquad \text{(A-13)}$$

equation (A-12) can be simplified to give

$$\frac{S}{\pi}\ \alpha_{eff} - \epsilon\,\sigma\,T^4 = 0 \qquad \text{(A-14)}$$

or

$$T = \left[\frac{S \alpha_{eff}}{\pi \epsilon \sigma} \right]^{\frac{1}{4}} \qquad \text{(A-15)}$$

Figure A-1 presents the results of calculations using equation (A-15). For example, consider a solar cell with a cover glass having α/ϵ equal to 0.8. Figure A-1 shows that the equilibrium temperature is 168°C at six suns. A comparison of the effect of considering the power generated by the cell is presented in the body of this report.

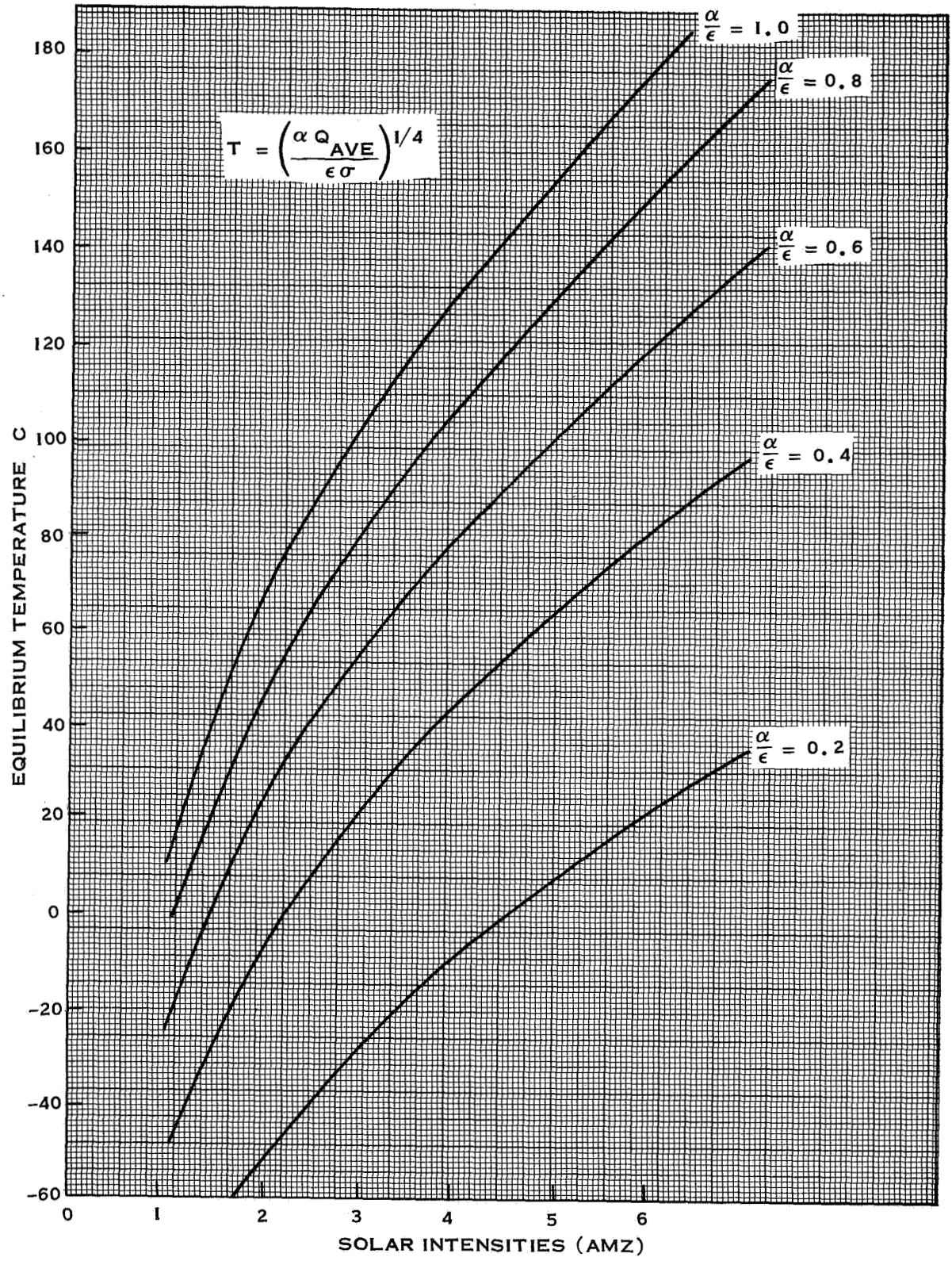

Figure A-1 Quasi Steady State Equilibrium Temperatures as a Function of Solar Intensity for Various α/ϵ Ratios

APPENDIX B

COMPARISON OF OCLI AND STRONG CARBON ARC SOLAR SIMULATORS

APPENDIX B

COMPARISON OF OCLI AND STRONG CARBON ARC SOLAR SIMULATORS

B.1 INTRODUCTION

The purpose of this appendix is to evaluate a comparison of the OCLI and Strong Carbon Arc solar simulators used in this program. The prime objective of this evaluation is to establish the validity of using the Strong Carbon Arc as a light source for high intensity solar cell evaluation. Of particular interest are the effects which occur when a blue/red interference filter is used with a solar cell subjected to carbon arc solar simulation as compared with its expected performance in space. This appendix briefly discusses and compares the two light sources as solar simulators. The results of measurements on solar cells is then presented.

The accepted standard solar spectrum is the data presented by F. S. Johnson (References 20 and 22). These data are based on three sources: (1) the NRL rocket data for wavelengths shorter than 0.318 μ, (2) Mount Lemmon data for the range 0.318 to 0.60 μ, and (3) Perry Moon's results for the wavelength range beyond 0.60 μ. The data presented by Johnson is well published and appears in this appendix on graphs marked "Johnson".

Although not an ideal black body, an examination of the solar spectrum shows that the sun in the region of solar cell response approximates the spectral energy distribution of a black body at a temperature in the range of 5700°K. The solar cell is only responsive to incident light in the spectral range from approximately 0.4 to 1.2 μ. Thus, for solar cell performance evaluation, where the cell temperature is actively controlled, the spectrum need be considered only in this range.

B.2 OCLI SOLAR SIMULATOR

The OCLI Model 31 solar simulator is used in the Philco-Ford photovoltaic laboratory specifically for evaluation of individual silicon solar cells at intensity levels of one solar constant or less. This device allows reproduction of the solar spectrum in the region of response of silicon solar cells through the mixing of two light sources, xenon and tungsten. This simulator successfully meets the AIEE Solar Simulation Specification (Reference 21) in 1000 Angstrom intervals; the tungsten lamp provides radiation with wavelengths longer than 6500 Angstroms and the xenon provides the remainder. The output of each lamp is filtered to provide the desired spectral content. They are then combined with respect to relative intensity.

The output provides 1 A.U. AMZ simulation over a 1-inch by 1-inch target. The spectral deviation of the OCLI solar simulator from Johnson's data on the solar spectrum is presented in Figure 6 which illustrates why the OCLI solar simulator is one of the accepted laboratory standards for testing solar cells at one sun AMZ intensities.

B.3 STRONG CARBON ARC SOLAR SIMULATOR

The strong carbon arc solar simulator is a Standard Model 75000-2 modified by the substitution of a 30 hp motor generator power supply for the usual rectifier supply. The operation of the carbon arc is supervised by personnel skilled and specially trained in its use and maintenance (through the motion picture industry). Although the carbon arc is not an ideal solar simulator, particularly for thermal control work, it can be shown to be acceptable for high intensity silicon solar cell measurements.

The performance of the carbon arc is limited by many factors; particularly the inherent flicker, the limited duration of test due to electrode life, the source uniformity, the spectral characteristics and the carbon "C" lines in the range of .35 to .5 micron, and the possible chromatic aberrations which are caused by the lens system. This appendix will address each of these limitations with the intent of establishing the relative value of the carbon arc as a solar simulator.

B.3.1 Carbon Arc Flicker

The flicker associated with the carbon arc systems results from several sources; however, two are the prime contributors: (1) current flucations and (2) inconsistancy in the composition of the electrodes.

The substitution of the 30 hp motor generator power supply for the usual rectifier supply has produced a very stable power supply for this light source. This modification has substantially reduced the amount of flicker usually associated with this type of simulator. The electrode feed systems have been mechanically checked to insure proper and continual electrical contact also tending to improve stability of the current to the electrodes. The distance between the electrodes is also important and the gap is maintained to insure proper current delivery.

Equally important is the quality and care of the carbon electrodes used. For this project, the electrodes were the highest quality available from National Carbon Company, with the positive being the 13.6 mm by 20-inch high intensity type, and the negative being the 1/2 by 9-inch oroty cored heavy duty type. Carbon electrodes readily absorb moisture from the atmosphere. Since much of the typical flicker results from the moisture in the electrodes being evaporated, the resulting flicker can be substantially reduced by insuring storage in a dry atmosphere. Philco-Ford stores the carbon electrodes openly exposed in an oven at approximately 150°C for at least two weeks prior to use.

B.3.2 Duration of Test

The 20-inch positive electrode is completely consumed in approximately one hour. When using the carbon arc for thermal control or in programs requiring quasi-steady-state thermal consideration, problems are encountered in the duration of test; however, when cell temperatures are actively controlled the allowable test duration is more than adequate due to the small mass of the silicon solar cell and its relatively instantaneous electrical response.

B.3.3 Uniformity and Collumation Angle

To provide the most consistent test section, the uniformity of the test plane was determined at various simulator intensities for different focusing lens positions. The short circuit current of a standard solar cell was used to map the uniformity across the given test plane. As expected, the most uniform test planes were consistently obtained with the lamp in the most unfocused position. A typical mapping of a test plane of the carbon arc is presented in Figure 11.

This completely defocused source has other advantages which are discussed in this appendix; however, it also has the disadvantage of substantially increasing the collumation angle. The larger collumation angle is only

a problem if it affects the solar cell performance parameters in any way.

The strong carbon arc solar simulator is located in the light source room of Philco-Ford's photovoltaic laboratory. The light source room is painted throughout with optically absorbing flat black paint to minimize stray reflections and background light. Thus, the light incident on a solar cell can be assumed to originate from the source only.

A mapping of the shadow line as a function of distance from the arc head in the defocused condition produced the graph of spot diameter presented in Figure B-2. This figure allowed the determination of the collumation half angle ($\theta/2 = 15^{\circ}\ 39'$) which is much larger than is generally quoted for carbon arc simulators. The problem associated with solar cells is twofold: (1) determining incident intensity and (2) determining angle of incidence. The description of the light source location and the description of the test apparatus presented in the main body of this report confirm the elimination of stray light to alter incident intensity measurements. Thus, if all the incident light comes from the source, only the collumation need be evaluated. However, when the size of the solar cell is considered relative to the distance from the source, it becomes obvious that the angular variation across the solar cell is inconsequential.

B.3.4 Spectral Characteristics

The most reliable data available on carbon arc spectral distribution, which has been confirmed by Philco-Ford measurements, is given by Gibson and Weinard (Reference 24). The Gibson and Weinard measurements are reproduced in Table B-1 for comparison with the relative spectral measurements performed by Philco-Ford (Table B-2).

The Gibson and Weinard data is compared to the NRL-Johnson data in Figure B-2. The carbon arc data has been adjusted to provide a graphical presentation of the comparison. This graphical comparison illustrates a

very acceptable comparison of the two data, particularly if the hash is averaged over the spectrum. However, the major concern is the spectral intensity effects on silicon solar cells. Also presented in Figure B-1 is the relative spectral response curve for a typical silicon solar cell. Figure B-2 presents the product of the NRL-Johnson data and the relative spectral response. For comparison, comparable data points are presented from the carbon arc data. This figure illustrates the very favorable result showing that the carbon spikes have substantially less effect than the portion of the spectrum from .45 μ to 1.0 μ. This argument is further enhanced by the consideration of the energy content of the carbon line spikes. Considering the relative spectral response of the solar cell and the very narrow band width of these spikes tends to place great credence upon the consideration of averaging the spectral intensity over the spectral spikes, particularly when the uncertainty associated with the measurement of these spikes exceeds 10%. The effect illustrated here will be further amplified in the discussion of solar cell performance comparisons presented in this appendix.

While the argument concludes that the carbon spikes have second order effects on solar cells, it also illustrates the fact that severe "chromatic aberrations" could produce much larger uncertainties. The magnitude of the effect of chromatic aberrations is greater at the longer wavelengths and can be a serious problem for thermal testing. In the range of solar cell response, chromatic aberrations in the simulator are relatively insignificant. This can be clearly seen from the fact that the position of the image formed by a lens depends upon the wavelength of the light (the ultraviolet closest to the lens, and the infrared the more distant). In the selected defocused condition, the test planes all fall well within the expected focus point of light with wavelengths greater than 4 μ. Thus, it is expected that the effects on solar cell performance due to chromatic aberrations are minor at the higher intensities (greater than one sun AMZ). This fact was confirmed by measurements of solar cell short circuit current behind the seventeen Philco-Ford narrow band filters, the data for which is presented in Table B-4.

B.4 COMPARISON OF SIMULATORS

The topic consideration is the value of the carbon arc as a light source for evaluating solar cell performance. A classic work is presented by Bell Labs (Reference 25) illustrating that any light source can be used if the solar cell quantum efficiency as a function of wavelength is accurately known and the spectral content of the source is known (particular emphasis being related to air mass zero solar cell performance). Since there are uncertainties associated with Johnson's data, it is observed that the Bell Labs method is at best cumbersome to apply and direct simulation is the best method to follow. The value of the OCLI solar simulation is well established industry-wide and Philco-Ford performs continued performance checks with industry (for example, Reference 26). This appendix compares the carbon arc solar simulator to the OCLI simulator through actual solar cell performance. Of major concern is the evaluation of solar cell performance employing blue red interference filters at high angles of incidence.

B.4.1 Comparison Using Interference Filters

Two comparisons were made using interference filters: (1) Tests using the five filter-cell fixture normally used as a course check on the OCLI simulator test facility and (2) tests using the seventeen narrow bandpass interference filters and the Heliotek standard cell.

The averaged results of many measurements are presented in Table B-3 along with the 50% cut on and cut off wavelength of the particular filter. The relative value of this data is to indicate that the carbon arc is a little weak (~ 20%) in ultraviolet (filter No. 2) and a little strong in infrared (~ 10% for No. 5). These results tend to confirm the spectral distribution presented in Figure B-1.

A more comprehensive spectral check using the seventeen selective bandpass filters is given in Table B-4, again illustrating a defficiency in

ultraviolet and a slight excess in infrared. All of these measurements are made at normal incidence; however, the values are so consistent, that in the range of solar cell responses, their comparison appears very favorable.

B.5 SOLAR CELL PERFORMANCE COMPARISON

To confirm the above described expected conformity between the light sources when testing silicon solar cells, a series of one sun performance tests were conducted. These tests were performed on two categories of test specimens used in this program: (1) in the as received condition and (2) with blue-red filters attached.

This section of the appendix presents the comparison of the data obtained from the two light sources, and illustrates the outstanding correlation. It is obviously expected that the open circuit voltage and short circuit current would exhibit better correlation than the area around maximum power, and this is seen in the data; however, the deviation of a single measurement is expected to be (by error analysis) approximately 2% while the deviation of the mean is expected to be somewhat less, approximately 1%. This is again confirmed by the results.

The curves presented in Figures B-3 through B-6 are labeled to describe the particular cell configuration and document the very acceptable correlation of solar cell performance. The deviation on normal curve for cell 3-A-24 presents the largest percentage error on any curve obtained; however, if the carbon arc curve is compared to the one sun OCLI cabi-bration curve, very close agreement exists, suggesting an operator error in adjusting the x-y plotter for the referenced OCLI curve.

The curves presented illustrate the very good comparison between all these samples tested; however, the blue-red filter used in these tests had a nominal cut on wavelength of approximately 0.405 μ and a very wide band-pass filter. The questions concerning the effect of the carbon spikes on

a narrower bandpass blue-red filter still remain to be considered. Reference 2 presents the recommendation that at increasing intensities, narrower bandpass filters would be required for maximum thermal control. An oriented array at 25 solar constants incident at 75 degrees would provide a maximum insolation of 25 cos 75 = 6.48 solar constants.

Reference 2 also shows that if this oriented array were rotating (as would be the case for a truncated cone) a calculated optimum "cut on" wavelength for an ideal filter would be at about 0.56 μ. This corresponds very closely to the cut on point for Filter No. 2 employed in this reference which gives the following spectral shifts as a function of wavelength. (Reference 2, Table 5, Page 51).

Incident Angle	Filter Cut on Wavelength
0	.590
15	.585
30	.5715
45	.553
60	.532
75	.517

This data illustrates the worst case, as the cell's relative spectral response is still very high at a wavelength of 0.5 μ (~ 50%) and the filter cut on wavelength is moving toward the carbon line spikes. However, it must be observed that the "cut on" wavelength is defined as the point where the transmission is 50% of the maximum transmission for that orientation. Reviewing the specific data on transmission as a function of angle of incident illustrates that no filter is an ideal filter and hence, the definition of "cut on" is defined for approximations and computational purposes. The fact remains that the filter begins to transmit energy at lower values of relative transmissivity at much lower wavelengths and the spectral shift into the carbon peaks is very slow. The combination of (1) decreasing solar cell response, (2) spectral transmission curves, (3) energy contained in the spikes (4) spectral uncertainty and especially

(5) the time deviations, confirm the argument that while the carbon arc is not the optimum light source it can be used with great advantage for high intensity testing and that, with the exception of the inherent flicker, the effects of spectral irregularities tend to average themselves out and represent a very small contribution to the experimental uncertainty of the overall program.

TABLE B-1*

Spectral Energy Distribution of the
13.6mm H.I. Carbon Bare Arc at 160 Amps

Conditions	Wavelengths (μ)	Energy: Microwatts/ cm^2 at 1 m from a 1 mm^2 source per 0.1μ interval
Photomultiplier	0.280	4.50
IP-28 Tube (600V)	0.290	6.68
	0.305	9.62
Slit Width - 0.0128 mm	0.330	$1.31 \cdot 10^{1}$
Cain - 10	0.350	$2.34 \cdot 10^{1}$
Full Scale - 10	0.352	$2.51 \cdot 10^{1}$
Relative Humidity - 32%	0.356	$5.03 \cdot 10^{1}$
	0.359	$2.36 \cdot 10^{1}$
	0.364	$2.11 \cdot 10^{1}$
	0.370	$2.26 \cdot 10^{1}$
	0.372	$3.51 \cdot 10^{1}$
	0.374	$2.85 \cdot 10^{1}$
	0.375	$2.75 \cdot 10^{1}$
	0.382	$5.14 \cdot 10^{1}$
	0.386	$9.45 \cdot 10^{1}$
	0.390	$7.78 \cdot 10^{1}$
	0.392	$9.73 \cdot 10^{1}$
	0.394	$3.58 \cdot 10^{1}$
	0.398	$5.52 \cdot 10^{1}$
	0.400	$3.84 \cdot 10^{1}$
	0.403	$4.94 \cdot 10^{1}$
	0.406	$3.77 \cdot 10^{1}$
	0.408	$4.55 \cdot 10^{1}$
	0.410	$3.67 \cdot 10^{1}$
	0.412	$5.24 \cdot 10^{1}$
	0.414	$3.72 \cdot 10^{1}$
	0.420	$5.17 \cdot 10^{1}$
	0.430	$3.43 \cdot 10^{1}$
	0.432	$4.41 \cdot 10^{1}$
	0.443	$3.49 \cdot 10^{1}$
	0.470	$4.71 \cdot 10^{1}$
	0.476	$3.47 \cdot 10^{1}$
	0.490	$3.85 \cdot 10^{1}$
	0.493	$3.36 \cdot 10^{1}$
	0.510	$4.03 \cdot 10^{1}$
PbS Cell	0.610	$4.60 \cdot 10^{1}$
	0.672	$4.18 \cdot 10^{1}$
Slit Width - 0.0392 mm	0.920	$1.71 \cdot 10^{1}$
Cain - 13	0.990	$1.73 \cdot 10^{1}$
Full Scale - 10	1.02	$1.81 \cdot 10^{1}$
Relative Humidity - 32%	1.05	$1.74 \cdot 10^{1}$
	1.10	$1.59 \cdot 10^{1}$
	1.12	$1.67 \cdot 10^{1}$
	1.26	$1.24 \cdot 10^{1}$
	1.48	9.00
	1.69	6.47
	2.04	4.04
	2.25	2.90
	2.68	1.35
Thermocouple	2.70	1.61
	3.05	$7.20 \cdot 10^{-1}$
Slit Width - 0.0954 mm	3.25	$5.60 \cdot 10^{-1}$
Cain - 18	3.70	$3.78 \cdot 10^{-1}$
Full Scale - 15	4.35	$2.67 \cdot 10^{-1}$
Relative Humidity - 28%	4.82	$2.07 \cdot 10^{-1}$
	5.60	$9.39 \cdot 10^{-2}$

*Obtained from Reference 24.

TABLE B-2

PHILCO-FORD SPECTRAL MEASUREMENTS OF
STRONG CARBON ARC

λ	X	K	$A\frac{X}{K}$	S_J
.40	1.57	2.68	.176	.154
.41	1.68	2.72	.185	.194
.42	1.75	2.88	.182	.192
.43	1.72	2.90	.178	.178
.44	1.75	3.03	.173	.203
.45	1.95	3.22	.182	.220
.46	2.10	3.42	.184	.216
.47	2.37	3.65	.195	.217
.48	2.40	3.85	.187	.216
.49	2.57	4.00	.193	.199
.50	2.68	4.15	.193	.198
.51	2.90	4.25	.205	.196
.52	2.93	4.30	.205	.187
.53	2.87	4.30	.200	.195
.54	2.83	4.15	.205	.198
.55	2.40	3.62	.199	.195
.56	2.20	3.35	.197	.190
.57	1.90	3.05	.187	.187
.58	1.72	2.75	.187	.187
.59	1.48	2.42	.184	.184
.60	1.30	2.15	.181	.181
.61	1.10	1.85	.178	.177
.62	.875	1.55	.169	.174
.63	.735	1.30	.169	.170
.64	.580	1.04	.167	.166
.65	.450	.810	.167	.162
.66	.325	.610	.160	.159
.67	.237	.440	.162	.155
.68	.161	.300	.161	.151
.70	.061	.125	.146	.144
.71	.033	.068	.145	.141
.72	.0187	.036	.156	.137
.73	.0100	.0185	.162	.134
.74	.0045	.0092	.147	.130

NOTE: λ - Wavelength in Microns

X - Meter Reading $X10^8$ in Amps

K - Sensitivity Factor X 10^6 in Amps-cm^e-μ/Watt

A - Adjustment Factor = 30

S_J - Johnson Solar Spectral Irradiance in Watts/cm^2-μ

TABLE B-3

SPECTRAL COMPARISON OF OCLI & STRONG SOLAR SIMULATORS
USING FIVE FILTER SPECTRAL TEST FIXTURE

CELL #	FILTER		OCLI SHORT CIRCUIT CURRENT	CARBON ARC SHORT CIRCUIT CURRENT
	NORMAL CUT ON	NORMAL CUT OFF		
	MICRONS	MICRONS		
1	Clear	Clear	68.6	68.6
2	.405	.583	18.3	15.3
3	.590	.694	14.7	14.7
4	.701	.810	11.9	13.6
5	.810	----	19.0	20.9

TABLE B-4

SPECTRAL COMPARISON OF OCLI & STRONG SOLAR SIMULATORS

USING SEVENTEEN BANDPASS FILTERS

FILTER	WAVELENGTH		MEASURE SHORT CIRCUIT CURRENT - MILLIAMP											
			OCLI			CARBON ARC								
						1 SUN			3 SUN			7.6 SUN		
	CUT ON μ	CUT OFF μ	RUN 1	RUN 2	RUN 3	RUN 1	RUN 2	RUN 3	RUN 1	RUN 2	RUN 3	RUN 1	RUN 2	RUN 3
1	.390	.411	0.189	0.189	0.188	0.16	0.16	0.17	0.45	0.48	0.49	1.30	1.34	1.34
2	.438	.454	0.470	0.471	0.470	0.40	0.39	0.37	1.21	1.19	1.19	2.70	2.70	2.80
3	.493	.507	0.940	0.942	0.943	0.77	0.77	0.78	2.22	2.22	2.20	6.05	5.85	6.00
4	.540	.558	1.470	1.480	1.470	1.29	1.28	1.28	3.67	3.65	3.65	9.75	9.80	9.90
5	.587	.607	1.51	1.51	1.51	1.31	1.31	1.32	3.92	3.85	3.75	10.00	9.95	10.05
6	.639	.661	1.72	1.72	1.72	1.69	1.65	1.65	5.10	4.90	4.90	13.05	12.60	12.90
7	.694	.720	1.99	1.98	1.99	1.96	1.95	1.95	5.80	5.75	5.80	15.00	14.75	15.00
8	.735	.765	1.60	1.59	1.59	1.61	1.60	1.62	4.85	4.80	4.80	12.05	12.20	12.10
9	.780	.815	1.67	1.67	1.67	1.55	1.57	1.58	4.70	4.70	4.70	11.70	11.60	11.60
10	.830	.860	1.382	1.378	1.378	1.27	1.26	1.28	3.80	3.78	3.75	9.50	9.35	2.45
11	.880	.905	1.255	1.261	1.265	1.11	1.13	1.14	3.38	3.35	3.35	8.40	8.35	8.35
12	.925	.960	1.122	1.119	1.121	1.00	1.02	1.01	3.05	3.05	3.05	7.70	7.60	7.60
13	1.010	1.040	0.760	0.754	0.758	0.72	0.74	0.73	2.15	2.20	2.18	5.60	5.40	5.55
14	1.050	1.090	0.385	0.381	0.383	0.35	0.37	0.37	1.10	1.09	1.10	2.80	2.65	2.80
15	1.115	1.145	0.113	0.111	0.118	0.105	0.11	0.11	0.34	0.34	0.34	0.83	0.84	0.85
16	1.150	1.200	0.143	0.141	0.144	0.13	0.14	0.13	0.41	0.41	0.42	0.99	1.03	1.02
17	1.190	1.220	0.060	0.060	0.067	0.06	0.06	0.06	0.17	0.17	0.17	0.46	0.45	0.48
None			61.2	61.2	61.2	61±1	61±1	61±1	182±2	182±2	182±2	343±2	343±2	343±2

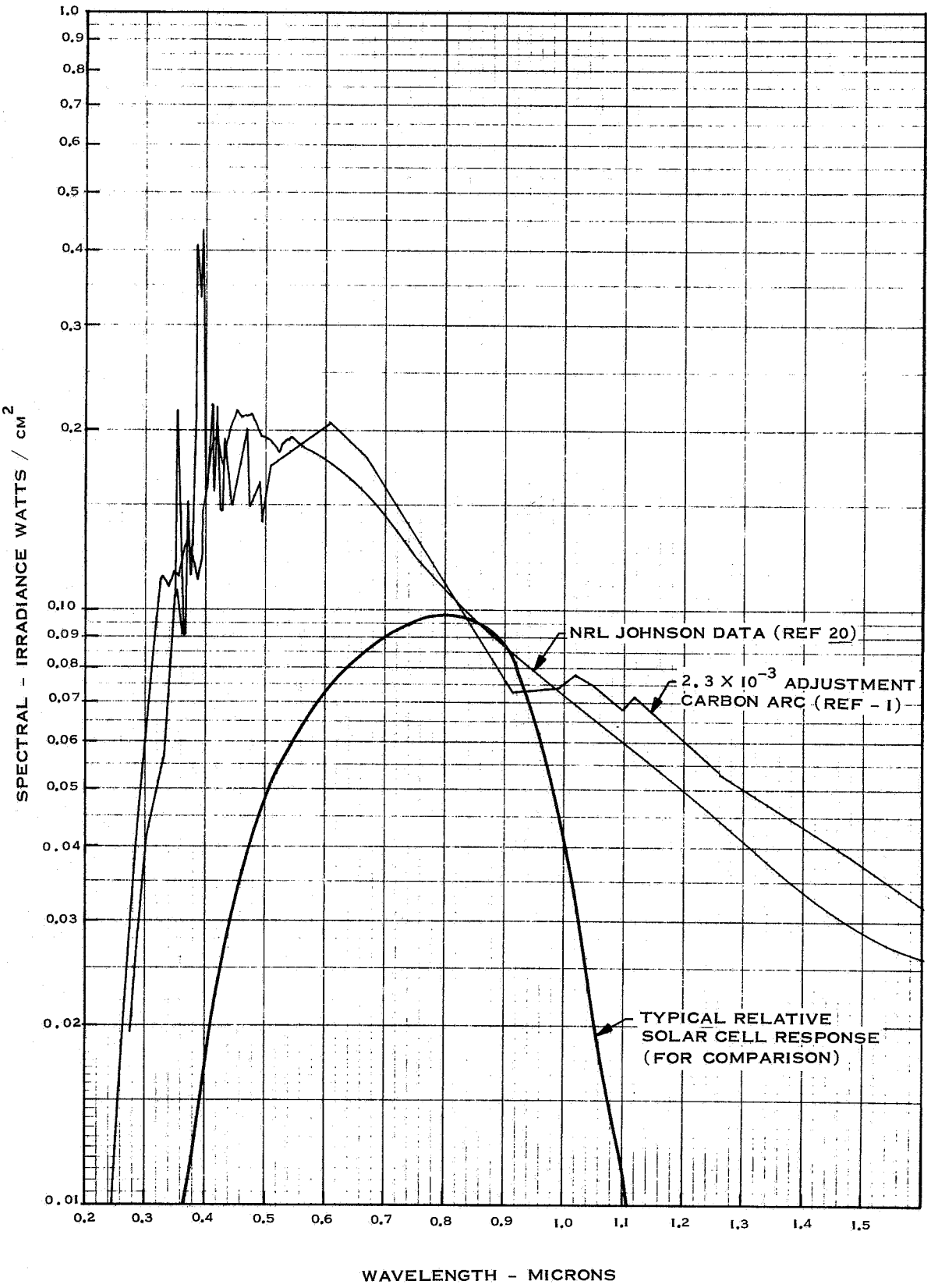

Figure B-1 Spectral Distribution of Carbon Arc

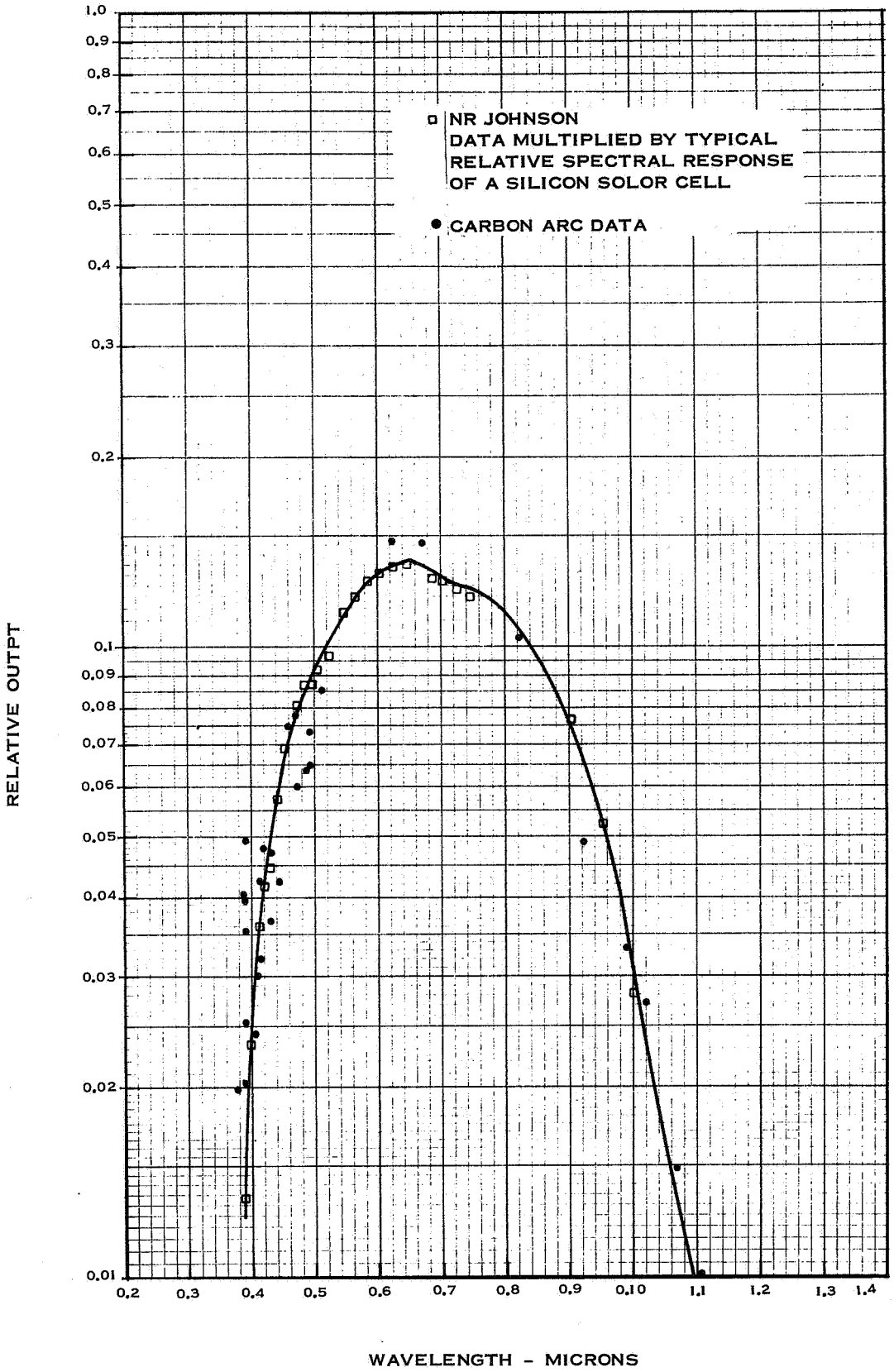

Figure B-2 Solar Cell Response and Solar Spectrum Comparison

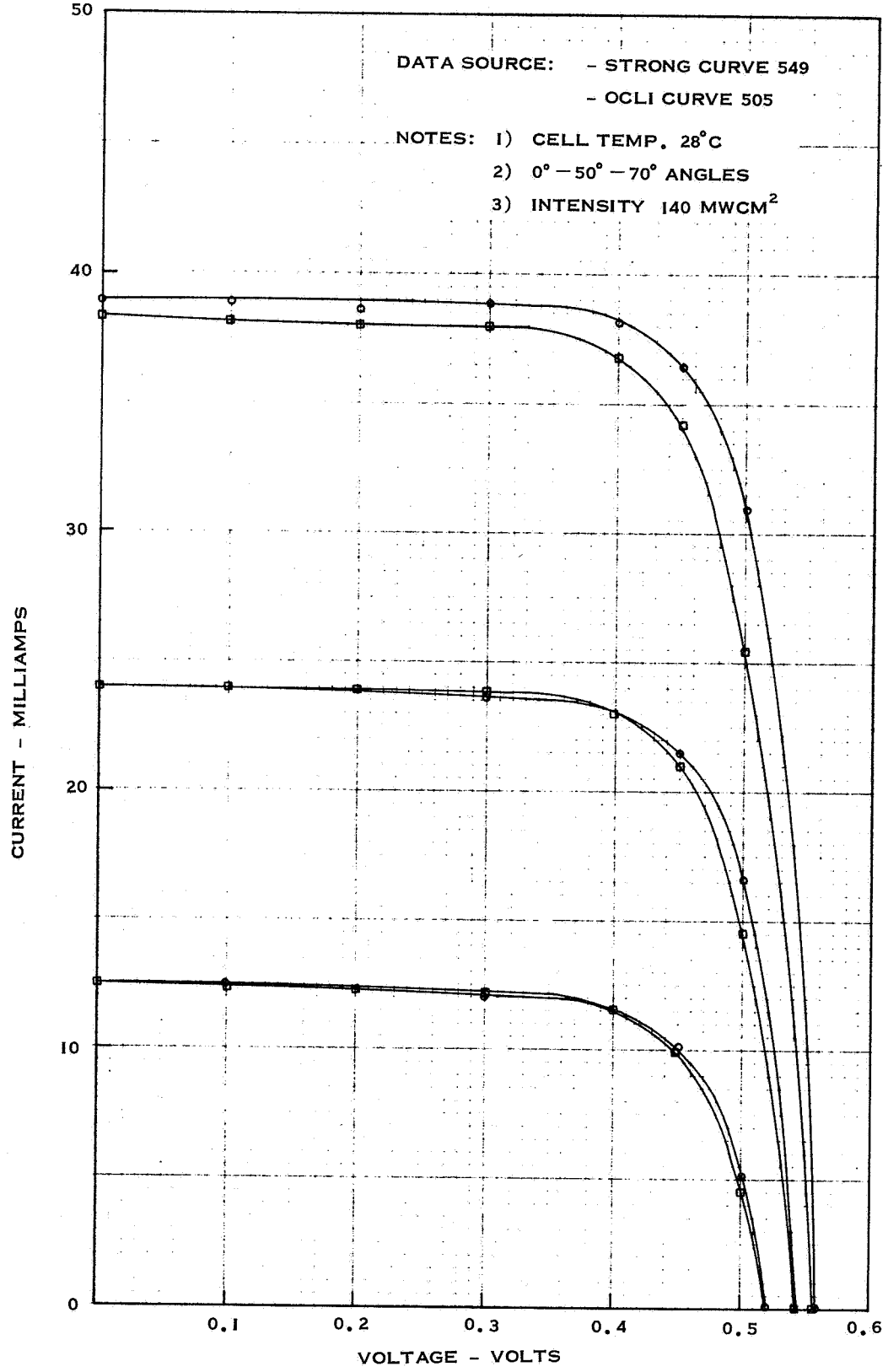

Figure B-3 I-V Comparison of Solar Cell Performance (Carbon Arc and OCLI Simulator)

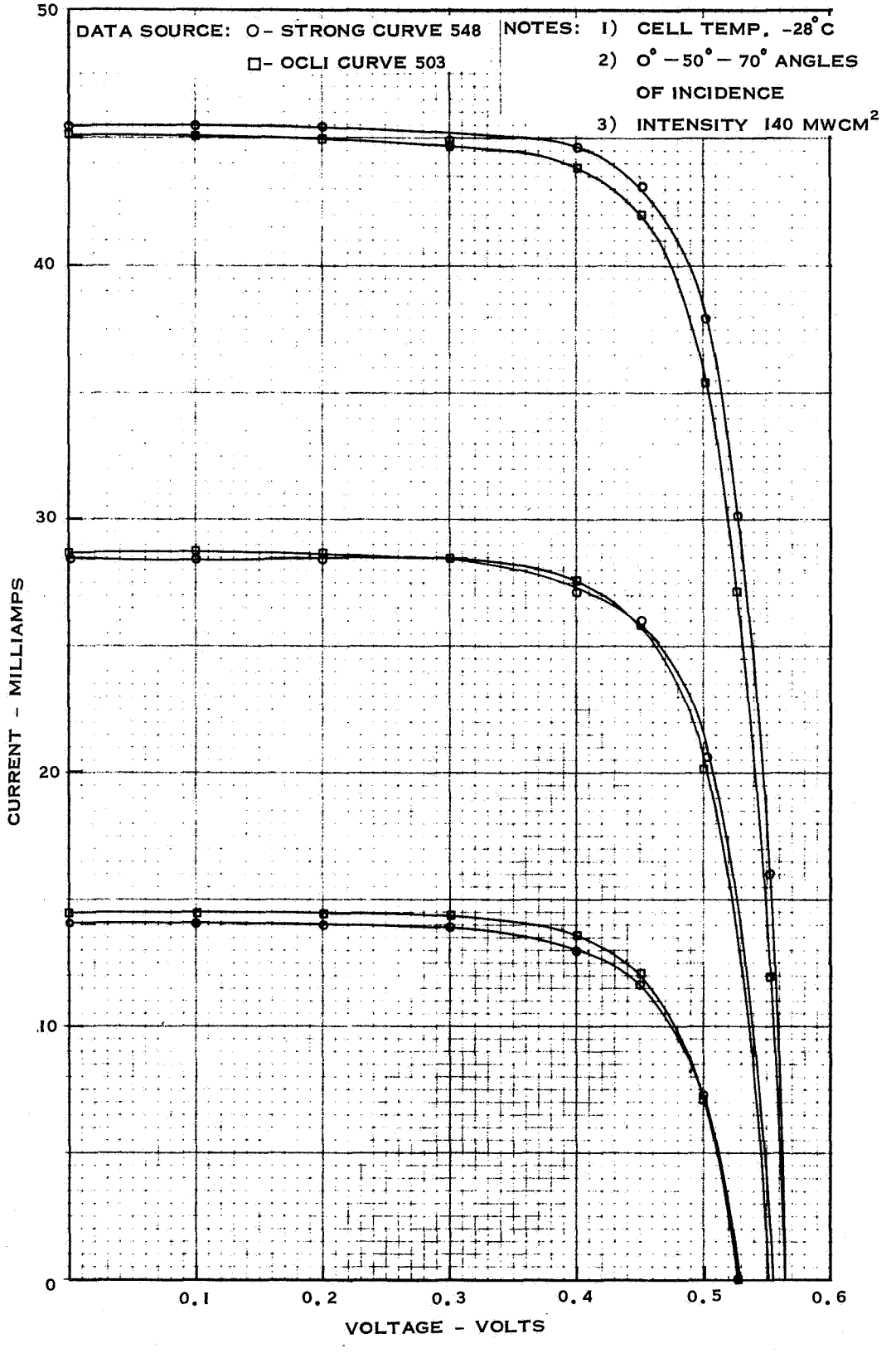

Figure B-4 I-V Comparison of Solar Cell Performance (Carbon Arc and OCLI Simulator)

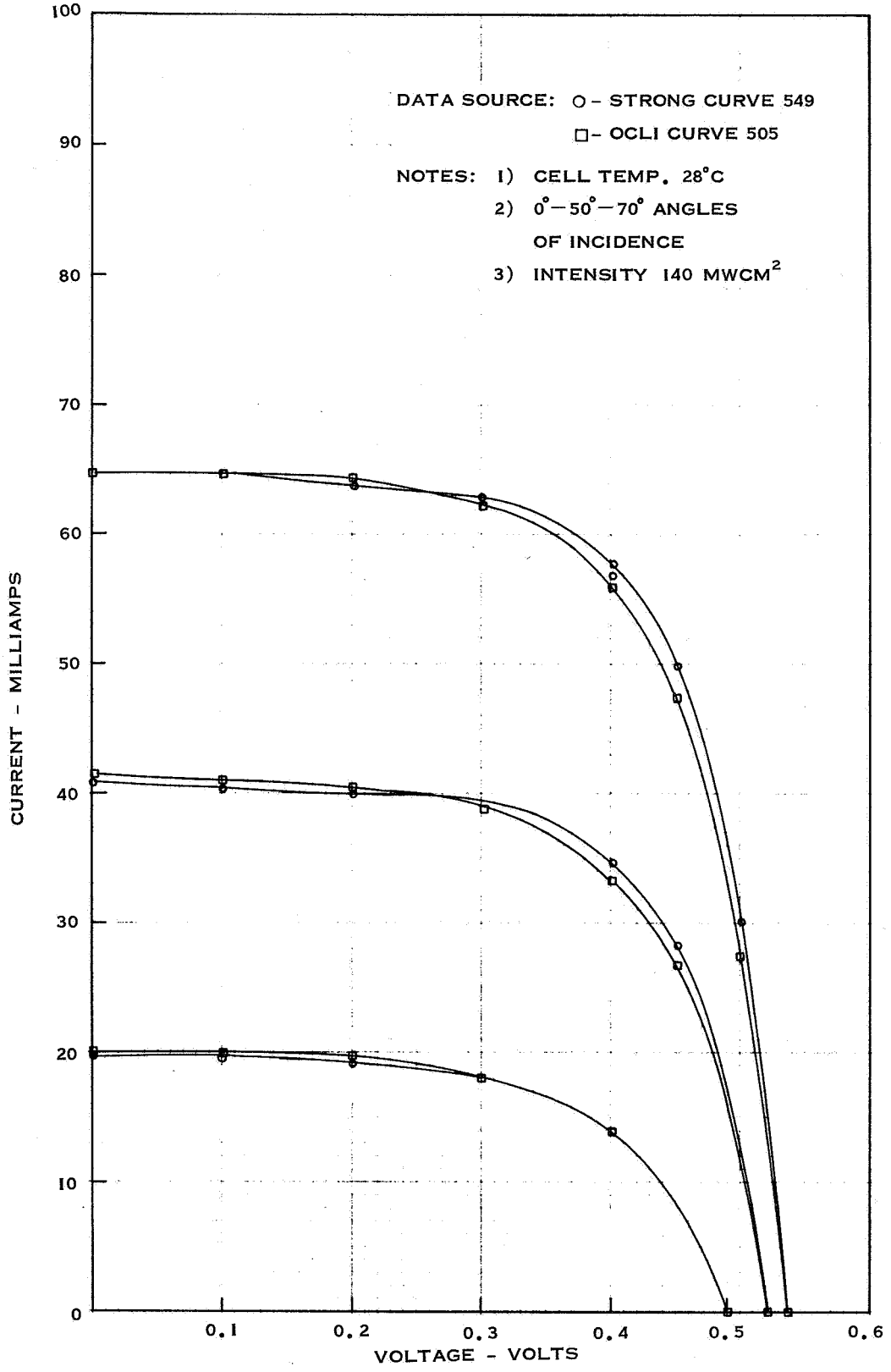

Figure B-5 I-V Comparison of Solar Cell Performance (Carbon Arc and OCLI Simulator)

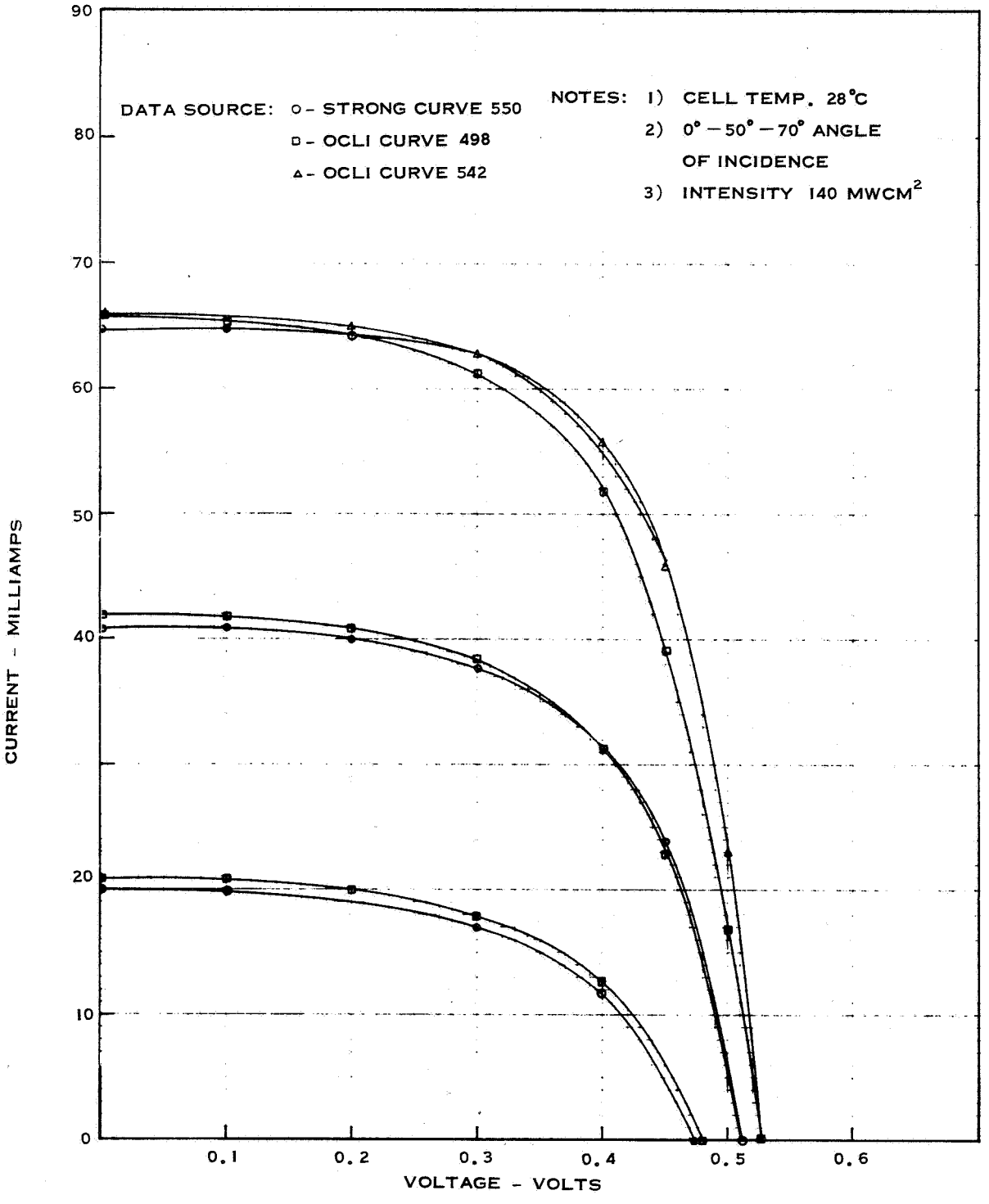

Figure B-6 I-V Comparison of Solar Cell Performance (Carbon Arc and OCLI Simulator)

APPENDIX C

EVALUATION OF EXPERIMENTAL ACCURACY

APPENDIX C

EVALUATION OF EXPERIMENTAL ACCURACY

C.1 INTRODUCTION

The data presented in this report covers many experimental techniques and procedures. For purposes of evaluating the experimental accuracy only the four basic experimental configurations will be considered: (1) the relative spectral response, (2) the OCLI solar simulator one sun test facility and (3) the carbon arc facility and (4) the measurement of series resistance. It is to be noted that the uncertainty and not the error is estimated by the methods herein employed. The uncertainty is a possible value of the error. The error in a single observation cannot be treated statistically; however, the uncertainty can be treated in part by the methods of statistics. The basis for the treatment of the evaluation of experimental accuracy is discussed in detail in Reference 36.

The procedure followed consists of three steps. These steps are:

1. Estimate and record in concise form the uncertainty in each of the variables.

2. Calculate the uncertainty in the result due and the uncertainty in each of the variables.

3. Combine the uncertainties to give a total uncertainty in the result.

Although the method is brief, some preliminary discussion is necessary. Uncertainties in the variables arise from possibilities for error. Errors can be classified as: fixed errors, random errors, and human errors. Fixed errors are errors which are constant for a given procedure. Random errors

are those errors which vary from reading to reading. Statistically, random errors can be reduced approximately as the square root of the number of readings by repeating and averaging the results. Human errors are those attributable to mistakes by the observer rather than sampling or instrumentation.

Some method is needed for establishing the estimates of uncertainties in a meaningful form. Rather than use the so-called "maximum uncertainty" an uncertainty interval of 1 in 20 will be employed in this analysis. This uncertainty interval is recognized as a simple guesstimate of a confidence interval. Combined with the assumption of normal distribution of errors, an uncertainty interval of 1 in 20 reflects approximately a 95% confidence limit.

C.2 UNCERTAINTY ASSOCIATED WITH RELATIVE SPECTRAL RESPONSE

The uncertainty associated with the measurement and determination of the relative spectral response can be contributed to the current measurement, light source stability, spectral characteristics of the filters, and the error in the given spectral response of the reference standard.

The cell temperature was measured to an accuracy of $\pm 1/2^{\circ}C$ and the tungsten light source was power through a stabline voltage regulator, hence, to simplify the analysis, the uncertainties will be attributed only to the current measurements and the standard cell data. The relative spectral response is determined from the ratio of the short circuit currents of the standard cell and the unknown cell, both of which are measured with the same equipment; hence, both measurement have the same experimental uncertainty. In addition, the bandpass characteristics of the filters tend to cause a fixed error in the readings. This error can be attributed to the uncertainty in the short circuit current at a particular wavelength. A detailed examination of these effects was performed which illustrates that the effect on the value of the relative spectral response is a function of how close the spectral response of the source is

to the reference standard. Since all cells tested in this program are, basically, comparable, the error introduced into the current measurement by these filters is estimated to be ±2%. These errors are additive; therefore, the uncertainty in each current reading is estimated at ±3%.

The relative spectral response of the Heliotek standard cell was measured using a filter wheel monochromator. Thus it is assumed that the reference standard used had an experimental uncertainty of ±3%. The uncertainty of the spectral response determined from measured short circuit currents is obtained from the following relation:

$$R^* = \frac{I_1}{I_s} R_s^* \qquad \text{(C-1)}$$

Differentiating,

$$d(R) = \frac{R_1^*}{I_1} dI_1 + \frac{R_1^*}{I_2} dI_2 + \frac{R_1^*}{R_s^*} dR_s$$

$$dR_1 = \frac{R_s^*}{I_s} dI_1 + \left(\frac{-I_1 R_s^*}{I_s^2} dI_s \right) + \frac{I_1}{I_s} dR_s^* \qquad \text{(C-2)}$$

Dividing C-2 by C-1 and from statistical errors propagation analysis,

$$\left(\frac{dR_1^*}{R_1} \right)^2 = \sqrt{\left(\frac{dI_1}{I_1} \right)^2 + \left(\frac{dI_s}{I_s} \right)^2 + \left(\frac{dR_s^*}{R_s} \right)^2} \qquad \text{(C-3)}$$

The current measurement was made on laboratory precision milliampmeters with a calibrated accuracy of 0.5%. The smallest scale division of the meter is consistent with the meter requirements for readings within this uncertainty. Combining possible human errors current measurement can be expected to be well within 1% of the current reading. The readings of both short circuit currents were accomplished in an identical manner; hence, response of the Philco-Ford standard cell can be determined from Equation C-3 as follows:

$$\frac{dR_s^*}{R_s} = \sqrt{3^2 + 3^2 + 3^2} = \pm 5.2\% \qquad \text{(C-4)}$$

Therefore, the uncertainty in this experiment is evaluated from equation C-3 as follows:

$$\frac{dR_1^*}{R_1^*} = \sqrt{3^2 + 3^2 + 5.2^2} = \sqrt{36} = \pm 6\% \qquad \text{(C-5)}$$

Which illustrates an expected uncertainty comparable to the Heliotek standard use throughout this program.

C.3 UNCERTAINTY ASSOCIATED WITH THE OCLI SOLAR SIMULATOR TEST FACILITY

The basic data obtained from the OCLI solar simulator test facility is in the form of I-V characteristic curves. The two independent variables (current and voltage) must be separately considered, thus there is an uncertainty associated with short circuit current and an uncertainty associated with open circuit voltage and a combined uncertainty associated with intermediate points.

The factor affecting the short circuit current are: light intensity, cell temperature, measurement error. In addition the I-V curves plotted on the X-Y plotter have an additional uncertainty resulting from the adjustment of the current axis. The light intensity is determined by measurement of the standard cell short circuit current which has been evaluated to have an uncertainty of approximately 1%. The temperature of the cell is determined to $\pm 1^{\circ}C$ which will cause less than .01% error and hence will have a negligible effect on the measured short circuit current. The short circuit current measurement error is identical to that discussed in Section C.2 and is

approximated to be 1%; hence, the measured short circuit current is determined from error propagation analysis to be:

$$\left(\frac{dI}{I}\right)_{sc} = \sqrt{1^2 + 1^2} = \pm 1.4\% \qquad \text{(C-6)}$$

In addition, the X-Y recorder adjustment is expected to introduce a possible 1% error addition to the uncertainty. Thus

$$\left(\frac{dI}{I}\right) = \sqrt{\left(\frac{dI}{I}\right)^2_{sc_1} + \left(\frac{dI}{I}\right)^2_{sc_2}} = \sqrt{2 + 1} = \pm 1.7\% \qquad \text{(C-7)}$$

The open circuit voltage measurement is affected primarily by temperature. Basic analysis of solar cell characteristics show that open circuit voltage can be basically used to measure cell temperature. The analysis of the test results illustrate that $2^{o}C$ temperature error can cause an absolute error of .006 volts for a specific cell which is approximately 1.5% uncertainty.

The best estimate of the magnitude of the uncertainty in power output including calibration errors is obtained from the error propagation analysis as the square root of the sum of the squares as follows:

$$\frac{d(P)}{P} = \sqrt{\left(\frac{dI}{I}\right)^2 + \left(\frac{dV}{V}\right)^2} = \sqrt{(1.7)^2 + (1.5)^2} = \pm 2.3\% \qquad \text{(C-8)}$$

The errors in the current measurement are generally random errors while the errors in voltage measurement result from the possible error in cell junction temperature determination. The uncertainty can be reduced somewhat by repeated measurement of the short circuit current. A useful rule which can be derived from statistics is that accidental errors can be reduced approximately as the square root of the number of readings by repeating and averaging results. In addition, throughout this testing program, several cells were tested so that mean readings tend to be more reliable.

C.4 UNCERTAINTY ASSOCIATED WITH THE STRONG CARBON ARC TEST FACILITY

The basic data obtained from the strong carbon arc solar simulator test facility is basically equivalent to that described in the previous section; however, several other sources of error must be evaluated. In addition, the established levels of uncertainty must be evaluated at particular solar intensities; thus, this analysis will consider the one sun and six sun experiments, assuming that the three sun uncertainty is between these two values.

C.4.1 One Sun Uncertainty

The cell voltage measurements at one sun are felt to be comparable to the OCLI data and analysis present in Section C.3. Since the measured cell temperatures are in the same general range, the calculated uncertainty interval of ±1.5% is applicable to this experiment.

The current measurement is affected by all the identical parameters as previously described; however, the flicker of the carbon arc caused an additional problem. The maximum flicker measured on the carbon arc has been somewhat less than 10%. A 10% flicker will affect a 10% efficient solar cell by approximately 1%. Assuming this in addition to the parameters considered the uncertainty for the measured short circuit current (following equation C-6) is

$$\left(\frac{dI}{I}\right)_{sc} = \sqrt{1^2 + 1^2 + 1^2} = \pm 1.7\% \qquad \text{(C-9)}$$

and the error in the current axis of the 1-V curves follows

$$\frac{dI}{I} = \sqrt{(1.7)^2 + 1^2} = \pm 2\% \qquad \text{(C-10)}$$

and thus the error in the power following equation C-8 is given by

$$\frac{dP}{P} = \sqrt{2^2 + 1.5^2} = \pm 2.5\% \qquad \text{(C-11)}$$

C.4.2 Six Sun Uncertainty

The six sun measurement was made at substantially higher cell temperature as well as the elevated intensity. The analysis of the uncertainty interval is identical to that prescribed in the previous sections with the exception of the uncertainty associated with the measurement of total incident intensity and cell temperatures.

The error in the measurement of total intensity is approximated to be about ±2.5% which will cause an equal error in the short circuit current. The problems of insuring an accurate measurement of short circuit current have been presented in the body of this report from which it can be concluded that the measurement errors are comparable to those presented above. Thus assuming the uncertainty in the short circuit current due to light source intensity measurements to increase from 1% to2.5%, the total uncertainty in measured short circuit current is calculated to be approximately 2.9%.

Similarly the temperature uncertainty is expected to increase primarily resulting from the temperature gradients across the cell. Thus the absolute error in voltage is expected to be about 2%. From these values the uncertainty for power can be calculated as 3.5%.

C.5 UNCERTAINTY ASSOCIATED WITH THE VALUES OF SERIES RESISTANCE

The series resistance calculations followed the method described by Wolf and Rauschenbach (Reference 4) which employs the following equation.

$$R_S = \frac{V_2 - V_1}{I_{L_2} - I_{L_1}} \qquad \text{(C-12)}$$

differentiating

$$dR_S = \frac{R_S}{I_{L_1}} dI_{L_1} + \frac{R_S}{I_{L_2}} dI_{L_2} + \frac{R_S}{V_2} dV_2 + \frac{R_S}{V_1} dV_1 \qquad \text{(C-13)}$$

dividing equation C-13 by C-12, determining each term, and employing the statistical error propagation criteria the following is obtained

$$\frac{dR_S}{R_S} = \sqrt{\left(\frac{dI_{L_1}}{I_{L_2} - I_{L_1}}\right)^2 + \left(\frac{dI_{L_2}}{I_{L_2} - I_{L_1}}\right)^2 + \left(\frac{dV_2}{V_2 - V_1}\right)^2 + \left(\frac{dV_1}{V_2 - V_1}\right)^2}$$

(C-14)

Examination of equation C-14 illustrates that the uncertainty associated with the calculated series resistance is related to the percentage error in each measurement as compared to the difference in the current and voltage measurements. This illustrates the effect of small differences in large numbers on uncertainty of the final results. A further analysis of this effect illustrates that the measurement of large series resistance can be accomplished much more accurately than cells with very small series resistance since the value of $(V_2 - V_1)$ can be determined more accurately for solar cells with larger series resistance.

Assuming that the error in I_{L_1} is equal to the error in I_{L_2} and the error in V_2 is equal to the error in V_1, equation C-14 can be simplified to

$$\frac{dR_S}{R_s} = \sqrt{2\left(\frac{dI_{L_1}}{I_{L_2} - I_{L_1}}\right)^2 + 2\left(\frac{dV_1}{V_2 - V_1}\right)^2} \qquad \text{(C-15)}$$

Observing that I_L is about 1/10 of I_{L_1} the quantity $I_{L_1}/I_{L_2} - I_{L_1}$ is evaluated from the OCLI analysis to be about 10%.

Eliminating the fixed error utilized in evaluating dV_1 the previous analysis allows evaluation of $dV_1/V_2 - V_1$ to be about 30%. These extremely large uncertainties are the result of light intensity levels relatively close together, however, many other parameters must be considered for large light level differences. Other problems associated with the measurement of series resistance are discussed in the body of this report.

Equation C-15 gives the following results

$$\frac{dR_S}{R_S} = \sqrt{2(10)^2 + 2(30)^2} = \pm 45\% \qquad \text{(C-16)}$$

which is felt to be a conservative estimate of the uncertainty associated with the determination of series resistance. The problems encountered in practice should be evaluated if more detailed investigations of series resistance are to be considered.

C.6 ERRORS ASSOCIATED WITH THE SPECTROPHOTOMETRIC MEASUREMENTS

The errors in each measurement are primarily instrumentation errors associated with the equipment. The emittance data from the Lion Emissometer is expected to have an uncertainty of approximately 5%. The data on relative transmittance from the Perkin-Elmer spectrophotometer is expected to also have an uncertainty of approximately 5%. The Gier-Dunkel data, was measured on assembled samples and is expected to have an associated uncertainty of approximately 10 to 15%. The spectrophotometric data was used only for the evaluation of the equilibrium temperatures of solar cell assemblies bonded to but thermally insulated from a spinning spacecraft. It is felt that the calculated temperatures are accurate with 5%. However, this does not enter into the uncertainty analysis for the characteristic curves, because the calculated temperatures were only used as guides for establishing test conditions.